AD/A-004 666

SPECIFIC IMPULSE LOSSES IN SOLID PROPELLANT ROCKETS

Paul Kuentzmann

Foreign Technology Division
Wright-Patterson Air Force Base, Ohio

17 December 1974

AD/A-004666

DOCUMENT CONTROL DATA - R & D

(Security classification of title, body of abstract and indexing annotation must be entered when the overall report is classified)

1 ORIGINATING ACTIVITY (Corporate author)	2a. REPORT SECURITY CLASSIFICATION
Foreign Technology Division Air Force Systems Command U. S. Air Force	Unclassified
	2b. GROUP

3. REPORT TITLE

SPECIFIC IMPULSE LOSSES IN SOLID PROPELLANT ROCKETS

4. DESCRIPTIVE NOTES *(Type of report and inclusive dates)*

Translation

5. AUTHOR(S) *(First name, middle initial, last name)*

Paul Kuentzmann

6 REPORT DATE	7a. TOTAL NO. OF PAGES	7b. NO. OF REFS
1973	222	98

8a. CONTRACT OR GRANT NO.	9a. ORIGINATOR'S REPORT NUMBER(S)
b. PROJECT NO.	FTD-HC-23-2719-74
c.	9b. OTHER REPORT NO(S) *(Any other numbers that may be assigned this report)*
d.	

10 DISTRIBUTION STATEMENT

Approved for public release;
distribution unlimited.

11 SUPPLEMENTARY NOTES	12. SPONSORING MILITARY ACTIVITY
	Foreign Technology Division Wright-Patterson AFB, Ohio

13. ABSTRACT

21

DD FORM 1473
1 NOV 65

EDITED TRANSLATION

FTD-HC-23-2719-74   17 December 1974

SPECIFIC IMPULSE LOSSES IN SOLID PROPELLANT ROCKETS

By: Paul Kuentzmann

English pages: 215

Source: A L'Universite de Paris vi le Grade de
          Docteur es Sciences Physiques, 26 June
          1973, pp. 1-157

Country of Origin: France
Translated under: · F33657-72-D-0854
Requester: AFRPL/XPI
Approved for public release;
distribution unlimited.

ia

U. S. BOARD ON GEOGRAPHIC NAMES TRANSLITERATION SYSTEM

Block	Italic	Transliteration	Block	Italic	Transliteration
А а	*А а*	A, a	Р р	*Р р*	R, r
Б б	*Б б*	B, b	С с	*С с*	S, s
В в	*В в*	V, v	Т т	*Т т*	T, t
Г г	*Г г*	G, g	У у	*У у*	U, u
Д д	*Д д*	D, d	Ф ф	*Ф ф*	F, f
Е е	*Е е*	Ye, ye; E, e*	Х х	*Х х*	Kh, kh
Ж ж	*Ж ж*	Zh, zh	Ц ц	*Ц ц*	Ts, ts
З з	*З з*	Z, z	Ч ч	*Ч ч*	Ch, ch
И и	*И и*	I, i	Ш ш	*Ш ш*	Sh, sh
Й й	*Й й*	Y, y	Щ щ	*Щ щ*	Shch, shch
К к	*К к*	K, k	Ъ ъ	*Ъ ъ*	"
Л л	*Л л*	L, l	Ы ы	*Ы ы*	Y, y
М м	*М м*	M, m	Ь ь	*Ь ь*	'
Н н	*Н н*	N, n	Э э	*Э э*	E, e
О о	*О о*	O, o	Ю ю	*Ю ю*	Yu, yu
П п	*П п*	P, p	Я я	*Я я*	Ya, ya

*ye initially, after vowels, and after ъ, ь; e elsewhere.
When written as ё in Russian, transliterate as yё or ё.
The use of diacritical marks is preferred, but such marks
may be omitted when expediency dictates.

* * * * * * * * *

GRAPHICS DISCLAIMER

All figures, graphics, tables, equations, etc.
merged into this translation were extracted
from the best quality copy available.

RUSSIAN AND ENGLISH TRIGONOMETRIC FUNCTIONS

Russian	English
sin	sin
cos	cos
tg	tan
ctg	cot
sec	sec
cosec	csc
sh	sinh
ch	cosh
th	tanh
cth	coth
sch	sech
csch	csch
arc sin	$\sin^{-1}$
arc cos	$\cos^{-1}$
arc tg	$\tan^{-1}$
arc ctg	$\cot^{-1}$
arc sec	$\sec^{-1}$
arc cosec	$\csc^{-1}$
arc sh	$\sinh^{-1}$
arc ch	$\cosh^{-1}$
arc th	$\tanh^{-1}$
arc cth	$\coth^{-1}$
arc sch	$\sech^{-1}$
arc csch	$\csch^{-1}$

Russian	English
rot	curl
lg	log

This work was conducted between November 1967 and March 1973 at ONERA (National Bureau for Aerospace Studies and Research) at the "High Temperature" Division of the Scientific Direction of Energetics. I would like to thank the Directors of the Bureau for allowing this thesis to be undertaken and carried through; my gratitude goes particularly to Mr. Barrère whose help and encouragement was of the greatest assistance to me. I also pay my homage to the dedication of the staff who contributed to the physical conduction of the experiments.

The topic was proposed by Professor Siestrunck to whom I express my gratitude for his continuing interest in my work and his plentiful advice. Professor Fortier was kind enough to accept a place on the Examining Committee and to propose the topic of the second thesis.

The work was done under a contract with the Direction of Powders, then the National Company of Powders and Explosives, which authorized publication of the results.

TABLE OF CONTENTS

SPECIFIC IMPULSE LOSSES IN SOLID PROPELLANT ROCKETS

SUMMARY

The discrepancy between experimental and theoretical specific impulses of metallized propellants is partly due to the presence of a condensed phase in combustion products. The theoretical analysis and the experimental study of this condensed phase both indicate a noteworthy increase in size of the particles during their evolution within the motor. The two-phase flow general equations are established and applied to a nozzle flow; the loss in specific impulse due to irreversible exchanges between phases is expressed analytically in a few particular cases. The condensed layer forming along the nozzle has little influence on the wall loss. Analytical predictions of the overall specific impulse loss compare well with measurements made on actual rocket motors.

1. · INTRODUCTION

The development in aerospace research over the last 15 years could never have taken place without the progress achieved in chemical propulsion. This method of propulsion is based on simple physical principles but implementation comes up against difficult technological problems and demonstrates the existence of unexpected operating states -- dangerous or simply unfavorable from the performance standpoint.

The unsteady and periodic states (combustion instability) are an important category of problems; instabilities are manifested both in liquid-propellant rockets where they may be accompanied by structural vibrations and unsteady response of pipes (Pogo effect), and in solid-propellant rockets where the acoustics of the combustion chamber play a large part. A second category of problems concerns the permanent or almost-permanent operating state; the performances obtained are generally inferior to theoretical predictions. This effect, known as "specific impulse loss" is particularly felt with solid propellants and it is the subject of this study.

A solid propellant is made of an intimate mixture of substances which, when they react in the combustion chamber, produce combustion products at high temperatures. Solid propellants are generally divided into two classes: double-base or homogeneous propellants where the oxidizer and the fuel are part of the same molecule (nitrocellulose, nitroglycerin) and the composite heterogeneous group where the oxidizer and the fuel are two different chemicals. Composite propellants give the best performances. Accordingly, attempts have been made to define the optimal composition from the energy standpoint alone, it being understood that other consider-ations will enter into the final choice (mechanical properties, manufacturing cost, ease of manufacturing, aging, and safety of use).

Using thermochemistry, we select the pairs of compounds with the best energy potential. Specific impulse, which physically represents the thrust produced per unit weight of fuel, is the most interesting overall parameter since it includes both the energy released by combustion and the fraction of this energy recuperated in expansion. The influence of the various factors involved in specific impulse may be defined by a simplified reasoning [1]. The study of isentropic expansion in a nozzle with the simplest hypo-theses gives the following expression for specific impulse [2]:

$$I = \frac{1}{g_o} \sqrt{2 \overline{C_p} T_o} \sqrt{1 - \left(\frac{p_s}{p_o}\right)^{\frac{\gamma-1}{\gamma}}}$$

where T_o is the temperature of the combustion products in the chamber,

p_o and p_s are the pressures in the chamber and at the nozzle outlet,

$\overline{\gamma}$ is the isentropic exponent and $\overline{C_p}$ the mass heat (two-phase mixture in equilibrium).

$\overline{C_p} T_o$ can be expressed as a function of the mass enthalpy vari-ation of the reaction at reference temperature T_R:

$$\overline{C_p} (T_o - T_R) = -\Delta h_R$$

The isentropic exponent of the combustion products is linked
to $\overline{C_p}$ by:

$$\frac{\overline{\gamma}-1}{\overline{\gamma}} = \frac{R}{(1+K)\,M\,\overline{C_p}} \quad ,$$

where R is the universal constant of the gases,
M is the molar mass of the gas combustion products,
K is the mass flow ratio of the condensed and gas-
eous phases.

For given operating conditions there is thus an advantage in
releasing substantial energy in the chamber and for the mass heat
of the combustion products, the mean molar mass of the gaseous
products, and the quantity of condensed phase to be as small as
possible.

The energy Δh_R is linked to the endothermic nature of the
reactions by which the propellant components are formed and the
exothermic nature of the reactions by which the combustion products
are formed, the latter having to be more stable at high temperatures.
Solely from the energy standpoint, a condensed phase and a high mass
heat of combustion products limiting combustion temperature and
dissociations can be favorable. Due to the effect of K and $\overline{C_p}$
on the fraction of energy recuperated in the nozzle it is desirable
to seek a compromise, and because of this we examine the reaction
product formation energies and the components linked with their
molar mass.

In the reaction products the oxides and fluorides are the
most interesting. The hydrogen (H_2O and HF) occupies a privileged
position by reason of the stability and low molar mass of these
compounds. Also, the oxides BeO, MgO and Al_2O_3 are characterized

-3-

by great exothermicity and appear in the condensed form in the useful temperature range. The components should be examined from the viewpoint of endothermicity and molar mass; the bonding energies should be as low as possible while being compatible with safety. The most interesting oxidizers are formed from S, O, Cl, and N while it is useful for the propellants to contain hydrogen and light metals.

These considerations explain why the introduction of metal into a classical composite propellant (ammonium perchlorate + plastic binder -- polyvinyl, polyurethane, or polybutadiene) markedly increases performance. Aluminum is the most widely used metal since its energy properties are good and its price, in the powder form, is moderate.

It was noticed fairly early on that the increase in specific impulse due to the metal is always less than calculations had predicted. This difference may be characterized by a general index such that:

$$\xi_I = \frac{I_{exp.}}{I_{th.}}$$

The numerator is detemined by bench tests while the denominator is given by thermodynamic calculation.

For non-metallized solid propellants the index ξ_I is on the order of 0.97 while it is often less than 0.93 for metallized propellants. This 4% decrease of ξ_I translates an extra loss of specific impulse of about 10 seconds. Such a loss, if not predicted, can irrevocably compromise a space mission; one can convince oneself of this by using the formula connecting the potential velocity increase to the ejection increase and the mass ratio.

$$\Delta V \simeq v_s \, Log \, \frac{M_2}{M_1}$$

For a given payload, the increase in velocity is directly proportional to v_s or I and it must be controlled very precisely,

particularly for injection into orbit. Calculation shows that a decrease of one second in the specific impulse of the third and last stage of a launcher means that the apogee drops by more than 100 km.

Thus the problem is first of all to precisely predict the performances of a given engine, which cannot be done without some explanation of the differences found; the next problem is to optimize the propellant configuration to maximize these performances.

2. ORIGIN OF SPECIFIC IMPULSE LOSSES

Since the total specific impulse loss results from the difference found between prediction and experiment we should investigate the two terms of the difference.

Calculation methods used have centered essentially on the thermochemical aspect of the phenomenon and have proved adequate for liquid propellant or non-metallized solid propellants. For metallized solid propellants it is assumed that the condensed and gaseous phases are in kinetic and thermal equilibrium.

For expansion in a nozzle we use the hypothesis of permanent one-dimensional flow in sections. Computer programs are distinguished by the number of chemicals considered and the hypothesis taken for the speed of chemical reactions. Chemical relaxations in the flow can be introduced into the calculation but this gives rise to large computing difficulties; for this reason the problem is tackled by calculations for extreme conditions: frozen expansion (reaction speeds infinitely slow) and equilibrium expansion (reaction speeds infinitely fast). The correct value is between the values calculated by the two hypotheses and actually depends on the time spent in the nozzle, and thus on the scale. Another hypothesis: frozen expansion in the throat or at a given temperature is also used.

The specific impulse values calculated for a typical propellant with 16.4% aluminum are as follows: (p_o = 70 atm. p_s = 1 atm.).

Frozen expansion:	257.3 sec
Mixed expansion (frozen in throat):	258.4 sec
Equilibrium expansion:	261.6 sec

The thermodynamic magnitudes at high temperatures are not always well known and the manner of decomposition of certain compounds is a matter of controversy: this is the case of Al_2O_3 whose existence in the vapor state is contested as chemical reactions in the gas phase between Al_2O, AlO, $(AlO)_2$ produce the condensed phase. These uncertainties may be at the origin of the slight differences from theoretical specific impulse.

However, the maximum difference between the values is about 2% and with small motors the experimental specific impulse is the same as the theoretical value. The uncertainty as to theoretical specific impulse cannot thus explain the loss.

Experimental specific impulse is measured at the testing station: the immobilized motor is fired and the evolution of thrust and chamber pressure is measured. From these two curves and the consumed mass one calculates a mean specific impulse and mean characteristic velocity. These two magnitudes are defined from formulas established for the ideal isentropic nozzle and adapted for average operation:

$$I_{exp} = \frac{F}{\dot{m} g_o} \simeq \frac{\int_0^{t_b} F dt}{\Delta m \, g_o}$$

$$C^*_{exp} = \frac{p_o A_c}{\dot{m}} \simeq \frac{\overline{A_c} \int_0^{t_b} p_o dt}{\Delta m}$$

The measurement precision of these two magnitudes will be discussed below. We will point out briefly that it is essential to take into consideration:

- the precision of instantaneous pressure and thrust measurements,
- the precision of measuring the exhausted mass (combustion of part of the inhibitor and the nozzle heat shielding, deposits in the chamber and on the nozzle, and unburnt substances),
- variation of throat cross section during firing,
- unsuitability of nozzle, chamber pressure varies through time (evolution of combustion surface, erosion of nozzle throat).

With a fine analysis of tests it has been shown that the experimental specific impulse can be ascertained with an accuracy of 0.2%. The relative difference between the theoretical value (fixed) and the experimental value on small motors , which is about 7 to 8% or about 20 seconds, is thus significant.

The specific impulse losses of non-metallized propellants are broken down in the classical way into elementary losses each attributed to a particular phenomenon. One generally distinguishes the following losses:

- chemical loss
  This loss corresponds to incomplete yield of chemical reactions. It happens for example when the propellant mixture is imperfect.

- wall losses
  The interactions with the wall are mainly friction and heat transfer.

- loss by jet divergence
  This loss is linked to the one-dimensional description of flow. For a conical divergent this loss is estimated by the classical formula [2]:
  $$\frac{1 + \cos \alpha}{2}$$

For the metallized propellants the importance of these various losses must be examined in detail.

2.1. CHEMICAL LOSS

We will first note that the oxidizer and plastic fuel of the propellant are intimately mixed in the propellant matrix such that the chemical reactions between these two components are likely to have an excellent yield. There might be some question, however, as to the combustion efficiency of the added metal. This efficiency has been evaluated by various methods.

2.1.1. Measuring Characteristic Velocity

The isentropic theory of the flow of an ideal gas in a nozzle enables the specific impulse to be expressed by:

$$I = \frac{C^* C_F}{g_o}$$

C* is the characteristic velocity:

$$C^* = \frac{P_o A_c}{\dot{m}} = \frac{\sqrt{r T_o}}{\Gamma(\gamma)}$$

This is thus a specific magnitude of combustion.

C_F is the thrust coefficient.

$$C_F = \frac{F}{P_o A_c} = \Gamma(\gamma) \sqrt{\frac{2\gamma}{\gamma-1}\left[1-\left(\frac{P_s}{P_o}\right)^{\frac{\gamma-1}{\gamma}}\right]} \qquad \text{(adapted nozzle)}$$

C_F characterizes the quality of expansion in the nozzle.

Attempts have been made to estimate the combustion efficiency by comparing the theoretical and experimental values of the characteristic velocity. The experimental value is always very close to the theoretical value, or even higher. The same is found with metallized lithergols leading to impairment of specific impulse greater than that of metallized solid propellants (specific impulse loss over 10%). We would thus be tempted to say that the combustion efficiency is excellent and the specific impulse loss is only connected with impairment of the thrust coefficient.

-8-

In actual fact this analysis is too simplistic; on the one hand the measurement of C* is fairly imprecise since little is known of nozzle throat erosion during firing; on the other hand the theoretical value of C* is very sensitive to the two-dimensional aspect of flow in the throat region, to wall losses, and above all to the two-phase nature of the flow: with respect to just this point the condensed phase would be translated by an increase in characteristic velocity connected with irreversible exchanges between phases and displacement of the sonic section toward the divergent [62]. The characteristic velocity measurement is thus insufficient for finding out the combustion efficiency.

2.1.2. Direct   Measurement of Combustion Efficiency of Aluminum

Analysis of the condensed phase enables the proportion of unburnt aluminum to be determined directly. Two types of deposits have been analyzed;

- a fraction of the condensed phase is deposited on the nozzle and collected after firing. This finely pulverized deposit can be treated chemically (attacked by average-concentration hydrochloric acid); postulating that alumina is totally insoluble in acid and that the volume of gas released comes from attack of free aluminum, we find that at least 99% of the aluminum is in the combined form; this result is in good agreement with that of Colucci [3].

- traps are placed in the jet to measure the grain size of the condensed phase. The trapped particles form a very thin film on the glass plates and the mass collected is extremely small. For this reason the X-ray diffraction method of analysis was chosen. The particles are removed from the plate with a razor blade, mixed with an amorphous glue, and the powder obtained is spread in a thin but dense film. The identification method (Debye-Scherret) shows bands of different kinds of alumina (principally α, δ, χ, γ).

-9-

)

The aluminum band is too small for direct quantitative assaying. A quantitative assaying method was developed for comparing the analyzed specimen with reference specimens composed of α alumina and a small quantity of aluminum.

These results enable us to state that less than 3% of the aluminum is in the free form.

The influence of a proportion of unburnt aluminum on performance is sought by thermodynamic calculation. One need only modify the computer program by considering the unburnt aluminum as an inert substance possessing the thermodynamic properties of aluminum. Figure 1 gives the variations in specific impulse and characteristic velocity with the proportion of unburnt aluminum under standard operating conditions (p_0 = 70 atm. p_s = 1 atm.) of a propellant containing 16% aluminum. It is seen that the specific impulse loss due to incomplete aluminum combustion is at most 0.4% or about one second.
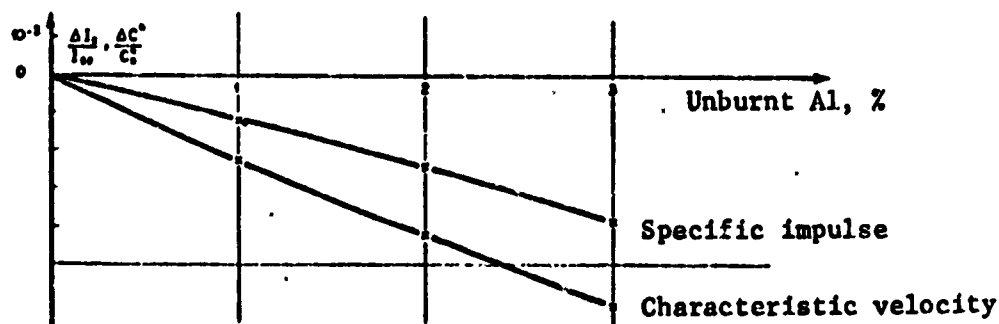

Figure 1. Influence of Percentage of Unburnt Aluminum on Performance.

2.1.3. Attempt to Improve Combustion Efficiency

An indirect determination of the combustion efficiency was made with a series of tests on a particular combustion chamber configuration. A grid made of tungsten bars (the only metal with satisfactory resistance to heat at the propellant combustion

temperature of about 3000°C) and placed between the propellant grain and the nozzle is charged to increase the turbulence in the chamber and intensify reactions between phases; this type of device has been used successfully in lithergol engines. The optimum specific impulse gain is about one second.

These various approaches lead us to assume that the combustion efficiency is very close to 1 and the corresponding loss, if it exists, is only a small fraction of the total specific impulse loss.

2.2. WALL LOSSES

The wall losses may, in a first approximation, be estimated with classic claculations for non-metallized propellants. The metallized propellants are characterized by a very high combustion temperature and the nozzles are not cooled; the wall temperatures reached are thus higher and the heat flow must remain in the same order of magnitude. The same applies to friction, far less sensitive to the temperature level than are thermal phencmena. Accordingly, the wall losses are comparable whether the propellants are metallized or not.

Experiments have shown that the problem is actually more complex due to formation of an alumina layer on the nozzle [3].

2.3. JET DIVERGENCE LOSSES

The nature of the problem is identical whether the propellant is metallized or not but in the first case the calculation is more complicated due to the non-uniform distribution of the condensed phase in the geseous phase and the relative movement of the two phases. However, the condensed phase is rather concentrated on the nozzle axis so that the loss can at most only be equal to its classical expression for a homogeneous fluid.

This brief discussion shows that classical losses are at most those of a nonmetallized propellant, but they do not suffice to explain the differences found, the origin of which must be sought in the existence of a condensed phase characterizing the metallized propellants and able to correspond to a mass fraction of combustion products greater than 40%.

Numerous studies on specific impulse losses have been conducted in the countries interested in chemical propulsion, principally the United States and the Soviet Union. In France the first studies were undertaken under contracts between the Direction of Powders and ONERA (Energy Direction).

Due to the large number of phenomena to be considered and the complexity and diversity of investigations to which they lead, only a few publications give a good overall approach to the problem [4]. On the other hand, there is abundant literature on particular aspects of the problem; in the field of multiphase flow we must cite the work of Marble [5] and Soo [6]. Some section of more general works also deal with the problem [7].

In the course of this study a number of developments proved necessary in varying directions. This diversity, found in the present account, led to the establishment of priorities of objectives. The first target we set ourselves was to pick out the most important phenomena and estimate by simple and realistic calculations the order of magnitude of the various losses. This led us to go more deeply into certain theoretical foundations and to conduct theory and experiment in parallel; experiment supplied physical data and enabled the calculations to be checked. It was noticed at an early stage that there were uncertainties as to the very description of certain phenomena and that we still have a poor quantitative knowledge of certain magnitudes. We did not thus feel the need to go into involved computer calculations while there was still uncertainty as to the basic premises.

The plan adopted here in describing the results obtained begins
with the study of the condensed phase since this plays the essential
part in specific impulse losses. Each loss is then analyzed on the
assumption that it is independent of the others, which is justi-
fied by their orders of magnitude, and corresponds to a small pertur-
bation in the ideal expansion of combustion products. We w l then
summarize the results and compare calculation and experiment.

3. STUDY OF THE CONDENSED PHASE

3.1. GENERAL

The condensed phase of the combustion products is formed by
alumina coming from combustion of the metallic propellant. It is
partly deposited on the chamber and nozzle walls but almost all of
it is in the form of very fine particles suspended in the gaseous
phase.

These particles influence all the phenomena to be taken into
consideration here. The flow is characterized by exchanges between
the gaseous and condensed phases: first of all, mass exchange due
to condensation of alumina, then momentum exchange connected with
entrainment of particles by the gaseous phase, then heat exchange.
These exchanges are irreversible in nature and may be expected to
have great effects on expansion of the combustion products. The
particles do not exactly follow the gaseous flow streamlines in
zones with a high velocity gradient, the condensed phase is not
uniformly distributed in the gaseous phase, and the two-dimensional
effects of flow are modified accordingly. A fraction of the par-
ticles is deposited on the walls to form a layer of alumina which
modifies wall phenomena and also corresponds to a loss in ejected
mass.

Each of these occurrences requires local knowledge of the
particle population. Since the number of particles is very large

(about 10^{14} for 1 kg of propellant containing 16.4% aluminum) we must resort to statistical methods to represent this population. At each point of flow we can define a particle distribution according to one or more variables which may be the mass or a characteristic geometric dimension, velocity, etc. The distribution density, assumed continuous, gives the number of particles per unit volume of the mixture of the two phases which possess a mass, a velocity, etc. within the given intervals.

The particles, collected on the outside of the motor, are essentially spherical in shape. The particles inside the motor are also assumed to be spherical although they can be deformed by sudden accelerations when liquid. We also noted the existence of exceptional particles, usually large and very limited in number, escaping this description; these were usually agglomerates. The photographs of Figures 2 and 3 taken under the scanning electron microscope show that most of the particles are almost spherical and that there is a large spread of diameter (between 0.1 and 20 μ under the experimental conditions of our tests).

The alumina remains in the liquid state (T > 2317°K) for most of the expansion, and solidification commences only in the divergent section of the nozzle. The liquid particles agglomerate by co - lision such that the particle size of the condensed phase is neither uniform nor constant. Particle growth is also accentuated by alumina condensation. The particle formation process, the colli - sions, and condensation give rise to the wide spread in particle diameter.

The condensed phase is thus characterized by the following three properties: interaction with the gaseous phase, development during expansion, and wide spread. As particle size is one of the most important parameters in calculating specific impulse losses (it will be seen that the square of the mean diameter comes into calculations of losses due to phase shifts), we can see that the
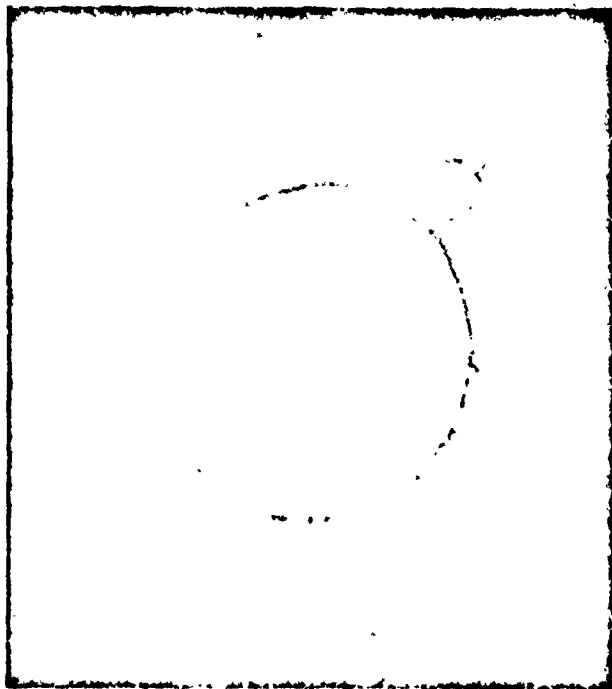
Figure 2. Particles Collected
Outside the Motor (x 1500).

Figure 3. Agglomerates Collected Outside the Motor.
General view and detail.
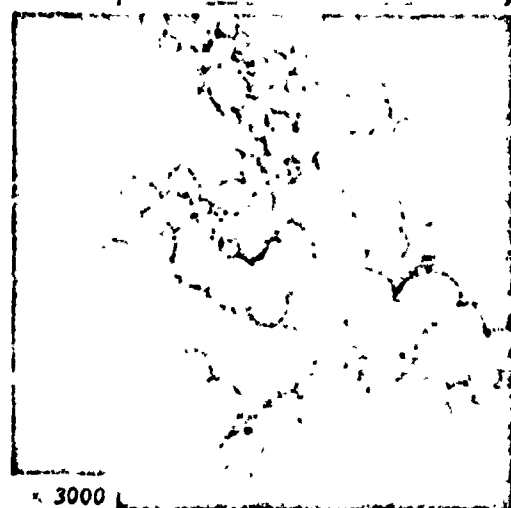
particle size of the condensed phase must be known locally and
accurately. This determination proved difficult; we thus called
on both experiment and theory at the same time.

3.2. EXPERIMENTAL DETERMINATION OF CONDENSED PHASE CHARACTERISTICS

The condensed phase of the combustion products of metallized
propellants was measured a number of times: for velocity, for
temperature, for particle concentration, and for particle size.
The latter called for the greatest amount of work as the other
magnitudes were more accessible by calculation. Experimental results
on particle size have been summarized elsewhere [8]. We will thus
confine ourselves to briefly summarizing results obtained abroad

-15-

with emphasis on the means used in the present study. We will also mention the measurement principles for the other magnitudes.

The first results on particle size of the condensed phase were published by Brown and MacArty [9]. Other investigators then took up the problem [10, 11, 12] but the lack of uniformity in results and conclusions induced us to continue the work started at ONERA in 1964 [13].

The experimental techniques may be classified into two groups: direct techniques, wherein particles are collected and analyzed, and indirect techniques where the particle size is deduced from another physical measurement.

The indirect techniques are principally based on optical measurements. These methods are particularly attractive since they do not perturb the flow and have great potential, especially since the development of lasers.

However, the measurements of Dobbins and Strand [12] showed a number of difficulties. Determination of the monochromatic flow transmission factor calls upon Mie's theory of light scattering by a cloud of particles. The calculation is extended to a particle distribution and enables a mean diameter to be calculated provided one assumes that the form of the distribution function is given. This is still poorly known, in particular its bimodal characteristic, and is still a subject of discussion although we will show its origin later in the present paper. This uncertainty probably explains the lack of coherence in results reported for various wavelength pairs.

We should also note that the alumina characteristics at high temperatures, particularly the complex refraction index, are still very imprecise. Crabol [14] showed in particular that the values of the absorption coefficients determined experimentally differ by

several orders of magnitude from those predicted by Mie's theory for saphire. Finally, as the measurements are usually made on revolutionally symmetric jets, we must take into account the non--uniform distribution of the condensed phase in the gaseous phase.

Optical methods are also used to measure the mean particle velocity calling on the Doppler effect [15]; the possibilities offered by holography [16] to determine mean velocity and part e size simultaneously seem to be promising. A spectropyrometer enables the mean temperature of the particles to be found and infrared emission to be measured; from this one deduces the gas temperature. The particle concentration comes into studies on radiation of a cloud of particles; its determination is thus not independent of particle size determination. These various techniques are fundamental in nature and have not yet reached a sufficient degree of accuracy. They will thus be used to supplement direct measurements.

One can collect alumina particles either by firing the motors in a box or by placing an obstacle in the flow. The box method is widely used in the United States (Atlantic Research Company, Hercules Powder Company, UTC, JPL); it is limited to small motors and furnishes a mean distribution of all the particles formed during the firing and after solidification. The results obtained are thus general. Sensing techniques permit a finer analysis of the phenomenon and were those mainly used in the present study.

3.2.1. Experimental Methods

The obstacles designed to pick up alumina particles can be fixed or mobile according to location and the motor characteristics; accordingly the exposure time is restricted by technological imperatives (particularly heat tolerance) as well as practical ones (number of particles collected).

The simplest and most widely-used device is a metal cross on which glass plates measuring 20 mm x 20 mm are placed. It is placed

in fixed fashion in the jet when firing takes no more than a few
seconds and at a fairly long distance from the outlet section of
the nozzle. This type of device is represented in Figure 4. The
distribution of the plates on the arms permits spatial exploration
of the jet.

When firing lasts more than some 10 seconds, or it is desirable
to collect the particles near the outlet section, it is necessary to
use a device not fixed in the jet. We built the retractable device
shown in Figure 5. This has a plate-carrying arm and a protective
arm cooled by water circulation. A kinematic system controlled by
a drum enables the two arms to be placed   in the jet, the protec-
tive element to be raised whereby the plates are exposed, and then
to be lowered before the two arms are raised.
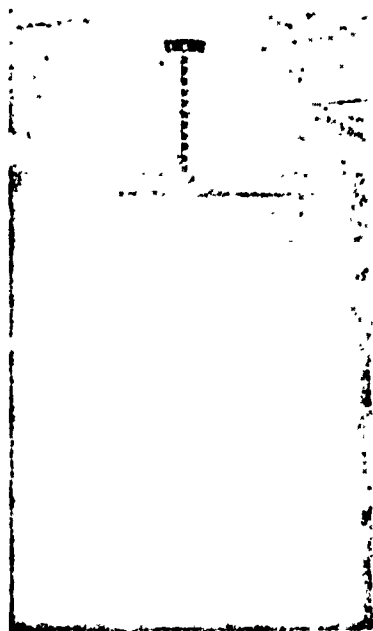
Figure 4. Collecting
on a Fixed Obstacle.
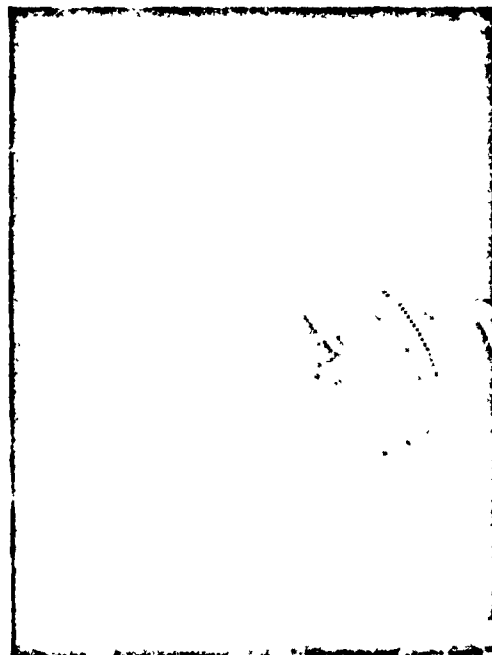
Figure 5. Collecting on
a Retractable Obstacle.

Other devices have been developed to capture particles inside
the motor instead of in the jet. These are double-acting jacks one
end of which has a quartz plate measuring 6 mm x 6 mm and is exposed
for a short time (less than 0.1 sec.) in the flow.

-18-

This collector can be mounted either on the nozzle or on the front bottom of the motor (Figure 6). Particles can only be collected near the wall due to the high chamber temperature. The jacks were originally controlled pneumatically but are now controlled pyrotechnically which permits the collector to be withdrawn and emplaced more quickly and gives better-controlled exposure times.

Figure 6. Particle Collector
Mounted on the Front Bottom
of a Motor.

3.2.2. Statistical Analysis

Whether the particles are gathered on the walls of a box or on collecting plates, statistical analysis raises the same difficulties.

The particles collected on the plates form a very thin film. They can be removed by scraping, but industrial particle size measurements (variation of the resistance of a particle suspension in an electrolyte, for example) cannot be used because the particles are too small. They must thus be studied optically.

The magnification of a microscope is limited to about 3000 and the field depth is accordingly reduced such that particles with different diameters are not seen sharply at the same time (Figure 7). The scanning electron microscope permits better image definition and

offers numerous magnification possibilities. The plates are vacuum-
-metallized (the thickness of the metal film is very much smaller
than the smallest particle diameter) before being placed under the
electron microscope. Photographs are taken at each point, examined,
and at different magnifications.

We attempted automatic photograph analysis with the aid of
an image-analyzing computer (Quantimeter 720 by Metals Research).
This did not work, as the agglomerated and superimposed particles
were not distinguished by the computer and completely distorted the
statistics. It was thus necessary to operate by hand. The parti-
cles were classified by an instrument of the sliding caliper type;
the information was coded on punched tape then stored on magnetic
tape for processing by the computer.

Microphotograph x 3000   Electron microphotograph x 2800

Figure 7. Particles Collected on Plates.

We could not analyze all the particles on a plate since there
were more than 10^4 of them. We thus took a sample of about 1000
particles. This sample usually corresponded to the photographs of
the center of the plate.

This method of analysis led to rather large uncertainties for
the smallest and largest diameters. A large number of small parti-
cles are classified in the small diameter group ($d_p < 0.5\mu$). The
large particles are limited in number and the probability of their

-20-

appearing in the sample is slight. As a result, the high-order moments of distribution have a fairly wide spread.

3.2.3. Interpreting the Results.

All obstacles perturb the flow, and we may ask ourselves whether the sample analyzed truly represents the particle population. The problem of capturing particles by an obstacle is a classical one and was tackled at an early stage of aeronautics [17, 18].

The two-phase nature of the flow is not usually taken into consideration in calculating the velocity field of the gaseous phase: one assumes that the number of particles is sufficiently limited not to perturb gaseous phase flow. In the velocity field so calculated the particle movement comes down to a problem of point mechanics.

For rectangular obstacles such as those used, we come to the classical velocity problem. If we assume that the Mach number is sufficiently small, the fluid may be considered incompressible; at higher velocities calculations become more complex and two-phase relaxation phenomena more important.

With a suitable transformation we can find the velocity field analytically in implicit form:

$$X = \frac{1}{\pi}\left(\frac{1}{2} \log \frac{(u^2+v^2-1)^2+4v^2}{[(u-1)^2+v^2]^2} + 2u\, \frac{u^2+v^2-1}{(u^2+v^2-1)^2+4v^2} \right),$$

The coordinates and velocity components are small (Figure 8).

A suitable choice of variable auxiliaries p and q enables us to give the parametric expressions:

$$Y = \frac{1}{\pi}\left(\text{Arc tg} \frac{-2v}{u^2+v^2-1} + 2v\, \frac{u^2+v^2+1}{(u^2+v^2-1)^2+4v^2} \right).$$

-21-
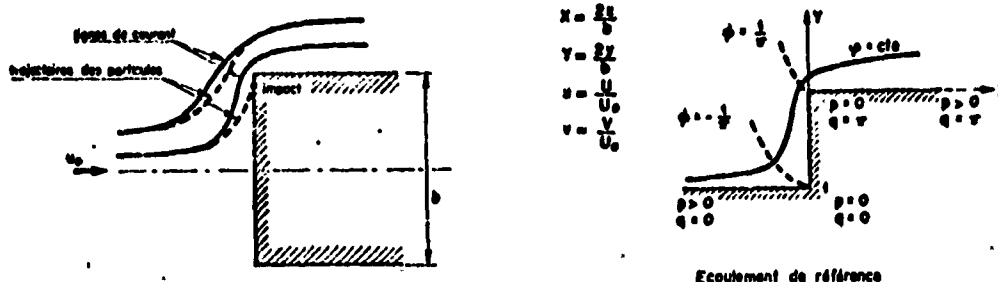
Figure 8. Capturing Particles by an Obstacle.

$$X = -\frac{1}{\pi}\left(p + sh\,p\cos q\right) \quad,$$

$$Y = \frac{1}{\pi}\left(q + ch\,p\sin q\right) - 1 \quad,$$

$$u = \frac{sh\,p}{ch\,p + \cos q} \quad,$$

$$v = \frac{\sin q}{ch\,p + \cos q} \quad.$$

The streamlines and potential lines are written, respectively:

$$\Psi = \frac{1}{\pi}\,sh\,p\sin q = Cte \quad,$$

$$\Phi = -\frac{1}{\pi}\,ch\,p\cos q = Cte.$$

The particle movement equations, in reduced variables are:

$$\frac{du_p}{d\tau} = \frac{C_D Re_R}{24}\,\frac{1}{I}\left(u - u_p\right) \quad,$$

$$\frac{dv_p}{d\tau} = \frac{C_D Re_R}{24}\,\frac{1}{I}\left(v - v_p\right) \quad.$$

In these equations, C_D is the drag coefficient and Re_R the Reynolds number based on the particle diameter and velocity difference between fluid and particle. The term $\frac{C_D Re_R}{24}$ thus characterizes the flow regime around the particle with respect to Stokes law.

The parameter I is often called inertia parameter; it summarizes the capturing conditions:

$$I = \frac{2\,u_o\,d_i^2\,\rho_s}{9\,\mu\,b} = \frac{2\,u_o}{b}\,Tu \quad,$$

where Tu is the velocity relaxation constant, ρ_s the particle density, and μ the dynamic viscosity of the fluid.

-22-

A computer application for a moderate velocity values shows that $Re_R < 1$ and $I \ll 1$. It is thus legitimate to study the problem with Stokes law for small values of parameter I. A perturbation method is thus very suitable for the problem.

The position of the particle at each point is well determined by the corresponding value ψ and ϕ or:

$$z = \psi \quad , \quad r = -\phi \; .$$

With order I we find:

$$\frac{dz}{dr} = \frac{2I}{\pi} \cdot \frac{zr}{\left[\left(\frac{1}{\pi}+r\right)^2 + z^2\right]^{\frac{1}{2}} \left[\left(\frac{1}{\pi}-r\right)^2 + z^2\right]^{\frac{1}{2}}} \; .$$

We will assume that the particle impinges when the distance of its trajectory to the obstacle is equal to its radius; we thus assume that it neither slips nor ricochets. These being the conditions, we look for the relationship between the value Z_∞ at infinity upstream, the particle diameter d_p, and the small distance k of the point of impact at the axis.

An approximate integration method may be found and we determine the relation Z_∞ (I, d_p, k) by computer. For capturing conditions:

$$\frac{d_p}{b} < 10^{-3} \; ,$$
$$\frac{k}{b} < 0,2 \; ,$$
$$I \ll 1 \; ,$$

we have shown that the following analytic expression gives a good representation of the phenomenon:

$$Z_\infty = \frac{\pi k}{4} \left(\frac{d_p}{b}\right)^{\exp\left(-\frac{\pi}{2}I\right)} \; .$$

This formula may be applied to the problem of correcting the experimental distribution of particles collected on plates. We will consider an elementary capturing zone defined by its position k (k < 0.2) and its extent dk. At infinity upstream it has a capture cross section defined by:

-23-

$$d\Sigma_\infty = \frac{\pi}{4} \left(\frac{d_p}{b}\right)^{\exp\left(-\frac{\pi}{4}I\right)} dR \ .$$

If we assume that particles of differing dimension are regularly distributed at upstream infinity, the real distribution density according to the radius will be deduced from the experimental density by the relation:

$$f(r) = C \ \frac{f_{exp}(r)}{\left(\frac{2r}{b}\right)^{\exp\left(-\frac{\pi}{4}I\right)}} \ ,$$

where C is a normalization coefficient and I is proportional to r^2.

We find numerically that the correction to be made to the experimental density is particularly large for the smallest particles (d_p on the order of 0.1µ). The influence of this correction is thus felt only on deduced mean radii with rather low orders, i.e., the least interesting ones.

We tried to verify whether the order of magnitude of the correction coefficient was exact by the following simplified calculation. For a mean radius value we sought the number of particles formed in one firing and the corresponding number of the particles which should be captured and observed on the surface of a plate seen under the microscope. The calculation gives an exactly correct order of magnitude for this number of particles.

The correction requires knowing the velocity before the capturing obstacle. It proved difficult to calculate this velocity with the application considered:

- internal capturing (nozzle converging section); it was possible to use a theoretical value;

- external capturing (motor jet); because of technological requirements we had to place the capturing apparatus rather far from the nozzle outlet section (distance 6 m with outlet diameter 60 mm).

The jet structure is poorly known at a large distance from the nozzle; from measuring the velocity with two Pitot tubes in the center of the jet we concluded that the velocity is small and the correction negligible. The flow is very turbulent in this zone; the effect of this on particle deposition is not known.

3.2.4. Results

From a fundamental viewpoint, it is necessary to determine the size of alumina particles to specify changes in the condensed phase in the motor. We also tried to explain variations in the specific impulse loss and particle size appeared to be a magnitude to be measured systematically. Since the particle-size measurements were very time-consuming we cannot make multiple captures with each firing. The tests were thus specialized:

- a series of tests was specially directed to particle size measurements. Particles were captured inside and outside the motor.

- tests wherein specific impulse was measured systematically included capturing in the jet.

Preliminary tests enabled us to define the number and position of plate adequate for determining particle size.

3.2.4.1. Presentation of Results

All the information is contained in the distribution density as a function of radius or diameter. This datum is essential for studying collisions, for example. On the other hand, for other applications, it is useful to characterize the particle size by one or more mean radius or diameter values, calculated from the moments of the distribution law.

The mean diameter d_{pq} is defined by the expression:

$$d_m = \left[\frac{\int_0^\infty \delta^r f(\delta) \, d\delta}{\int_0^\infty \delta^q f(\delta) \, d\delta} \right]^{\frac{1}{r-q}} .$$

The median diameter of order i, d_{mi} is given by the relation:

$$\int_0^{d_{mi}} \delta^i f(\delta) \, d\delta = \frac{1}{2} \int_0^\infty \delta^i f(\delta) \, d\delta .$$

Different mean and median diameters are used in the literature, which makes it difficult to compare results of different origins. The most frequent are:

$$d_{10}, \ d_{20}, \ d_{32}, \ d_{43}, \ d_{63} \ \text{et} \ d_{m_3} .$$

The mean radius d_{53} is the most significant for specific impulse losses, as we shall see later.

Attempts are often made to fit the experimental distribution law to known analytic laws. The most commonly used are laws of the logarithmic or exponential types. These laws of unimodal character today appear somewhat unsuitable for our problem: certain indications seem to show that the law is bimodal. However, the precision of the results is still insufficient to enable analytic functions with more than three parameters to be used.

3.2.4.2. Qualitative Results

Some remarks must first be made with respect to the form of the experimental distribution laws (outside capture).

In general shape this law is a decreasing one, extending from 0.1 μ to some 10 μ (Figure 9). There are still some uncertainties at low and high diameter values.

A lower limit for small particles is observed (d_p = 0.1 μ). We might be tempted to attribute this limit to a perturbing effect of capture. It is more logical to regard this as an effect connected with the particle formation process: the smaller the particle,

-26-

the more rapid the growth by condensation. The shape of the distribution law at very low diameter values is uncertain. Experimental laws generally increase while calculations based on collision growth give a decreasing law. This discrepancy can be explained either by the capture conditions or by the fact that theory fails to take into account a maximum particle diameter. In any case, it has little importance since it is only negligibly involved in calculations of high-order moments.
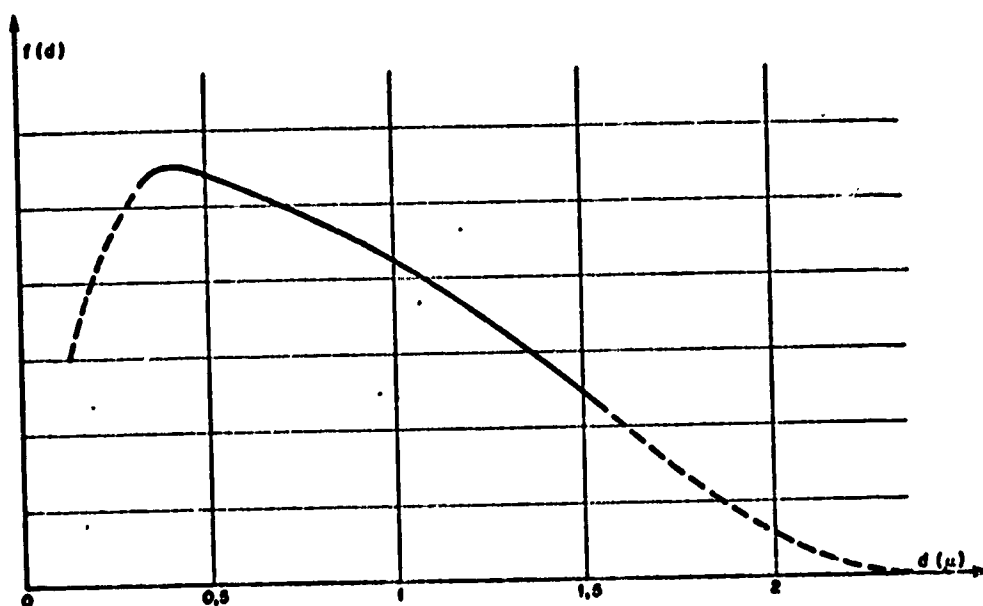
Figure 9. Example of Experimental Particle Distribution Law According to Particle Diameter (Outside Capture).

Large-particle statistics are imprecise. The existence of particles with diameters of about 10 μ has been observed experimentally and a theoretical explanation has been proposed (see Section 3.3.2.). These particles occur only randomly in the statistics due to the size of the samples studied. High-order moments and the corresponding mean radii are thus necessarily imprecise. As a result it appears necessary to develop techniques of analysis suitable for this class of particles.

The growth of the particles as they change in the motor is a phenomenon of primordial importance and has been checked by experiment; on the other hand, theoretical calculation methods are more abundant. This disparity of effort has to do with difficulties of measurement and measurement interpretation. Our tests prove the reality of the phenomenon and, despite their relative imprecision, give the beginnings of quantitative estimation.

The table below shows the most characteristic results (ϕ_c = 15 mm, P_o = 70 b):

CAPTURE	FRONT BOTTOM	CONVERGENT	OUTSIDE
d_{10} µm	0.35	0.54	0.90
d_{30} µm	0.40	0.60	1.17
d_{53} µm	0.63	0.75	3.90

The measurements in the bottom front are more significant than those in the nozzle. Particles which are still liquid in these two zones are partially crushed on the plate of the convergent capturing device due to their great velocity.

3.2.4.3. Quantitative Results

The results presented here are confined to those obtained under this study. For the bibliography of results obtained abroad, see Reference [8]. The plates analyzed are those for outside capture; the values given are thus representative of the final state of the condensed phase after solidification.

For each test about ten plates were analyzed and averages were taken for all the plates. We took a mean diameter of d_{32} to permit comparison with foreign results. We established statically the relation:

We first sought the influence of the plate position on particle
size. These results are summarized in Figure 10. We chose the
plates arranged on the horizontal arms of the capture cross-piece.
d_{32} increases with distance between plate and jet axis, which is
linked with the existence of more numerous large particles. The
means presented relate to plates situated less than 20 cm from the
jet axis and seem to be the most representative.
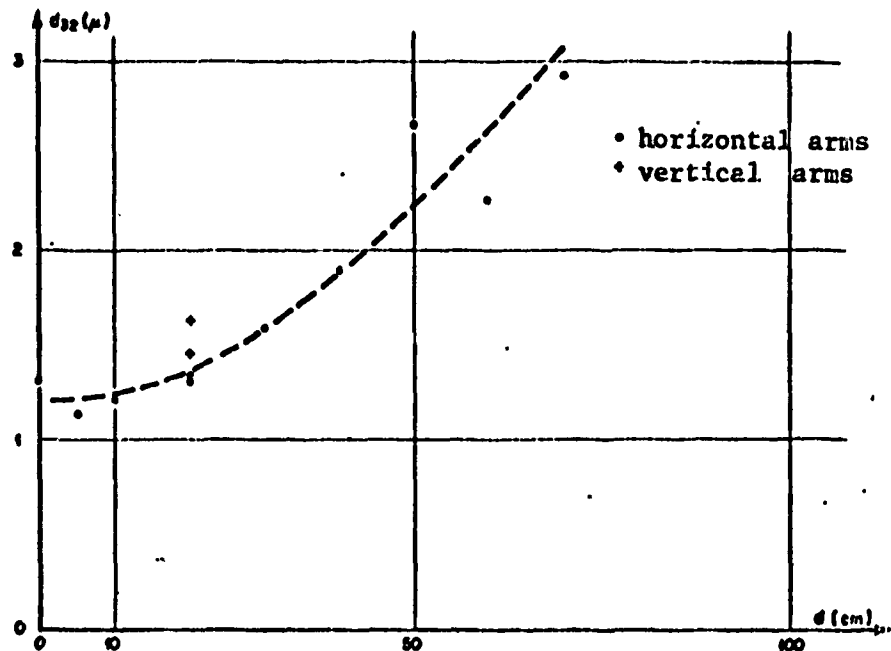
Figure 10.   Influence of Capturing Position on Mean Particle
Diameter.   (ϕ_c = 30 mm;   D = 6 m; P_o = 40 b)

INFLUENCE OF THE NATURE OF THE PROPELLANT

The results in the literature indicate that the particle size
of the condensed phase is independent of the propellant's composi-
tion, its aluminum content, and the aluminum or ammonium perchlorate
particle size. The conclusions are contradictory with respect to
the influence of the aluminum content. Our tests compared two pro-
pellants with identical composition by weight (ammonium perchlorate-
-aluminum-polyurethane binder) but different as to particle size and

the origin of the aluminum. A 9% difference for d_{32} was found; this is corroborated by a difference in specific impulse. This result shows that each type of propellant must be studied from the viewpoint of its condensed phase.

INFLUENCE OF OPERATING PRESSURE

The influence of operating pressure has not yet been clearly established. Our tests on small motors showed a moderate variation of d_{32} with p_o (Figure 11). This effect is in good agreement with conclusions of Dobbins and Strand [12].
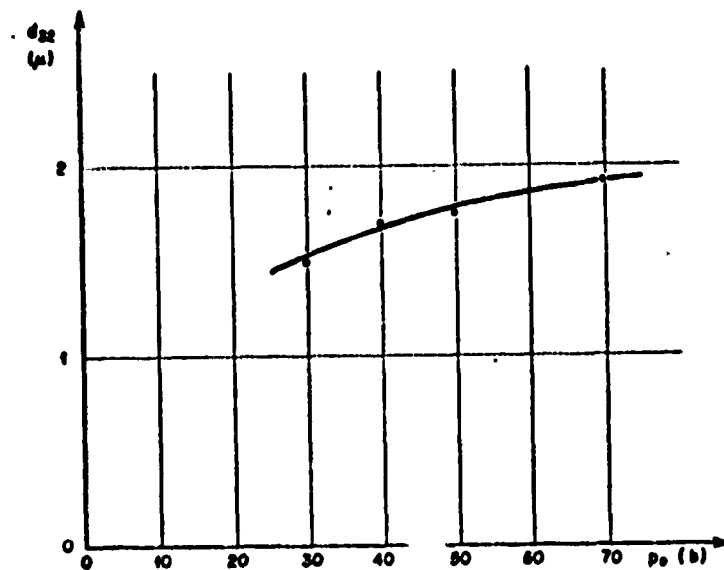
Figure 11. Influence of Operating Pressure on Mean Particle Diameter (ϕ_c = 20 to 30 mm).

INFLUENCE OF MOTOR SCALE

The literature indicates a considerable increase of condensed phase with the scale of the motor: d_{32} reaches 9 μ for ϕ_c = 10 cm. Our tests did not show any substantial influence of motor size when

ϕ_c varied from 1.5 to 3 cm. Beyond these values collaboration with other laboratories should be envisaged.

INFLUENCE OF MOTOR GEOMETRY

Our tests were done mainly on the influence of nozzle geometry. For a biconical nozzle whose convergent angle and throat radius of curvature are made to vary, no variation in mean diameter is manifested. On the other hand, when the nozzle entrance ratio diminished or when integration of the nozzle and the motor increases, diameter d_{32} increases (the proportion of large particles is higher). This increased particle size is correlated by an increase in specific impulse loss.

3.2.5. Conclusions

Experimental determination of the particle size of the condensed phase thus proves difficult and relatively imprecise due to the wide dispersion of particle diameters, their growth in the course of expansion, and their irregular distribution in the flow.

The measures we made, however, enabled us to prove the reality and importance of particle growth and to propose values for the final mean particle diameter which seem substantially more realistic than those found in the foreign literature. Some improvements still have to be made in these measurements, but they seem an essential tool for designing a motor.

Despite our efforts, the data gathered is too fragmentary to be connected quantitatively with specific impulse losses, and we attempted to predict the evolution of the condensed phase by calculation.

3.3. THEORETICAL STUDY OF CONDENSED PHASE

The condensed phase must be known at each point of the motor both with regard to local particle concentration and with regard to

particle diameter distribution. In principle, a study of these characteristics is inseparable from a study of flow. However, one can, under certain conditions defined later, determine the particle movement and growth without taking the gaseous phase into account. This approximation enables a first representation of the phenomenon to be given.

The mechanisms involved appear sufficiently varied for the various motor zones to be distinguished. The specific impulse loss mainly concerns the nozzle; the first studies were thus performed for this type of flow and it appeared essential to find out the characteristics of the condensed phase in the entrance section. Accordingly, we studied the phenomenon in the chamber, then particle formation in the combustion process. Here we will follow the particles in their evolution at the same time as summarizing some results published elsewhere [19, 20].

3.3.1. Relative Influence of Different Phenomena

The development of the particles is the result of a set of phenomena whose importance must be estimated before a calculating method is set up. In the first place one must study the combustion mechanism of the aluminum particles in the propellant and the formation of alumina particles. A large number of fundamental studies have been devoted to particle combustion but most of them were oriented to the kinetic aspect of combustion rather than to studying the combustion products [13, 21]. The useful qualitative indications can, however, be deduced from the results obtained at ONERA by ultra-rapid cinematography of the solid propellant combustion surface. One notes the following particularities (Figure 12):

- combustion occurs essentially in the vapor phase (diffusion of combustive and combustible species) and very fine alumina particles appear in the flame zone. These particles can form very thin asymmetric bubbles due to the movement, with long tails,

which may be collected by stopping combustion suddenly. These
bubbles can explode spontaneously.

- on the aluminum particle there is a brighter zone shaped like a
  cap and is assumed to be made of alumina resulting from surface
  oxidation of the aluminum during the particle heating period pre-
  ceding ignition, and also from heterogeneous combustion near the
  cap.

1 - aluminum particle

2 - alumina cap

3 - alumina layer

4 - wake of fine
    alumina particles
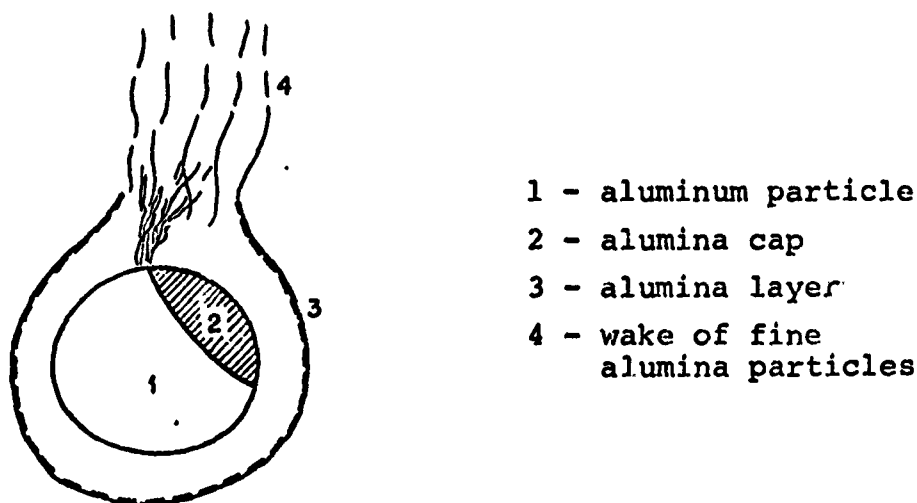
Figure 12.   Combustion
of an Aluminum Particle
of a Solid Propellant.

Three mechanisms are simultaneously involved in this stage of
development of alumina particles: formation of condensed nuclei ,
growth of these nuclei by deposition of new alumina molecules, and
agglomeration of the particles by collision. Later only the latter
two mechanisms subsist.

The most simplified model for predicting the radius and speed
of appearance of the nuclei is that of the liquid droplet (homo-
geneous nucleation). There is a limit value of the radius above
which the nucleus, formed by the fluctuations in the vapor phase,
is stable and can continue to grow; the most generally used expres-
sion is that of Kelvin:

$$r^* = \frac{2\sigma M}{\rho_e RT \log \frac{p}{p_\infty}},$$

where M is the molar mass of the gas and R the universal constant, τ the surface tension, ρ_e the liquid density, T the temperature, and p and p_∞, the partial vapor pressures of the liquid in droplets and in mass. r* is always in the vicinity of about 100 Å and is thus very much less than the particle radii observed experimentally.

The number of nuclei formed by unit of time and volume is given by expressions of the type:

$$I = K \exp\left(-\frac{W}{kT}\right),$$

where W is the work of formation of the nucleus, k the Boltzmann constant and K a factor linked to the frequency of molecular collisions.

The exponential term appears to be very temperature-sensitive, explaining why condensation occurs very suddenly when the vapor expands.

The growth of the nuclei under our conditions (generally under high pressure) largely in the continuum domain (Knudsen number << 1) where it is controlled by the diffusion of the species, in particular the condensable species. On this point we should note that the existence of alumina in the vapor phase is not proved: alumina is probably formed through reactions involving other aluminum components, principally the chlorides. To take this uncertainty into account we define a partial ficticious alumina pressure in the vapor phase. Thermodynamic calculation enables the proportion of liquid alumina to be found as a function of temperature upon equilibrium: nearly 80% of the alumina is condensed in the chamber (approximately 3300°K); condensation continues in the nozzle and terminates before the alumina solidifies (approximately 2300°K).

In our publication [19] we established the particle growth law by condensation due to the lack of clarity in the literature with respect to the hypotheses used and how calculations were made. The equations are written for the Zvab-Zeldovitch approximation [22]: stationary mechanism, absence of viscosity forces and distant forces, constant pressure, insensitivity of diffusion to the thermal gradient, Levis number equal to 1. In this way we come out with two equations, a continuity equation for vapor and an energy equation which in this problem with spherical symmetry are simply integrated and the linking of pressures leads to an expression for the growth rate:

$$r\frac{dr}{dt} = \left(1 - \frac{r^*}{r}\right)\frac{\lambda}{C_{pF}\rho_e} \quad \frac{Log\frac{P_{1\infty}}{P_{v_1}(T_\infty)}}{\frac{P_\infty - P_{1\infty}}{P_\infty}\left[\frac{\mathcal{M}_2}{\mathcal{M}_1} + \left(1 - \frac{\mathcal{M}_2}{\mathcal{M}_1}\right)\frac{P_{1\infty}}{P_\infty}\right] + \frac{L^*}{r_1 C_{pF}T_\infty^*}}$$

where the index 1 is reserved for condensable vapor and index 2 for the inert species.

When the radius is far greater than the critical radius we find the classic r^2 law. Gyarmathy [23] proposes that this formula be extended to the molecular regime by replacing the second r member by $r + \alpha\bar{e}$, where $\bar{e}$ is the mean free path and α a numeric coefficient.

Collisions are induced by several phenomena; when the particles are very small they have Brownian motion. This motion quickly becomes negligible when the radius exceeds $0.05\ \mu$. Other phenomena are of random origin (vortices) or organized origin (acoustic field or acceleration of flow). We try to define these different modes of collision in a unique manner by defining a collision function. We will call the particle distribution function according to mass, for example, $f(m)$. The frequency of collisions for the two classes of particles $(p, p + dp)$ and $q, q + dq)$ is presented in the form:

$$f(p)f(q)\,\phi(p,q)\,dp\,dq \ .$$

When writing collision function ϕ, only the masses of particles considered appear but it is evident that other variables implicitly take into account the collision mechanism and the local conditions;

we try to make these variables appear in the form of coefficients. Thus, Jenkins and Hoglund [24] give:

- for Brownian motion:

$$\phi(p, q) \text{ proportional to } 2 + (p/q)^{1/3} + (q/p)^{1/3}$$

- for turbulent scattering:

$$\phi(p, q) \text{ proportional to } (p^{1/3} + q^{1/3})^3,$$

- for collisions of acoustic origin:

$$\phi(p, q) \text{ proportional to } (p^{1/3} + q^{1/3})|p^{2/3} - q^{2/3}|.$$

For collisions due to flow accelerations it is easy to show in near equilibrium (see Section 3.3.4) that $\phi(p, q)$ is proportional to $(p^{1/3} + q^{1/3})^2 \, |p^{2/3} - q^{2/3}|$.

To each of the above phenomena there corresponds a characteristic time, and comparison of the various times enables the predominant phenomenon in each zone of the motor to be defined. Nucleus production is almost instantaneous and quickly becomes negligible.

For condensation in the continuum, the balance equation for the condensable species is written:

$$\frac{d\rho_1}{dt} = -4\pi n_p \rho \mathcal{D} r F (\rho_\infty, \rho_{\cdots}, T_\infty) ,$$

where n_p is the number of particles per unit volume and D the binary scattering function. In the vicinity of equilibrium and for a large dilution of the condensable species, the expression of F can be simplified to:

$$F \simeq \frac{\rho_1 - \rho_{v_1}(T_\infty)}{\rho}$$

The time constant is thus:

$$\hat{\tau}_c = \frac{1}{4\pi n_p \mathcal{D} r} = \frac{r^2 \rho_\ell^2}{3\kappa \rho \mathcal{D}}$$

Marble [25] has shown that the characteristic condensation time in the molecular region is very much less than τ_c.

For agglomerations in the chamber it will be shown later that it is advisable to use a collision function of the form:

$$\phi(p,q) = \beta(p+q)$$

The number of particles is then expressed by the relation:

$$\frac{n_p}{n_{p_o}} = \exp\left(-\beta p_o t\right)$$

The time constant will thus be defined by the expression:

$$\tau_A = \frac{1}{p_o \beta}$$

For agglomerations in the nozzle due to flow acceleration, we can use the quantity already mentioned:

$$\tau_u = \frac{2r^2 \rho_o}{9\mu}$$

We see that T_c and T_u are of the same order of magnitude: condensation and two-phase disequilibrium between phases must be studied simultaneously. In the chamber T_A may be calculated for a reasonable variation in mean radius as to volume and an upper limit of T_c can be proposed; T_A is always larger than T_c, which indicates that agglomerations are always the most important phenomenon in the chamber. These characteristic times are always less than the mean dwell times in the chamber and in the nozzle, so the corresponding phenomena have time to develop.

These general considerations should enable us approach the study of the various motor zones.

3.2.2. Study of the Combustion Zone

This zone is a strongly heterogeneous medium due to the existence of condensed phases and to that of strong variations in temperature and concentrations. As far as we know there is no

theoretical model taking into account all the phenomena and in particular particle formation and growth. However we can advance some observations enabling this problem to be circumscribed.

a) Extent of Combustion Zone

The study of combustion mechanisms, that of rate of combustion for example, is carried out in chambers with observation windows (Figure 13). Near the combustion surface we observe a very bright zone whose thickness varies characteristically for metallized propellants (Figure 14). We will show that this zone corresponds to particle combustion by studying particle movement.

The flow of the combustion products is characterized by fairly substantial velocity gradients and particles under combustion whose initial diameter reaches 100 μ. As for a large number of two-phase flows, we will define a reference flow and we will study the trajectory of the particles in the calculated velocity field. In the case of a channel with a constant cross section the simplest flow corresponds to the irrotational movement of an incompressible fluid. In the plane we obtain:

$$u = v_0 \frac{x}{h} , \qquad\qquad v = -v_0 \frac{y}{h} ,$$

with the notations of Figure 14 and u_0 corresponding to the injection velocity at the wall.

Assuming that flow around particles takes place within Stokes hypotheses and that the particles burn as soon as they leave the combustion surface in an r^2 law, we can establish the differential equations giving the particle position as a function of time rather simply. Changes in variables bring these equations to Bessel equations. We can thus give solutions of the form:

Figure 13. Motor with Observation Window.
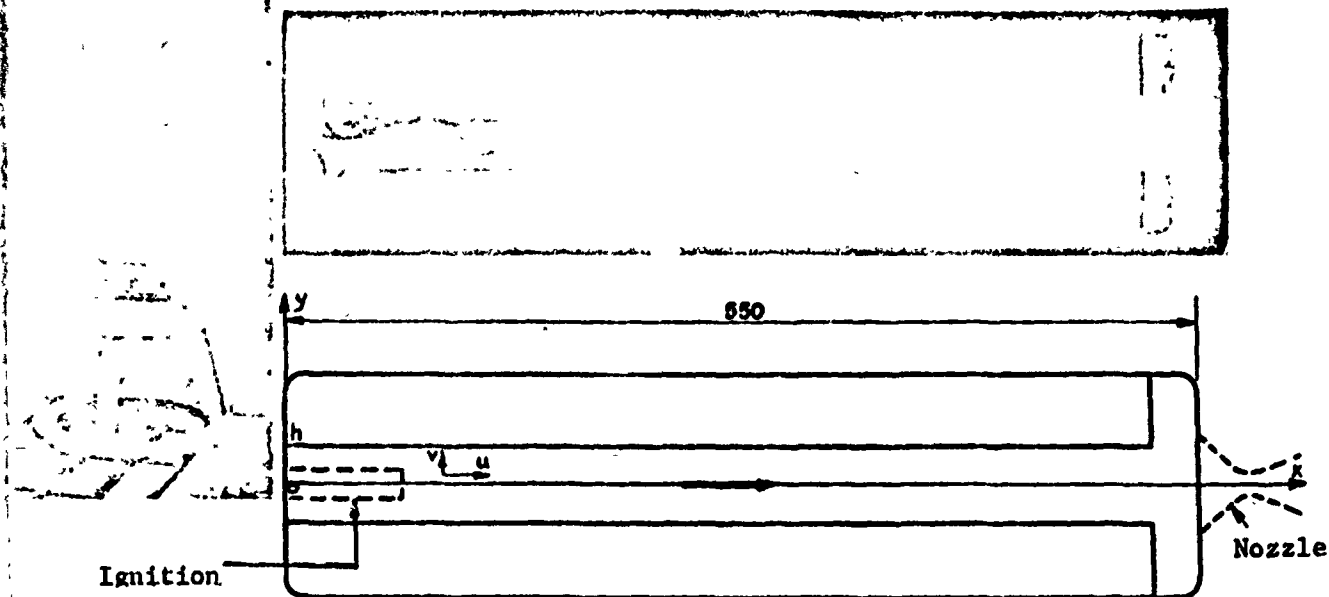
Figure 14. Diagram of Combustion Zone.

$$\frac{x_p}{x_{p_0}} = A_3^{\nu} I_{\nu}(\sqrt{b}_3) + B_3^{\nu} K_{\nu}(\sqrt{b}_3),$$

$$\frac{y_p}{h} = C_3^{\nu} J_{\nu}(\sqrt{b}_3) + D_3^{\nu} Y_{\nu}(\sqrt{b}_3),$$

where $\nu = \dfrac{1+\alpha}{\alpha}$, $b = \dfrac{4 \tau_{u_0} v_0}{h \alpha^2}$, $3^2 = 1 - \alpha \dfrac{t}{\tau_{u_0}}$,

$\alpha = R_c \dfrac{\tau_{u_0}}{d_{p_0}^2}$, $\qquad k_c$ being the combustion constant.

Taking into account the initial conditions we determine the coordinates of the point where combustion ceases:

$$\frac{x_{pf}}{x_{p_0}} = \frac{2^{\nu-1} \Gamma(\nu)}{(\sqrt{b})^{\nu-1}} I_{\nu-1}(\sqrt{b}), \quad \frac{y_{pf}}{h} = \frac{2^{\nu-1} \Gamma(\nu)}{(\sqrt{b})^{\nu-1}} J_{\nu-1}(\sqrt{b}).$$

We note that $\nu - 1$ is independent of the particle size while $\sqrt{b}$ is proportional to the initial diameter:

$$\nu - 1 = \frac{18 \mu}{R_c \rho_{Ae}},$$

$$\sqrt{b} = \frac{2}{R_c} \sqrt{\frac{v_0 \rho_{Ae}}{18 \mu h}} d_{p_0}.$$

For reasonable numerical values taken from the literature (in particular, 1.25×10^{-3} cm^2/sec $< k_c < 3.75 \times 10^{-3}$ cm^2/sec [21]), we calculate, starting from the border of the bright zone, the initial mean diameter of the particles at each point of the combustion surface. This result is plotted on Figure 15. The decrease in dp_0 with abscissa x is to be connected with the influence of flow which disintegrates the largest agglomerates. The order of magnitude of the diameter at low values of x is in good agreement with experimental observations.
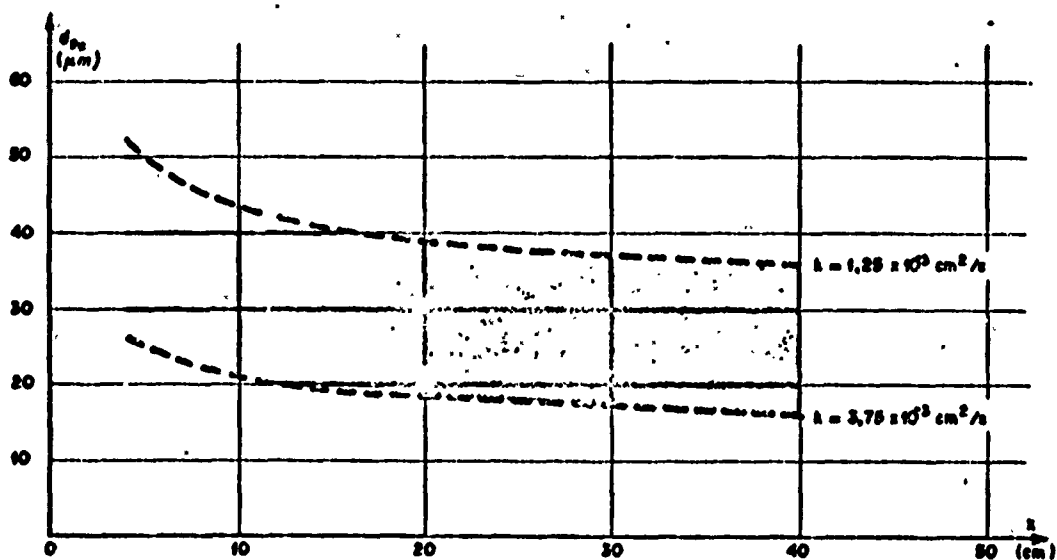
Figure 15. Mean Aluminum Particle Diameter on the Combustion Surface.

Thus, the bright zone observed is indeed the combustion zone. This zone is rather thin because of the dimensions of the motor with observation window and will be negligible with a real motor such that the initial problem comes down to that of finding out the alumina particle distribution on the combustion surface.

b) Particle Distribution

The alumina particles are formed very early in the vapor phase and their growth in the rarefied domain is very rapid such that there are no particles with diameters less than 0.01 µ. This value

fits the measurements of Caruso [26] and the results of captures at the front bottom of a motor.

The large particles come from the alumina which collects on aluminum particles in combustion. We estimated their mean diameter from photographs such as that of Figure 16a, calculating the relative volume of alumina with respect to that of aluminum.

The two liquids are assumed not to be miscible, so we write the equilibrium equation of the internal surface and of the line common to the three media as follows:

$$\frac{\sigma_{10}}{R_{10}} - \frac{\sigma_{20}}{R_{20}} + \frac{\sigma_{12}}{R_{12}} = 0 ,$$

$$\sigma_{10} \sin \alpha_{10} - \sigma_{20} \sin \alpha_{20} + \sigma_{12} \sin \alpha_{12} = 0 ,$$

$$\sigma_{10} \cos \alpha_{10} - \sigma_{20} \cos \alpha_{20} + \sigma_{12} \cos \alpha_{12} = 0 ,$$

with the notations and the internal surface concavity of Figure 16b. Eliminating T_{12} we can express the ratio R' of R_{12} to R_{10} as a function of the ratio R of R_{20} to R_{10}, the ratio T of T_{20} to T_{10}, and of angle δ:

$$R' = \frac{\sqrt{1 + \sigma^2 - 2T \cos \delta}}{\left| \frac{\sigma}{R} - 1 \right|} ,$$

V the concavity.
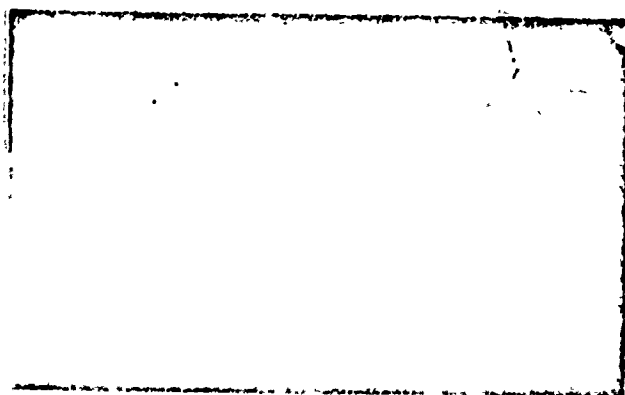
∙∙∙∙∙∙∙ surface tensions

a) shown by photograph   h) section in the plane of
                                          symmetry
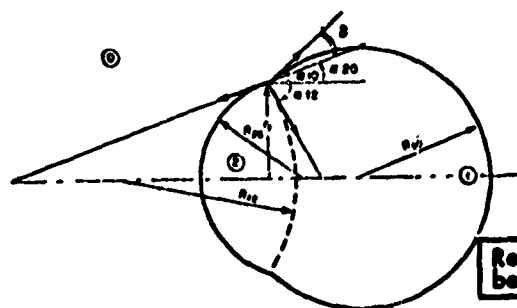
Figure 16. Alumina Cap Formed on an Aluminum Particle.

Reproduced from best available copy.

-41-

The relative volume for which we are seeking is determined in a purely geometric manner:

$$\mathcal{V} = \frac{\left(R - \sqrt{R^2 - r^2}\right)^2 \left(2R + \sqrt{R^2 - r^2}\right) \pm \left(R' - \sqrt{R'^2 - r^2}\right)^2 \left(2R' + \sqrt{R'^2 - r^2}\right)}{\left(1 + \sqrt{1 - r^2}\right)^2 \left(2 - \sqrt{1 - r^2}\right) \mp \left(R' - \sqrt{R'^2 - r^2}\right)^2 \left(2R' + \sqrt{R'^2 - r^2}\right)},$$

avec $\quad r = \dfrac{r_c}{R_{10}}$.

For the same exterior geometry, u depends on the ratio τ of the surface tensions. At high temperatures these characteristics are poorly known; for liquid alumina we find a value close of 650 dynes/cm and for aluminum 840 dynes/cm at 700°C. These data lead us to taking a τ/R near to 1. To simplify, we will assume that R' is infinite such that the expression of u is simplified.

The computer calculation, made for probable density values which are also poorly known at high temperatures, enables us to suggest:

- that the large particles have mean diameters between 8 and 16 μ,

- that they represent a mass fraction of the condensed phase of about 4%.

3.3.3. Evolution of Particles in the Combustion Chamber

Contrary to the case with the combustion zone, a number of articles have been written on the chamber. The hypotheses of Fein [27] are very much simplified: flow in sections, continuous condensation, growth law with r. The analysis of Jenkins and Hoglund [24] is a finer one except with regard to the flow pattern, and uses an initial distribution which is somewhat unrepresentative of the actual phenomenon. We re-performed this analysis in the light of the information in the preceding paragraph; in particular we considered two-dimensional flow (cylindrical channel) which enables us to better define the distribution in space

of the condensed phase, and we assume that the particles fall into two classes.

a) Two-Phase Aspect of Flow

The velocity field is now:

$$v_{\delta} = 2v_0 \frac{\delta}{R} \,,$$

$$v_r = -v_0 \frac{r}{R} \,.$$

The reduced movement equations of a particle of constant diameter are

$$\begin{cases} \dfrac{d^2x}{d\tau^2} + \dfrac{dx}{d\tau} - 2Ix = 0 \,, \\[2mm] \dfrac{d^2y}{d\tau^2} + \dfrac{dy}{d\tau} + Iy = 0 \,, \\[2mm] \text{avec}: \quad \tau = 0, \quad x = y = 1, \quad \dfrac{dx}{d\tau} = 2I, \quad \dfrac{dy}{d\tau} = -I, \\[2mm] \qquad I = \dfrac{\tau_0 v_0}{R} \,. \end{cases}$$

These equations are easily integrated to give:

$$\frac{x_p}{x_{p_0}} = \frac{\alpha + (1 + 4I)}{2\alpha} e^{-\frac{\alpha-1}{2}\tau} + \frac{\alpha - (1 + 4I)}{2\alpha} e^{-\frac{\alpha+1}{2}\tau} \,,$$

$$\frac{y_p}{R} = \frac{\beta + (1 - 2I)}{2\beta} e^{-\frac{1-\beta}{2}\tau} + \frac{\beta - (1 - 2I)}{2\beta} e^{-\frac{1+\beta}{2}\tau} \,,$$

$$\text{où} \quad \alpha = \sqrt{1 + 8I} \,,$$

$$\beta = \sqrt{1 - 4I} \,.$$

Even for large particles, I is always very much less than 1. Developing the above expression in the neighborhood of I = 0, we find the movement of a fluid particle to the nearest second order.

We can thus say that the small particles perfectly follow the streamlines of the gaseous phase while the large ones deviate from it but little. Segregation of the condensed phase in the combustion products flow is negligible; however, for more complex geometries (machined blocks, one-piece nozzle) this effect could be more marked locally.

Since the characteristic condensation is of the same order as that characterizing velocity disequilibrium, we deduce that condensation is practically terminated in the combustion zone. We also know that compressibility effects are small in the chamber; the Mach number is usually less than 0.2 while higher velocities modify the rate of combustion of the propellant grain (erosion).

We can thus assume that the density of the condensed phase is constant in the chamber. The problem thus comes down to studying the agglomeration of particles in each streamline.

In the absence of experimental information on particle distribution at the combustion zone outlet, we will assume it can be represented analytically, as a function of mass, by the expression:

$$f_o(m) = A \delta(m - m_1) + B \delta(m - m_2),$$

where δ is the Dirac function, m_1 and m_2 are the masses of the small and large particles $(m_2 \gg m_1)$ and A and B the numerical fraction of each class of particles $(A \gg B, A + B = 1$ if the law is normalized).

b) Particle Growth Pattern

Let $f(m, t)$ be the normalized particle distribution law according to mass and π_p the number of particles per unit volume. The frequency of collisions between particles of classes $(p, p + dp)$ and $(q, q + dq)$ is written:

$$n_p^2 \, f(p,t) \, f(q,t) \, \phi(p,q) \, dp \, dq .$$

The balance of particles in class $(m, m + dm)$ can be written by the equation:

$$\frac{\partial}{\partial t}\left(n_p \, f(m,t) \, dm \right) = \frac{n_p^2}{2} \int_{p+q=m} f(p,t) \, f(q,t) \, \phi(p,q) \, dp \, dq$$

$$- n_p^2 \int_{p=0}^{\infty} f(m,t) \, f(p,t) \, \phi(m,p) \, dp \, dm .$$

-44-

The first term of the second member represents the number of particles formed at binary collisions, coefficient 1/2 resulting from p and q symmetry.

The corresponding integral can be rewritten:

$$\int_0^m f(p,t)\, f(m-p,t)\, \phi(p,m-p)\, dp\, dm .$$

We see immediately how useful it is to use the collision function form proposed by Golovin to simplify this production term:

$$\phi(p,q) \simeq \beta(p,q) .$$

Accordingly:

$$\frac{\partial}{\partial t}\left(n_p \cdot f(m,t)\right) = n_p^2 \frac{\beta m}{2} \int_0^m f(p,t)\, f(m-p,t)\, dp$$
$$- n_p^2 \beta f(m,t)\left[\int_0^\infty p\, f(p,t)\, dp + m\right] ;$$

hence, by integration:

$$\frac{dn_p}{dt} = -n_p^2 \beta \int_0^\infty p\, f(p,t)\, dp .$$

Now, we know that the density of the condensed phase is constant:

$$\rho_p = n_p \int_0^\infty p\, f(p,t)\, dp = C^{te} .$$

From the last two equations we immediately get:

$$\frac{n_p}{n_{p_0}} = \exp\left(-\beta \rho_p t\right).$$

The mean mass of the particles is given by:

$$\bar{m} = \frac{\rho_p}{n_{p_0}}\exp\left(\beta \rho_p t\right).$$

Calculations can be continued when all binary collisions are characterized by the same factor ß [19]. However, as there are two classes of particles with very different diameters, collisions probably do not come about by the same mechanism.

As the small particles are characterized by index 1 and the large particles by index 2 we must define three collision functions:

-15-

- ϕ_{11} (p, q), for small-particle collisions. We will take;

- ϕ_{22}(p,q), for large-particle collisions. Due to their very small number and their inertia the frequency of such collisions is very slight and the phenomenon can be neglected.

- ϕ_{12}(p,q), for mixed collisions. A new parameter β' is defined by the relation:

$$\phi_{12}(p,q) = \beta'(p+q) \simeq \beta'p,$$

p being the mass of the large particles (p/q >> 1).

The equation of the balance for small particles is written:

$$\frac{\partial}{\partial t}\left(n_{P_1} f_1\right) = \frac{\beta n_{P_1}^2}{2} m \int_0^m f_1(p,t) f_1(m-p,t)\,dp$$
$$- \beta n_{P_1}^2 f_1(m,t)\left[m + \int_0^\infty p\, f_1(p,t)\,dp\right]$$
$$- \beta' n_{P_1} n_{P_2} f_1(m,t) \int_0^\infty p\, f_2(p,t)\,dp.$$

We deduce from this equation:

$$\frac{d n_{P_1}}{d t} = -\beta n_{P_1}^2 \int_0^\infty p\, f_1(p,t)\,dp - \beta' n_{P_1} n_{P_2} \int_0^\infty p\, f_2(p,t)\,dp,$$

and $\quad \frac{\partial f_1}{\partial t} = \frac{\beta n_{P_1}}{2} m \int_0^m f_1(p,t) f_1(m-p,t)\,dp - \beta n_{P_1} m\, f_1(m,t).$

Writing:
$$\frac{d\mathfrak{z}}{dt} = -\beta n_{P_1},$$

we obtain for f_1 an equation identical in form to that for a single class of particles ($\zeta = 1/\overline{m}$):

$$\frac{\partial f_1}{\partial \mathfrak{z}} + \frac{m}{2} \int_0^m f_1(p,\mathfrak{z}) f_1(m-p,\mathfrak{z})\,dp - m\, f_1(m,\mathfrak{z}) = 0.$$

This intego-differential equation must be integrated, taking into account the initial condition:

$$f_{10}(m) = \delta(m-m_{10}).$$

We have shown that the exact solution is:

$$F_i(x, z) = \sum_{i=1}^{\infty} \frac{i^{i-1}}{i!} z^{i-1} e^{-iz} \delta(x-1) ,$$

with
$$x = \frac{m}{m_{10}} ,$$
$$z = m_{10}(\mathfrak{z}_0 - \mathfrak{z}) .$$

When t increases this distribution tends to a limit form which, for $m \gg m_{10}$ corresponds to:

$$F_1\left(\frac{m}{m_{10}}, z\right) \simeq \frac{1}{\sqrt{2\pi}} \left(\frac{m_{10}}{m}\right)^{\frac{3}{2}} .$$

This is a decreasing law.

The large particles are constant in number and uniform in diameter such that the equation of the balance is written:

$$n_{P_2} \frac{dm_2}{dt} = \beta' n_{P_1} n_{P_2} m_2 \int_0^{\infty} P F_1(P, t) dP ,$$

or
$$\frac{dm_2}{dt} = \beta' n_{P_1} m_2 \overline{m_1} .$$

Using the fact that the density of the condensed phase is constant, we come out with a system of differential equations:

$$\left\{
\begin{array}{l}
\dfrac{dz}{dt} = \beta n_{P_1} m_{10} , \\[2mm]
\dfrac{dn_{P_1}}{dt} = -\beta n_{P_1} \rho_P + (\beta - \beta') n_{P_1} n_{\theta_0} m_2 , \\[2mm]
\dfrac{dm_2}{dt} = \beta' m_2 (\rho_P - n_{P_{20}} m_2) , \\[2mm]
\text{with} \quad t = 0 : \quad z = 0 , \quad n_{P_1} = n_{P_0} , \quad m_2 = m_{20} , \\[2mm]
\text{and} \quad \overline{m_1} = \dfrac{\rho_P - n_{P_{20}} m_2}{n_{P_1}} .
\end{array}
\right.$$

These equations can be integrated analytically. We have shown:

- reduced time: $\quad \tau = \dfrac{v_0 t}{R} ,$

- reduced collision parameters:

$$\delta = \frac{\beta \rho_P R}{v_0} ; \quad \delta' = \frac{\beta' \rho_P R}{v_0} , \quad \varepsilon = \frac{\delta'}{\delta} = \frac{\beta'}{\beta} ,$$

- the mass fraction of the large particles α $(\alpha(0) = \alpha_0)$,

- the numbers N_1 and N_2 of the particles of each class brought down to their initial values.

We find finally:

$$
\begin{cases}
\alpha = \dfrac{\alpha_0}{\alpha_0 + (1-\alpha_0)\exp(-\delta'\tau)}, \\[2mm]
Z = 1 - \left(\dfrac{\alpha}{\alpha_0}\right)^{-\varepsilon}, \\[2mm]
N_1 = \dfrac{1-\alpha}{1-\alpha_0}\left(\dfrac{\alpha}{\alpha_0}\right)^{-\varepsilon}, \quad N_2 = 1, \\[2mm]
\dfrac{\overline{m_1}}{m_{10}} = \left(\dfrac{\alpha}{\alpha_0}\right)^{\varepsilon}, \quad \dfrac{\overline{m_2}}{m_{20}} = \dfrac{\alpha}{\alpha_0}.
\end{cases}
$$

To eliminate the time, we need only take the equations of motion of a fluid particle. It is easy to see that:

$$
\exp(-\delta'\tau) = \left(\frac{r}{R}\right)^{\delta'},
$$

where R is the radius of the cylindrical channel and r the distance between the axis and the point considered in the terminal section of the grain.

The simplest result relates to the mass fraction α of the large particles:

$$
\frac{\alpha}{\alpha_0} = \left[\alpha_0 + (1-\alpha_0)\left(\frac{r}{R}\right)^{\delta'}\right]^{-1}
$$

α is larger at the center of flow than at the periphery, since the dwell time in the chamber is longer in the first case than in the second.

The average value of α is given by: $\overline{\alpha} = \dfrac{1}{\pi R^2}\displaystyle\int_0^R \alpha(r)\, 2\pi r\, dr$.

for $\delta' \ll 1$, we get: $\overline{\alpha}/\alpha_0 = 1 + (1 - \alpha_0)(\delta'/2)$.

In the absence of data on the value of δ', we sought for an order of magnitude assuming that a longitudinal harmonic acoustic field was superimposed on the average velocity field and that the differential response of the small and large particles is the cause of the collisions.

The equation containing x for for motion of a particle is written:

$$\frac{d^2 x_p}{dt^2} + \frac{1}{\tau_u}\frac{d x_p}{dt} - \frac{2 v_c}{R \tau_u} x_p = \frac{U}{\tau_u}\sin\omega t ,$$

with $\quad t = 0, \quad x_p = x_{p_0}, \quad \frac{dx}{dt} = 0 ,$

and U, amplitude of acoustic velocity.

This equation can be integrated analytically. The difference in instant velocity is at the origin of the collisions. The expression for this difference can be established by noting that the small particles almost perfectly follow the motion of the gas:

$$\Delta u_p = |u_{p_2} - u_{p_1}| = U \sin\psi_2 \, |\cos(\omega t - \psi_2)| ,$$

with $\quad tg\,\psi_2 = \omega \tau_{u_2} ,$

or, on the average:

$$\overline{\Delta u_p} = \frac{2}{\pi} U \frac{\omega \tau_{u_2}}{\sqrt{1 + (\omega \tau_{u_2})^2}} .$$

The collision cross section is πr_2^2. Elementary reasoning easily leads to:

$$\delta' \simeq \frac{3}{2\pi} \cdot \frac{U R \rho_p}{v_0 \, r_2 \, \rho_c} \cdot \frac{\omega \tau_{u_2}}{\sqrt{1 + (\omega \tau_{u_2})^2}}$$

Computer application for acoustic intensity values and the reference frequency [24] and our experimental data gives $\delta' = 0.06$. This value leads us to suppose that the diameters of the large particles vary little on the average if the acoustics are assumed to be responsible for the collisions.

-49-

The role played by turbulent scattering still remains to be defined. The value proposed by Jenkins and Hoglund leads to a value β on the order of 10^5 and a considerably overestimated value for the increase in the mean mass of the small particles.

c) Conclusions

By reason of the uncertainties remaining as to the numerical coefficients of the collision functions, the results are still only qualitative in nature. Despite this restriction, the calculation method proposed shows that the condensed phase remains homogeneously distributed in the flow, that the distribution of small particles tends to a decreasing law, and that the large particles tend to develop in the center of the flow. We may expect a more marked particle growth as the scale of the motor increases such that the average dwell time in the chamber increases. For this method to be improved a finer study has to be made of particle behavior in real flow, requiring local particle size measurement techniques to be developed.

3.3.4. Evolution of Particles in the Nozzle.

The nozzle problem is the most important from the viewpoint of specific impulse losses due to the two-phase disequilibrium due to flow acceleration.

We assume that the characteristics of the condensed phase in the nozzle inlet section are known either by computation or by measurement. Determination of these characteristics from the preceding results is not always immediate. We have to note that between the terminal grain section and the nozzle inlet section is a connection zone whose influence can be substantial; this is the case when evolution of the section is very rapid or when vortices develop. Nozzle integration also leads to complications. This aspect of the problem, which depends on the chosen geometric configuration, will

be left aside; we can however state that from the condensed phase viewpoint alone it is always appropriate to avoid zones with sharp velocity gradients.

The study of the flow of combustion products in the nozzle is extremely complex in its general form. We will only note here that two-dimensional effects are difficult to take into account even for expansion of an ideal gas due to the existence of the transonic zone. Most proposed patterns take the hypothesis of sectional flow and do not take into account segregation of the condensed phase in the flow, which must be studied separately.

a) Role of Condensation in Particle Growth

The same mechanisms act together to create particle growth in the chamber and the nozzle. We can, however, look for the preponderant mechanism.

We still assume that condensation, which will take place due to displacement of chemical equilibria due to temperature and pressure drops, occurs almost instantaneously (local thermodynamic equilibrium) and according to an r^2 law. An elementary calculation was made to find the effect of this phenomenon alone on the condensed mean radius.

The rate of growth can be characterized by the variation in the minimum radius r_1 or by the fraction R defined by the relation:

$$R^2 = r_1^2 - r_{10}^2$$

Considering the particle distribution function according to the radius, $f(r, t)$, we establish the equation:

$$\frac{\partial f}{\partial t} + \dot{r} \frac{\partial f}{\partial r} + \frac{\partial \dot{r}}{\partial r} f = \sigma$$

-51-

Solving for $\overset{\circ}{r}$, we get:

$$\frac{\partial}{\partial R^2}\left(\frac{f}{r}\right) + \frac{\partial}{\partial r^2}\left(\frac{f}{r}\right) = 0 \,,$$

or

$$f(r,t) = r\, F(r^2 - R^2) \,.$$

The function F is determined from the initial particle distribution:

$$f(r,t) = \frac{r\, f_0(\sqrt{r^2 - R^2})}{\sqrt{r^2 - R^2}} \,.$$

The various moments of the distribution law come in the form:

$$r_{no}^n = \int_0^\infty (r^2 + R^2)^{\frac{n}{2}} f_0(r)\, dr \,.$$

The function $R^2(r)$ is obtained by establishing the condensed phase balance, its density ρ_p being known at each point by thermodynamic calculation. We get:

$$\frac{\int_0^\infty (r^2 + R^2)^{\frac{3}{2}} f_0(r)\, dr}{\int_0^\infty r^3 f_0(r)\, dr} = \frac{\frac{\rho_c}{\rho_{p_0}} - \alpha}{1 - \alpha_e} \,.$$

To simplify calculation we chose for $f_0(r)$ the decreasing exponential law which has the same shape as the small particle theoretical distribution law:

$$f_0(r) = \frac{1}{r_m} e^{-\frac{r}{r_m}} \qquad (r_{io} = 0) \,.$$

Defining a function $I_n(z)$ by the relation:

$$I_n(z) = \int_0^\infty (v^2 + z^2)^{\frac{n}{2}} e^{-v}\, dv \,,$$

we get finally:

$$I_3\left(\frac{R}{r_m}\right) = 6 \frac{\frac{\rho_c}{\rho_{i_0}} - \alpha_0}{1 - \alpha_0} \,,$$

$$\frac{r_{no}}{(r_{no})_0} = \left[\frac{I_n\left(\frac{R}{r_m}\right)}{n!}\right]^{\frac{1}{n}} \,.$$

Calculation shows that condensation occurs principally on the smallest particles and that high-order moments are little affected by this. As these moments are the most important ones in practice, condensation appears here to be a second-order phenomenon which can be left out in the first approximation. This result is corroborated by more complete calculation [24] which also show that the acoustic effect is negligible. The only collisions to be taken into account in the nozzle are thus those resulting from differential entrainment by the gaseous phase.

b)   Particle Growth Pattern in the Nozzle [20]

We study binary collisions between particles in a permanent sectional flow. We generally assume that two particles encountering one another agglomerate instantaneously and definitively.

The condensed phase is described locally by the distribution law according to the radius we will define here, and normalized: $f(r, x)$, and the velocities and mean temperatures of particles with the same radius: $u_p(r, x)$ and $T_p(r, x)$.

Since collisions are due to differences in average velocities the collision function is expressed simply; the collision frequency between particles of classes $(a, a + da)$ and $(b, b + db)$ is written:

$$\pi (a+b)^2 n_p^2 f(a,x) f(b,x) |u_p(a,x) - u_p(b,x)| \, da \, db ,$$

and these collisions create particles with radius $(a^3 + b^3)^{1/3}$.

A balance made for particles of one and the same class leads to the equation:

$$\frac{\partial f}{\partial x} = \pi n_p \left[\frac{-f I_1 + r^2 I_2}{u_p} - f \int_o^\infty \frac{-f I_1 + r^2 I_2}{u_p} dr \right] .$$

The terms I_1 and I_2 corresponding to disappearance of particles in collisions and formation of new particles are given by the expressions:

$$I_1(r,x) = \int_0^\infty (r+a)^2 \, f(a,x) \, \left| u_p(r,x) - u_p(a,x) \right| \, da \, ,$$

$$I_2(r,x) = \frac{1}{2} \int_0^r \left[a + (r^2 - a^2)^{\frac{1}{2}} \right]^2 \, f(a,x) \, f((r^2-a^2)^{\frac{1}{2}}, x) \, \frac{\left| u_p(a,x) - u_p((r^2-a^2)^{\frac{1}{2}}, x) \right|}{(r^2 - a^2)^{\frac{1}{2}}} \, da \, .$$

Evolution of the condensed phase is linked, through the inter-mediary of particle velocities, to gaseous phase flow. Computer calculations can take this coupling into account; the distribution function is made discrete and a differential equation is set up for each class of particles [28, 29, 30]. These calculations require a great deal of computer time; they show that pressure, nozzle scale, condensed mass fraction, and initial distribution have a great impact on the final distribution. Moreover, the imperfect collision yield seems to be an important phenomenon [30].

Rather than developing this type of calculation we looked to see whether, by an analytical route, the problem could be uncoupled from the flow problem. The simplification used is that of the near equilibrium [31] and results from the following considerations: if the particle velocity relaxation constant, τ_u, is much smaller than the dwell time of the combustion particles in the nozzle, in the first approximation the particle velocity can be determined as a function of local gaseous phase flow characteristics, and is itself very close to two-phase equilibrium flow of the combustion products (index (o)) which is well known (thermodynamic calculation).

With this hypothesis we get:

$$u_p(r,x) = u^{(o)} - \tau_u(r) \cdot u^{(o)} \frac{du^{(o)}}{dx} \, ,$$

provided that:

$$\tau_u \left| \frac{du^{(o)}}{dx} \right| \ll 1 \, .$$

This inequality is verified in most practical cases for the majority of particles. Only the large particles ($d_p > 10 \, \mu$) do not permit such an approximation and require separate treatment. The actual flow pattern around the particles can also have non-trivial importance.

Assuming that the u_p expression is valid for all particles, the collision frequency is proportional to the difference of the squares of the radii.

The distribution function can be defined by its different moments.

The equation for moment of order n, r_{no}, is written:

$$\frac{dr_{no}^n}{dx} = \frac{K\dot{m}}{\frac{8}{3}\rho_c A u^{(t)^2} r_{30}^3}\left[\iint_D (y+z)^2 f(y,x) f(z,x)\left|u_p(y,x)-u_p(z,x)\right| \times \right.$$
$$\times \left[(y^3+z^3)^{\frac{n}{3}}-(y^n+z^n)\right] dy\,dz$$
$$\left. + r_{no}^n \iint_D (y+z)^2 f(y,x) f(z,x)\left|u_p(y,x)-u_p(z,x)\right| dy\,dz\right],$$

where K represents the ratio between the condensed phase mass flow and the gaseous phase mass flow, $\dot{m}$ the total mass flow, and A the straight section of the nozzle. The domain D is the first quadrant in the plane (y, z). The near equilibrium hypothesis simplifies this relation:

$$\frac{dr_{no}^n}{dx} = \frac{K\dot{m}\frac{du^{(t)}}{dx}}{6 A \mu u^{(t)} r_{30}^3}\left[\iint_{D'} (y+z)^2 (y^2-z^2)\left[(y^3+z^3)^{\frac{n}{3}}-(y^n+z^n)\right] f(y,x) f(z,x) dy\,dz \right.$$
$$\left. + r_{no}^n \iint_{D'} (y+z)^2 (y^2-z^2) f(y,x) f(z,x) dy\,dz\right].$$

The domain D' is now between the y axis and the first bisector. To continue the calculation we must give an analytical expression for f(y, x) and f(z, x). We chose the form:

$$f(r,x) = \frac{a^{b+1}}{\Gamma(b+1)} r^b e^{-ar}, \quad a>0, \quad b>-1.$$

Taking b = 0, i.e., the decreasing exponential law, we find the mean radius expression proposed by Marble [31]. This one-parameter approximation is, however, insufficient to describe the agglomeration [20]. We assume in the expression of f(r, x) that a and b vary with x. It is useful to relate a and b to more physical characteristics. We find without difficulty:

$$r_m = \frac{b+1}{a} \qquad (= r_{10}, \text{ mean radius in number}),$$

$$\sigma^2 = \frac{b+1}{a^2} \qquad (\text{root mean square}).$$

We keep b and substitute the variable r_m for a:

$$f(r,x) = \frac{1}{r_m} \cdot \frac{(b+1)^{b+1}}{\Gamma(b+1)} \left(\frac{r}{r_m}\right)^b e^{-(b+1)\frac{r}{r_m}} .$$

We chose to utilize the first moments to define the distribution law. We can show an auxiliary variable characterizing the evolution in the section:

$$z = \frac{1}{6} \frac{K \overset{\circ}{m} r_{m_0}}{A_c/\mu} \int_0^x \frac{A_c}{A} \frac{1}{\mu^{(c)}} \frac{d\mu^{(c)}}{dx} dx .$$

z does not depend on the nozzle geometry but only on the straight section.

Replacing f by its expression as a function of b and r/r_m then coming back to a and b we find:

$$\frac{da}{dz} = \frac{a_o}{b_o+1}(b+1) \left[(2b+3) J_1(b) - (b+1) J_2(b) \right],$$

$$\frac{db}{dz} = \frac{a_o}{b_o+1} \frac{(b+1)^2}{a} \left[(2b+4) J_1(b) - (b+1) J_2(b) \right],$$

with:

$$J_1(b) = \frac{(b+1)^{2b+5}}{\Gamma(b+1)\Gamma(b+4)} \iint_{D'} (Y+Z)^2 (Y^2-Z^2) Y^b Z^b \times$$
$$\times \left[(Y^3+Z^3)^{\frac{1}{3}} - (Y+Z) + 1 \right] dYdZ,$$

$$J_2(b) = \frac{(b+1)^{2b+5}}{\Gamma(b-1)\Gamma(b+4)} \iint_{D'} (Y+Z)^2 (Y^2-Z^2) Y^b Z^b \times$$
$$\times \left[(Y^3+Z^3)^{\frac{2}{3}} - (Y^2+Z^2) + b+2 \right] dYdZ.$$

The differential equations can be integrated and give:

$$z - z_o = \frac{b+1}{L(b_o)} \left[M(b) - M(b_o) \right],$$

$$\frac{r_m}{r_{m_o}} = \frac{b+1}{b_o+1} \times \frac{L(b_o)}{L(b)},$$

$$\frac{\sigma^2}{r_m^2} = \frac{b_o+1}{b+1},$$

-56-

with:

$$L(b) = \exp\left[\int_0^b \frac{(2b+3)J_1 - (b+1)J_2}{(2b+4)J_1 - (b+1)J_2} \cdot \frac{db}{b+1} \right],$$

$$M(b) = \int_0^b \frac{L(b)}{(2b+4)J_1 - (b+1)J_2} \cdot \frac{db}{(b+1)^2}.$$

Computation of J_1 and J_2 is analytical except for expressions of the form:

$$I = \int_0^1 t^b \left(1 - \frac{3}{4}t\right)^{\frac{n}{3}} dt \qquad (n = 1 \text{ ou } 2),$$

which are calculated by means of a development. Thus the initial problem has been brought down to a series of quadratures.

Computer application was done on a biconical nozzle. The initial particle distribution is the decreasing exponential law ($b_0 = 0$). For simplification we chose:

$$\frac{K p_0 r_m}{c^* \mu} = 1$$

Figure 17 gives the variation in the various mean radii ralated to their nozzle inlet value and to the relative spread of the particles along the abscissa. The following comments can be made:

α> The mean radius in number tends to decrease, which can be justified analytically: the collisions disperse the particles toward the small and large radii.

β> High-order mean radii increase rapidly in the throat region independently of nozzle geometry. This result disagrees with the calculations of Crowe and Willoughby [28] which indicate that the converging section is a privileged agglomeration region and that the geometry has a noteworthy influence. However these effects have not been demonstrated by other investigators [29, 30].

γ> Particle growth is moderate in the diverging section and practically negligible when the particles begin to solidify with a section ratio on the order of 3.

Despite the orders of magnitude obtained which can be considered satisfactory when compared to the experimental results (Paragraph 3.2.4.2.) this calculation method furnishes only a qualitative approach to the problem and should be improved with regard to the following points: representation of the particle population in the nozzle inlet section (bimodal law), collision yield, and expression of the velocity difference between particles. Whatever the case may be, the primordial importance of the particle agglomeration phenomenon seems clearly demonstrated.
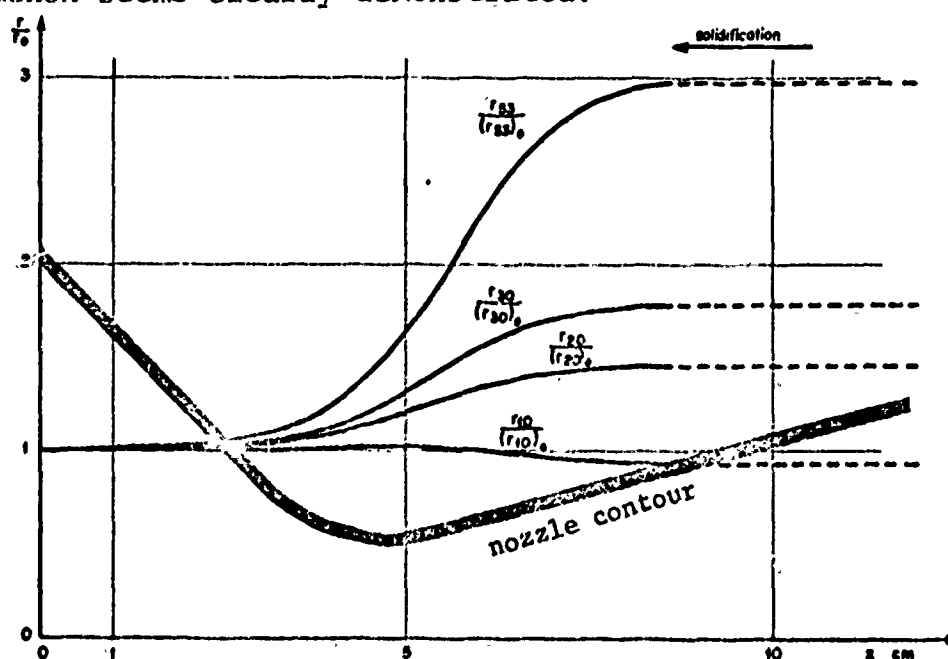
Figure 17.   Particle Growth in Nozzle.

c)   Spatial Distribution of the Condensed Phase in the Flow

The particle drag is also manifested in the flow perpendicularly to the nozzle axis and we often observe in the outlet section that the jet central zone is far brighter than the peripheral zone (Figure 18) which would suggest that the condensed phase tends to

group around the center of the jet. The study of this phenomenon requires a two-dimensional description of flow. We know that the transverse velocity gradients are much greater in the throat region, i.e., the transonic zone. Analysis of two-phase flow in the transsonic zone is a difficult problem which has not been tackled as a whole (collisions, particle growth); only Regan, Thompson and Hoglund [32] treated this problem on the computer for particles of uniform and constant diameter.
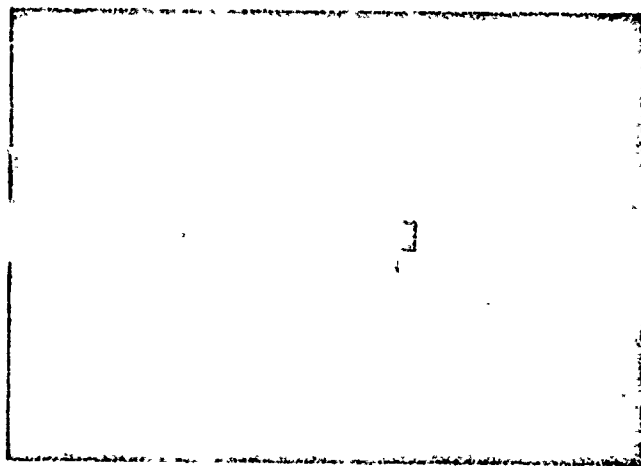
Figure 18. Segregation of Condensed Phase in Flow (Motor with Observation Window).

A calculation method was developed to give an approximate representation of the phenomenon. To give an account of two-dimensional flow effects we used a system of natural curvilinear coordinates in each nozzle zone (Figure 19): spherical system for converging section (conical), toric spherical system for the throat (with constant radius of curvature), spherical or toric spherical system for the diverging section (conical or "egg-cup" shape). Only the throat is examined here and particle motion is deduced by a perturbation method; the reference flow corresponds to two-phase equilibrium; the streamlines here are ζ = Cte lines and the velocity depends only on ψ (which means that the sound barrier in this case is the plane of the throat and the approximation has greater validity according as the ratio between the throat radius of curvature and the throat radius is large).

$$\frac{R_i}{r_c} = 2$$
$$\alpha = 15°$$
$$\beta = 45°$$
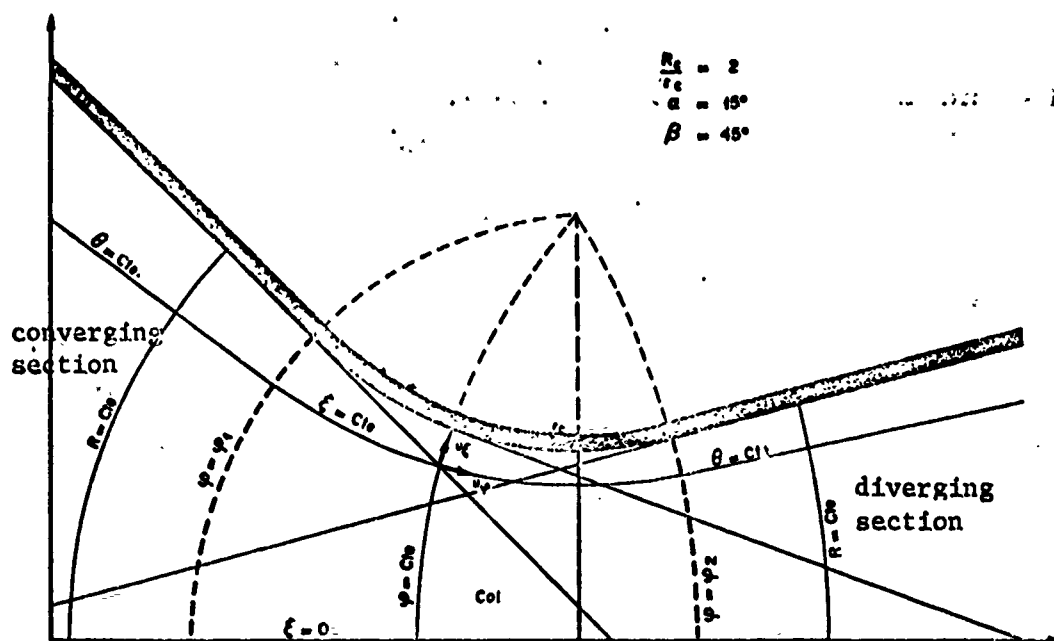
Figure 19. Systems of Coordinates for Studying Two-
-Dimensional Phenomena in the Nozzle.

Motion of a particle in the reference velocity field is described
by the equations:

$$
\begin{cases}
du_\varphi = u_\zeta \left(\frac{\sin\varphi}{a} u_\zeta + \frac{sh\zeta}{a} u_\varphi \right) + \frac{v(\varphi) - u_\varphi}{I}, \\
\frac{du_\zeta}{dr} = -u_\varphi \left(\frac{\sin\varphi}{a} u_\zeta + \frac{sh\zeta}{a} u_\varphi \right) - \frac{u_\zeta}{I},
\end{cases}
$$

where $a = \sqrt{1 + 2\dfrac{Rc}{rc}}$

and $I = \dfrac{\tau_u U_1}{rc}$, inertia parameter based on the maximum velocity and
the throat radius.

We write:
$$u_\varphi = v(\varphi) + I u_\varphi^{(1)} + \ldots$$
$$u_\zeta = \qquad I u_\zeta^{(1)} + \ldots$$

We get immediately:
$$u_\varphi^{(1)} = -\frac{dv}{d\varphi},$$
$$u_\zeta^{(1)} = -\frac{sh\zeta}{a} v^x.$$

-60-

Here we are only interested in the lateral phase shift due to use u_γ. The position of a particle is noted by ψ and γ, so we establish the equation:

or

$$\frac{d\gamma}{\mathrm{sh}\,\gamma} = -\frac{I}{a}\,v(\varphi)\,dv\,,$$

$$\mathrm{Log}\,\frac{\mathrm{th}\,\frac{\gamma_2}{2}}{\mathrm{th}\,\frac{\gamma_2}{2}} = \frac{I}{a}\int_{\varphi_1}^{\varphi_e}v\,d\varphi\,.$$

For the numerical values we have taken we find the relation between positions γ_1 and γ_2 in the throat inlet and outlet sections of a particle whose diameter is denoted by I:

$$\gamma_2 - \gamma_1 \simeq -0.0045\,I\,\mathrm{sh}\,\gamma_1\,.$$

This formula shows that the largest particles tend to approach the nozzle axis and enables the limit position of a particle of given size ($\gamma_1 = \gamma_p$) to be defined in the section.

The spatial distribution of the condensed phase in the flow is described by the density ρ_p of the condensed phase. To calculate ρ_p we can start from the continuum equation:

$$\mathrm{div}\,\rho_p\,\vec{u}_p = 0\,.$$

We will also write:

$$\rho_p = \rho_p^{(0)} + I\rho_p^{(1)} + \dots$$

We will assume, to simplify uniform spatial distribution in the inlet section 1: $\rho_p^{(0)}(\psi_1)$ is independent of γ. The terms of order 0 lead to:

$$\frac{\rho_p^{(0)}(\varphi,\gamma)}{\rho_p^{(0)}(\varphi,0)} = \left(\frac{\mathrm{ch}\,\gamma + \cos\varphi}{\mathrm{ch}\,\gamma + \cos\varphi_1} \times \frac{1+\cos\varphi_1}{1+\cos\varphi}\right)^2\,.$$

This relation indicates that even in the absence of two-phase effects the density is greater at the center of flow than at the periphery.

-61-

This result has good agreement with what we know of the trans-sonic zone.

The terms of order I lead us, for particles of uniform diameter, to the relation:

$$\frac{I\rho_r^{(4)}}{\rho_P^{(e)}} = \frac{2I}{a} \frac{1+ch\zeta\cos\psi_1}{ch\zeta+\cos\psi_1} \int_{\psi_1}^{\psi} v\,d\psi .$$

Thus, for example, we have on the jet axis:

$$\left(\frac{\rho_P}{\rho_P^{(e)}}\right)_{\zeta=0} = 1 + 0{,}0090\,I .$$

The two-phase effects thus contribute to increasing the density of the condensed phase at the center of flow.

These calculations can be extended to an initial particle distribution $f_1(r, \zeta)$ (collisions left out of account). The density of particles with radius r is, at one point:

if $0 \leq \zeta \leq \zeta_L$
and $d\rho_p = 0$, if $\zeta_L \leq \zeta \leq \zeta_p$,
where ζ_L is the limit position of a particle.

At each point (ψ, ζ) we can conversely assign an upper limit value of radius r_L, such that the density is written:

$$\frac{\rho_r}{\rho_P^{(e)}} = \frac{\int_0^{r_L(\psi\zeta)} r^3 f_1(r,\zeta)\left(1+\frac{2I}{a}\frac{1+ch\zeta\cos\psi}{ch\zeta+\cos\psi_1}\int_{\psi_1}^{\psi} v\,d\psi\right)dr}{\int_0^{\infty} r^3 f_1(r,\zeta)\,dr} .$$

The distribution law is given by:

$$f(r,\psi,\zeta) = \frac{f_1(r,\zeta)\left(1+\frac{2I}{a}\frac{1+ch\zeta\cos\psi_1}{ch\zeta+\cos\psi_1}\int_{\psi_1}^{\psi} v\,d\psi\right)}{\int_0^{r_L(\psi\zeta)} f_1(r,\zeta)\left(1+\frac{2I}{a}\frac{1+ch\zeta\cos\psi}{ch\zeta+\cos\psi}\int_{\psi_1}^{\psi} v\,d\psi\right)dr} ,$$

for $r \leq r_L$,

and $f(r, \psi, \zeta) = 0$ for $r > r_L$.

We applied this on the computer assuming that the initial particle distribution was independent of $\hat{\gamma}$ and exponential:

$$f_i(r,\hat{\gamma}) = \frac{1}{r_{m_i}} e^{-\frac{r}{r_{m_i}}}.$$

Figure 20 gives the variation in density reduced as a function of the position shown by the angle θ of the diverging section in Section 2 for some values of I based on the mean radius r_{ml} (in practice we find that I is on the order of unity). The curves are characterized by a sharp downward slope in the vicinity of the wall; this shape is to be compared with the variation in luminous intensity of the jet (Figure 18). The curves giving the variation in local mean radius and scattering function are similar.

We thus observe that two-dimensional phenomena are marked by this type of two-phase flow. Segregation of the condensed phase in the flow can increase particle growth at the flow center and complicate calculation of divergence losses. It will thus be necessary to develop a flow pattern which takes into account both collisions and lateral phase shifts.
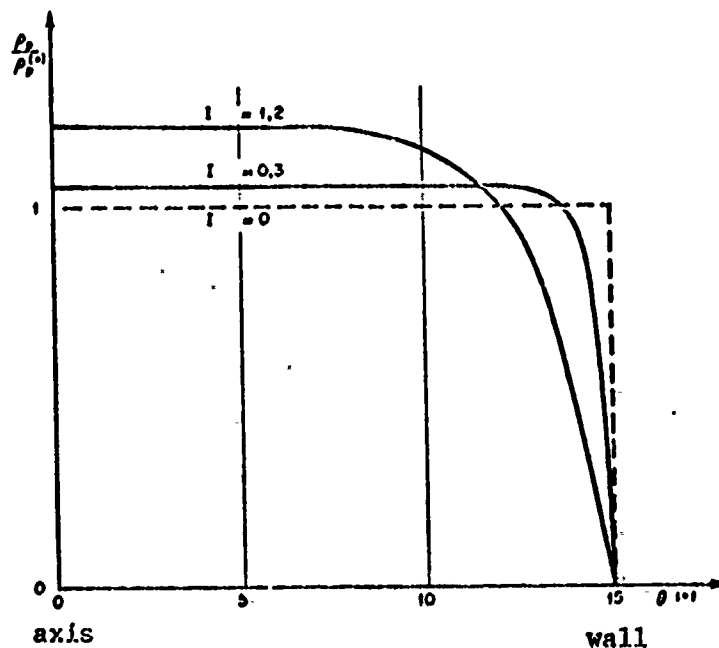
Figure 20. Variation in Density of Condensed Phase After the Throat.

3.4. CONCLUSIONS

The condensed phase requires both experimental and theoretical means of study. The particle growth, in particular, sets a limit on the accuracy of the results since the fundamental collision phenomena are still imperfectly known. Due to these difficulties and although the qualitative description of the condensed phase may be considered established the computer data still have a substantial margin of uncertainty and we must expect this inaccuracy to turn up again in the final estimate of specific impulse losses.

4. STUDY OF TWO-PHASE FLOWS

The interactions between the two phases have thus far been simplified when our objective was to find out more about condensed phase behavior. To define their role in expansion of combustion products in order to estimate specific impulse losses we must now study two-phase flows more thoroughly. We will cite some data from [33]:

4.1. CONDENSED FLOW SCHEMATIZATION

The particles formed in the combustion process are very numerous due to their small diameters. Although they represent a noteworthy mass fraction of the combustion products, they correspond only to a very small volume fraction. These two features: small size and small relative volume of dispersed elements characterize the suspensions [34]. We can define elementary volumes which are very small with respect to the area considered but whose dimensions are far greater than those of the particles and which contain a large number of particles.

Application of homogeneous flow methods to suspension comes up against the difficulty of correctly defining the control volume or volumes. A volume for the whole of both phases is broken down into a volume occupied by the gaseous phase and the volume occupied by the condensed phase. Due to the particle motion in the gaseous phase these volumes are constantly changing such that, by nature,

multi-phase flow is unsteady and three-dimensional. From the theoretical viewpoint alone we can study the gaseous phase and each particle. This approach enables us to demonstrate the rules of similarity of the flow but the very high number of equations to which it leads is unsuitable for computation. We may believe that, when the dimensions of the general control volume become large enough while being much smaller than those of the enclosed area considered, fluctuations in the gaseous phase and condensed phase volumes will decrease and statistical methods will be useable. The basic idea is thus to try to represent the condensed phase as a continuum mixed with the gaseous phase and interacting with it.

The most demanding step in arriving at this result consists of defining a mean in time and space for each magnitude [35, 36]. These magnitudes must be insensitive to the order in which the means are made, which requires the following two conditions:

- The fluctuations in the number of particles in the volume considered are very small in comparison with the average number of particles in this volume;

- The time it takes for a particle to pass a point is very much smaller than the time interval used to establish the mean.

These two conditions establish the lower space and time limits below which continuum equations can no longer be used. In the equations for gas and the gaseous phase, terms appear due to particle velocity and temperature fluctuations and, analogously, to the Reynolds terms of the classic turbulent theory. These terms linked to the passage from real flow to its continuous description even subsist if the gaseous flow is assumed to be laminar. A condensed phase pressure exists which is independent from that sometimes calculated when the particles move in random motion. The supplementary fluctuation terms are difficult to evaluate and make it cumbersome to use general equations. However, it has been shown

-65-

that, if the medium is very dispersed (volume portion occupied by
particles much less than 1), the fluctuation terms are negligible
as is the pressure of the condensed phase. If the gaseous flow is
turbulent, Reynolds terms exist in both phases, which must be
correlated.

The possibility of going on to a continuous description of the
condensed phase being granted, the general equation can be obtained
by two methods: either by studying separately the evolution of each
class of particles characterized by a diameter value, or by directly
establishing equations for the mean magnitudes of the condensed
phase. In the first case we must expand the terms for interactions
between the various classes of particles, which is possible when
the particles are solid [6] but not so easy when the particles are
liquid and agglomerate. The second attitude is more common [5] and
we have chosen it here.

Simplifying hypotheses were made with respect to interactions
between particles and between phases. We neglect distant forces
and exchanges between particles by radiation. We assume that the
interface between the gaseous phase and the particles is an ideal
surface through which exchanges occur and on both sides of which
properties can be defined for each phase. The interface is only a
pressure and density discontinuity. Finally we will assume that
the particles are always spherical, which was checked experimentally
by the capture technique described in Paragraph 3.2, but which
fails in high-acceleration zones where the liquid particles are
deformed.

4.2. CONDENSED PHASE EQUATIONS

The condensed phase is described locally by a distribution function f which depends on spatial variables x_i, on velocity components c_j, on the internal mass energy e of the particles (the temperature is assumed to be uniform in each particle), on the radius τ, and on time t. This function f may be assumed continuous with respect to the different variables.

The quantity: $f(x_i, c_j, e, \tau, t)\, d^3x_i\, d^3c_j\, de\, d\tau$

represents, at time t, the number of particles contained in the volume defined by x_i, $x_i + dx_i$ and with a velocity whose components are between c_j and $c_j + dc_j$, an internal energy of between e and e + de, and a radius between τ and $\tau + d\tau$.

4.2.1. Fundamental Condensed-Phase Equation

The function f obeys a balance equation of the Liouville-Boltzmann type, which is written:

$$\frac{\partial f}{\partial t} + \sum_i \frac{\partial}{\partial q_i}(f \dot{q}_i) = h(q_i, t).$$

In this equation, the q_i are coordinates of the space occupied by the phases. The derivatives $\dot{q}_i$ are functions of q_i and t given by outside phenomena while the function $h(q_i, t)$ is on the contrary due to phenomena internal to the particle population.

a) Expression for derivatives in the phase space:

We note first of all that: $\dfrac{dx_i}{dt} = c_i$.

Thus we get:

$$\sum_{i=1}^{3} \frac{\partial(f \dot{x}_i)}{\partial x_i} = \operatorname{div}(f \vec{c}),$$

$\vec{\psi}$ represents the force exerted on a particle of mass m, the particle motion equation is written:

$$\frac{d\vec{c}_d}{dt} = \frac{\varphi_d}{m} \quad .$$

whence:

$$\sum_{d=1}^{3} \frac{\partial (f\vec{c}_d)}{\partial c_d} = div_{\vec{c}} \left(\frac{f\vec{\varphi}}{m} \right) \quad .$$

The force $\vec{\psi}$ represents the resultant of the elementary forces acting on an isolated particle; these are:
- the weight of the particle: $\psi_{\gamma 1} = mg_\gamma$,
- the force exerted by the gaseous phase on the particle:
$\psi_{\gamma 2} = T_\gamma$.

The drag force T depends on a large number of parameters such as the shape, dimension, and surface condition of each particle, the velocity field in the gaseous phase, and the history of the particle's movement.

Experimental results obtained on particles of millimetric size are generally extrapolated for microscopic particles. The simplest expression for drag is obtained, for an incompressible fluid and in Stokes' regime, when the Reynolds number based on the particle diameter and the velocity difference between gas and particle is very much less than 1. Due to the great density differences between the gas and the particle, we can neglect the transitory drag terms. To take into account the effects of inertia, compressibility, and possibly rarefaction (diverging section with a large expansion ratio), we correct the drag coefficient established in the Stokes regime by a factor ℓ_u established semi-empirically [37, 38] and depending on the Reynolds number, the Mach number and the Knudsen number. Many formulas are presented in the literature covering all operational domains of motors. The differences in specific impulse resulting from using the different formulas are fairly moderate for average chamber pressures [39] and the uncertainty subsisting as to certain phenomena connected with the condensed phase is greater than that concerning drag laws.

In short, we will write:

$$\frac{\vec{\varphi}}{m} = \vec{g} + \frac{\ell_u (\vec{u_g} - \vec{c})}{\tau_u},$$

and we will often use the simplification:

$$\ell_u \equiv 1.$$

Likewise, as q is the heat flux received by a particle, we can write:

$$\frac{\partial (f \dot{e})}{\partial c} = \frac{\partial}{\partial c}\left(\frac{f q}{m}\right).$$

In the absence of radiative exchanges between particles or between the particles and the enclosure, the heat flux is only due to the convective exchange between the gaseous phase and the particle whose temperatures are different. This condensation occurs on the particles, the heat released in the process is entirely evacuated by the gaseous phase. Calculation of flux q as a function of other values raises the same problems as that of the drag coefficient; it is treated similarly. With Stokes regime we have a heat transfer by pure conduction which gives a characteristic value for the Nusselt number:

$$Nu = 2.$$

This value is corrected to take into account real gas effects. The corrective factor is noted ℓ_T; several expressions for this are given in the literature [38]. Finally we get:

where
$$\frac{q}{m} = \frac{\ell_T \overline{C_c}(T_g - T_P)}{\tau_T} \simeq \frac{\ell_T e(T_g) - e}{\tau_T},$$

$$\tau_T = \frac{\sigma^2 \rho_c \overline{C_c}}{3 \lambda} = \tau_u \times \frac{3}{2} \overline{\tau_r} \times \beta$$

We will often take: $\ell_T \equiv 1.$

M is the mass flow deposited on a particle, so that we finally have:

$$\frac{\partial (f \dot{r})}{\partial \tau} = \frac{\partial}{\partial \tau}\left(\frac{f M \sigma}{3 m}\right).$$

An expression for M can be deduced from the calculations presented when considering formation of alumina particles (Section 3.3.1.).

b) **Expression of the second member:**

The phenomena of the particle population which modify the state of a particle are collisions and disintegrations (formation of new particles is left out of count here).

The role and importance of collisions and their varied origins have already been shown. We will remember simply that at a collision between two solid particles, considered to be perfectly elastic, only the velocities are modified while liquid particles can agglomerate.

Disintegration of a liquid particle is able to occur without impact in a strongly accelerated flow. The most common burst criterion is based on the Weber number:

$$W_e = \frac{\rho |\vec{u_q} - \vec{c}| d_p}{\sigma},$$

where γ is the surface tension.

When the Weber number exceeds a critical value of about 10 to 20 the particle disintegrates. Certain authors believe that this phenomenon limits the maximum particle dimension [40], which would seem to prove the experimentally-found variation of this characteristic with nozzle size. In actual fact we know that the phenomenon is not instantaneous and that particles begin first to deform progressively under the effect of various surface forces; moreover the existence of an upper limit for the particle diameter must be connected to the mechanism of formation and the dwell time in the nozzle. Thus, spontaneous disintegrations are not systematic; at most they involve a limited number of very large particles, i.e., the population class which is still poorly known. The phenomenon will thus be left out of count in the following remarks.

For collisions, we will consider first the case of solid particles and then liquid particles.

In all cases we write the number of collisions occurring per unit of volume and time between two classes of particles in the form:

$$f(x_i, c_j, e, \sigma, t) \, f(x_i, c_j', e', \sigma', t) \, \Phi(x_i, c_j, c_j', e, e', \sigma, \sigma', t)$$
$$d^3 c_j \, de \, d\sigma \, d^3 c_j' \, de' \, d\sigma'.$$

The function Φ is the collision function. It is symmetrical with respect to the particles and should in principle take the form:

$$\Phi\left(|\vec{c} - \vec{c}'| , |\sigma - \sigma'| , (\sigma + \sigma') , x_i, t \right).$$

The expression for Φ results from studying the intimate mechanism of collisions and Φ must often be given a simplified form; several expressions were given in Section 3.3.1.

All collisions of particles in the class $d^3 g \, de \, d\tau$ with all others are obtained by integration and are translated by a vanishing term in the second member of the basic equation, which is:

$$h(q_i, t) = -f \iint_D f(x_i, c_j', e', \sigma', t) \, \Phi \, d^3 c_j' \, de' \, d\sigma.$$

The other term of the second member linked to collisions is a production term; we must consider all inter-particle collisions resulting in formation of a particle of the given class to be binary. The form of this term differs according to whether the particles are solid or liquid.

- <u>Solid Particles</u>:

The production term is written:

$$h_{2s}(q_i, t) = \iint_{D_s} f(x_i, c_j', e, \sigma, t) \, f(x_i, c_j'', e'', \sigma'', t) \cdot \Phi$$
$$d^2 c_j' \, d^2 c_j'' \, de'' \, d\sigma'' \, d^2 \sigma_j \, ,$$

The domain of integration D_S being such that:

$$\begin{cases} c_j' + \frac{2}{1+\left(\frac{z'}{z}\right)^3}\left[(c_j'' - c_j')(1-d^2) - |\vec{c}'' - \vec{c}'|\sqrt{1-d^2}\,d_j\right] = c_{dj} \\ |\vec{\delta}| \leqslant 1, \quad \sum_j \delta_j(c_j'' - c_j') = 0 \end{cases}$$

- Liquid Particles:

The problem for liquid particles is more complex since colli-sion may take place in several stages as pointed out by several authors [30]. It has been noted that, if the velocity difference between two incident particles is large enough, agglomeration is followed by a burst, i.e., the intermediate particle formed is unstable. This phenomenon is said to depend on two dimensionless numbers characterizing the impact conditions:

$$R_e = \frac{2|\vec{c} - \vec{c}'||\tau - \tau'|\rho_c}{\mu_c},$$

$$\Gamma = \frac{\mu_c^2}{2|\tau - \tau'|\,z\,\rho_c} \quad .$$

We must thus define a new function $G(c_\gamma''', e''', \tau''', |\tau - \tau'|,$ $|\vec{cc}|)$ giving the number of particles in class d^3c_γ''', $de'''d\tau'''$ formed in the collisions of particles $(\tau, \vec{c})$ and $(\tau', \vec{c}')$. The internal energy and the velocity of the particles formed after the burst are those of the intermediate particle and are calculated quite easily. G is thus presented in the form:

$$G\left(\tau''; |\tau - \tau'|, |\vec{c} - \vec{c}'|\right),$$

and the production term is written:

$$h_{2L}(q_{ij}, t) = \frac{1}{2}\iint_{D_L} f(x_i, c_j', e', \tau', t)\, f(x_i, c_j'', e'', \tau'', t)\, \Phi$$
$$G\left(\tau_j|\tau - \tau''|, |\vec{c} - \vec{c}''|\right)d^3c_j'\,d^3c_j''\,de'\,de''\,d\tau'd\tau'',$$

the domain of integration D_L being such that:

$$\begin{cases} \dfrac{c'_d + c''_d \left(\dfrac{\sigma''}{\sigma'}\right)^3}{1 + \left(\dfrac{\sigma''}{\sigma'}\right)^3} = c_d \ , \\[2ex] \dfrac{c' 4 \left(\dfrac{\sigma''}{\sigma'}\right)^3 c'' + \dfrac{1}{2}|\vec{c}'-\vec{c}''|^2 \dfrac{\left(\dfrac{\sigma''}{\sigma'}\right)^3}{1+\left(\dfrac{\sigma''}{\sigma'}\right)^3}}{1+\left(\dfrac{\sigma''}{\sigma'}\right)^3} = c \ , \\[2ex] \left(\sigma'^3 + \sigma''^3\right)^{\frac{1}{3}} = \sigma \ , \end{cases}$$

and the coefficient 1/2 taking into account the symmetrical role played by the collisions. In the condensed form, the second member of the basic equation is written as follows:

$$h = -f \int_{D_1} f'\Phi \, d\upsilon_1 + \int_{D_s} f'f'\Phi \, d\upsilon_s \ , \quad \text{(solid particles)}$$

$$h = -f \int_{D_1} f'\Phi \, d\upsilon_1 + \frac{1}{2}\int_{D_L} f'f''\Phi G \, d\upsilon_L \ , \quad \text{(liquid particles)}.$$

We must admit that the collision function Φ and production G are rather poorly known. These uncertainties have a direct impact on the evolution of the condensed phase. On the other hand, in equations characterizing the average behavior of the condensed phase, these functions will not appear explicitly since the collisions themselves obey certain conservation laws.

To establish these equations we proceed in the normal manner: after multiplying the two members of the equation by the same quantity, one integrates them over space (c_j, e, τ). The mean magnitudes thus appear naturally.

4.2.2. Continuity Equation

The multiplying factor is $m(\tau)$. We define the density of the condensed phase an its velocity by the relations:

$$\rho_P = \iint m(\sigma) f \, d^3c_j \, de \, d\sigma \ ,$$

$$u_{P_i} = \frac{1}{\rho_P} \iint m(\sigma) \, c_i \, f \, d^3c_j \, de \, d\sigma .$$

-73-

ρ_p represents the mass of condensed phase contained in a unit volume of the mixture; it is thus a fictitious density which is connected with the true density of the particles ρ_c through the intermediary of the volume fraction occupied by the condensed phase:

$$\rho_p = \varepsilon \rho_c \, .$$

The first member contains first the term involving the time and space variables:

$$\frac{\partial \rho_p}{\partial t} + \sum_i \frac{\partial}{\partial x_i}(\rho_p u_{pi}) \, .$$

Other terms involve other phase space variables (c_j, e, τ); only that for the radius is not zero and is written:

$$-\iint M f \, d^3c_j \, de \, d\tau = - \overset{\circ}{w}_p \, .$$

This is a term corresponding to mass production by condensation.

As the mass is conserved in collisions, the second member is identically zero such that the continuity equation of the condensed phase takes the classic form:

$$\frac{\partial \rho_p}{\partial t} + \text{div}(\rho_p \vec{u}_p) = \overset{\circ}{w}_p \, .$$

4.2.3. Momentum Equation

The multiplying factor is $m(\tau)c_k$.

When the equation is integrated the first member (as well as magnitudes already defined) has terms such as:

- the force exerted per unit volume by the gaseous phase on the condensed phase, the components of which are:

$$F_{PA} = \iint \varphi_A \, f \, d^3\vec{\zeta} \, d\mathbf{c} \, d\sigma$$
$$= \rho_P g_A + \iint \frac{\partial}{\partial c_\iota}(u_A - c_A) \, m(\sigma) \, f \, d^3\vec{\zeta} \, d\mathbf{c} \, d\sigma$$
$$= F_{PA\prime} + F_{PA\prime\prime} \quad ,$$

- terms coming from particle scattering in barycentric movement.
We write:

$$\mathbb{D}_{P_\iota A} = -\iint (c_\iota - u_{P\iota})(c_A - u_{PA}) \, m(\sigma) \, f \, d^3\vec{\zeta} \, d\mathbf{c} \, d\sigma \, ,$$
$$K_{PA} = \iint (c_A - u_{PA}) \, M \, f \, d^3\vec{\zeta} \, d\mathbf{c} \, d\sigma \, .$$

The momentum is conserved in the collisions such that the second member is again identically zero. We thus obtain:

$$\frac{\partial}{\partial t}(\rho_P u_{PA}) + \sum_\iota \frac{\partial}{\partial c_\iota}(\rho_P u_{PA} u_{P\iota}) = F_{PA} + \dot{w}_P u_{PA} + \sum_\iota \frac{\partial \mathbb{D}_{P_\iota A}}{\partial x_\iota} + K_{PA} \, .$$

This equation can be combined with the continuity equation multiplied by u_{pk}. It thus appears in the vectorial form:

$$\rho_P \frac{\partial \vec{u}_P}{\partial t} + \rho_P \vec{u}_P \cdot \overrightarrow{\text{grad}} \, \vec{u}_P = \vec{F}_P + \overrightarrow{\text{div}} \, \overrightarrow{\mathbb{D}}_P + \vec{K}_P \, .$$

When compared to the classical momentum equation for a homogeneous fluid we note the absence of a pressure term and the presence of a force term and a scatter term. In the absence of condensation the supplementary term $\vec{K}_p$ does not exist.

4.2.4. Energy Equation

The multiplying factor is $m(\tau)e$. The internal mass energy is obtained by adding:

$$e_P = \frac{1}{\rho_P} \iint m(\sigma) \, e \, f \, d^3\vec{\zeta} \, d\mathbf{c} \, d\sigma \, .$$

We define:

- the heat transmitted by the gas to the condensed phase per unit of volume and time:

$$Q = \iint q\, f\, d^3c_j\, de\, d\sigma$$

$$= \iint \frac{\mathcal{E}_\tau}{\tau_\tau}\left[e(T_j) - e\right] m(\sigma)\, f d^3c_j\, de\, d\sigma.$$

- scatter terms such as:

$$G_{P_i} = \iint (c_i - u_{P_i})(e - e_P) m(\sigma)\, f d^3c_j\, de\, d\sigma,$$

$$L_P = \iint M(e - e_P)\, f d^3c_j\, de\, d\sigma.$$

We note that energy is conserved in the collisions such that
the terms of the second member are zero.

The energy equation is thus written:

$$\frac{\partial}{\partial t}\left(\rho_P e_P\right) + \sum_i \frac{\partial}{\partial x_i}\left(\rho_P u_{P_i} e_P\right) = Q + \dot{w}_P e_P - \sum_i \frac{\partial G_{P_i}}{\partial x_i} + L_P.$$

It can be combined with the continuity equation multiplied by e_P to
give:

$$\rho_P \frac{\partial e_P}{\partial t} + \rho_P \vec{u}_P \cdot \overrightarrow{grad}\, e_P = Q - div\, \vec{G}_P + L_P$$

The form of this equation is that relative to homogeneous flow
with a heat source, yet the pressure term does not exist here.

By combining the momentum and energy equations we establish
the total energy equation:

$$\rho_P \frac{\partial}{\partial t}\left(e_P + \frac{u_P^2}{2}\right) + \rho_P \vec{u}_P \cdot \overrightarrow{grad}\left(e_P + \frac{u_P^2}{2}\right)$$

$$= \vec{u}_P \cdot \vec{F} + Q + \vec{u}_P \cdot div\, \overrightarrow{D_P} - div\, \vec{G}_P + \vec{u}_P \cdot \vec{K}_P + L_P.$$

The general equations of the condensed phase are thus presented
in a classical form, where interactions with the gaseous phase are
translated by force terms and definition of the mean magnitude by
supplementary terms. We can define a derivative in barycentric move-
ment by:

$$\frac{d(\ )}{dt} = \frac{\partial(\ )}{\partial t} + \vec{u}_P \cdot \overrightarrow{grad}(\quad).$$

4.2.5. Entropy Balance

The muliplying factor is $m(\tau)s$. The mass entropy of the condensed phase is obtained by adding:

$$s_P = \frac{1}{\rho_P} \iint m(\tau)sf\,d^3c_g\,dc\,d\tau.$$

The s_p equation is established like the other equations and new terms must be defined. This equation can be combined with the energy equation such that:

$$T_P \frac{ds_P}{d\tau} = \frac{de_P}{d\tau} + T_P \mathcal{G}_P.$$

G_p is a term linked on the one hand to dispersion of mean magnitude and on the other hand to irreversible changes occurring during the collisions (liquid particles). The presence of this term is an obstacle to studying the two-phase mixture by classic thermodynamic methods since it throws out the local equilibrium hypothesis [41]. Fortunately, one can show that G_p is of the second order with respect to temperature deviations; thus in most cases it will be neglected.

4.3. GASEOUS PHASE EQUATIONS

The gaseous phase equations, even for a multi-reactive mixture, can be established in a more classical manner [42]; these equations will thus be established more briefly. They must, however, be modified to take into account the presence of the condensed phase. By comparison with equations for a homogeneous fluid, a particularity resides in the definition of the density. We define a fictitious density ρ_γ for each species j which is assumed to occupy the entire volume of the mixture; this quantity is linked to the real density ρ_{gj} by the relation:

$$\rho_\gamma = \rho_{gj}\,(1-\varepsilon).$$

In the general balance equation the ρ_γ quantities are used while in the equations of state the ρ_{gj} equations are used. We must, however, note that in the type of suspension studied the volume fraction ε occupied by the condensed phase is always very small such that the differences between ρ_γ and ρ_{gj} are negligible.

4.3.1. Continuity Equation

The continuity equation for each species shows the mass production rates $\overset{\circ}{w}_\gamma$. The mass conservation principle in the chemical reactions is translated by:

$$\sum_{j=1}^{N} \overset{\circ}{w}_j = - \overset{\circ}{w}_p .$$

If Y_γ is the mass fraction of species j in the gaseous mixture, the corresponding continuity equation is:

$$\frac{\partial}{\partial t}\left(\rho Y_j\right) + \operatorname{div}\left(\rho Y_j \vec{v}_j\right) = \overset{\circ}{w}_j ,$$

where ρ is the density of the gaseous phase obtained by adding:

$$\rho = \sum_{j=1}^{N} \rho_j .$$

The barycentric velocity of the gaseous phase is defined by:

$$\vec{u} = \sum_{j=1}^{N} Y_j \vec{v}_j .$$

The rate of scatter of species j in barycentric motion will be given by:

$$\vec{V}_j = \vec{v}_j - \vec{u} .$$

Expressing $\vec{v}_j$ as a function of $\vec{u}$ and $\vec{V}_j$ in the continuity equation of species j then adding all the species, we arrive at the overall equation:

$$\frac{\partial \rho}{\partial t} + \operatorname{div} \rho \vec{u} = -\mathring{w}_P$$

This equation is distinguished from the classical equation only by the source term of the second member. It can be rewritten introducing the particular derivative in barycentric motion.

$$\frac{d\rho}{dt} + \rho \operatorname{div} \vec{u} = -\mathring{w}_P .$$

4.3.2. Momentum Equation

The variation in momentun of any volume is due to surface stresses, volume forces, production of species, and action of the condensed phase. Accordingly, terms such as the following enter the momentum equation:

- the scattering tensor whose components are defined by:

$$D_{i\ell} = -\rho \sum_{d=1}^{N} Y_d V_{di} V_{d\ell} ,$$

- the stress tensors which break down in the classical manner into a pressure term and a viscosity term:

$$\vec{\vec{\sigma}}_d = -P_d \vec{\vec{\delta}} + \vec{\vec{\tau}}_d ,$$

hence by adding:

$$\vec{\vec{\sigma}} = -P\vec{\vec{\delta}} + \vec{\vec{\tau}} .$$

Finally, after combination with the continuity equation, we get:

$$\rho \frac{d\vec{u}}{dt} + \overrightarrow{\operatorname{grad}} P = \overrightarrow{\operatorname{div}} (\vec{\vec{\tau}} + \vec{\vec{D}}) + \rho\vec{g} - \vec{F}_R + (\vec{u} - \vec{u}_P)\mathring{w}_P - \vec{R}_P .$$

This equation differs from its classical expression only by the existence of terms due to the condensed phase. We will note that it is only the component of interaction between the two phases which intervenes in the forces.

The equation for kinetic energy is deduced without difficulty from the momentum equation.

4.3.3. Energy Equation

To establish the energy equation we operate with the total energy. Its variation in any volume results from the work of the surface stresses and the volume forces, the heat transfer by conduction, and exchanges with the condensed phase. The classical terms appear:

- the dissipation function:

$$\phi = (\overset{\Rightarrow}{\mathcal{C}} + \overset{\Rightarrow}{\mathcal{D}}) : \overrightarrow{\text{grad}}\ \overrightarrow{u}\ ,$$

- the heat flux density $\overrightarrow{q^*}$ modified to take scattering effects into account.

With the usual simplifications and after combining the equation obtained with the continuity and kinetic energy equations, we finally obtain:

$$\rho \frac{d\mathcal{E}}{dt} + p\,\text{div}\,\overrightarrow{u} - \phi + \text{div}\,\overrightarrow{q^*} =$$

$$= \overset{\cdot}{w}_p \left(\mathcal{E} - \mathcal{E}_p + \frac{u^2 - u_p^2}{2} - \overrightarrow{u}(\overrightarrow{u} - \overrightarrow{u}_p)\right) + (\overrightarrow{u} - \overrightarrow{u}_p) \cdot (\overrightarrow{F}_{p_x} + \overrightarrow{R}_p) - (\mathcal{O} + L_p).$$

The first member of this equation is classical; the second groups all the terms of interaction with the condensed phase.

The enthalpy equation is easily deduced from the above equation:

$$\rho \frac{dh}{dF} - \frac{dp}{dF} - \dot{\phi} + \operatorname{div}\vec{q}^{*} =$$

$$= \dot{w}_P \left(h - e_T + \frac{4e - u_P^2}{2} - \vec{u}\cdot(\vec{u} - \vec{u}_P) \right) + (\vec{u} - \vec{u}_P)\cdot(\vec{F}_{P_2} + \vec{\tau}_P) - (Q + L_P).$$

4.3.4. Entropy Balance

Between the entropy, the internal energy, the density, and the mass fractions exists Gibbs relation:

$$de = Tds + \frac{p}{\rho^2}d\rho + \sum_{d=1}^{N} \mu_d dY_d \,;$$

where μ_j is the mass chemical potential of species j.

The mass entropy equation is thus deduced from the equations established above. It appears that the entropy flux is not modified by the presence of the condensed phase which, on the contrary, is manifested as internal production, which corresponds well to the irreversible nature of inter-phase exchanges.

4.4. MIXTURE EQUATIONS

Although the equations of the two phases in principle are sufficient for describing the flow, it could be useful to study the average behavior of the mixture. As with the condensed phase, we need first to make a suitable definition of the mean magnitudes, then establish the corresponding equations.

4.4.1. Continuity Equation

The density of the mixture is simply written:

$$\overline{\rho} = \rho + \rho_P \,.$$

The barycentric velocity is defined by the relation:

$$\bar{\rho}\,\vec{u} = \rho\,\vec{u} + \rho_P\,\vec{u_P} \;.$$

The scatter velocities of the phases in barycentric motion can now be introduced:

$$\vec{V} = \vec{u} - \vec{u} \;,$$
$$\vec{V_P} = \vec{u_P} - \vec{u} \;.$$

By adding the continuity equations of the two phases we obtain the overall continuity equation directly:

$$\frac{\partial \bar{\rho}}{\partial t} + div(\bar{\rho}\,\vec{u}) = 0 \;.$$

A new particular derivative in the barycentric motion of the mixture can be defined by:

$$\frac{d(\;)}{dt} = \frac{\partial(\;)}{\partial t} + \vec{u}\cdot grad(\;) \;,$$

such that the overall continuity equation is written:

$$\frac{d\bar{\rho}}{dt} + \bar{\rho}\,div\,\vec{u} = 0 \;.$$

4.4.2. Momentum Equation

The momentum equations for the two phases can be presented in the form:

$$\frac{\partial}{\partial t}(\rho_P\,\vec{u_P}) + div(\rho_P\,\vec{u_P} \otimes \vec{u_P}) =$$
$$= \vec{F_P} + \dot{w}_P\,\vec{u_P} + div\,\vec{\mathbb{D}_P} + \vec{K_P} \;,$$

$$\frac{\partial}{\partial t}(\rho\,\vec{u}) + div(\rho\,\vec{u} \otimes \vec{u}) =$$
$$= -grad\,p + \cdots (\vec{\tau} + \vec{\mathbb{D}}) + \rho\,\vec{g} - \vec{F_{P*}} - \dot{w}_P\,\vec{u_P} - \vec{K_P} \;.$$

-82-

We will define a two-phase scattering tensor by:

$$\vec{\vec{B}} = -\left(\rho\,\vec{V}\otimes\vec{V} + \rho_P\,\vec{V}_P\otimes\vec{V}_P\right),$$

and a generalized scattering tensor by:

$$\vec{\vec{\mathcal{J}}} = \vec{\vec{B}} + \vec{\vec{B}}_P + \vec{\vec{B}}.$$

By adding the two above equations we arrive directly at the equation we are looking for:

$$\frac{\partial}{\partial t}\left(\bar{\rho}\,\vec{u}\right) + \overrightarrow{\text{div}}\left(\bar{\rho}\,\vec{u}\otimes\vec{u}\right) = -\overrightarrow{\text{grad}}\,p + \bar{\rho}\,\vec{g} + \overrightarrow{\text{div}}\left(\vec{\vec{\mathcal{E}}} + \vec{\vec{\mathcal{J}}}\right),$$

or again, by combination with the continuity equation:

$$\bar{\rho}\,\frac{d\vec{u}}{dt} + \overrightarrow{\text{grad}}\,p - \bar{\rho}\,\vec{g} - \overrightarrow{\text{div}}\left(\vec{\vec{\mathcal{E}}} + \vec{\vec{\mathcal{J}}}\right) = 0.$$

The kinetic energy equation is deduced from this:

$$\bar{\rho}\,\frac{d}{dt}\left(\frac{\vec{u}^{\,2}}{2}\right) = \bar{\rho}\,\vec{g}\cdot\vec{u} - \vec{u}\cdot\overrightarrow{\text{grad}}\,p + \vec{u}\cdot\overrightarrow{\text{div}}\left(\vec{\vec{\mathcal{E}}} + \vec{\vec{\mathcal{J}}}\right).$$

4.4.3. Energy Equation

The internal mass energy is obtained by adding:

$$\bar{\rho}\,\bar{e} = \rho\,e + \rho_P\,e_P.$$

The mass enthalpy may be deduced immediately:

$$\bar{h} = \bar{e} + \frac{p}{\bar{\rho}}.$$

The energy equations for each phase can be written:

$$\frac{\partial}{\partial t}\left(\rho_P\,e_P\right) + \text{div}\left(\rho_P\,e_P\,\vec{u}_P\right) = Q + \dot{w}_P\,e_P - \text{div}\,\vec{G} + L_P,$$

$$\frac{\partial}{\partial t}\left(\rho e\right) + \text{div}\left(\rho e\,\vec{u}\right) = -p\,\text{div}\,\vec{u} + \Phi - \text{div}\,\vec{q}^{\,*}$$
$$+ \dot{w}_P\left(-e_P + \frac{u_{-\mu\nu}^{2}}{2} - \vec{u}\cdot(\vec{u}-\vec{u}_P)\right) + (\vec{u}-\vec{u}_P)\cdot(\vec{F}_P + \vec{K}_P) - (Q+L_P).$$

-83-

By adding, we get:

$$\frac{\partial}{\partial t}\left(\bar{\rho}\,\bar{e}\right)+\mathrm{div}\left(\bar{\rho}\,\bar{e}\,\vec{u}\right) = -p\,\mathrm{div}\,\vec{u} + \phi -\mathrm{div}\,\vec{q}^{\,\varkappa} -\mathrm{div}\left(\rho e\vec{V}+\rho_P e_P\vec{V}_P\right)$$
$$+\,\dot{w}_P\left(\frac{u_P^2-u^2}{2}-\vec{u}\cdot(\vec{u}-\vec{u}_P)\right)+(\vec{u}-\vec{u}_P)(\vec{F}_{P_2}+\vec{K}_P)-\mathrm{div}\,\vec{G}\ .$$

It is thus appropriate to define a generalized dissipation
function and an overall heat flux density with the aid of relations:

$$\bar{\Phi} = \phi +\vec{V}\cdot\overrightarrow{\mathrm{grad}}\,p +\dot{w}_P\left(\frac{u_P^2-u^2}{2}-\vec{u}\cdot(\vec{u}-\vec{u}_P)\right)+(\vec{u}-\vec{u}_P)\cdot(\vec{F}_{P_2}+\vec{K}_P)\ ,$$

$$\vec{q} = \vec{q}^{\,\varkappa} +\rho h\vec{V}+\rho_e e_P\vec{V}_P+\vec{G}\ .$$

The energy equation then takes the classical form after com-
bination with the continuity equation:

$$\bar{\rho}\,\frac{d\bar{e}}{dt} = -p\,\mathrm{div}\,\vec{u} + \bar{\Phi} -\mathrm{div}\,\vec{q}\ .$$

The enthalpy equation is deduced immediately:

$$\rho\,\frac{d\bar{h}}{dt} = \frac{dp}{dt} + \bar{\Phi} -\mathrm{div}\,\vec{q}\ .$$

4.4.4. Entropy Balance

The two-phase mixture is to be considered a composite system
made of two sub-systems which are not in mutual equilibrium but are
in individual equilibrium and can thus be described by an equation
of state.

We can write equations of state for any quantity of mixture.
Expressing internal energy and entropy as additive magnitudes we
arrive at the mixture equation then at the Gibbs equation. Going on
to barycentric motion in the mixture, then expressing the particular
derivatives with the aid of the equations already established, we
arrive at the general expression of the form:

$$\bar{\rho}\,\frac{d\bar{s}}{dt} = -\mathrm{div}\,\vec{J}_s +\overline{\sigma_s}\ .$$

The entropy flux $\vec{J}_s$ has a heat-transfer term and scattering terms. The production $\vec{\tau}_s$ is broken down mainly into terms relating to the gaseous phase (dissipation, chemical reactions, and heat flux) and in terms due to two-phase exchanges.

It is useful to establish the relative order of magnitude of these production terms. We will take the case of permanent flow in sections. Viscous dissipation in the gaseous phase is given by:

$$\Phi \approx \frac{4}{3}\mu\left(\frac{du}{dx}\right)^2 , \qquad \text{(Stokes hypothesis)}.$$

The friction term of the condensed phase is approximately:

$$F_p(u-u_p) = \frac{18\rho_p\mu\,(u-u_p)^2}{\rho_c\,\bar{d}_p^{\,2}} , \qquad \begin{array}{l}\text{(Stokes law and}\\ \text{uniform particle}\\ \text{diameter)},\end{array}$$

i.e., using the near equilibrium hypothesis:

$$F_p(u-u_p) = \frac{\rho_c\rho_p\,\bar{d}_p^{\,2}}{18\mu}\,u^2\left(\frac{du}{dx}\right)^2 .$$

The ratio between the production term due to the condensed phase and that due to the gaseous phase finally comes out in the form:

$$\frac{1}{24\varepsilon}\left(\rho_c\frac{u\,\bar{d}_p}{\mu}\right)^2 .$$

For realistic operating conditions, the Reynolds number appearing between parentheses is always greater than 1; ε is accordingly very small. We could thus say that in suspension flows the irreversible exchanges between phases are almost exclusively at the origin of the entropy growth within the flow.

The performance degradation phenomena must thus be studied first from the viewpoint of two-phase effects. It is certain that these

effects are more marked in zones where there are sharp velocity and temperature gradients, in particular in the nozzle.

4.5. APPLICATION OF GENERAL EQUATIONS TO FLOW OF A SUSPENSION IN A NOZZLE

Besides the two-phase effects we are trying to define, which are linked to the existence of a condensed phase with complex characteristics (wide spectrum of particles, growth by agglomeration), we must, in principle, take into account in our flow pattern more classical phenomena such as wall losses and chemical reactions in the gaseous phase, since the flow studied here is at a high temperature and at high pressure. In practice, these phenomena also partly depend on the condensed phase, and even if it is possible to establish the most general flow equations, the associated computing problem exceeds present computer capabilities [30]. We are thus compelled to make simplifications on either the condensed phase or the gaseous phase, or the number of dimensions considered. Due to the large number of possible simplifications, a great many articles have been written on flow of suspensions in nozzles. However, very few calculations methods reported are realistic enough to give firm results.

There is something to be said for beginning from the most elementary basis in order to bring out certain characteristics common to this type of flow. We will briefly report results from the most simplified model before attempting to define the requirements of a realistic model.

4.5.1. Simplified Flow Model

The following hypotheses are made:

- permanent flow is in sections,

- the particles are of uniform diameter and are regularly
distributed in the gaseous phase; they undergo neither collisons
nor phase changes, their volume is negligible in the mixture, and
their physical properties are constant;

- the gaseous phase is made of a non-viscous ideal gas (except
with regard to its effect on the particles) whose properties are
constant;

- exchanges between phases are calculated for the Stokes
law;

- the interactions between the flow and the nozzle wall are
neglected.

Equations for this type of flow are fairly classical [5]. There
are three conservation equations for each phase, obtained easily from
the general equations of Section 4, and the gas equation of state.
It is useful to combine the momentum equations and energy of the
two phases equations to eliminate the F and Q exchange terms. We
come out with:

$$\begin{cases} \rho u A = \overset{\circ}{m} , \\[4pt] \rho_p u_p A = \overset{\circ}{m}_p , \\[4pt] \rho u \dfrac{du}{dx} + \rho_p u_p \dfrac{du_p}{dx} + \dfrac{dp}{dx} = 0 , \\[4pt] \rho u \dfrac{d}{dx}\left(C_p T + \dfrac{u^2}{2}\right) + \rho_p u_p \dfrac{d}{dx}\left(C_s T_p + \dfrac{u_p^2}{2}\right) = 0 , \\[4pt] u_p \dfrac{du_p}{dx} = \dfrac{1}{\tau_u}\left(u - u_p\right) , \\[4pt] u_p \dfrac{dT_p}{dx} = \dfrac{1}{\tau_T}\left(T - T_p\right) , \\[4pt] p = \rho r T . \end{cases}$$

We can eliminate the volume masses and pressure by noting that the mass flows are in a constant ratio K, and integrate the overall energy equation. We will denote:

- H, the mass enthalpy of the mixture under generating conditions (phase equilibrium),

- $T = \frac{1}{A} \frac{dA}{dx}$, the abscissa function characterizing the evolution of the straight section.

The system reduces to:

$$
\begin{cases}
\left(1 - \frac{rT}{u^2}\right) \frac{d}{dx}\left(\frac{u^2}{2}\right) + r\frac{dT}{dx} = rT\,\sigma - Ku\frac{du_p}{dx} , \\[2mm]
C_p T + \frac{u^2}{2} + K\left(C_s T_p + \frac{u_p^2}{2}\right) = H(1+K) , \\[2mm]
u_p \frac{du_p}{dx} = \frac{1}{\tau_u}(u - u_p) , \\[2mm]
u_p \frac{dT_p}{dx} = \frac{1}{\tau_T}(T - T_p) .
\end{cases}
$$

Rather than eliminating T in the energy equation to come out with three differential equations containing u, u_p, and T_p, we preferred to show reduced magnitudes and phase disequilibria by writing:

$$
m \equiv \frac{1}{\gamma M^2} = \frac{rT}{u^2} ,
$$

$$
n \equiv \frac{u_p}{u} ,
$$

$$
p \equiv \frac{T_p}{T} .
$$

The function m was preferred to the Mach number M in the gas to facilitate writing the equations; it is easy to pass from m to M. A reduced variable can be introduced, as well as a new function F:

$$
X = \frac{x}{\tau_u \sqrt{2H(1+K)}} ,
$$

$$
F = \frac{1}{A}\frac{dA}{dx} .
$$

After the transform, we obtain:

$$\left\{ \frac{dm}{dx} = -\frac{m\left(2m + \frac{\gamma-1}{\gamma}\right)}{\frac{1}{\gamma} - m} F - \left(1 + Kn^2 + \frac{2\gamma}{\gamma-1} n(1 + K\beta p)\right)^{\frac{1}{2}} \left[\frac{1-n}{n} + (m+1)\frac{\left(\frac{\gamma-1}{\gamma}n - 1\right)\frac{1-n}{n} + \frac{2}{3\sigma_r}\frac{1-p}{n}m}{\frac{1}{\gamma} - m}\right], \right.$$

$$\left\{ \frac{dn}{dx} = -\frac{mn}{\frac{1}{\gamma} - m} F + \left(1 + Kn^2 + \frac{2\gamma}{\gamma-1} m(1 + K\beta p)\right)^{\frac{1}{2}} \left[\frac{1-n}{n} - Kn \frac{\left(\frac{\gamma-1}{\gamma}n - 1\right)\frac{1-n}{n} + \frac{2}{3\sigma_r}\frac{1-p}{n}m}{\frac{1}{\gamma} - m}\right], \right.$$

$$\left\{ \frac{dp}{dx} = \frac{\frac{\gamma-1}{\gamma}p}{\frac{1}{\gamma} - m} F + \left(1 + Kn^2 + \frac{2\gamma}{\gamma-1} m(1 + K\beta p)\right)^{\frac{1}{2}} \left[\frac{2}{3\sigma_r}\frac{1-p}{\beta n} + \frac{Kp}{m}\left\{\frac{1-n}{n} + (1-m)\frac{\left(\frac{\gamma-1}{\gamma}n - 1\right)\frac{1-n}{n} + \frac{2}{3\sigma_r}\frac{1-p}{n}m}{\frac{1}{\gamma} - m}\right\}\right]\right\}$$

These equations define a class of flows characterized by the loading parameter K, the thermal factor β, the Prandtl gas number (often taken as equal to 2/3) and the function F which depends on the nozzle contour, its scale (established by the throat radius r_c, for example) and the adimensional parameter:

$$\frac{\tau_u u_L}{r_c} ,$$

where u_L is the limit velocity of the mixture in equilibrium $(u_L = \sqrt{2H})$.

There is a single point for $m = 1/\gamma$, i.e., when the speed of sound is reached by the gas. At sonic velocity we must check:

$$F + K\left(1 + Kn^2 + \frac{2}{\gamma-1}(1 + K\beta p)\right)^{\frac{1}{2}}\left(\frac{1-p}{n} + \gamma \frac{1-n}{n}\left(\frac{\gamma-1}{\gamma}n - 1\right)\right) = 0 .$$

In a nozzle, velocity increases upon expansion, while temperature decreases, which makes it necessary for:

$$n < 1 , \quad p > 1 .$$

We deduce the condition for $M = 1$:

$$\frac{1-p}{n} + \gamma \frac{1-n}{n}\left(\frac{\gamma-1}{\gamma}n - 1\right) < 0$$

This inequality implies that the sonic section is always located downstream of the geometric throat $(F > 0)$.

The singularity for $m = 1/\gamma$ corresponds to a boundary condition. The two other conditions necessary for completely defining the problem are data for values n and p at the nozzle entrance for example.

All the flow values are deduced from m, n, and p, in particular the specific impulse delivered by the nozzle:

$$I = \frac{\sqrt{2H(1+K)}}{g_0(1+K)}\left\{\frac{1+Kn}{\left(1+Kn^2+\frac{2\tau}{\sigma-1}m(1+K\beta p)\right)^{\frac{1}{2}}}\right\}_{m=\frac{1}{\gamma}}$$

The specific impulse is thus affected by the values of magnitude m, n, and p taken in the outlet section, which in their turn depend on the whole history of the flow since its entrance into the nozzle, if for no other reason because of displacement of the sonic section due to phase shifts.

Variation in mass entropy of the mixture is given by the relation:

$$\frac{1}{\Gamma}\frac{dS}{dX} = \frac{K}{1+K}\left(1+Kn^2+\frac{2\tau}{\sigma-1}m(1+K\beta p)\right)\left[\frac{(1-n)^2}{nm}+\frac{2}{3\tau}\frac{(1-p)^2}{np}\right].$$

The local increase in the mixture's entropy does indeed depend upon the square of the kinetic and thermal deviations.

An important simplification occurs when we assume that inter-phase equilibrium is produced locally at every point in the nozzle.

Starting again from the initial system of equations -- without the condensed phase equations, replaced by the two kinetic equilibrium and thermal equilibrium hypotheses -- it is easy to show that the mixture behaves like an ideal non-viscous gas; this feature may be found from the general mixture equations (Section 4.4.): the mixture obeys the equations of a gas whose apparent viscosity becomes negligible when the phase lags are small. The properties of the equivalent gas are easily calculated:

$$\bar{\gamma} = \frac{\gamma(1+K\beta)}{1+K\beta\gamma} \quad,$$

$$\bar{r} = \frac{r}{1+K} \quad.$$

A new Mach number for the mixture can then be defined, based on the speed of sound at equilibrium ($a_c^e = \bar{\gamma}\bar{r}T$). The relation between the straight section of the nozzle and the Mach number upon equilibrium is given by the classical relation:

$$\frac{A}{A_c} = \frac{1}{\bar{M}}\left(\frac{1+\frac{\bar{\gamma}-1}{2}\bar{M}^2}{\frac{\bar{\gamma}+1}{2}}\right)^{\frac{\bar{\gamma}+1}{2(\bar{\gamma}-1)}} \quad.$$

Between the two Mach numbers we have the relation:

$$\bar{M} = M\sqrt{\frac{(1+K)(1+K\beta\gamma)}{1+K\beta}}$$

This relation shows that at the geometric throat: $\bar{M} = 1$ and $M < 1$; the sonic section for the gas is indeed situated in the diverging section.

The point of simplifying the two-phase equilibrium is to come out with a definition of a reference flow: this flow is the limit of the real flow when, at a constant load rating, the particle diameter becomes infinitely small; this fixes the upper limit of a nozzle performance for a given suspension.

We will briefly examine calculation methods when kinetic and thermal phase lags are taken into account.

a) Analytic Solutions:

Analytic solutions to the problem are known for certain types of nozzle. The contours are not known a priori but deduced from

-91-

other magnitudes assuming a given variation law for one of these magnitudes; the problem is thus one of squaring.

The most classic solution is that of "constant phase-shift" nozzles [44, 45]. We will assume that the ratio n of the velocities of the two phases is constant. The equation of particle motion is integrated to give:

$$u = \frac{1}{\tau_u} \frac{1-n}{n^2} x ,$$

$$u_p = \frac{1}{\tau_u} \frac{1-n}{n} x .$$

If we also assume that the ratio:

$$q = \frac{T_o - T_p}{T_o - T} ,$$

is constant, the heat equation of the particles and the overall energy equation are consistent provided that n and q are linked by the relation:

$$\frac{1-q}{q} = 3\sigma_r \beta \frac{1-n}{n} .$$

This gives:

$$T_o - T = \frac{1+Kn^2}{2} \left(\frac{1}{\tau_u} \frac{1-n}{n^2} \right)^2 \frac{x^2}{C_p + KC_s q} ,$$

$$T_o - T_p = \frac{1+Kn^2}{2} \left(\frac{1}{\tau_u} \frac{1-n}{n^2} \right)^2 \frac{x^2 q}{C_p + KC_s q} .$$

The nozzle is between the abscissas $x = 0$ and $x = x_i$, for which the limit velocity of flow is reached: the nozzle section for these two abscissa values is infinite. It is easily seen that the corresponding nozzle contours have very open converging and diverging sections; the throat is very long.

It is possible to show that a mixture behaves like a gas; the properties of this gas depend upon n the choice of which establishes the nozzle length.

Due to their shape, "constant phase-shift" nozzles are not used
a great deal for propulsion; they would lead increased losses, prin-
cipally because of the sharp divergence of the jet. However, this
theory is sometimes used to make a rough estimate of loss due to
phase shifts for a given nozzle: we know that phase shifts are at
their maximum in the throat region; we thus call the nozzle's throat
a "constant phase-shift" nozzle. The following relation will be
used:

$$\frac{d\bar{u}}{dx}\Big|_c = \frac{\varepsilon}{\bar{\gamma}+1}\sqrt{\frac{\bar{\gamma}\bar{r}T_c}{\bar{r}_c R_c}} = \frac{1}{\bar{r}_u}\frac{1-n}{n^2}\frac{1+Kn}{1+K}$$

$\bar{\gamma}$ and $\bar{r}$ are dependent upon n; we thus obtain an algebraic equation
for n which is resolved according to the problem data.

This calculating technique can be extended to other nozzle
contours, either considering a given function n(x) [33] or a given
$u_p(x)$ function [46, 47]. It is generally essential to use
the computer except for laws: $u_p = kx$ and $u_p = k\sqrt{x}$.

b) Approximate Solutions:

The equations proposed are valid whatever the flow loading and
particle diameter. The flows studied here are characterized by a
moderate loading and particles of microscopic size, and it is legit-
imate to investigate whether these features can give rise to useful
simplifications.

The general equations can be brought down to an adimensional
form. The parameter characterizing the particle size is written:

$$\varepsilon = \frac{\bar{r}_u u_r}{\bar{r}_c} \quad ,$$

the throat radius, for instance, being chosen as the reference
length. This parameter is, at most, about unity for large motors.
If absolutely necessary it can serve as a perturbation parameter
[5, 48]. The principle of the perturbation method is to assume

that all the functions can be developed according to a certain sequence of ε functions (the whole powers of ε, in a large number of problems). For example, we write:

$$u = u_0 + \varepsilon u_1 + \varepsilon^2 u_2 + \ldots ,$$

$$u_s = u - u_p = u_{s_0} + \varepsilon u_{s_1} + \varepsilon^2 u_{s_2} + \ldots$$

The initial system of equations leads, by identification of the powers of ε, to a system of new equations enabling us to determine, in succession, the functions of u_0, u_{s_0} ..., u_1, u_{s_1} ..., etc. Calculations are rarely taken beyond the first order due to the increasing complexity of the expression. The particle motion equation is written, in reduced variables:

$$\varepsilon u_p^* \frac{du_p^*}{dX} = u^* - u_p^* = u_s^*$$

or, after substituting for u_p^* and u_s^* their developments with ε and ordering the power of ε in each member:

$$\varepsilon (u_0^* - u_{s_0}^*)\frac{d}{dX}(u_0^* - u_{s_0}^*) + \varepsilon^2 \left[(u_1^* - u_{s_1}^*)\frac{d}{dX}(u_0^* - u_{s_0}^*) + (u_0^* - u_{s_0}^*)\frac{d}{dX}(u_1^* - u_{s_1}^*)\right]$$

$$+ \ldots = u_{s_0}^* + \varepsilon u_{s_1}^* + \varepsilon^2 u_{s_2}^* + \ldots$$

We immediately get:

$$u_{s_0}^* = 0 ,$$

then:

$$u_{s_1}^* = u_0^* \frac{du_0^*}{dX} .$$

In the same way, we find:

$$T_{s_0} = 0 ,$$

$$T_{s_1} = \frac{3\sigma_r}{2} u_0^* \frac{dT_0}{dX} .$$

These relations signify on the one hand that non-perturbed flow ($\varepsilon = 0$) is that corresponding to two-phase equilibrium and, on the other hand, that the first terms of the perturbation are deduced from the local state of non-perturbed flow. This is an

asymptotic theory when it is limited to the first order: the two-phase relaxation times are sufficiently slow compared with the dwell time in the nozzle for the condensed phase to reach almost instantaneously a state fixed by the reference flow gradients. We judge the validity of this hypothesis, for example:

$$\varepsilon \; \frac{u_{s_1}}{u_o} \; << 1 \; .$$

For classic nozzles the velocity gradient is at its maximum in the throat region. We must thus verify:

$$\frac{\ell \, \tau_u}{\overline{\gamma} + 1} \sqrt{\frac{\overline{\gamma r T_o}}{r_c \, R_c}} \; << 1 \; .$$

This condition is fulfilled for fairly large motors and the great majority of particles. This method can thus be usefully applied; we must, however, note that the phase shifts calculated in this way have discontinuities of slope linked with discontinuities of curvature of the meridian (biconical nozzles, for example). These calculations are unsuitable for certain contours (nozzles with cylindrical throats).

When the particles are no longer small enough for the near equilibrium theory to be applicable, one can proceed by successive approximations [49]. Since the reference flow corresponds to phase equilibrium, we study the evolution of velocity and temperature of the particles in this flow. We can thus calculate the inter-phase interaction terms in the first approximation, then give a second approximation for gaseous flow, etc. In this method, which takes into account inter-phase relaxation phenomena, it is necessary to make numeric calculations.

c) <u>Computer Solutions</u>

Computer processing of a system of reduced differential equations is made difficult by the existence of a single point for

-95-

$m = 1/\gamma$ ($M = 1$, in the gas) and by the fact that the position of this single point is not known a priori. For a given nozzle, there is only one initial value m_o which permits passage of the single point; all the different values of this value lead to solutions with infinite branches, physically unacceptable. Little work has been done on the computer problem linked to investigating this initial value [50, 51, 52]. It is possible [53] to use a different variable, of the form:

$$\mathcal{Z} = \left(\frac{1}{\gamma} - m\right)^2 ,$$

A computer program was developed with the aid of the ONERA computer center. It has the following three parts:

- search for initial value m_o: this is done by successive approximations. If the value chosen is too high, dm/dx cancels out in one computing step. If it is too low, $1/\gamma - m$ cancels out in one computing step without the n, p, F condition being fulfilled. Starting from the two extreme values given by the two hypotheses: two-phase equilibrium flow, and flow of just one gas, one progressively reduces the interval in which m_o may be found. The calculation is done in double precision.

- passage of single point: when one estimates that the value m_o is sufficiently approximate, namely that integration can be done up to a very close value without difficulty, one passes the single point by an analytical method, for example assuming that u_p is a linear function of x. Values are thus defined shortly after the single point.

- integration in the nozzle's supersonic zone.

The computing time is fairly long, even for a high-capacity computer (IBM 360). For this reason, and also because of the poor representativeness of the model used, these calculations were not run systematically.

Figure 21 shows results with n and ρ under the given operating
conditions. Approximation of the near equilibrium is indicated
for comparison; discrepancy with calculations is substantial despite
the high ratio between the throat radius of curvature and the throat
radius. Indeed, we find that the near equilibrium theory is not
applicable in this case:

$$\frac{2\tau_u}{\delta+1} \sqrt{\frac{\delta - T_0}{r_c R_c}} = 0.712 .$$
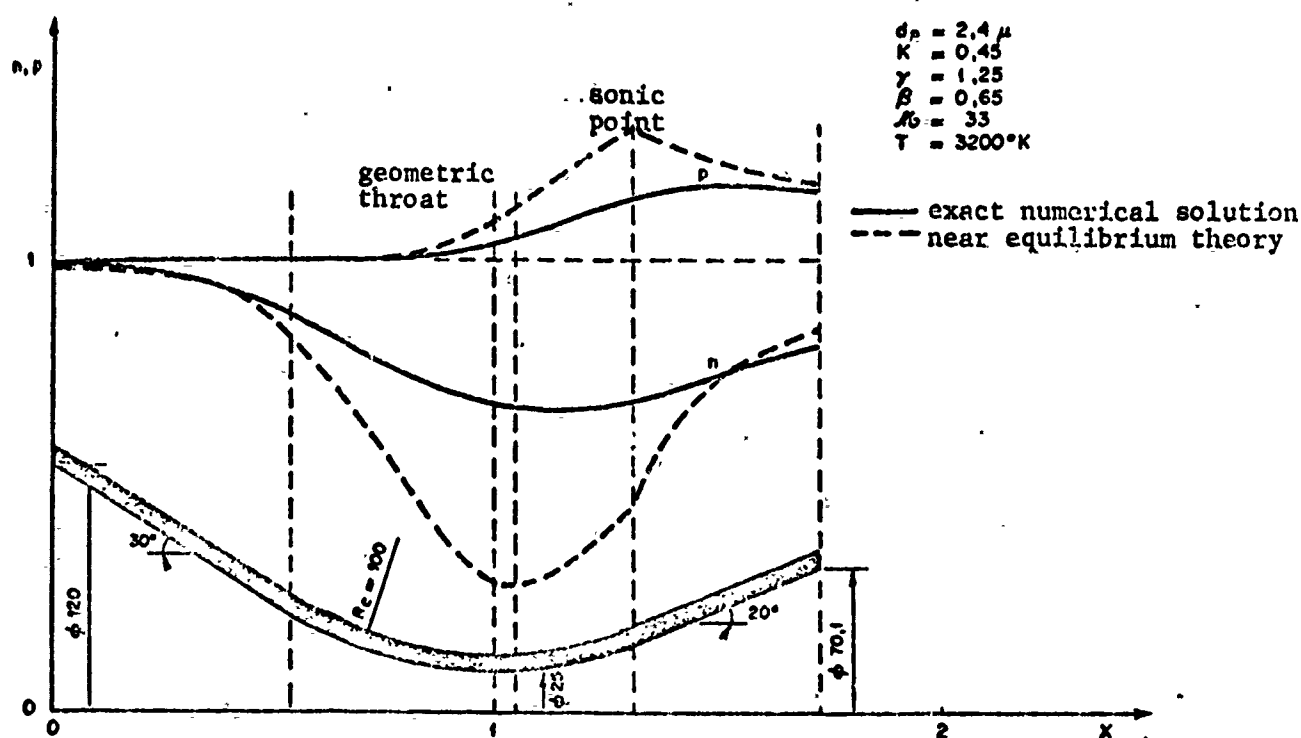
Figure 21. Kinetic and Thermal Phase Shifts in a Biconical
Nozzle (Simplified Model).

4.5.2. Representativeness of Simplified Model

We need to investigate whether the simplified scheme presented
is realistic enough for the suspension being studied. We must
examine, first, whether the behavior of the gaseous phase or the con-
densed phase is truely represented, and secondly whether the
hypothesis of flow in sections is adequate.

-97-

a) Behavior of Gaseous Phase:

The gaseous phase is not an ideal gas, rather a multi-reactive
high-temperature and high-pressure mixture. The chemical relaxations
make it difficult to process this type of flow on the computer. In
principle, we can take chemical relaxation into account by assuming
that the gaseous phase is comparable witha Lighthill gas; we showed
that the system then has four equations for gas temperature and velo-
city and phase shifts n and p, and that the single   point is reached
when the gas velocity is equal to the speed of sound fixed in the
gas. Unfortunately this comparison is far from realistic here.
Accordingly, we generally confined ourselves to calculations with
the hypothesis that the reactions were frozen in the chamber condi-
tions (infinitely slow rate of reaction) or the hypothesis of con-
tinuous thermodynamic equilibrium (reaction rates infinitely fast).
In both these conditions, and taking into account the actual thermo-
dynamic properties of the combustion products, the system of equa-
tions cannot be reduced as in the simplified scheme, but its
processing does not raise any further problems.

We must also take into account the variation in transfer para-
meters with temperature. This can be included when viscosity μ and
conductivity λ are substantially proportional to the square root of
the temperature, which is a good approximation to Sutherland's law
at high temperatures:

$$\mu = \mu_0 \sqrt{\frac{T}{T_0}} \, ,$$

$$\lambda = \lambda_0 \sqrt{\frac{T}{T_0}} \, .$$

We can then define the characteristic relaxation length of the
flow using the speed of sound in the gas:

$$\lambda_u = a \, \tau_u = a_0 \, \tau_{u_0} \, ,$$

$$\lambda_T = a \, \tau_T = a_0 \, \tau_{T_0} \, .$$

The reduced equations are very much comparable in this case to the case when μ and λ are constant. The only changes are the substitution of:

$$\left(\frac{2\gamma}{\gamma-1}m\right)^{\frac{1}{2}} \geqq \left(1+Kn^{2}+\frac{2\gamma}{\gamma-1}m(1+K\beta\rho)\right)^{\frac{1}{2}},$$

and:

$$\tilde{u}_{o}\sqrt{2H(1+K)} \geqq \tilde{u}\sqrt{2H(1+K)}.$$

Finally we should note that flow around the particles can be considerably different from that of Stokes law. The correction coefficients ℓ_{u} and ℓ_{T} to be made to the drag coefficient and the Nusselt number bring in the relative Reynolds and Mach numbers:

$$Re_{R} = \frac{\dot{m}d_{p}}{\mu_{o}A_{c}} \times \frac{\mu}{\mu_{o}} \times \frac{1-n}{\frac{A}{A_{c}}},$$

$$M_{R} = \frac{1-n}{\sqrt{\gamma m}}.$$

We see a new parameter of similitude for this type of flow. This corresponds to the coefficient Re_{R}:

$$\frac{\dot{m}d_{p}}{\mu_{o}A_{c}} \simeq \frac{P_{o}d_{p}}{C^{*}\mu_{o}},$$

where C*. can be calculated in the first approximation for equilibrium.

The equations are only slightly modified by introducing ℓ_{u} and ℓ_{T}. The effects of these corrections can be fairly striking since in the Stokes law · the drag coefficient is under-estimated and the particles actually drag less than this hypothesis predicts. These effects, of course, depend on the nozzle size.

b) Behavior of Condensed Phase:

The hypothesis of particles with uniform and constant diameters is unrealistic since we have shown that the particles have a broad diameter distribution and agglomerate during expansion. We must

also check whether the volume fraction of the particle is indeed negligible, and modify the equations to take solidification into account.

The equations can be established without too much difficulty taking account of the volume occupied by the condensed phase. When the general equations were established it was shown that a fictitious volume mass of the gaseous phase had to be established and the equation of state had to be modified as a consequence. The two-phase equilibrium flow is no longer equivalent to that of a gas; the sonic point for the mixture is situated upstream of the geometric throat. The relaxed two-phase flow is again described by three relations containing n, m, and p. A new parameter of similitude appears:

$$\eta = \frac{\overset{o}{m}}{K \rho_c A_c \sqrt{2H(1+K)}} \approx \frac{P_o}{K C^* \rho_c \sqrt{2H(1+K)}}.$$

The single point corresponds to:

$$m = \frac{1}{\gamma} - \eta \frac{\left(1 + Kn^2 + \frac{2\gamma}{\gamma-1} m \left(1 + K\beta p\right)\right)^{\frac{1}{2}}}{n \frac{A}{A_c}}$$

Rudinger [55] integrated the equations for different suspension loadings. These calculations showed that the particle volume became large only when ε was greater than 0.01. For all metallized propellants and all utilization conditions, ε is always far lower than this value. Thus the volume of the condensed phase is indeed negligible.

When alumina solidifies in the diverging section of the nozzle, the equations giving the temperature of the condensed phase can no longer be used. The condensed phase temperature is constant during solidification and a new variable f, corresponding to the volume fraction of the condensed phase which is solidified, must be introduced. The heat balance of a particle gives the equation for f:

$$u_p \frac{df}{dx} = - \frac{c_L \mathcal{C}_T}{\mathcal{C}_T L_f} (T - T_{pf}) \quad , \quad (0 \leqslant f \leqslant 1),$$

The general energy equation must also be modified:

$$C_p T + \frac{u^2}{2} + K(C_s T_{pf} + \frac{u_p^2}{2}) = H(1+K) + K f L_f.$$

After solidification, one uses the initial equations again, but with a new value for generating enthalpy. Reference [33] shows the equations with m, n, and p to be used during and after solidification. To find out the influence of this phenomenon on phase lags   we used a perturbation method. The non-perturbed flow leads to knowledge of function $f^{(o)}(x)$ which depends only on the section ratio; u varies much more slowly than in the absence of solidification, which is favorable from the viewpoint of kinetic phase lags.   In the first order it appears that temperature deviation tends to increase. The influence of solidi-- fication on specific impulse must thus be determined by calculation.

We must also take into consideration the particle distribution and evolution. This evolution is not independent of the flow of the combustion products as collisions are principally due to differences in average velocity between particles of different sizes. The most complete calculations are those in which the particles are divided into a limited number of classes, a series of equations is established for each of these classes, and account is explicitly taken of collisions and agglomerations [29]. The precision of these calculations is limited by uncertainties as to collision yields [30]. When the near equilibrium theory is applicable, in the first approximation the flow problem is separated from the particle agglomeration problem; indeed the particle veloci- ties can be calculated from the flow characteristics in equilib- rium and the changes in the various mean radii calculated in expansion, as shown in Section 3.3.4. In these circumstances, local particle distribution is a datum to be inserted in the flow calculation and it is useful to be able to characterize the condensed phase by a single mean diameter. Attempts in this direction are limited [48] and a wide variety of "effective"

diameters are found in the literature: these are d_{32}, d_{43}, d_{53} ....
It is however possible to show that a single definition agrees with
the initial hypotheses.

Let us go back to the expressions for u_p and e_p:

$$u_P = \frac{1}{\rho_P} \iiint m(\sigma) c f \, d^3 c_d \, dc \, d\sigma ,$$

$$e_P = \frac{1}{\rho_r} \iiint m(\sigma) e f \, d^3 c_d \, dc \, d\sigma .$$

If we assume:

$$c \simeq u^{(e)}\left(1 - \tau_u \frac{du^{(e)}}{dx}\right) ,$$

$$e \simeq e^{(e)}\left(1 - \tau_T \frac{u^{(e)}}{T^{(e)}} \frac{dT^{(e)}}{dx}\right) ,$$

we immediately get:

$$u_P = u^{(e)}\left(1 - \overline{\tau_u} \frac{du^{(e)}}{dx}\right) ,$$

$$T_P = T^{(e)}\left(1 - \overline{\tau_T} \frac{u^{(e)}}{T^{(e)}} \frac{dT^{(e)}}{dx}\right) ,$$

where $\overline{\tau}_u$ and $\overline{\tau}_t$ are based on the mean radius r_{53} defined by the
relation:

$$r_{53}^2 = \frac{\iiint \sigma^5 f \, d^3 c_d \, dc \, d\sigma}{\iint \sigma^3 f \, d^3 c_d \, dc \, d\sigma}$$

With the same hypotheses, the between-phase coupling terms are
written:

$$\overline{\tau}_{Px} \simeq \rho_P u^{(e)} \frac{du^{(e)}}{dx} ,$$

$$Q \simeq c_e \rho_P u^{(e)} \frac{dT^{(e)}}{dx} .$$

In fact, all we need to do is to find out the change in r_{53} as a function of A/A_c or x to perform the calculation in the classical manner. It has been already shown that high-order moments of the distribution law are those most poorly known experimentally and that they undergo considerable variation during expansion. Because of this, particle agglomeration appears to be something which cannot be left out of a realistic calculation method and incomplete knowledge of the condensed phase will necessarily result in fairly large uncertainty in predicting specific impulse losses.

c) Two-Dimensional Effects:

The hypothesis of flow in sections must be considered as a first approximation; this description is known to be inadequate even for a homogeneous fluid (calculation of wall pressures in the throat region, optimization of contour, etc.). This inadequacy is even more marked for suspension flows due to the non-uniform distribution of the condensed phase in the gaseous phase.

This distribution is generally uniform in the chamber due to the reduced particle size, the low flow velocities, and the small geometric variations of the cavity. On the other hand the nozzle flow is characterized by contraction then expansion of the jet, considerable accelerations, and particle growth. Differences between the velocity components normal to the nozzle access are thus produced. Their effect is that the condensed phase tends to concentrate in the nozzle axis. This segregation is amplified by the fact that when the particles concentrate, collision frequencies and their mean dimensions increase as a consequence.

To our knowledge there are no two-dimensional calculation methods which take particle growth into account; introduction of a particle distribution according to particle diameter is very rare [43]. The particle diameter is almost always assumed to be constant and uniform, and collisions are accordingly neglected.

All the nozzle zones are not treated identically. The converging section flow is treated like a well flow with uniform spatial distribution of the condensed phase or in one-dimensional analysis. Analysis of the transsonic zone requires us to resort to some simplifications due to its complexity. We can calculate trajectories in the velocity field determined by phase equilibrium; this is an extension to the two-dimensional problem of the perturbation method [32, 56, 57].

The constant phase lag hypothesis can also be generalized to the two-dimensional problem [43]. These calculations enable initial conditions to be defined so that we can start a calculation of characteristics in the supersonic portion of flow [58, 59, 60]. The results of this calculation can be compared to those of the one-dimensional approximation when corrected by the jet divergence effect: we find that this underestimates the loss linked with the condensed phase [56, 61]. The influence of non-homogeneous distribution of the condensed phase is thus injurious.

The actual behavior of combustion products of a solid metallized propellant is thus incompletely described by the simplified scheme of Paragraph 4.5.1. A realistic scheme must take into consideration the multireactive nature of the gaseous phase (in one or the hypotheses, frozen or in equilibrium), particle growth, and segregation of the condensed phase in the flow. Formulas can be established to calculate the specific impulse loss due to the condensed phase under the most general conditions provided that the particles are either very small or very large; an estimate of two--dimensional effects can also be made.

4.6. FORMULAS FOR CALCULATING SPECIFIC IMPULSE LOSS

Specific impulse loss depends on the entire history of the particles and exchanges between phases starting from the nozzle entrance, which explains why the flow must be fully calculated before we can find out the specific impulse. Apart from the case of nozzles

with a constant velocity gradient, not useable for propulsion, there
are no absolutely general formulas for calculating losses. If we
assume, however, that the particles are very small, their velocity
and temperature will be very close to those of the gaseous phase
(near equilibrium) and we may seek a valid formula under these
conditions. Also, if the particles are very large, they virtually
do not participate in expansion and a formula can also be sought.
The usefulness of these approximate formulas is to permit a rapid
estimate of the specific impulse loss for very small or very large
motors and relatively simple discussion of the influence of the
various operating parameters.

4.6.1. Specific Impulse Loss in Near Equilibrium

Near equilibrium calculation is relatively classical [5, 7]
although it still needs to be extended to a condensed phase whose
particles are growing and a multireactive gaseous mixture. This
was done in [62]. The demonstration calls upon the mean entropy
of the mixture as a characteristic of irreversible exchanges
between phases. Here we propose to establish the same formula by
a slightly different route.

We will take the general equations for a chemically frozen
gaseous flow: .

$$
\begin{cases}
\rho u A = \dot{m}_g , \\[4pt]
\rho_p u_p A = \dot{m}_p , \\[4pt]
\rho u \left(\dfrac{du}{dx} + K \dfrac{du_p}{dx} \right) + \dfrac{dp}{dx} = 0 , \\[4pt]
h(T) + \dfrac{u^2}{2} + K \left[c_p(T_p) + \dfrac{u_p^2}{2} \right] = (1+K) H , \\[4pt]
p = \rho r T ,
\end{cases}
$$

+ condensed phase equations.

We will define some new functions:

$$\begin{cases} \rho' = \rho(1+K) , \\[6pt] u' = u , \qquad u_s = u - u_p , \\[6pt] T' = T , \qquad T_s = T - T_p , \\[6pt] h'(T') = \dfrac{h(T) + K\, c_p(T)}{1+K} , \\[6pt] P' = P , \\[6pt] r' = \dfrac{r}{1+K} . \end{cases}$$

This is not only a change of functions: the magnitudes marked with
the ' are different from the average magnitudes of the mixture.
When we group the terms depending on u_s and T_s in the second member,
we obtain:

$$\begin{cases} \rho' u' A = \overset{\circ}{m} , \\[8pt] h'(T') + \dfrac{u'^2}{2} = H + \dfrac{K}{1+K}\left(c_s T_s + u\, u_s - \dfrac{u_s^2}{2}\right) , \\[8pt] \rho' u' \dfrac{du'}{dx} + \dfrac{dp'}{dx} = \dfrac{K}{1+K}\, \rho' u' \dfrac{du_s}{dx} , \\[8pt] P' = \rho' r' T' , \\[4pt] + \text{condensed phase equations} \end{cases}$$

For infinitely small particles the velocity and temperature
differences between phases u_s and T_s are identically zero and the
' magnitudes relate to the mixture at two-phase equilibrium. Since
the particles are of finite size, the temperature and velocity dif-
ferences between phases which arise perturb the flow of the mixture,
as the equations show. We can define an entropy variation by:

$$dh' = T' ds' + \dfrac{dp'}{\rho'} .$$

From this we get:

$$ds' = \dfrac{K}{1+K} \cdot \dfrac{c_s\, dT_s + u_s\, du' - u_s\, du_s}{T'} .$$

The momentum equation can then be replaced by:

$$s'(T') - s'(T_0) = \frac{K}{1+K} \int_0^\infty \frac{c_s dT_s + u_s du' - u_s du_s}{T'}.$$

Calculation is done as follows:

- A first approximation of u_s and T_s, anotated $u_s^{(0)}$ and $T_s^{(0)}$ is given
  by studying the condensed phase equations. The result is classical:

$$u_s^{(0)} = \bar{\tau}_u \, \bar{u}^{(0)} \frac{d\bar{u}^{(0)}}{dx}, \qquad T_s^{(0)} = \bar{\tau}_T \, u^{(0)} \frac{dT^{(0)}}{dx}.$$

The variables with an overbar correspond to the two-phase mixture
and the $^{(0)}$ indicates that we are talking about the first approxima-
tion; $\bar{u}^{(0)}$ and $T^{(0)}$ are evidently the velocity and temperature of
the reference flow (two-phase equilibrium). $\bar{\tau}_u$ and $\bar{\tau}_t$ are calcu-
lated with the local mean diameter r_{53}.

- We enter terms $u_s^{(0)}$ and $t_s^{(0)}$ in the preceding equations, neglect-
  ing the second-order terms, and calculate the ' magnitudes. A
  linearized method is still used. We define the differences:

$$\delta\rho' = \rho' - \bar{\rho}^{(0)},$$
$$\delta u' = u' - \bar{u}^{(0)} \ldots,$$

The linearized system is written:

$$
\begin{cases}
\dfrac{\delta\rho'}{\bar{\rho}^{(0)}} + \dfrac{\delta u'}{\bar{u}^{(0)}} = \dfrac{\delta \overset{\circ}{m}}{\overline{m}^{(0)}}, \\[2mm]
\overline{c_{pf}}^{(0)} \, \delta T' + \bar{u}^{(0)} \delta u' = \dfrac{K}{1+K}\left(c_s T_s^{(0)} + \bar{u}^{(0)} u_s^{(0)}\right) = (\delta h')_a, \\[2mm]
\overline{c_{pf}}^{(0)} \dfrac{\delta T'}{\overline{T}^{(0)}} - r' \dfrac{\delta\rho'}{\bar{\rho}^{(0)}} = \dfrac{K}{1+K} \int_0^\infty \dfrac{c_s dT_s^{(0)} + u_s d\bar{u}^{(0)}}{\overline{T}^{(0)}} = (\delta s')_a, \\[2mm]
\dfrac{\delta p'}{\bar{p}^{(0)}} = \dfrac{\delta\rho'}{\bar{\rho}^{(0)}} + \dfrac{\delta T'}{\overline{T}^{(0)}}.
\end{cases}
$$

-107-

Resolution of the system by matrix calculus leads to expressions for $\delta p'$, $\delta u'$, etc. In particular:

$$\begin{cases} \delta u' = -\bar{u}^{(e)} \dfrac{\dfrac{\delta \dot{m}}{\bar{\dot{m}}^{(e)}} + \dfrac{(\overline{\delta s'})_a}{\Gamma'} - \dfrac{(\overline{\delta h'})_a}{\bar{a}_f^{(e)2}}}{\dfrac{\bar{u}^{(e)2}}{\bar{a}_f^{(e)2}} - 1} \, , \\[3em] \delta p' = \bar{\rho}^{(e)} \dfrac{\bar{u}^{(e)2} \dfrac{\delta \dot{m}}{\bar{\dot{m}}^{(e)}} + \dfrac{\overline{C_{pf}^{(e)} T^{(e)}} + \bar{u}^{(e)2}}{\overline{C_{pf}^{(e)}}} (\overline{\delta s'})_a - (\overline{\delta h'})_a}{\dfrac{\bar{u}^{(e)2}}{\bar{a}_f^{(e)2}} - 1} \, . \end{cases}$$

The denominator cancels out at the geometric throat for $\bar{u}^{(o)} = \bar{a}_f^{(o)}$. The common condition for cancelling out the numerators of the second members is written:

$$\frac{\delta \dot{m}}{\bar{\dot{m}}^{(e)}} = - \frac{(\overline{\delta s'})_a^*}{\Gamma'} + \frac{(\overline{\delta h'})_a^*}{\bar{a}_\rho^{(e)2*}}$$

Variation in characteristic velocity is directly connected to variations of mass flow. We find, assuming that C_s varies but little:

$$\frac{\delta C^*}{\bar{C}^{*(e)}} = - \frac{\delta \dot{m}}{\bar{\dot{m}}^{(e)}} \simeq \frac{\varepsilon}{\Gamma'} \int_0^{x^*} \overline{\tau_u} \frac{\bar{u}^{(e)}}{\bar{T}^{(e)}} \left(\frac{d\bar{u}^{(e)}}{dx}\right)^2 \left[1 + \frac{3}{2} \overline{\sigma_f^{(e)}} \beta^2 \frac{\bar{u}^{(e)2}}{\overline{C_{pf}^{(e)} T^{(e)}}}\right] dx$$

$$- \varepsilon \left[(\overline{\tau_u} + \beta(\overline{\sigma_f^{(e)}} - 1) \overline{\tau_f}) \frac{d\bar{u}^{(e)}}{dx}\right]^* .$$

The two terms have opposite signs, so that we can conclude only as to the sign of the characteristic velocity variation.

Specific impulse is defined with the hypothesis of a suitable reference flow corresponding to:

$$\bar{I}_A^{(e)} = \frac{\bar{u}_A^{(e)}}{g_0} \quad , \quad \left(\bar{p}_A^{(e)} = p_A\right) .$$

The actual specific impulse is linked on the one hand to the velocity difference in the outlet section and on the other hand to the pressure difference translating the unsuitability of the nozzle. We get:

$$\frac{\delta I}{I^{(o)}} = \frac{\delta u_A'}{u_A^{(o)}} + \frac{A_A \; \delta p_A'}{\mathring{m}^{(o)} \; u_A^{(o)}} - \varepsilon \; \frac{u_S^{(o)}}{u_A^{(o)}} \quad .$$

The sought-for result is obtained by substituting for $\delta u'$, $\delta p'$, $u_s^{(o)}$ their expression as functions of $u^{(o)}$ and $T^{(o)}$. Many te are eliminated and, extending calculations to the solidification case, we finally obtain, neglecting variations of C_s:

$$\frac{|\delta I|}{I^{(o)}} = \varepsilon \; \frac{T_A^{(o)}}{u_A^{(o)^2}} \int_{x_o}^{x_o} \tau_u \; \frac{u^{(o)}}{T^{(o)}} \left(\frac{d u^{(o)}}{dx}\right)^2 \left[1 + \frac{3}{2} \sigma_{rp}^{(o)} k^2 \frac{u^{(o)^2}}{C_p^{(o)} T^{(o)}}\right] dx$$

where $k = \beta$ without solidification,
and $k - 1/\varepsilon$ during solidification.

a)   Domain in Which Formula is Valid

The proposed formula generalizes the results obtained by the same process but with far less realistic hypotheses [7]. Its accuracy is, however, limited by the necessary simplifications. Local velocity of the condensed phase is obtained in near equilibrium and as it has been demonstrated that this hypothesis over-estimates the phase lags (Figure 21) and the influence of the largest particles. This effect is accentuated by the increase in the drag coefficient with respect to the value calculated with Stokes law when the Reynolds number in question is greater than 1. Linearization of the equations around the equilibrium values also introduces an approximation, which can however be avoided by directly determining the magnitudes rather than their differences with respect to equilibrium. We should finally point out that the useful diameter r_{53} is rather poorly known due to the fragmentary analysis of the large particles.

Strictly speaking, the proposed formula should only be used when the following condition is fulfilled:

$$\tau_u \; \frac{d u^{(o)}}{dx} \ll 1 \quad .$$

This formula relates to large motors only. We might try to extend it empirically to smaller motors in view of experimental results.

b) Practical Calculation of Specific Impulse Loss

In the calculation, $\bar{\tau}_u$ is a magnitude which varies with x due to particle growth in the nozzle and can be brought back to its nozzle entrance value:

$$\frac{\overline{\tau_u}}{\tau_{u_o}} = \left(\frac{d_{53}}{d_{53_o}}\right)^2 \times \left(\frac{\rho_c}{\rho_{c_o}}\right) \times \left(\frac{\mu}{\mu_o}\right)^{-1}.$$

The quantity characterizing the particle size changes is:

$$q(x) = \left(\frac{d_{53}}{d_{53_o}}\right)^2$$

Figure 16 gives an example of function q(x); variations in q(x) are large in the present problem and cannot be neglected.

The formula is written in the form:

$$\left|\frac{\delta I}{I^{(o)}}\right| = \varepsilon\, \overline{\tau_{u_o}}\, \frac{\overline{T_A^{(o)}}}{U_A^{(o)2}} \int_{x_o}^{x_A} q(x) \frac{\rho_c}{\rho_{c_o}}(T^{(o)}) \frac{\mu_o}{\mu}(T^{(o)}) \frac{U^{(o)}}{T^{(o)}}\left(\frac{dU^{(o)}}{dx}\right)^2 \left[1 + \frac{3}{2}\overline{U_q^{(o)}}^2 R^2 \frac{U^{(o)2}}{C_p^{(o)} T^{(o)}}\right] dx$$

$$= \varepsilon\, \overline{\tau_{u_o}}\, \frac{\overline{T_A^{(o)}}}{U_A^{(o)2}} \int_0^{\zeta_A} \frac{\rho_c}{\rho_{c_o}}(T^{(o)}) \frac{\mu_o}{\mu}(T^{(o)}) \frac{U^{(o)}}{T^{(o)}}\left(\frac{dU^{(o)}}{d\zeta}\right)^2 \left[1 + \frac{3}{2}\overline{U_q^{(o)}}^2 R^2 \frac{U^{(o)2}}{C_p^{(o)} T^{(o)}}\right] d\zeta,$$

$$\text{où}\quad \zeta = \int_{x_o}^x \frac{dx}{q(x)}.$$

Particle growth is translated by a distortion of the integration interval. This distortion particularly concerns the areas furthest from the nozzle entrance; where the particles are largest. Although

in the expansion of a solid particle suspension the throat plays a
predominant role, in the case of liquid particles the diverging
section is the important element.

To simplify calculation it is useful to introduce non-dimensional
magnitudes into the formula. We will write:

$x = x/L$, where L is a characteristic length, $\quad \overline{M}^{(i)} = \dfrac{\overline{u}^{(i)}}{\overline{a}^{(i)}}$.

We get:

$$\left|\frac{\delta I}{I^{(i)}}\right| = \varepsilon \, \frac{\overline{\tau}_{u_0} \overline{a}_0^{(i)}}{L} \, \frac{\overline{\delta}_0}{\overline{\delta}_A \overline{M}_A^{(i)2}} \int_{X_0}^{X_s} q \, \frac{\rho_c}{\rho_{c_0}} \, \frac{\mu_0}{\mu} \left(\frac{T^{(i)}}{T_0}\right)^{\frac{1}{2}} \left(\frac{\gamma}{\gamma_0}\right)^{\frac{3}{2}} \overline{M}^{(i)}\left(1 + \gamma(\overline{\gamma}-1)\overline{M}^{(i)2}\right) \times$$

$$\times \left(\frac{1 + \frac{\overline{M}^{(i)}}{2\overline{\gamma}} \frac{d\overline{\gamma}}{d\overline{M}^{(i)}}}{1 + \delta \frac{\overline{\gamma}-1}{2} \overline{M}^{(i)2}}\right)^2 \left(\frac{d\overline{M}^{(i)}}{dX}\right)^2 dX ,$$

where $\gamma = \frac{3}{2} \tau_{rf}^{\overline{(o)}} k^2$ and $\delta = 1$ during isentropic expansion ($k = \ell$),
$\delta = 0$ during solidification of the condensed phase.

The influence of the operating parameters of the motor can be
summarized briefly [62]:

- This loss is directly proportional to the metal charge of the
  propellant by means of ε.

- The influence of the geometry will be examined later on when we
  investigate the possibilities of reducing specific impulse losses.
  The nozzle entrance section ratio should not have any substantial
  effect although the organization of flow in the entrance zone
  acts on the particle size.

- The nozzle outlet section ratio is linked to the expansion ratio.
  Calculation enables us to plot the curve of Figure 22 which gives,
  as a function of expansion ratio, the relative specific impulse
  loss brought to its value in the reference conditions. We see
  that it increases with the expansion ratio but remains in the
  same order of magnitude.

- The scale of the motor is manifested explicitly by L; in the first
  analysis the loss will be inversely proportional to the motor scale.
  In actual fact when the motor scale increases the dwell time also
  increases as does growth in the mean particle size at the nozzle
  entrance (there is possibly more marked growth of particles in
  the nozzle [28] but this effect has not been confirmed). The
  scope of validity of the formula is limited, but its application
  to estimating total specific impulse losses permits surprisingly
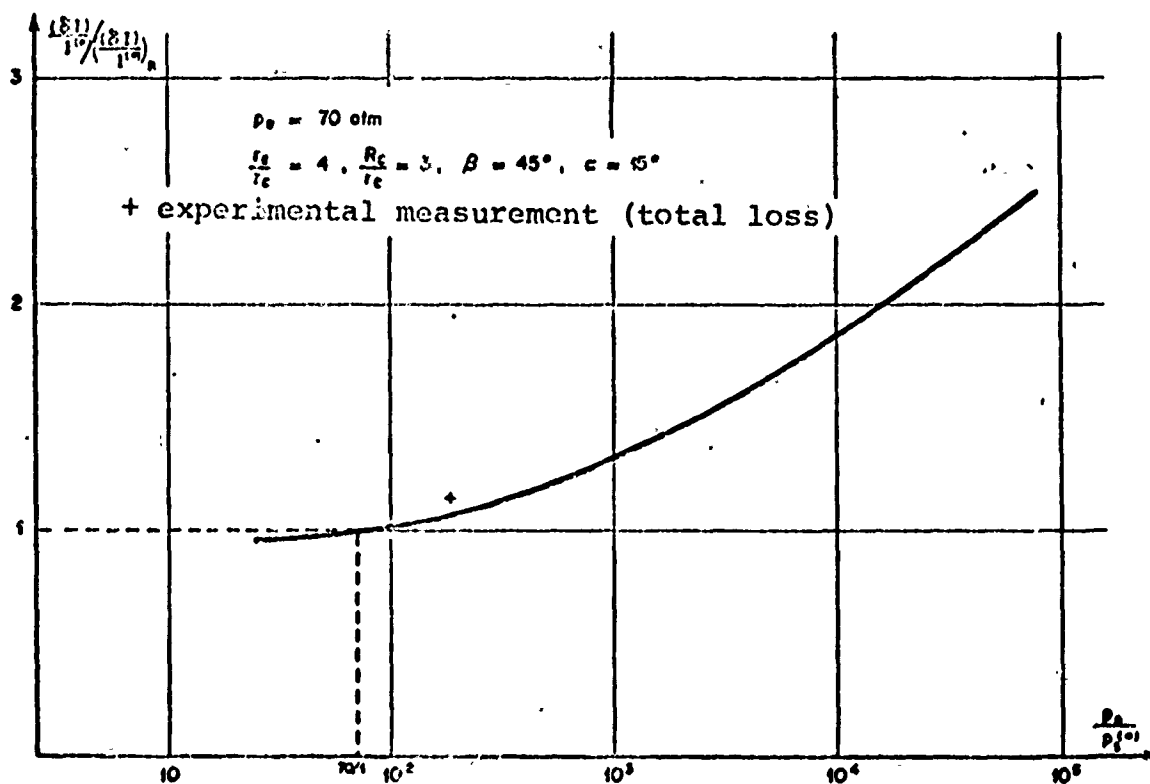 good correlations [62].

Figure 22. Influence of Expansion Ratio on Specific Impulse
Loss Due to Phase Lags.

4.6.2. Specific Impulse Loss with Near Frozen Flow

Calculation for large particles or a small motor is useful for
many practical applications (micro-rockets) but far less classical

than in near equilibrium since there is no publication on the subject.
We will show that, nevertheless, a formula may be arrived at by a
process comparable to that used in the preceding paragraph.

We depart from the same system of equations, namely:

$$\left\{ \begin{array}{l} \rho u A = \dot{m}_g \, , \\[6pt] \rho_p u_p A = K \dot{m}_g \, , \\[6pt] \rho u \left(\dfrac{du}{dx} + K \dfrac{du_p}{dx} \right) + \dfrac{dp}{dx} = 0 \, , \\[6pt] h(T) + \dfrac{u^2}{2} + K \left[c_p(T_p) + \dfrac{u_p^2}{2} \right] = (1+K) H \, , \\[6pt] + \text{condensed phase equations.} \end{array} \right.$$

We are looking at the case where the particles are large, i.e.,
they are only slightly accelerated by the gaseous phase and only
slightly cooled in expansion. We keep the functions describing the
gaseous phase, but for the condensed phase we write:

$$u_d = u_p \, ,$$

$$T_d = T_o - T_p \, .$$

The terms containing magnitudes u_d and T_p are grouped in the second
members of equations:

$$\left\{ \begin{array}{l} \rho u A = \dot{m}_g \, , \\[6pt] \rho u \dfrac{du}{dx} + \dfrac{dp}{dx} = - K \rho u \dfrac{du_d}{dx} \, , \\[6pt] h(T) + \dfrac{u^2}{2} = h_o + K \left(C_s T_d - \dfrac{u_d^2}{2} \right) \, , \\[6pt] p = \rho r T \, , \\[6pt] + \text{transformed condensed-phase equations.} \end{array} \right.$$

For very large particles (small in number) the magnitudes u_d
and T_d are practically zero. The reference flow is thus here the
flow of gaseous combustion products only. When the particles are

such that u_d and T_d take on substantial values, gaseous phase flow is perturbed. A variation in entropy is defined by:

We get:
$$ds = K \frac{C_s T_d + u\, du_d - u_d\, du_d}{T} .$$

The momentum equation in the latter system of equations can be replaced by:

$$s(T) - s(T_0) = K \int_0^x \frac{C_s T_d + u\, du_d - u_d\, du_d}{T} .$$

A first approximation of u_d and T_d is given by examining the condensed phase equations; $u_d^{(0)}$ and $T_d^{(0)}$ are then introduced into the gaseous phase equation and we calculate the resulting perturbations of gaseous flow.

In its general form the momentum equation of the condensed phase is written:

$$\rho_p u_p \frac{du_p}{dx} = \iiint \frac{\mathcal{C}_u}{\mathcal{T}_u} (u-c)\, m(r)\, f\, d^2 c_j\, dc\, dr .$$

Near frozen flow is expressed simply in the second member, considering:

$$c \ll u ,$$
$$u \simeq u^{(e)} .$$

Thus we get:

$$\rho_p u_p \frac{du_p}{dx} \simeq u^{(e)} \iint \frac{\mathcal{C}_u}{\mathcal{T}_u}\, m(r)\, f\, d^2 c_j\, dc\, dr .$$

The corrective coefficient certainly has great influence due to the high Reynolds number values. We will thus define a mean value for the time constant $\bar{\tau}_u$ by the formula:

$$\bar{\tau}_u = \frac{\rho_p}{\iiint \frac{C_u}{\tau_u} m(\sigma) f d^3 g \, d\sigma \, d\tau}.$$

An identical formula defines the mean quadratic diameter to be used. We will merely note that if we assume $C_u \equiv 1$, $\bar{\tau}_u$ must be calculated with the diameter d_{31}.

The equation enabling $u_d^{(o)}$ to be calculated is thus reduced to:

$$u_d^{(o)} \frac{d u_d^{(o)}}{dx} = \frac{u^{(o)}}{\bar{\tau}_u}.$$

Integration gives:

$$u_d^{(o)} = \frac{1}{\sqrt{\bar{\tau}_{uo}}} \left[2 \int_0^x \frac{\bar{\tau}_{uo}}{\bar{\tau}_u} u^{(o)} dx \right]^{\frac{1}{2}}.$$

Likewise the energy equation of the condensed phase is at first:

$$\rho_p u_p \frac{dT_p}{dx} = \iiint \frac{C_T}{\tau_T} \frac{e(T_g) - e}{C_c} m(\sigma) f d^3 g \, d\sigma \, d\tau.$$

Near frozen flow leads us to take:

$$e \simeq C_c T_o \, ,$$

$$e(T_g) \simeq C_c T^{(o)}.$$

A mean value for the time constant $\bar{\tau}_t$ is given by:

$$\bar{\tau}_t = \frac{\rho_p}{\iint \frac{C_T}{\tau_T} m(\sigma) f d^3 g \, d\sigma \, d\tau} \, ,$$

and $\bar{\tau}_t$ is calculated with d_{31} if $C_t \equiv 1$ (Nu = 2).
The equation giving $T_d^{(o)}$ is finally:

$$u_d^{(o)} \frac{d T_d^{(o)}}{dx} = \frac{T_o - T^{(o)}}{\bar{\tau}_t}.$$

Integration leads to:

$$T_d^{(e)} = \frac{1}{\sqrt{\bar{u}_o}} \cdot \frac{\bar{u}_o}{\bar{c}_{T_0}} \int_0^{\infty} \frac{\frac{\bar{c}_{T_0}}{\kappa}(T_0 - T^{(e)})}{\left[2\int_0^{\infty} \frac{\bar{u}_o}{\bar{c}u} u^{(e)} dx \right]^{\frac{1}{2}}} \cdot$$

Putting $u_d^{(o)}$ and $T_d^{(o)}$ in the gaseous phase equations, keeping to first-order terms and linearizing the system, we obtain:

$$\begin{cases} \dfrac{\delta\rho}{\rho^{(e)}} + \dfrac{\delta u}{u^{(e)}} = \dfrac{\delta \dot{m}_g}{\dot{m}_g^{(e)}} \; , \\[2mm] c_{pf}^{(e)} \delta T + u^{(e)} \delta u = K c_s T_d^{(e)'} = (\delta h)_a \; , \\[2mm] c_{pf}^{(e)} \dfrac{\delta T}{T^{(e)}} - r \dfrac{\delta p}{p^{(e)}} = K \int_0^{\infty} \dfrac{c_s T_d^{(e)'} + u^{(e)} d u_d^{(e)}}{T^{(e)}} = (\delta s)_a \; , \\[2mm] \dfrac{\delta p}{p^{(e)}} = \dfrac{\delta\rho}{\rho^{(e)}} + \dfrac{\delta T}{T^{(e)}} \; . \end{cases}$$

Resolution of the system enables us to explain each lag δu, δp, etc. explicitly. The geometric throat is a single point which enables us to find the variation in the gas flow $\overset{o}{m}g$; however no conclusion can be found as to the sign of $\delta \overset{o}{m}g$.

The reference specific impulse corresponds to a suitable gaseous flow and is calculated for the total flow of the combustion products.

$$I^{(e)} = \frac{u^{(e)}}{(1+K) g_o} \; .$$

The specific impulse lag is written in the form:

$$\frac{\delta I}{I^{(e)}} = \frac{\delta u}{u^{(e)}} + \frac{A_a \delta p}{\dot{m}_g^{(e)} u_A^{(e)}} + K \frac{u_d^{(e)}}{u^{(e)}} \; .$$

Calculation leads to:

$$\boxed{\frac{\delta I}{I^{(e)}} = \frac{K T_0^{(e)}}{u_A^{(e)2}} \int_0^{x_A} \frac{u^{(e)}}{T^{(e)}} \left[\frac{c_s}{c_{pf}^{(e)}} \frac{T_d^{(e)'}}{T^{(e)}} + \left(1 + \frac{u^{(e)2}}{c_{pf}T^{(e)}}\right) \frac{u_d^{(e)}}{u^{(e)}} \right] \frac{du^{(e)}}{dx} dx \, .}$$

116

We see that δI is positive, which is natural because in the reference flow the condensed phase does not participate in propulsion.

As with the near equilibrium, we may wonder to what extent the formula is valid. The condition is established fairly easily:

$$\frac{\sqrt{\overline{\tau_{\omega_o}}}\, u^{(e)}}{\left[2\int_0^x \frac{\overline{\tau_{\omega_o}}}{\overline{\tau_\omega}}\, u^{(e)}dx\right]^{\frac{1}{2}}} \gg 1 \quad .$$

We must also note that the formula remains valid only if solidification of the condensed phase does not occur in the nozzle ($T_d^{(o)} <$ $T_o - T_{pf}$).

The discussion on the influence of the operating parameters on specific impulse is made complex since $u_d^{(o)}$ and $T_d^{(o)}$ take into account the entire history of the particles. We note that the increase in specific impulse remains proportional to the metal concentration of the propellant.

4.7. INFLUENCE OF FLOW STRATIFICATION

As a first approach to the phenomenon of condensed phase segregation in flow, we proposed [63] to consider the flow as perfectly stratified, where the density of the condensed phase varies from one streamline to another. We also assumed that there is always kinetic and thermal equilibrium between phases, which enables us to define an equivalent gas in each streamline, and say that the gaseous phase is made of a thermically perfect gas. The connection condition which enables us to define the problem fully is the uniformity of pressure in each straight nozzle section.

Only local pressure depends solely on the abscissa along the nozzle axis. We will thus express all magnitudes as a function of the reduced pressure by classical formulas:

117

$$\frac{T}{T_0} = \left(\frac{p}{p_0}\right)^{\frac{\bar\gamma-1}{\bar\gamma}} \; ;$$

$$\frac{\bar\rho}{\bar\rho_0} = \left(\frac{p}{p_0}\right)^{\frac{1}{\bar\gamma}} \; , \qquad \text{with } \bar\rho = \rho(1+K) ,$$

$$\left(\frac{u}{U_L}\right)^2 = 1 - \left(\frac{p}{p_0}\right)^{\frac{\bar\gamma-1}{\bar\gamma}} , \text{ with } U_L = \frac{2\bar\gamma}{\bar\gamma-1} r T_0 ,$$

$$\frac{dr_c^2}{(dr^*)_c} = \left(\frac{\bar\gamma-1}{2}\right)^{\frac{1}{2}} \left(\frac{\bar\gamma+1}{2}\right)^{-\frac{\bar\gamma+1}{2(\bar\gamma-1)}} \frac{\left(\frac{p}{p_0}\right)^{-\frac{\bar\gamma+1}{2\bar\gamma}}}{\sqrt{\left(\frac{p}{p_0}\right)^{-\frac{\bar\gamma-1}{\bar\gamma}}-1}} \; .$$

The isentropic exponent of the mixture $\bar\gamma$ depends on the streamline considered by means of K:

$$\bar\gamma = \frac{\gamma(1+K\beta)}{1+K\beta\gamma} \; .$$

As a result, the minimum streamline section $(dr^2)_c$ is not reached by a common value of the reduced pressure and it is thus appropriate to refer all magnitudes to values in a reference section such as the entrance section. Writing:

$$\frac{p_c}{p_0} = 1-\varepsilon \; , \quad \varepsilon \ll 1 ,$$

we get, for example:

$$\frac{dr^2}{(dr^2)_c} = \sqrt{\frac{\bar\gamma-1}{\bar\gamma}} \, \varepsilon \left(\frac{p}{p_0}\right)^{-\frac{\bar\gamma-1}{2\bar\gamma}} \left[\left(\frac{p}{p_0}\right)^{-\frac{\bar\gamma-1}{\bar\gamma}}-1\right]^{-\frac{1}{2}} \; .$$

Expressing the elementary flows of the two phases in each streamline then integrating over the straight section we obtain the mean value for the ratio between the flows of the two phases $\bar K$:

$$\bar K = \frac{\int_0^1 \frac{K}{\sqrt{1+K}} R^{-\frac{1}{\bar\gamma}} d(r_c^{*2})}{\int_0^1 \frac{1}{\sqrt{1+K}} R^{-\frac{1}{\bar\gamma}} d(r_c^{*2})} \; ,$$

where $r^* = r/r_{wall}$, $R = p_0/p$.
In the entrance section we have, more simply:

$$\overline{K_e} = \frac{\int_o^1 \frac{K}{\sqrt{1+K}} \, d(r_c^{*2})}{\int_o^1 \frac{1}{\sqrt{1+K}} \, d(r_c^{*2})} \; .$$

For computer applications we chose a law with a shape comparable to that of the Figure 20 curves and characterizing the particle concentration in the center of flow:

$$K = K_m \left(1 - r_c^{*e}\right) \; .$$

We deduce from this the relation between K_m and $\overline{K_e}$:

$$K_m = \frac{3}{2}\left(1 + 2\overline{K_e} - \sqrt{1 + \frac{4}{3}\overline{K_e}}\right) \; .$$

This enables K_m to be calculated from the propellant's metal concentration.

To obtain the evolution of pressure along the nozzle we also proceed by integration:

$$\frac{A}{A_c} = \sqrt{\varepsilon} \int_o^1 \sqrt{\frac{\gamma-1}{\gamma}} \left(\frac{p}{p_o}\right)^{-\frac{\gamma+1}{2\gamma}} \left[\left(\frac{p}{p_o}\right)^{-\frac{\gamma-1}{\gamma}} - 1\right] d(r_c^{*2}) \; .$$

However ε is not known a priori. To determine it we must, after referring A to is value A_c at the geometric throat, write that its derivative with respect to the reduced pressure at the geometric throat is zero. An approximate method enables the critical ratio $(p/p_o)^*$ to be calculated in the case of stratified flow; numerical application shows that this ratio is very close to its value for homogeneous flow. The pressure appears insensitive to the intensity of stratification.

The distribution of the velocity, temperature, or flow in the jet can be found in each section. We first establish the relation giving the position of a streamline characterized by the parameter K, where the pressure ratio comes in as a parameter:

$$r^*_e = \frac{\displaystyle\int_{\frac{\gamma-1}{\gamma}\frac{1}{1+K_m\beta}}^{\frac{\gamma-1}{\gamma}\frac{1}{1+K\beta}} \frac{dr}{r^{\frac{3}{2}}\sqrt{R^\epsilon(R^\epsilon-1)}}}{\displaystyle\int_{\frac{\gamma-1}{\gamma}\frac{1}{1+K_e\beta}}^{\frac{\gamma-1}{\gamma}} \frac{dr}{\epsilon r^{\frac{3}{2}}\sqrt{R^\epsilon(R^\epsilon-1)}}} \qquad \text{(for the } K(r^*_e)\text{ law} \atop \text{taken)},$$

If we compose r^* at this corresponding value r_e^* in the entrance section we find that:

$$r^* > r_e^* \,, \ \forall K.$$

This inequality signifies that expansion of the mixture increases 'in proportion to the size of the condensed phase.

Each magnitude is referred to its value on the axis and is plotted against distance from the axis for three sections: the entrance section, the throat section, and the outlet section defined by an expansion ratio of 70:1. The wall velocity is greater than the axis velocity; this difference tends to decrease upon expansion. This finding agrees with the more precise calculations [64]. The wall temperature, on the other hand, is greater than the axis temperature and this effect tends to increase in expansion. The mass flow at the periphery of flow is greater than that at the center but the difference tends to disappear. The sound barrier for stratified flow (M = 1 in gas) has a shape comparable to that of two-dimensional homogeneous flow.

The influence of flow stratification on the performance parameters appears as an application of the above calculations. We show first of all that the characteristic velocity is not sensitive to stratification. For specific impulse of a suitable nozzle we establish, with the hypotheses of stratified flwo and non-stratified flow, the expressions:

$$I = \sqrt{2rT_0}\ \frac{\int_0^1 \sqrt{\frac{\overline{\gamma}}{\overline{\gamma}-1}\left(1-R^{-\frac{\overline{\gamma}-1}{\overline{\gamma}}}\right)}\,d\left(r_c^2\,\varepsilon\right)}{\int_0^1 \sqrt{1+K}\ d\left(r_c^2\,\varepsilon\right)}\ ,$$

and $\quad I_0 = \sqrt{2rT_0}\ \sqrt{\dfrac{\overline{\gamma}}{\overline{\gamma}-1}\ \dfrac{1-R^{-\frac{\overline{\gamma}-1}{\overline{\gamma}}}}{1+K}}\ ,\quad$ where $\quad \overline{\gamma}\,(\overline{K})$.

The loss for infinite expansion appears to depend on β: it is zero if $\beta = 1$ and positive if $\beta \neq 1$. Figure 23 gives the evolution of specific impulse loss due to stratification as a function of the expansion ratio. The relative loss for realistic expansion ratios is about several thousandths, i.e., the limit of values worthy of being considered.

The loss by jet divergence was also calculated by integration, assigning to the momentum of each streamline a locally-calculated correction coefficient. It seems that the general classical formula for homogeneous flows with $\frac{1 + \cos \alpha}{2}$ is still applicable to stratified flow as long as the divergent angle does not exceed 20°.
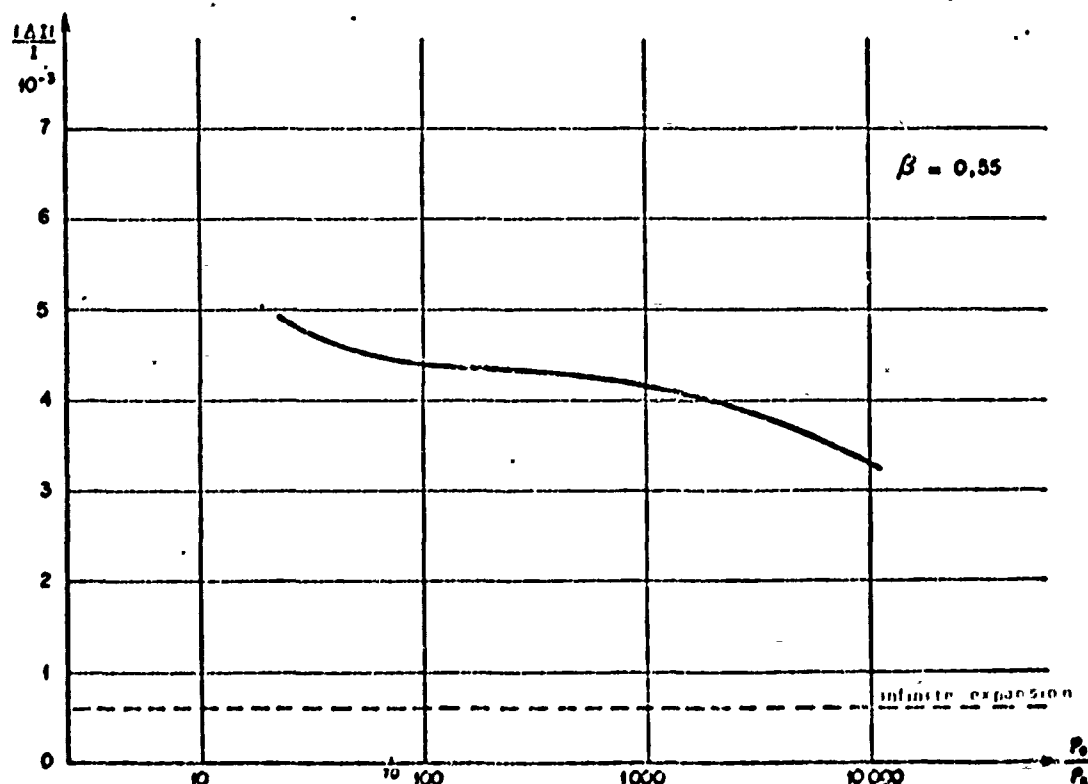

Figure 23. Specific Impulse Loss Due to Jet Stratification as a Function of Expansion Ratio.

These approximate and somewhat elementary calculations thus prove that segregation of the condensed phase in the flow is an unfavorable phenomenon. They enable us to verify the fact that the classical one-dimensional calculation tends to under-estimate specific impulse loss, as shown by two-dimensional calculations. Although the order of magnitude of the specific impulse loss due to imperfect distribution of the condensed phase obtained with this simplified method is correct, it can only be considered a first approximation as phase lags play an active role in the phenomenon.

*   *

*

5. EXAMINATION OF WALL PHENOMENA

The wall phenomena are responsible for the greatest specific impulse loss when the propellant is not metallized. The effect of these exchanges on the flow make us question two hypotheses: the flow is in actual fact neither adiabatic due to heat transfer nor isentropic due to wall friction and heat loss. In the case of a metallized propellant we must add a mass exchange between the flow and the wall due to deposition of the condensed phase.

Even with a nonmetallized propellant it is difficult to estimate heat flow and wall friction: differences of as much as 50% have been found between experiment and theory. The difficulties come from the unsteady nature of the heat phenomena and the complex configuration of the boundary layer developing on the nozzle wall. First of all "outside" flow is accelerated with the negative pressure gradient and the nozzle section varies rapidly. Due to the temperature level of the phenomena we must take into account chemical reactions in the boundary layer; even neglecting concentration variations, the high temperature differences between outside flow and wall make it difficult to estimate the average fluid properties. We should also take radiation exchange into account. The nature of the boundary layer is in itself somewhat poorly known; experimentally, observations give it a turbulent character. We know,

however, that stabilization of flow tends to occur in the throat, i.e., in the zone where exchange coefficients are highest [65]. Also, the thickness of the boundary layer can be large enough to have a substantial impact on outside flow.

Metallized propellants result mainly in formation of a condensed layer on the wall which has a great effect on heat transfer. We must also point out that the particles perturb the laminar sub-layer; in the very schematic case of a laminar layer of the plane sheet for a suspension in an incompressible fluid, it has been shown [5] that the friction and heat transfer coefficients calculated for the fluid alone must be multiplied by the corrective factor to take the condensed phase into account:

$$\sqrt{1+K} \left[1 + 943 \frac{a_0 \tau_u}{x} \frac{K}{1+K} \right] \text{ , if } \frac{x}{a_0 \tau_u} \gg 1.$$

For more general hypotheses we would have to develop the theory of two-phase boundary layers: as yet, little is known about these.

The existence of a condensed layer which complicates already difficult calculations and very strict experimental conditions (temperature in particular) explain why the literature on wall phenomena when the propellant is metallized is so scanty. We are thus stepping into the almost-unknown.

The approach we made consisted, in order to simplify calculations, of trying to uncouple the phenomena. Emphasis will be laid on new phenomena and we will use theory and experiment simultaneously. The nozzle examined here does not represent large motors but, when we choose a nozzle fully machined in a graphite block for calculations and tests, we get rid of phenomena such as ablation of heat shields which would complicate the problem still further.

5.1. EXAMINATION OF BOUNDARY LAYER

The problem of the boundary layer for a metallized propellant is stated in the same manner as for a non-metallized propellant

except that the surface temperature can be that of the condensed
phase and the gas-condensed layer interface has a velocity which
can generally be neglected. We must also calculate the heat flow
and friction coefficient to take momentum and energy contributed
by particles into account. The radiation exchange, which could
be quite substantial in the converging section if the results of
[65] are extrapolated, is estimated.

As the heat problem is unsteady by its very nature, the
density of the heat flux at a point changes with time. Thus we
are trying to show a characteristic value for heat exchange which
would be a constant quantity with the simplest hypotheses. The
heat transfer coefficient h is defined by:

$$q_r = h \left(h_f - h_p \right),$$

where q is the heat flux density,

h_p is the wall enthalpy,

h_r is the friction enthalpy (athermanous wall).

To coefficient h are linked two important non-dimensional numbers:

- the heat flux coefficient or enthalpy transport coefficient:

$$C_h = \frac{q_r}{\rho_e u_e \left(h_f - h_p \right)} = \frac{h}{\rho_e u_e} \qquad \text{(Margoulis or Stanton number)},$$

- the Nusselt number:

$$Nu = \frac{h \dot{C}_p L}{\lambda} \qquad \text{where L is a reference length.}$$

For wall friction we use the friction coefficient:

$$C_f = \frac{\tau_p}{\frac{\rho_e u_e^2}{2}}$$

The problem is to calculate C_h or Nu and C_f locally. We can
either start from general boundary layer equations or use formulas
of a more or less empirical character.

The formulas are due to the work of Bartz [67] and are presented in the general form:

$$Nu = C \, Re^{0,8} \, \sigma_r^{0,4},$$

where the constant C is 0.023 or 0.026.
Nu and Re are based on the local diameter D of the nozzle and according to Colucci [3] the Prandtl number τ_r is near to 1 under our experimental conditions. The reference temperature to which the gas properties must be calculated is the static temperature:

$$Nu_e \simeq 0,023 \, Re^{0,8}.$$

The major drawback of this formula is that it is fully independent of the nozzle entrance conditions and in particular of the boundary layer thickness. The formula was thus extended by theoretically justified considerations to give:

$$Nu = 0,0346 \, Re^{0,8} \cdot \sigma_r^{7/15} \left(\frac{2\ell}{D_o}\right)^{-\frac{1}{5}} \left(\frac{D_o}{D}\right)^{-\frac{1}{25}} \left(\frac{T^*}{T_e}\right)^{-0,6},$$

provided $2\ell/Do$ is sufficiently large. The reference temperature T* is in the first approximation the arithmetic mean of the local static temperature and the wall temperature while the gas properties are calculated with the outside flow pressure and composition but with temperature T*.

This formula was developed for liquid propellant motors and gives a generally satisfactory representation of the phenomenon since the nozzle is preceded by a fairly long combustion chamber. The case is different for solid propellant motors where the origin of the boundary layer is very near to the nozzle, and strictly speaking only elementary formulas can be used.

In principle, the general equations would give more general and more complete results (simultaneous examination of heat transfer and wall friction). Although it requires more complex computing, this method was chosen for these applications and we will summarize the principal stages of the theory [67, 68, 69].

The boundary layer is assumed to be entirely turbulent and
to remain in the throat region, which would probably lead to the
heat transfer coefficient in this zone being over-estimated and,
for simplification, we grant that its thickness is always very
small at the local nozzle radius. The basic equation is from Von
Karman's integral momentum equation:

$$\frac{C_f}{2} = \frac{d\delta_2}{dx} + \delta_2 \left(\frac{H+2}{u_e} \frac{du_e}{dx} + \frac{1}{\rho_e} \frac{d\rho_e}{dx} + \frac{1}{R} \frac{dR}{dx} \right)$$

δ_2 is here the momentum thickness and H a shape parameter, the
quotient of the displacement thickness by the momentum thickness.
The outside flow magnitudes are given index e and R is the local
nozzle radius; x is the abscissa along the boundary layer.

We consider this equation as a differential equations for
δ_2, which can be integrated provided we know the velocity profile,
the law giving the friction coefficient, and the origin of the
boundary layer.

-C_f is assumed to be given by relation [68]:

$$\frac{C_f}{2} = \frac{b\,g}{R_{\delta_2}^{m_o}} ,$$

where b is a numerical coefficient,

m$_o$ is an exponent depending on the velocity profile used,

g is a corrective coefficient taking into account the effects
of real gas.

With Michel† we will take:

$$b = 0,0036 ,$$

$$m_o = \frac{1}{5} ,$$

$$g = \frac{\left(\frac{\mu^*}{\mu_e} \right)^{\frac{4}{15}}}{\frac{T^*}{T_e}} ,$$

_____

† Presumably reference [68]. Translator's Note.

The asterisk here relates to a reference temperature; Monaghan's relation will be used:

$$h^* - h_e = 0{,}54 \left(h_p - h_e\right) + 0{,}16 \left(h_f - h_e\right).$$

- The friction temperature is calculated from the wall heat factor:

$$r = \frac{T_f - T_e}{T_{la} - T_e}$$

The classic expression $r = \tau_r^{1/3}$ leads, with τ_r close to 1, to $T_f = T_{la}$, the local stoppage temperature of the outside flow.

- As the pressure gradient is negative we can assume that the velocity profile varies slowly enough for H to be determined by the expressions established for a plane sheet; moreover, as the role played by H is not very important we neglect the real gas effects:

$$H \simeq H_{inc.} + \alpha \, M_e^2 + \beta \, \frac{T_p - T_f}{T_e},$$

with

$$H_{inc.} = 1{,}4 \quad , \quad \beta = 1{,}222 \quad ; \quad \alpha = 0{,}222.$$

Writing:

$$Y = \delta_2^{\,m_0+1},$$

the integral equation takes the form:

$$\frac{dY}{dx} + P(x)\,Y = Q(x).$$

This equation can be integrated analytically. The origin of the layer was taken to be at the nozzle entrance, because of the geometric configuration of the motors we tested where the terminal face of the grain is in the nozzle entrance plane. We assumed that viscosity was proportional to $\sqrt{t}$.

Finally we get:

$$\left(\frac{\delta_2}{R_c}\right)^{1/2} F_1 \, E \left(\frac{R}{R_c}\right)^{-1/2} = 0{,}0103 \left(\frac{\ell_i}{R_c}\right)^{0{,}2} \int_0^{\frac{x}{R_c}} \frac{F_1 \, E}{g \, F_2} \left(\frac{R}{R_c}\right)^{1/2} d\left(\frac{x}{R_c}\right),$$

where F_1, F_2, and E are given by expressions:

$$F_1 = \frac{M_e^{4,08}}{(1 + 0,1\, M_e^2)^{6,905}} \quad , \quad (\gamma = 1,20),$$

$$F_2 = \frac{M_e^{0,2}}{1 + 0,1\, M_e^2} \quad ,$$

$$E = M_e^{-1,45\left(1 - \frac{T_p}{T}\right)}.$$

ℓ_i is a parameter characterizing the flow-generating conditions and is homogeneous at a length of:

$$\ell_i = \frac{\mu_i}{\rho_i\, a_i}.$$

Since we have calculated δ_2 we can deduce C_f and C_h.

- C_f is calculated with the aid of:

$$\frac{C_f}{2} = 0,0086\, g\left(\frac{\ell_i}{R_c}\right)^{m_o}\left(\frac{\delta_2}{R_c}\right)^{-m_o}.$$

We deduce the tangential friction stress at the wall by the expression:

$$\tau_p = \rho_e\, u_e^2\, \frac{C_f}{2}$$

whence:
$$\frac{\tau_p}{p_i} = 0,01032\, \frac{M_e^{1,8}}{(1 + 0,1\, M_e^2)^5}\, g\left(\frac{\ell_i}{R_c}\right)^{\frac{1}{5}}\left(\frac{\delta_2}{R_c}\right)^{-\frac{1}{5}}.$$

- C_h can also be calculated from an integral equation:

$$\frac{q_p}{\rho_e\, u_e\, h_{i_e}} = \frac{d\Delta}{dx} + \Delta\left(\frac{1}{u_e}\frac{du_e}{dx} + \frac{1}{\rho_e}\frac{d\rho_e}{dx} + \frac{1}{R}\frac{dR}{dx}\right),$$

where Δ is the ... ay thickness.
We write, to integrate this equation:

$$\frac{q_p}{\rho_e\, u_e\, h_{i_e}} = \frac{B}{R_\Delta^{\frac{1}{5}}} \quad ,$$

with:
$$B = 0,0086\, g\left(\Delta\, \frac{h_p - h_e}{h_{i_e}}\right)^{\frac{6}{5}}.$$

Whence $\Delta(x)$ then C_h and h.

-129-

We prefer to assume that the Reynolds analogy subsists, rather than repeating the calculations, i.e., that we can define a factor s such that:

$$C_h = s \, \frac{C_f}{2}$$

If Colburn's formula: $s = \tau_r^{-2/3}$ is extended to our problem we immediately get, with the hypotheses already made:

$$C_h \simeq \frac{C_f}{2} = \frac{0,0086}{F_2} \, g \left(\frac{\rho_i}{R_c} \right)^{m_o} \left(\frac{\partial_s}{R_c} \right)^{-m_o}$$

We deduce h or h', the heat transfer coefficient based on a temperature deviation and thus more directly usable in the rest of the calculation:

$$h' = \frac{q_p}{T_{ie} - T_p} = 0,0516 \, \frac{M_e^{0,8}}{\left(1 + 0,1 M_e^2 \right)^{4,5}} \, g \left(\frac{\rho_i}{R_c} \right)^{\frac{1}{5}} \left(\frac{\partial_e}{R} \right)^{-\frac{1}{5}} \frac{c_u \, p_i}{T_i}$$

Calculations were done for the following reference conditions:
- biconical nozzle:
        entrance ratio: Re/Rc = 6,
        outlet ratio: Rs/Rc = 3,
        throat raduis of curvature: 2Rc,
        converging angle: $\beta = 45°$,
        diverging angle: $\alpha = 15°$,
        throat radius: 10 mm.

- metallized propellant with 16.4% aluminum,

$$T_i = 3300°K,$$
$$P_i = 70b,$$
$$\mu_i = 4,9 \times 10^{-5} \; kg \, m^{-1} s^{-1}$$

Calculations were first run for a uniform wall temperature of 2317°K, the alumina melting point, then at two other temperatures (3300 and 1400°K). It appears that h' and τ_p are fairly insensitive

to wall temperature which only comes in when calculating the refer-
ence temperature. A posteriori this finding justifies the possibil-
ity of uncoupling the examination of heat transfer coefficent and
wall friction from examination of the condensed layer.

Figure 24 gives the variation in h' and τ_p as a function of
the abscissa taken along the nozzle axis. The coefficient h' is
compared to its value calculated by the formula:

$$Nu_a = 0,023 \, Re_c^{0,8} .$$

This formula rather clearly under-estimates coefficient h', mainly
in the throat region. This discrepancy probably comes from dif-
ferent hypotheses in the two calculations for the thickness of
the boundary layer at the nozzle entrance. The two curves come
close to each other in the diverging section as the initial con-
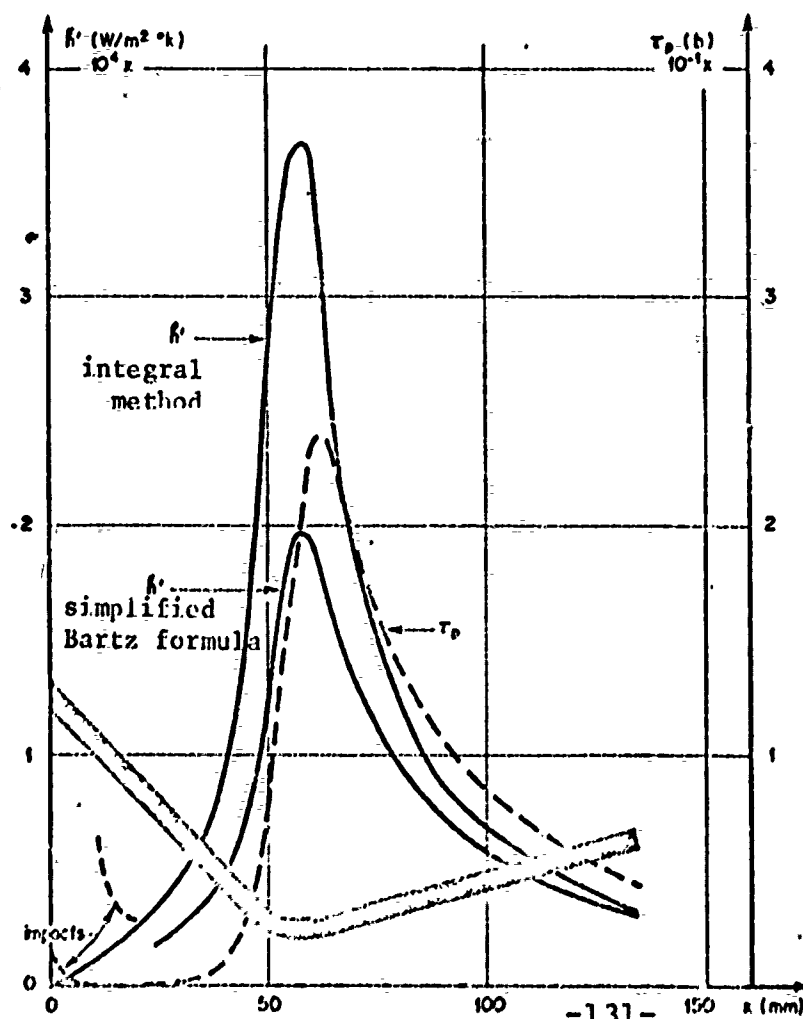ditions have less and less influence.

Figure 24. Heat
Transfer Coefficient
and Wall Friction in
a Nozzle.

To find out the influence of the motor operating conditions on the values of h' and τ_p we need only note that:

- h' is proportional to $\dfrac{ai\ Pi}{Ti}\left(\dfrac{Ti}{Rc\,Pi}\right)^{0.166}$

- τ_p is proportional to $pi\left(\dfrac{Ti}{Rc\ Pi}\right)^{0.166}$

with constant nozzle geometry

Since Ti changes but little with the operating pressure, we can conclude that h' and τ_p are substantially proportional to the group:

$$\frac{P_i^{0,834}}{R_c^{0,168}} \ .$$

Wall exchanges thus vary rapidly with pressure but decrease relatively little when the motor scale increases.

The two-phase nature of flow has been ignored thus far. We can take the condensed phase into account by defining the kinematic viscosity of the mixture [5]. We must also take into consideration the momentum and energy produced by the particles which stick against the wall. These contributions modify expressions for h' and τ_p by correction terms:

$$\tau_P = (\tau_P)_0 + \rho_c\, q_v\, u_c \ ,$$

$$h' = (h')_0 + \rho_c\, C_v\, q_v \ ,$$

where q_v is the flux density of the condensed phase (in volume) intercepting the surface.

We applied this to the computer assuming that 5% of the nozzle mass flow is collected in the first half of the converging section, the flow being a decreasing exponential function of the curvilinear abscissa along the wall. We find (Figure 4) that corrections are only large at the nozzle inlet; this heat phenomenon will be studied in greater detail below.

5.2. FORMATION OF CONDENSED LAYER

Although it is sufficient to know τ_p to determine friction loss, to find out the heat flux we need to know not only h' but also the wall temperature. This temperature comes out of a balance set up between the heat transmitted to the wall by the flow and the heat transmitted by conduction and we know that it is affected by the presence of an intermediate layer between the flow and the wall. We find, after cutting off the engine, that there is an alumina layer; this layer is formed by the impact of alumina particles (and aluminum particles in a smaller proportion) on the converging section of the nozzle, as shown experimentally. The possibility of impacts on the final portion of the diverging section has also been shown in the case of contoured nozzle [52] but this phenomena is mainly of structural importance (resistance of nozzle to erosion) and will not be considered in this study.

Besides the need to study impacts in the converging section to determine the nozzle surface temperature, it appears that this phenomenon has a direct effect on performance: the mass captured is not ejected (or is ejected in the form of sufficiently large droplets for the propulsion yield to be mediocre) and the ejected mass defect leads directly to specific impulse loss.

Despite its interest the impact problem has been given little attention. Zeamer [70] givesacriterion for the ability of a particle approaching the wall to strike it; the relation is established by comparing the stopping distance of a particle moving at some distance from the wall with a velocity component normal to the wall and the thickness of the boundary layer. This theory does not properly explain the particular role played by the boundary layer; the impact problem is in fact linked to the particle trajectories throughout the flow. Thus the phenomenon is particularly sensitive to the flow pattern in the nozzle inlet zone (inlet ratio value, converging section progressivity, and nozzle integration).

We can see that impacts are due to gaps between the streamlines of the gaseous phase and the particle trajectories at the flow periphery. Qualitatively, impact intensity depends both on the suddeness of flow contraction which has a repercussion on the curvature of the streamlines, and on the velocity level, itself linked to the section ratio. Abrupt converging sections and low inlet section ratios are thus unfavorable; moreover, the loss can be accentuated by more numerous particle collisions and greater particle growth, but this effect will be left out of count here. The case of the integrated nozzle is more complex due to the confluence of flows coming from upstream of the grain and from the zones situated behind the integrated part of the nozzle.

Impacts must be studied by two-dimensional analysis of two-phase flow in the inlet zone. In order to find out the order of magnitude of specific impulse loss due to impacts, which loss is unknown at present, we propose a simplified method of calculation for a nozzle with a conical converging section of moderate inlet ratio. The flow between the grain hole and the nozzle throat is schematized as follows:

- Gaseous flow in the grain hole is a sectional flow;

- Gaseous flow in the conical converging section is conical (well flow);

- The link between these two flow types is a flow of the same nature as that defined in Paragraph 3.3.4.c for the throat with constant radius of curvature (Figure 13); the streamlines in this zone belong to a group of secant circles while the lines of a meridian plane on which the magnitudes are constant are portions of circles of the conjugated group.

The particle trajectories are examined in this gaseous velocity field (Stokes law).

-134-

a) Examination of trajectories in the intermediate zone

In the grain hole, kinetic phase lags are very small, and the streamlines and trajectories are comparable to parallels to the motor axis. It is in this intermediate zone, described by the system of toric-spherical curvilinear coordinates, that the divergencies between streamlines and trajectories begin to be manifested.

Before determining the particle motion equations it is essential to proceed via the following steps: write the transformation formulas for the curvilinear coordiantes in rectangular coordinates, establish expressions for the natural base vectors then those for unit vectors of the ordinary base, and give the ordinary velocity components.

With the notations of Figure 25 we finally come out with the two following equations for components u and v of the velocity of one particle:

$$\frac{du}{dt} + v\ \frac{sh\ \gamma\ v + \sin\varphi\ u}{a} = \frac{1}{\tau_u}\left(u_g - u\right),$$

$$\frac{dv}{dt} - u\ \frac{sh\ \gamma\ v + \sin\varphi\ u}{a} = -\frac{1}{\tau_u}\ v,$$

with: $a = r_a$ and $v_g = 0$ hypothetical

$$u = \frac{a}{ch\ \gamma + \cos\varphi}\ \frac{d\gamma}{dt},$$

$$v = \frac{a}{ch\ \gamma + \cos\varphi}\ \frac{d\varphi}{dt}.$$

To resolve this system we use a perturbation method. The magnitudes are first reduced by choosing a reference velocity u_R and writing:

$$u^* = \frac{u}{u_R}\quad,\quad v^* = \frac{v}{v_R}\quad,\quad \tau = \frac{t\,u_R}{a}.$$

We get a dimensionless and very small quantity which will be chosen as a perturbation parameter:

-135-

$$\mathcal{E} \doteq \frac{\tau_u\, u_R}{a} \;.$$

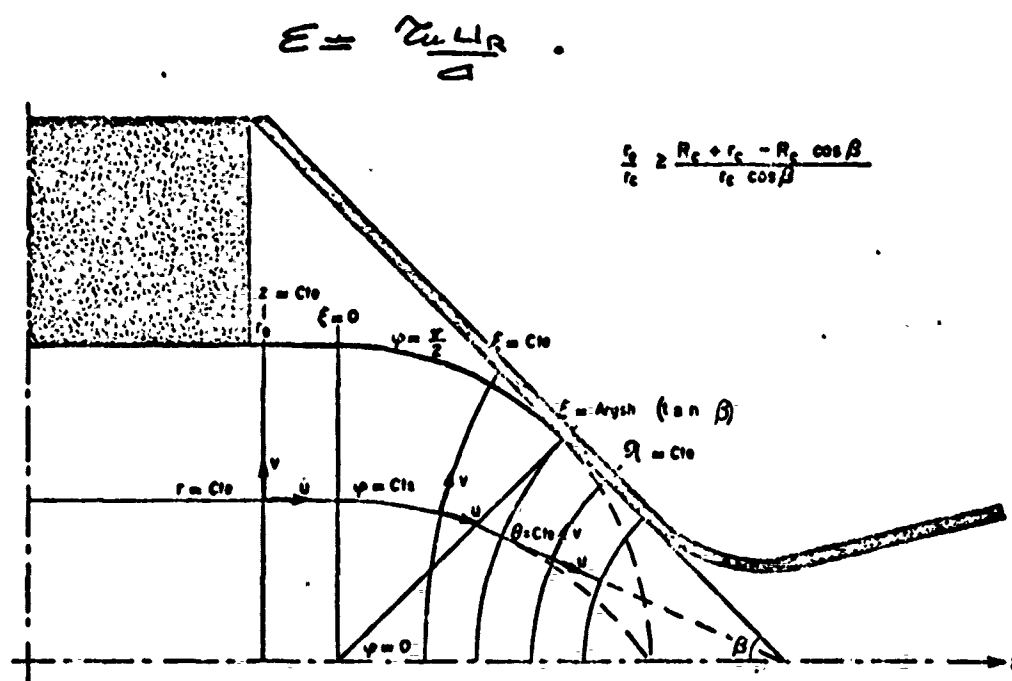$$\frac{r_g}{r_c} \geq \frac{R_c + r_c - R_c \cos \beta}{r_c \cos \beta}$$

Figure 25. Schematization of Gaseous Flow in the Nozzle Inlet Zone for Studying Impacts.

The reduced equations are written:

$$\begin{cases} \mathcal{E}\dfrac{du^*}{d\tau} + \mathcal{E}v^*\left(\operatorname{sh}\zeta\, v^* + \sin\varphi\, u^*\right) = u_g^* - u^*, \\[2mm] \mathcal{E}\dfrac{dv^*}{d\tau} - \mathcal{E}u^*\left(\operatorname{sh}\zeta\, v^* + \sin\varphi\, u^*\right) = -v^*. \end{cases}$$

With order 0 we obtain:

$$u^{(0)*} = u_g^*, \quad v^{(0)*} = 0 \;.$$

With order ε, the calculations give:

$$u^{(1)*} = -\frac{du_g^*}{d\tau}\,,$$

$$v^{(1)*} = u_g^{*2}\sin\varphi \;.$$

-136-

We are mainly interested in lags due to the transverse velocity v. We will thus confine ourselves to a approximation of order 0 for u and an approximation of order ϵ for v. Coming back to the non-reduced magnitudes we have:

$$
\begin{cases}
u = \dfrac{a}{\mathrm{ch}\,\gamma + \cos\varphi}\,\dfrac{d\gamma}{dt} \simeq u_g, \\[2mm]
v = \dfrac{a}{\mathrm{ch}\,\gamma + \cos\varphi}\,\dfrac{d\varphi}{dt} \simeq \dfrac{\tau_u}{a}\,u_g^2\,\sin\varphi .
\end{cases}
$$

The latter expression shows that v increases with particle size through the intermediary of the relaxation parameter τ_u, with the velocity and proximity of the wall (ψ close to $\pi/2$), and decreases with the inlet ratio.

Dividing the two equations member by member we obtain the trajectory equation in the differential form:

$$
\frac{d\varphi}{d\gamma} = \frac{\tau_u u_g}{a}\,\sin\varphi,
$$

or, after integration:

$$
\mathrm{Log}\ \frac{\mathrm{tg}\,\frac{\varphi_2}{2}}{\mathrm{tg}\,\frac{\varphi_1}{2}} = \frac{\tau_u}{a}\int_{\gamma_1}^{\gamma_2} u_g(\gamma)\,d\gamma
$$

This implicit relation enables us to calculate the trajectory lag locally and to calculate a streamline, these being characterized by the same initial conditions (ψ_1, γ_1).

b) Examination of trajectories in the conical converging zone

Calculation is performed in this zone as in the intermediate zone. The particle motion equations are here written:

$$
\begin{cases}
\dfrac{du}{dt} - \dfrac{v^2}{R} = \dfrac{1}{\tau_u}\,(u_g - u), \\[2mm]
\dfrac{dv}{dt} + \dfrac{u v}{R} = -\dfrac{v}{\tau_u},
\end{cases}
$$

with: $v_g = 0$ (hypothetical),

$$u = \frac{dR}{dt} ,$$

$$v = R \frac{d\Theta}{dt} .$$

To obtain the reduced equations we chose a velocity u_R and a reference length L_R and write:

$$\mathcal{E} = \frac{\tau_u u_R}{L_R} , \quad R^* = \frac{R}{L_R} , \quad u^* = \frac{u}{u_R} , \quad v^* = \frac{v}{u_R} , \quad \tau = \frac{t u_R}{L_R} .$$

We get:

$$\begin{cases} \mathcal{E} \dfrac{du^*}{d\tau} - \mathcal{E} \dfrac{v^{*2}}{R} = u_g^* - u^* , \\[2mm] \mathcal{E} \dfrac{dv^*}{d\tau} + \mathcal{E} \dfrac{u^* v^*}{R} = - v^* . \end{cases}$$

Calculation shows that $v^{(1)}$ is zero which indicates that the lateral lags are at most of the second order with respect to ε. This result is logical: in conical flow the streamlines are rectilinear; a lateral velocity v_0 is spread over a distance proportional to τ_u multiplied by v_0. We have shown that the initial velocity at the point where the two zones meet is itself proportional to τ_u. The lags in the conical converging section are thus of the second order and will accordingly be neglected; the formula set up in the intermediate zone is thus sufficient.

c) Calculation of captured mass and specific impulse loss

Once again we will take the formula:

$$\text{Log} \; \frac{\mathsf{b} \frac{\varphi_2}{2}}{\mathsf{b} \frac{\varphi_1}{2}} = \frac{\tau_u}{a} \int_{\tau_1}^{\tau_2} u_g(\tau) d\tau .$$

We must first expand the variations of u_g with τ. To do this we can assume that to simplify the incompressible reference flow:

$$u_g(\tau_1) A_1 = u_g(\tau) A .$$

Calculation of area A leads to:

$$A = \frac{2\pi a^2}{\mathrm{ch}\,\zeta\,(1+\mathrm{ch}\,\zeta)} \quad,$$

whence: $u_g(\zeta) = u_g(\zeta_1)\,\dfrac{\mathrm{ch}\,\zeta\,(1+\mathrm{ch}\,\zeta)}{\mathrm{ch}\,\zeta_1\,(1+\mathrm{ch}\,\zeta_1)} \quad,$

and:

$$\int_{\zeta_1}^{\zeta_2} u_g(\zeta)\,d\zeta = \frac{u_g(\zeta_1)}{\mathrm{ch}\,\zeta_1\,(1+\mathrm{ch}\,\zeta_1)}\left[\mathrm{sh}\,\zeta + \frac{\zeta+\mathrm{ch}\,\zeta\,\mathrm{ch}\,\zeta}{2}\right]_{\zeta_1}^{\zeta_2}.$$

We will consider that conditions 1 and 2 correspond to lines connecting the zones and that a wall impact is considered, i.e.:

$$\zeta_1 = 0\;,\quad \zeta_2 = \mathrm{Arg\,sh}\,(\mathrm{tg}\,\beta)\;,$$

$$\varphi_2 = \frac{\pi}{2}\;,\quad \mathrm{tg}\,\frac{\varphi_1}{2} = \frac{r_1}{r_a}\;.$$

We get:

$$-\log\frac{r_1}{r_a} = \frac{\bar{u}_a\,u_{g_c}}{r_a}\times\frac{\mathrm{tg}\,\beta + \frac{1}{2}\left[\log\left(\mathrm{tg}\,\beta + \frac{1}{\cos\beta}\right) + \frac{\mathrm{tg}\,\beta}{\cos\beta}\right]}{2}\;.$$

This relation determines the initial position of a particle of given radius meeting the wall at the inlet of the conical converging section. Conversely, considering an initial position characterized by r_1, we can calculate a radius value r_{pm} such that all particles of greater radii must necessarily be captured.

In a streamline of section $2\pi r_1 dr_1$, the mass flow of the condensed phase is:

$$d\dot{m}_p = \rho_p\,u_{p_c}\,2\pi r_1\,dr = 2\pi u_{g_c}\left(\int_0^\infty \tfrac{4}{3}\pi r_p^3 \rho_c\,f(r_p)\,dr_p\right) r_1\,dr_1.$$

The mass flow captured by the wall is:

$$d\dot{m}_{p_c} = 2\pi u_{g_c}\left(\int_{r_{pm}(r_1)}^\infty \tfrac{4}{3}\pi r_p^3 \rho_c\,f(r_p)\,dr_p\right) r_1\,dr_1.$$

The total captured flow is obtained by integration:

$$\dot{m}_{pc} = 2\pi u_{gc} \int_0^{r_e} \left(\int_{r_{Pn}(r_1)}^{\infty} \frac{4}{3}\pi r_p^3 \rho_c f(r_p) dr_p \right) r_1 dr_1$$

$$= \pi u_{gc} r_e^2 \int_0^1 \left(\int_{r_{Pm}\left(\left(\frac{r_1}{r_e}\right)^2\right)}^{\infty} \frac{4}{3}\pi r_p^3 \rho_c f(r_p) dr_p \right) d\left(\frac{r_1}{r_e}\right)^2 .$$

Or, bringing the captured flow back to the total flow:

$$\frac{\overset{\circ}{m}_{pc}}{\overset{\circ}{m}_p} = \varepsilon \frac{\int_0^1 \left(\int_{r_{pm}(b)}^{\infty} r_p^3 f(r_p) dr_p \right) db}{\int_0^{\infty} r_p^3 f(r_p) dr_p} ,$$

where $\varepsilon = \dfrac{K}{1+K}$, ratio between the condensed phase flow and the total flow.

The integral of the numerator can be transformed by permuting the order of integrations:

$$\int_0^1 \left(\int_{r_{pm}(b)}^{\infty} r_p^3 f(r_p) dr_p \right) db = \int_0^{\infty} \left(\int_{b(r_p)}^1 db \right) r_p^3 f(r_p) dr_p$$

$$= \int_0^{\infty} \left[1 - b(r_p) \right] r^3 f(r_p) dr_p ..$$

Now:

$$1 - b(r_p) = 1 - \frac{r_1^2}{r_e^2} \simeq -2 \log \frac{r_1}{r_e} = 2 \times \frac{2\eta^2 \rho_c u_{gc}}{9\mu r_e} \cdot \frac{\frac{1}{6}\beta + \frac{1}{2}\left[\log\left(\frac{1}{6}\beta + \frac{1}{\alpha\beta}\right) + \frac{1 \cdot \beta}{\alpha\beta}\right]}{\ell}$$

Integration thus shows the mean radius r_{53}. In fact we can write:

$$\frac{\overset{\circ}{m}_{pc}}{\overset{\circ}{m}_p} = \varepsilon \cdot \frac{\overline{a_{uo}} \, u_{gc}}{r_{cc}} \cdot g(\beta) ,$$

where the index 0 indicates that this is the mean radius in the chamber where the significance of $g(\beta)$ is obvious.

The relative specific impulse loss is proportional to the relative non-ejected mass which is less than the mass captured by the nozzle. Moreover, it is useful to bring velocity u_{gc} down to the speed of sound $\bar{a}_0^{(o)}$ at two-phase equilibrium in the chamber and radius r_e to throat radius r_c. After transformation we finally get, when r_e/r_c remains fairly large:

$$\frac{|\delta I|}{I^{(o)}} \leq \varepsilon \frac{\overline{a_{uo}}\,\overline{a_o}^{(o)}}{r_c}\left(\frac{\overline{\gamma}+1}{2}\right)^{-\frac{\overline{\gamma}+1}{\varepsilon(\overline{\gamma}-1)}}\left(\frac{r_c}{r_c}\right)^3\left[r_\beta\beta + \frac{1}{2}\left[\log\left(r_\beta\beta + \frac{1}{\cos\beta}\right) + \frac{r_\beta\beta}{\cos\beta}\right]\right]$$

This formula resembles that established for loss due to phase lags in near equilibrium: it is proportional to the metal content of the propellant through the intermediary of ε, to a dimensionless factor which brings in the mean particle relaxation content, a velocity $\overline{a}_o^{(o)}$ characterizing the condition of the combustion products in the chamber and the scale of the motor by the throat radius, and finally a geometric factor depending principally on the inlet ratio and the converging section angle. To extend this formula to more difficult inlet conditions (inlet ratio close to 1, very abrupt converging section) it is probably sufficient to modify the geometric factor.
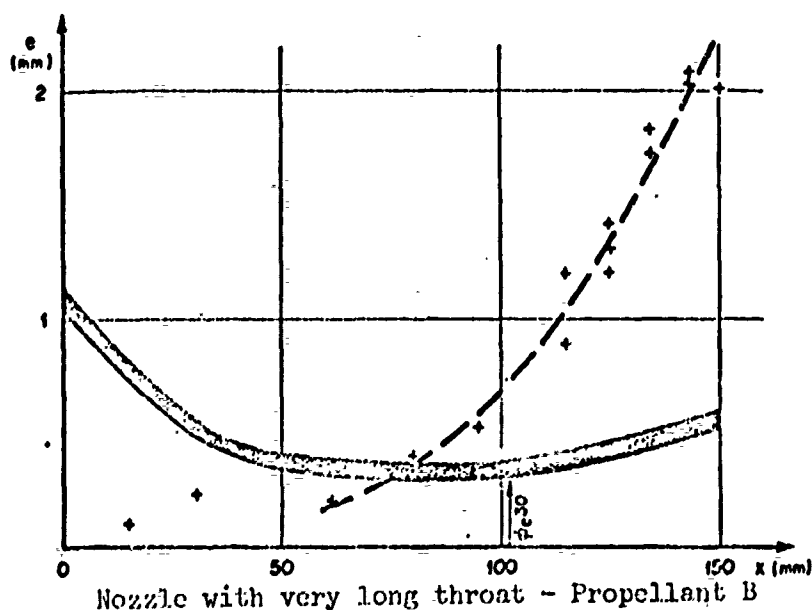
5.3. DEVELOPMENT AND DESTRUCTION OF CONDENSED LAYER

Development of the condensed layer depends both on the flow and the wall heat problem. Flow intervenes by the impact of the particles; the mass flow deposited locally depends on the time by reason of modification of the nozzle inlet geometry due to combustion of the propellant grain and increase in the mean hole diameter. Wall heating no longer depends not only on heat transfer due to the boundary layer but also on transfer through the condensed layer; the thickness of the layer and its physical conditions (liquid or solid according to temperature), and heat properties are thus involved. The condensed layer does not always develop over the entire surface: the nozzle geometry seems to play an important role as shown in Figure 26. The alumina film does not develop beyond the throat when the throat radius of curvature is small as compared to its radius, at least for small motors. We therefore need to look for the phenomenon which disintegrates the alumina layer and the results of this disintegration.

-141-

The condensed layer has not been studied to date, except for some very fragmentary results from Colucci [3] and Unger [71]. We will try to bring out certain general features of the problem which can have some impact on estimating specific impulse loss from the wall. Some simplifications will be made to permit a local heat transfer study: accumulation of heat in the layer is neglected by comparison with the quantity of heat transmitted [71]; conduction of heat parallel to the wall is a second-order phenomenon due to the intense flows, and the nozzle is considered to be infinitely thick which excludes external influences. The problem of conduction in the nozzle is brought to that of a semi-infinite wall with variable surface conditions; in actual fact we should take surface curvature into consideration but in the first approximation this phenomenon is neglected. Even for constant heat properties the relation between the wall flow temperature and density is not simple in form. Classical calculations [72] enable us to come to the integral equation:

$$T_P(t) - T_0 = \Theta_P(t) - \frac{\sqrt{a_P}}{\lambda_P \sqrt{\pi}} \int_0^t \frac{q(\tau)\,d\tau}{\sqrt{t-\tau}} \, ,$$

where a_p and λ_p are the diffusivity and heat conductibility of the nozzle material.

Nozzle with very long throat - Propellant B
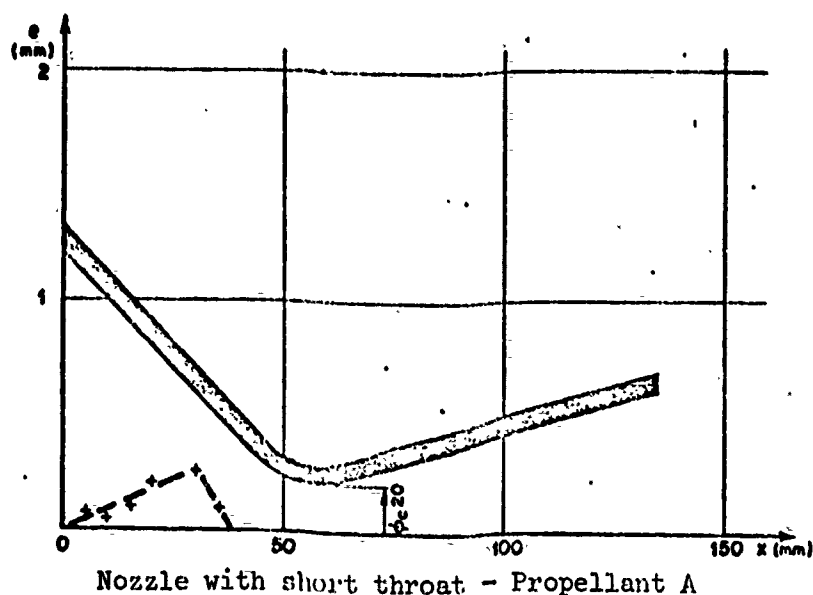
-142-

Nozzle with short throat – Propellant A

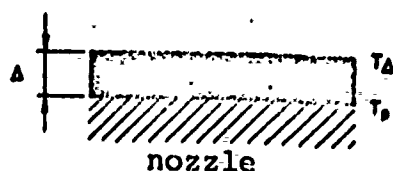Figure 26. Thickness of Alumina Deposit Collected After Firing.

The flux density can also be expressed by means of different heat transfers. With the notations of Figure 27, we get:

$$q = h'(\Theta_L - \Theta_\delta) = \frac{\lambda_e}{\delta}(\Theta_\delta - \Theta_\Delta) = \frac{\lambda_s}{\Delta}(\Theta_\Delta - \Theta_P) = \frac{\Theta_L - \Theta_P}{\frac{1}{h'} + \frac{\delta}{\lambda_e} + \frac{\Delta}{\lambda_s}}$$

Eliminating the wall temperature $T_{P'}$ we obtain an integral equation for flux:
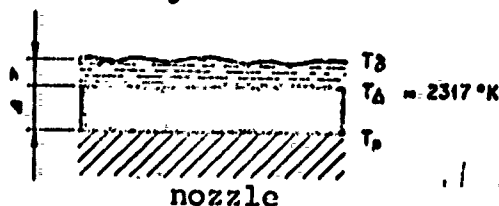
$$\frac{\sqrt{a_P}}{\lambda_P \sqrt{\pi}} \int_0^t \frac{q(\tau)d\tau}{\sqrt{t-\tau}} + \left(\frac{1}{h'} + \frac{\delta}{\lambda_e} + \frac{\Delta}{\lambda_s}\right) q(t) = \Theta_L .$$

$T_\Delta < 2317\,°K$ $T_\delta > 2317\,°K$

$T_\Delta = 2317\,°K$

nozzle   nozzle

solid layer   solid and liquid layer

Figure 27. Notations Used for Studying the Condensed Phase.

In this equation thicknesses δ and Λ and to a less extent coefficient h' (ignition phase, modification of inlet geometry over time) must be considered as functions of time. We may try to find out whether the presence of the layer is truly important; it could be neglected provided, for example, that:

$$\Delta \ll \frac{\lambda_S}{h'} .$$

Computer application leads to:

$$\Delta \ll 0.2 \text{ mm in the throat,}$$
$$\Delta \ll 1.7 \text{ mm in the middle of the converging section (Figure 26).}$$

These are in actual fact the order, of magnitude usually observed; we must thus study the phenomenon in a more precise fashion.

a) Thickness of negligible or non-existent deposit

Calculation is then done in the classical way as for a non-metallized propellant. If we consider h' constant we come out analytically to the solution:

$$\frac{q(t)}{h'\Theta_L} = \exp\left(\frac{a_p h'^2}{\lambda_p^2} t\right) \times \mathrm{erfc}\left(\sqrt{\frac{a_p h'^2}{\lambda_p^2} t}\right) ,$$

$$\frac{\Theta_P}{\Theta_L} = 1 - \exp\left(\frac{a_p h'^2}{\lambda_p^2} t\right) \times \mathrm{erfc}\left(\sqrt{\frac{a_p h'^2}{\lambda_p^2} t}\right)$$

We note that these formulas can be extended to the case where a layer of constant thickness Λ and exchange by radiation between the combustion products and the wall exist, the layer being transparent to radiation and the wall temperature rather small as compared to Ti. We then define an equivalent heat exchange coefficient $\bar{h}$ by the formula:

$$\frac{1}{\bar{h}} = \frac{1}{h'} + \frac{\Delta}{\lambda_s} \quad ,$$

or:

$$\bar{h} = \frac{h'\lambda_s}{\lambda_s + h'\Delta} < h' .$$

We get:

$$\frac{q(t)}{\bar{h}\Theta_L + a\sigma T_L^4} = \exp\left(\frac{a_p \bar{h}^2 t}{\lambda_p^2}\right) \times \mathrm{erfc}\left(\sqrt{\frac{a_p \bar{h}^2}{\lambda_p^2} t}\right),$$

$$\frac{\Theta_p}{\Theta_L + \frac{a\sigma T_L^4}{\bar{h}}} = 1 - \exp\left(\frac{a_p \bar{h}^2 t}{\lambda_p^2}\right) \times \mathrm{erfc}\left(\sqrt{\frac{a_p \bar{h}^2 t}{\lambda_p^2}}\right)$$

Figure 28 shows the shape of the flux and temperature curves for small magnitudes. Temperature increases with time while flux decreases. A change in $\bar{h}$ is translated simply by dilation of the time scale.
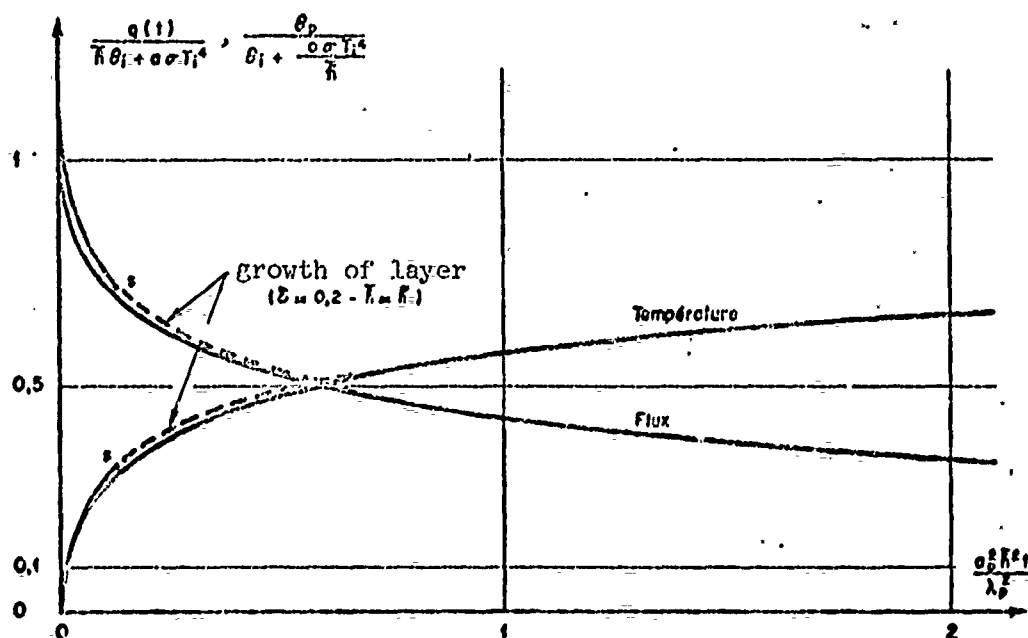

Figure 28. Change of Wall Flux and Temperature Through Time Without Variation of the Condensed Layer (h = cte).

Rather than the instant flow value it is the mean value during motor operation which enables the total heat loss to be estimated. We thus write:

$$\bar{q}(t) = \frac{1}{t_b} \int_0^{t_b} q(t)\,dt .$$

Calculation gives:

$$\frac{q}{\hbar\,\Theta_L + \sigma\tau\,T_L^4} = f\left(\sqrt{\frac{c_{\tau}\hbar^2 t_b}{\lambda_p^2}}\right), \text{ where } f(\zeta) = \sqrt{\pi}\frac{\zeta - (1 - e^{\zeta^2}\operatorname{erfc}\zeta)}{\zeta^2}.$$

The function f(z) can easily be tabulated; it decreases with combusiton time t_b (wall hotter on the average) and with the heat exchange coefficient $\bar{h}$ (more rapid wall heating).

b) Deposit thickness non-negligible, as layer is always solid

The layer remains solid if the surface temperature, in contact with the flow, does not exceed the alumina melting point; the particles solidify at their impact point which to some extent facilitates calculation of layer thickness.

The density of the flux transmitted to the nozzle wall is composed of the radiation flux density and the conduction flux density, through the solid layer, due to convection and to the heat energy introduced by the particles. We will call the mass density of the captured flow f, i.e., the condensed mass arising per unit time and surface on the layer. As the layer is solid, f is linked to the layer growth rate; the particles solidify almost instantaneously at the impact point, so that we have:

$$f = \rho_c \frac{d\Delta}{dt}.$$

The energy introduced by the particles is broken down into a large heat term and a change-of-state term (the kinetic energy of the particles, moderate in the converging section, is neglected):

$$q_p = f\left[c_c(T_c - T_A) + L_f\right],$$

where C_c is the mass heat of alumina, L_f its mass melting enthalpy, and T_c its temperature (T_c is close to T_i in the converging section).

We thus get:

$$q - \sigma\tau\,T_L^4 = \frac{\lambda_s}{\Delta}(\Theta_A - \Theta_P) = \hbar'(\Theta_L - \Theta_A) + \rho_c \frac{d\Delta}{dt}\left[c_c(\Theta_c - \Theta_A) + L_f\right]$$

θ_Δ is first eliminated to obtain θ_p. To simplify we also assume that Δ varies linearly with time:

$$\Delta = \alpha t .$$

This hypothesis implies that f is constant, i.e., the transient phenomena due, for example, to variations in inlet geometry linked to combustion have little effect on the impact.

The equation for flow q is finally written:

$$\frac{\sqrt{a_p}}{\lambda_p \sqrt{\pi}} \int_0^t \frac{q(\tau)d\tau}{\sqrt{t-\tau}} + \left(\frac{1}{h' + \rho_c C_c \alpha} + \frac{\alpha t}{\lambda_s}\right) q = \theta_i + a_\tau T_i^4 \frac{\alpha t}{\lambda_s} + \frac{a_\tau T_i^4 + \rho_c L_f \alpha}{h' + \rho_c C_c \alpha} .$$

It is interesting to write this equation for small magnitudes. As we are trying to compare q to its value without a condensed layer we will bring q to the quantity $\theta_i h' + a_\tau T_i^4$ and t to $\frac{\lambda p^2}{a_p h'^2}$.

The calculations show the existence of dimensionless parameters:

- $d = \dfrac{\rho_c C_c}{h'}$, the ratio between the perceivable heat introduced by the particles and that introduced by the boundary layer,

- $\beta = \dfrac{a_c \ell}{a_p} \dfrac{\lambda_p^2}{\lambda_{ce} \lambda_s}$, heat parameter linked to the nature of the materials (alumina, wall),

- $R = \dfrac{a_\tau T_i^4}{\theta_i h'}$, parameter characterizing the relative importance of radiation,

- $\ell = \dfrac{L_f}{C_c \theta_i}$, reduced melting enthalpy.

The reduced equation is:

$$\frac{1}{\sqrt{\pi}} \int_0^t \frac{q(\tau)d\tau}{\sqrt{t-\tau}} + \left[\frac{1}{1+d} + \beta d t\right] q = \frac{1+R+d(1+\ell)}{(1+R)(1+d)} + \frac{R}{1+R} \beta d t .$$

-147-

Computer calculation shows that d is on the order of 1 at most and less than 0.1 when the section ratio is less than 4. In the absence of an analytical solution we look for a solution by the perturbation method where d is the perturbation parameter.

We first use the Laplace transform to come down to a differential equation:

$$-\frac{\beta d}{2}\frac{dF}{d\sqrt{p}} + \left(1 + \frac{\sqrt{p}}{1+d}\right)F = \frac{(1+R)+d(1+\ell)}{(1+R)(1+d)}\frac{1}{\sqrt{p}} + \frac{R\beta d}{1+R}\frac{1}{p\sqrt{p}} .$$

At order 0 we get:

$$F^{(0)} = \frac{1}{\sqrt{p}\,(1+\sqrt{p})} \quad \text{or} \quad q^{(0)} = e^t erfc(\sqrt{t}),$$

classical solution in the absence of layer.

With order d, we obtain:

$$F^{(1)} = \frac{1}{(1+\sqrt{p})^2} + \frac{\beta}{2}\cdot\left[\frac{1}{(1+\sqrt{p})^3} - \frac{1}{p(1+\sqrt{p})}\right] + \frac{\ell R}{1+R}\frac{1}{\sqrt{p}(1+\sqrt{p})} + \frac{R\beta}{1+R}\frac{1}{p\sqrt{p}(1+\sqrt{p})} .$$

Inversion of function $F^{(1)}$ is fairly long; we will only the give the final result:

$$q^{(1)} = -\beta\left(\frac{1}{2}+\frac{R}{1+R}\right) + \sqrt{\frac{t}{\pi}}\left[\beta t + \beta\left(1+\frac{\ell R}{1+R}\right)-2\right] + \left[-\beta t + \left(2-\frac{3\beta}{2}\right)t + \frac{1+\ell}{1+R} + \beta\left(\frac{1}{2}+\frac{R}{1+R}\right)\right] \times$$
$$\times e^t erfc(\sqrt{t})$$

The approximate expression for flux density will thus be:

$$q \approx q^{(0)} + d q^{(1)} .$$

We can deduce from q the wall and surface temperatures θ_p and θ_Δ (reduced to $\theta_i(1 + R)$):

$$\Theta_p = \Theta_p^{(0)} + d\Theta_p^{(1)},$$

$$\Theta_\Delta = \Theta_\Delta^{(0)} + d\Theta_\Delta^{(1)},$$

with: $\Theta_P^{(6)} = \Theta_A^{(6)} = 1 - e^r \, \mathrm{erfc}(\sqrt{r})$

$$\Theta_P^{(1)} = \frac{\beta}{2} + \frac{\ell - R}{1+R} + \frac{R\beta}{1+R}(1+r) - \sqrt{\frac{r}{\pi}}\left[\beta r + \beta\left(1 + \frac{2R}{1+R}\right) - \ell\right] +$$
$$+ \left[\beta r^2 + \left(\frac{\beta}{2} - \ell\right)r - \left(\frac{\beta}{2} + \frac{\ell - R}{1+R} + \frac{R\beta}{1+R}\right)\right]e^r \, \mathrm{erfc}(\sqrt{r})$$

$$\Theta_A^{(1)} = \frac{\beta}{2} + \frac{\ell - R}{1+R} + \frac{R\beta}{1+R} - \sqrt{\frac{r}{\pi}}\left[\beta r + \beta\left(1 + \frac{2R}{1+R}\right) - \ell\right] +$$
$$+ \left[\beta r^2 + \left(\frac{3\beta}{2} - \ell\right) - \left(\frac{\beta}{2} + \frac{\ell - R}{1+R} + \frac{R\beta}{1+R}\right)\right]e^r \, \mathrm{erfc}(\sqrt{r})$$

We must check that the surface temperature Θ_A does not exceed the alumina melting point, namely, with a reduced value:

$$\Theta_A < \frac{T_F - T_0}{(T_i - T_0)(1+R)} .$$

It is also necessary to calculate the mean flow density through the time interval $(0, t)$. We brought this value to its value without a layer:

$$\frac{\bar{q}}{\bar{q}^{(0)}} = 1 + d\left\{ -\beta r^2 + \left(2 + \frac{\beta}{2}\right)r + \frac{\ell - R}{1+R} + \frac{\beta R}{1+R} - 1 + \right.$$
$$\left. + \frac{-\beta r^2 + \left(2 - \frac{\beta R}{1+R}\right)r + \sqrt{\frac{r}{\pi}}\left[2\beta r^2 - 4\left(1 - \frac{\beta R}{3(1+R)}\right)r\right]}{2\sqrt{\frac{r}{\pi}} - (1 - e^r \, \mathrm{erfc}(\sqrt{r}))} \right\}$$

For computer application we chose for h' the value relative to a mean ratio between the grain hole radius and throat radius of about 4, which aligns well with our tests and we chose for a the value of 0.1 mm/sec which appears fairly realistic. We deduce:

$$d \simeq 0,2 \ . \quad \beta \simeq 1 \ . \quad R \simeq 1 \ . \quad \ell = 0,24 \ .$$

We note that the value of d matches the domain of application of the perturbation method and we note the size of radiation at this point.

The results of calculation are shown in Figure 28:

- The flux is slightly greater than in the absence of a layer and the difference tends to diminish through time. This result is due in the first instance to the energy introduced by the particles.

- The wall temperature increases slightly faster than in the absence of a layer. This result could not be known a priori since the two effects offset each other: increase of flux due to impacts and blocking of flux by the condensed layer.

- The mean flux differs from its layer-less value only by about 10% at the beginning of the phenomenon; this difference is less than the accuracy one could expect from heat flux calculations.

We also observe that the alumina melting point is quickly reached in this place; calculation gives $t_2 \approx 1.2$ sec., a time at which $\theta_{ps} \approx 1000°C$ and $\Lambda_s \approx 0.12$ mm.

c) Solid condensed layer on nozzle wall, liquid at the flow interface

The surface temperature of the condensed layer exceeds the alumina melting point but the wall temperature is less than this. Thus there are actually two different layers: liquid and solid. To simplify we will say that the change of state is frank and without density change. The same time scale is retained. The relation between surface temperature and flux is thus:

$$\theta_P = \theta_{Ps} + \frac{\sqrt{a_p}}{\lambda_p \sqrt{\pi}} \int_{t_s}^{t} \frac{q(\tau) d\tau}{\sqrt{t-\tau}} \quad , \quad t \geq t_s .$$

q is broken down into a radiation term $a\tau T_i^4$ and a conduction term through the solid layer:

$$q_{cond_s} = \frac{\lambda_s}{\Delta} \left(\theta_{i\Delta} - \theta_P \right) .$$

This flux density is equal to that due to conduction in the liquid layer plus the heat released by solidification:

-150-

$$q_{conds} = \frac{\lambda_L}{\delta}\left(\Theta_\delta - \Theta_\Delta\right) + \rho_c L_f \frac{d\Delta}{dt}.$$

The conduction flux density in the liquid layer corresponds to
the convection flux density and to the perceptible heat introduced
by the particles (their kinetic energy is neglected):

$$\beta_i'\left(\Theta_L - \Theta_\delta\right) + f C_c\left(\Theta_L - \Theta_\delta\right).$$

Elimination between the various Θ_δ and Θ_p equations (Θ_Δ is a
constant, the solidification temperature) enables us to write the
two final equations:

$$\frac{\sqrt{a_p}}{\lambda_p \sqrt{\pi}} \int_{t_s}^{t} \frac{q(\tau) d\tau}{\sqrt{t-\tau}} + \frac{\Delta}{\lambda_s} q = \Theta_\Delta - \Theta_{Ps} + \frac{\Delta}{\lambda_s} \sigma \nabla T_L^4 ,$$

$$\rho_c L_f \frac{d\Delta}{dt} = q - \sigma \nabla T_L^4 - \left(\Theta_L - \Theta_\Delta\right) \frac{\beta_i' + f C_c}{1 + \frac{\delta}{\lambda_\ell}\left(\beta_i' + f C_c\right)}.$$

Since f is assumed to be known these equations contain only
three unknowns: q, δ, Δ; we are thus missing one equation obtained
by studying the liquid layer. The heat equation of this layer has
already been used and uncoupled from the other equations; we now
only need to exploit the continuum equation and the momentum
equation. Here we will leave out transient effects and assume
that the local variations in layer thickness are moderate.

The momentum equation is used implicitly assuming that the
velocity profile is parabolic in the liquid layer. This law
results from studying the equilibrium of a liquid element:

$$\frac{d\tau_{PL}}{dy} = \frac{dp}{dx} , \qquad \text{(x: curvilinear}$$
$$\text{abscissa)}$$

where pressure p is known from the flow.

When we assume that dynamic viscosity is constant, integration of this relation leads to the contour of which we spoke. The integration constants are determined by the velocity cancellation condition at the liquid-solid interface and the connection of tangential forces at the liquid-gas interface:

$$(\tau_{FL})_\delta = \tau_P ,$$

τ_p being determined by examination of the classical boundary layer (the interface velocity is small compared to the flow velocity) and the momentum introduced by the particles being neglected.

We thus get:

$$u = \frac{1}{2\mu_L} \frac{dp}{dx} y^2 + \frac{1}{\mu_L} \left(\tau_P - \delta \frac{dp}{dx}\right) y , \qquad 0 \leq y \leq \delta .$$

This expression enables us to calculate the local instant flowrate:

$$\overset{\circ}{m}_L = \frac{2\pi R \rho_c}{6 \mu_L} \left(3 \delta^2 \tau_P - 2 \delta^3 \frac{dp}{dx}\right), \qquad \frac{\delta}{R} \ll 1 .$$

The continuum equation indicates that the increase in flowrate according to x is due to the arrival of particles at the liquid layer minus the rate lost by solidification. Hence, finally:

$$\rho_c \frac{d\Delta}{dt} = f' - \frac{\rho_c}{6\mu_L} \frac{d}{dx} \left[3\delta^2 \tau_P - 2\delta^3 \frac{dp}{dx}\right] .$$

This is the third equation for which we were looking. The problem is thus fully defined by the three equations and the boundary conditions:

$$t = t_s : \qquad \delta = 0 , \quad \Delta = \Delta_s .$$

-152-

We see that there is a coupling between the local time varia-
tions of the characteristic magnitudes of the layer and their
spatial variations due to the liquid flow. Resolution of the
problem thus implies a thorough description of impacts and
rather cumbersome computation. We might think that streaming of
the liquid would first limit the thickness of the layer; tempera-
tures continue to grow, the solid layer will melt until it completely
disappears when the wall temperature reaches the melting point. It
is thus probable that the condensed layer does not increase in sub-
stantial proportions with respect to its value Λ_s and that, as a
consequence, perturbation introduced by this layer into the flux
and wall temperature calculation remains moderate.

Equations can also be established in the case of a fully
liquid layer $(\theta_p > \theta_\Delta)$

$$\left\{ \begin{array}{l} \dfrac{\sqrt{a_p}}{\lambda_p \sqrt{\pi}} \displaystyle\int_{t_L}^{t} \dfrac{q(\tau)\,d\tau}{\sqrt{t-\tau}} + \left(\dfrac{1}{h + f c_c} + \dfrac{\delta}{\lambda_L}\right) q = \theta_c - \theta_p + \sigma T_c^4 \left(\dfrac{1}{h + f c_c} + \dfrac{\delta}{\lambda_L}\right), \\[4mm] f = \dfrac{\rho_c}{6 \mu_L} \dfrac{d}{dx}\left[3\delta^2 \tau_p - 2\delta^3 \dfrac{dp}{dx}\right] \quad , \quad t \geq t_L \, , \end{array} \right.$$

with: $t = t_L$, $\delta = \delta_L$.
In this case the second equation can be integrated:

$$3\delta^2 \tau_p - 2\delta^3 \dfrac{dp}{dx} = \int_{x_0(t)}^{x} \dfrac{6\mu_L f}{\rho_c}\,dx,$$

$x_0(t)$ étant défini par $\delta = 0$.

$x_0(t)$ is defined by $\delta = 0$.

x_0 can be determined only by a complete study of the entire con-
densed layer.

d) Destruction of condensed layer

As the surface of the layer rapidly rises to the alumina
melting point, this layer should theoretically cover the entire

-153-

nozzle surface, which in fact it does not (Figure 26). There thus
exists a phenomenon which limits flow of the liquid alumina under
certain conditions; this phenomenon relates to the stability of the
liquid layer and has been studied in some depth [73 to 76]. Our
objective here is to find out the conditions under which the liquid
layer is unstable and the result of its destruction.

We will briefly set out the method of establishing the stabil-
ity criterion. We first assume that the surface equation is of the
form:

$$\bar{y} = \eta e^{\tau t} \cos(kx - \omega t),$$

where k is a given wave number (wavelength $\lambda = 2\pi/k$) and w and τ
are real constants which we will determine. First considering
the case of a non-viscous layer of infinite thickness in contact
with a non-viscous gas [74] we write the linear continuum and
momentum equations of the liquid layer which must be integrated
with two conditions: one relates to an infinite depth and the
other is of kinematic nature at the interface. In the gas we
can define a pressure perturbation due to interface variations;
we must then find out whether the flow is subsonic or supersonic.
The expressions for τ and w as a function of k are obtained by
writing the interface equilibrium under the effect of pressure
and surface tension forces. The calculation is then extended
to the case of a viscous layer of finite depth taking the boundary
layer and volume forces into account.

Applying the results of Chang and Russell, we can for example
plot, as a function of the Mach number, the wavelength characterizing
the limit of stability. We see from Figure 29 that at the nozzle
throat all perturbations with wavelengths greater than 1 micron
are amplified; since the scale of phenomena in a motor is always
greater than the micron, if for no other reason because of the
mean diameter of particles likely to deposit on the liquid layer,
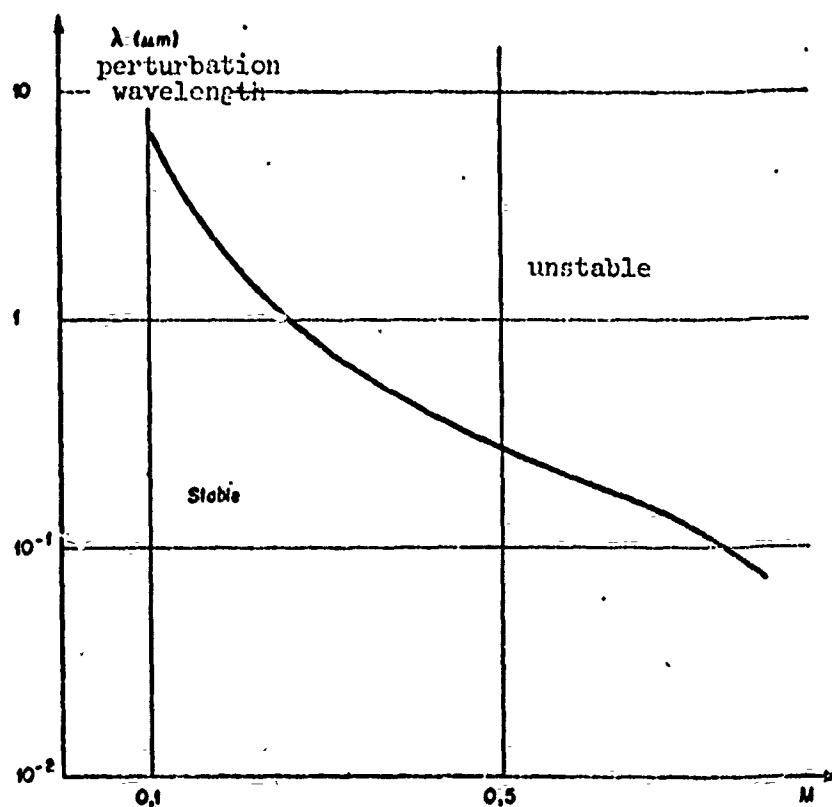we must assume that this layer is naturally unstable.

Figure 29. Stability of Boundary Layer.

To explain the discrepancies between the two results of Figure 26 we must remember that impacts take place almost exclusively in the converging section and that the physical condition of the layer depends on heat transfer. For the nozzle with a very large throat radius of curvature, the exchange coefficient h' remains moderate in the throat region such that the surface temperature does not reach θ_Λ during firing; alumina progresses in this direction by streaming over the wall but solidifies there before being destroyed by instability; the alumina deposited on the converging section passes the throat by this process and can then accumulate on the relatively cold wall of the diverging section. For the nozzle with a small radius of curvature at the throat the high value of the exchange coefficient implies that the surface temperature very quickly rises to θ_Λ which is checked experimentally

by heat measurements; the whole layer reaching the throat is liquid, it is destroyed by instabilities and is not found in the converging section.

The fragments of the liquid layer reinjected into the flow take on a spherical shape unless their diameters are too large to ensure stability in acceleration in which case they are likely to disintegrate. The particle size of the new formed particles is poorly known; the most we can do is to cite the results of Sherman and Schetz [75] whose conditions, however, are somewhat removed from those of our problem: the observed particle diameter extends up to 100 microns with an average diameter between 20 and 30 microns, which would correspond approximately to the wavelength giving the maximum instability rate of growth. In the absence of more precise information we will say that the order of magnitude mentioned applies to alumina particles formed from the condensed layer; these particles are only slightly accelerated by the flow which justifies definition of loss due to impact. We will note that experimental observations indicate that destruction of the layer cannot be an entirely continuous phenomenon: films of the jet show that, from time to time, flashes pass by -- probably formed from alumina.

5.4 EXPERIMENTAL STUDY OF WALL PHENOMENA

The various phenomena involved in the preceding calculations are insufficiently known and it appears essential to perform measurements to supplement theoretical developments. Among the magnitudes that can perhaps be determined by experiment comes first thickness of the alumina deposit on the wall. Tests were made for this purpose, cutting off a motor after different operating times; cutoff by expansion is a sudden phenomenon, adherence of the layer is imperfect, and rapid cooling of the nozzle often causes the solidified layer to detach and fragment such that it is a rather difficult matter to run these tests. Today we have only fragmentary qualitative information; for the operating conditions chosen, characterized by the type of propellant, motor, and nozzle (geometry and materials)

the alumina layer appears very rapidly at the nozzle throat then subsists only in the inlet zone of the converging section. Tests on a simulation assembly to define the instability of a liquid layer in a nozzle throat have also been undertaken but have not yet yielded practical results; during these tests one could study the particle size of the droplets formed by disintegration of the liquid layer.

Measurement of the temperature or heat flux of the wall, which magnitudes are linked by conduction in the later, is more classical. These measurements have often been done for the chamber or nozzle of liquid propellant rocket motors [67] but are far more scarce for solid metallized propellants; this is because the technological problems are more difficult in the latter case (higher temperatures) and the heat shield problem is different (utilization of ablating materials). Utilization of special metal nozzles designed for these measurements enables the total heat transfer coefficient of the combustion products to the nozzle to be determined [3, 71] but we may ask whether the condensed layer here develops in the same way as under real conditions. We thus choose to use flowmeters built into the real nozzle giving a local measurement and disturbing motor operation only slightly.

The demands placed on the flowmeter are severe: very short response time (rise from 0 to 1000°C in less than 0.1 sec when the motor ignites), high-temperature behavior (2000°C) under very intense flux densities (on the order of $10^4 kW/m^2$), small dimensions in order to have the least possible perturbation of nozzle conduction and remain integrated in nozzle which themselves are small. The type of flowmeter chosen is that performing according to the heat well principle; in fact we are measuring the temperature or a phenomenon linked to temperature and with the aid of conduction equations in the solid we go back to the wall flux. Platinum film thermometric probes [77, 78], developed for somewhat similar problems, were used without success as they were of inadequate resistance. A special material had to be developed.

The flowmeters developed and tested had the approximate shape
of a cylinder 4 mm in diameter and 13 mm long made of graphite,
i.e., the same material as the nozzle (grade 58-90 by Carbone-
Lorraine). The two types of flowmeters designed one after the
other differ only by temperature measurement. In the first type
(Figure 30) the temperature is measured at two distances from the
wall by small-diameter thermocouples (Chromel-Alumel thermocouples
clad in stainless steel 0.5 mm in diameter of the Philipps Thermo-
coax type). Conduction is only slightly perturbed by the longi-
tudinal arrangement of the two thermocouples, as the thermal
conductivities of the graphite and the metals are of the same order
of magnitude. The very precise position of the hot weld of the
thermocouples is determined after the flowmeter is completely fin-
ished by an X-ray photograph. This type of flowmeter proved to
have two major drawbacks: it implied a fairly imprecise method
of analysis because one had to go back from the temperature to
the point measured at the wall temperature, i.e., extrapolate in
a zone where the heat gradient is particularly intense; also it
is limited as to temperature (1200°C) because the Chromel Alumel
couples are destroyed. Use of stronger couples, for example
platinum and platinum-rhodium could only be considered when the
couples are available in a smaller clad diameter. It should,
however, be noted that this type of flowmeter is the only type
that can be used in the case of wall erosion, particularly in the
nozzle throat, provided that wall displacement can be arranged
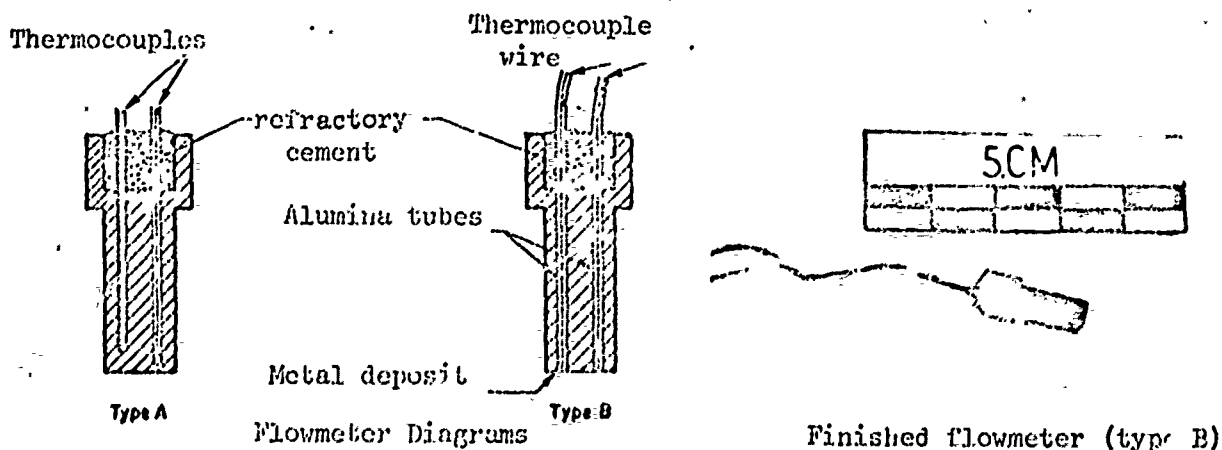for elsewhere.

Figure 30. Flowmeters Arranged on the Nozzle.

-158-

The second type of flowmeter aims to determine the surface temperature directly making the hot weld of a thermocouple by a very fine surface metal deposit. To permit operation at very high temperature the tungsten-rhenium 5% -- tungsten-rhenium 26% couple was used. The two wires are separated by alumina tubes themselves built into the graphite. The tungsten deposit proved to be the most difficult; several methods were tried: deposit of molten metal with the aid of a plasma jet, deposition in the vapor phase, and cathode pulverization. The latter method gave very encouraging results since, for an 8 μ deposit, a total operating time greater than 8 seconds was obtained; however, the technique seems inadequately mastered to give correctly reproducible results from the adherence standpoint. When these difficulties have been smoothed over this type of flowmeter should give substantially increased accuracy compared to the preceding type.

The final accuracy of the results is not only due to measurement but also the method of analysis which is delicate here due to the wide temperature differences found in one test. These differences are translated by a noteworthy variation (from 1 to 5) of the graphite heat properties, particularly heat conductivity. The heat conduction problem in the material is thus non-linear, which makes it necessary to resort to the computer or to approximate methods of calculation.

The computer must be used to determine the flow density when the surface temperature is imposed. For non-linear one-dimensional conduction it became possible to develop a finite-difference calculation method of the explicit type; the stability criterion is then given by relation [79]:

$$a_p \frac{\Delta t}{(\Delta x)^2} \leqslant \frac{1}{2} .$$

The computer program for this has not yet been developed; it will be as soon as the technological problems in building the flowmeter

have been overcome and the heat properties of the material have been
defined over a suitable temperature interval.

Approximate calculation methods were developed to analyze
the measurements made by both types of flowmeter. Reference [80]
summarizes all the analytic method developed for unsteady non-
linear conduction problems. The two methods developed are both
based on an algebraic representation of temperature.

The first method is an adaption of the variational methods
established by Biot [81] to the problem connected with the second
type of flowmeter and extended to the case of variable heat
properties [82]. The mathematical problem comes down to seeking
the solution of a partial derivative equation:

$$\frac{\partial^2 \Lambda}{\partial X^2} = \frac{1}{A(\Lambda)} \frac{\partial \Lambda}{\partial t^*} \quad , $$

$$\text{où} \quad \Lambda = \frac{\int_{T_R}^{T} \lambda(T)\, dT}{\lambda_R T_R} \quad ,$$

$$A = \frac{a(\Lambda)}{a(0)} \quad ,$$

$$X = \frac{x}{L} \quad , \quad t^* = \frac{t\, a_R}{L^2} \quad ,$$

and with boundary conditions:

$$t^* = 0 \quad , \quad \Lambda = 0 \quad \forall x ,$$

$$t^* > 0 \quad , \quad x = 0 \quad , \quad \Lambda = \Lambda_P .$$

We assume that Λ is of the form:

$$\Lambda = \Lambda_P \left(1 - \frac{x}{P}\right)^n \quad , \quad x \leqslant P , \quad n \geqslant 2 ,$$

where p here represents the thickness of heat penetration. We
establish that p is defined by the differential equation:

$$P \frac{dP}{dt^*} I_1(\Lambda_P) + \frac{P^2}{n} \frac{1}{\Lambda_P} \frac{d\Lambda_P}{dt^*} I_2(\Lambda_P) = n\, I_3(\Lambda_P) ,$$

where
$$I_1(\Lambda_P) = \int_0^1 \tau^{-\frac{1}{4}\hat{P}} \left[\int_0^\tau \frac{1-\tau^{\frac{1}{4}}}{A(\tau \Lambda_P)} d\tau \right] d\tau,$$

$$I_2(\Lambda_P) = \int_0^1 \tau^{\frac{1}{4}\hat{P}} \left[\int_0^\tau \frac{1-\tau^{\frac{1}{4}}}{A(\tau \Lambda_P)} d\tau \right] \left[\int \frac{\tau^{\frac{1}{4}}}{A(\tau \Lambda_P)} d\tau \right] d\tau,$$

$$I_3(\Lambda_P) = \int_0^1 \frac{(1-\tau)(1-\tau^{\frac{1}{4}})}{A(\tau \Lambda_P)} d\tau.$$

This equation can be integrated taking into account condition:

$$p = 0 \text{ for } r^* = 0.$$

The explicit solution for the flow density is deduced:

$$q = \frac{n \Lambda_P}{\left\{ 2n \exp \left[+\frac{2}{n} \int_0^{\Lambda_P} \frac{I_3}{I_1} \frac{d\Lambda_P}{\Lambda_P} \right] \times \int_0^t \frac{I_2}{I_1} \exp \left[-\frac{2}{n} \int_0^t \frac{I_3}{I_1} \frac{d\Lambda_P}{\Lambda_P} \right] dt \right\}^{\frac{1}{2}}}$$

The initial problem thus comes down to a series of squares. In practice calculations will be done by the computer.

The second method corresponds to the problem linked to the first type of flowmeter. In the vicinity of the wall we represent Λ in the form of a polynomial development such that:

$$\Lambda = \alpha_0 + \alpha X_1 + \alpha_2 X^2 + \alpha_3 X^3.$$

The partial derivative equation is extended to the case where the surface has a radius of curvature whose reduced value is R^*:

$$\frac{\partial^2 \Lambda}{\partial X^2} + \frac{1}{R^*} \frac{\partial \Lambda}{\partial X} = \frac{1}{A(\Lambda)} \frac{\partial \Lambda}{\partial \tau}.$$

Coefficients α_0, α_1, α_2, and α_3 are determined from the four following conditions:

$$\alpha_0 + \alpha_1 X_1 + \alpha_2 X_1^2 + \alpha_3 X_1^3 = \Lambda_1(\tau),$$

$$\alpha_0 + \alpha_1 X_2 + \alpha_2 X_2^2 + \alpha_3 X_2^3 = \Lambda_2(\tau),$$

$$\frac{\alpha_1}{R^*} + 2\left(1 + \frac{X_1}{R^*}\right)\alpha_2 + 3\left(2X_1 + \frac{X_1^2}{R^*}\right)\alpha_3 = \frac{1}{A(\Lambda_1)}\left(\frac{\partial \Lambda}{\partial \tau}\right)_{X_1} = L_1(\tau),$$

$$\frac{\alpha_1}{R^*} + 2\left(1 + \frac{X_2}{R^*}\right)\alpha_2 + 3\left(2X_2 + \frac{X_2^2}{R^*}\right)\alpha_3 = \frac{1}{A(\Lambda_2)}\left(\frac{\partial \Lambda}{\partial \tau}\right)_{X_2} = L_2(\tau).$$

Resolution of the system leads to the explicit expression for the sought-after results as a function of the measured quantity Λ_1 and Λ_2 and the quantities deduced from the preceding ones, L_1 and L_2. We have, for example:

$$\frac{qL}{\lambda_R T_R} = -\alpha_1 = -\frac{M_2 - M_1}{\Delta} \, ,$$

$$\Lambda_P = \alpha_0 = \frac{N_2 M_1 - N_1 M_2}{\Delta} \, ,$$

with:

$$N_1 = \frac{X_1 \left(12 + \frac{6 X_2}{R^{*}} + \frac{3 X_1 X_2}{R^{*2}} - \frac{X_1^2}{R^{*2}} \right)}{6 \left(2 + \frac{X_1 + X_2}{R^{*}} + \frac{X_1 X_2}{R^{*2}} \right)} \, ,$$

$$N_2 = \frac{X_2 \left(12 + \frac{6 X_1}{R^{*}} + \frac{3 X_1 X_2}{R^{*2}} - \frac{X_2^2}{R^{*2}} \right)}{6 \left(2 + \frac{X_1 + X_2}{R^{*}} + \frac{X_1 X_2}{R^{*2}} \right)} \, ,$$

$$M_1 = \Lambda_1 - X_1^2 \frac{L_1 \left(3 X_2 \left(2 + \frac{X_2}{R^{*}} \right) - 2 X_1 \left(1 + \frac{X_2}{R^{*}} \right) \right) - L_2 X_1 \left(4 + \frac{X_1}{R^{*}} \right)}{6 (X_2 - X_1) \left(2 + \frac{X_1 + X_2}{R^{*}} + \frac{X_1 X_2}{R^{*2}} \right)} \, ,$$

$$M_2 = \Lambda_2 - X_2^2 \frac{L_1 X_2 \left(4 + \frac{X_2}{R^{*}} \right) - L_2 \left(3 X_1 \left(2 + \frac{X_1}{R^{*}} \right) - 2 X_2 \left(1 + \frac{X_1}{R^{*}} \right) \right)}{6 (X_2 - X_1) \left(2 + \frac{X_1 + X_2}{R^{*}} + \frac{X_1 X_2}{R^{*2}} \right)} \, ,$$

$$\Delta = \frac{(X_2 - X_1) \left[12 - \frac{(X_2 - X_1)^2}{R^{*2}} \right]}{6 \left(2 + \frac{X_1 + X_2}{R^{*}} + \frac{X_1 X_2}{R^{*2}} \right)} \, .$$

Figure 31 gives the characteristic shape of the results obtained by these calculations for a measurement in the diverging section to get rid of the condensed layer problem. Qualitatively the surface temperature and flow density change as predicted by theory (Figure 28), if we exclude the ignition phase. On the other hand the heat exchange coefficient only stabilizes to a constant value after a fairly long time; its order of magnitude is indeed that predicted by calculation (Figure 23); the difference shown could come from differences in the nozzle geometries used.
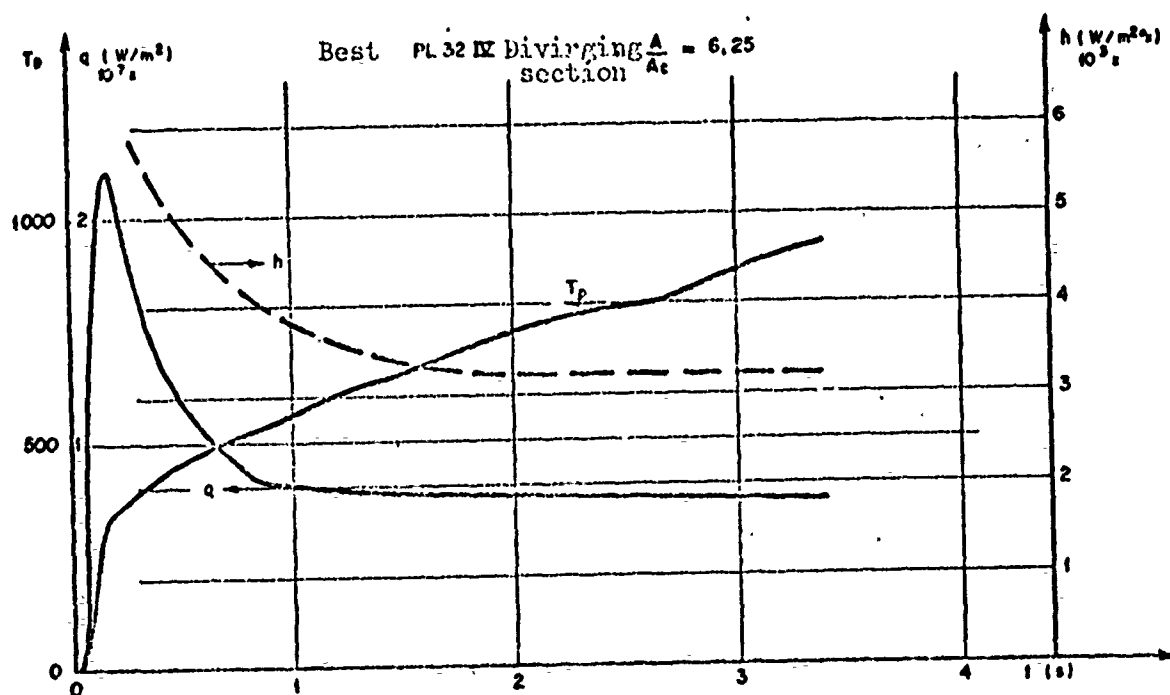
Figure 31. Results Given by Type B Flowmeter.

Flow measurements were made in an almost systematic manner
over a large number of tests and it is not possible to reproduce
all the results here. We will merely note that, despite the
manufacturing difficulties, operation of Type A and Type B flow-
meters was satisfactory and we are trying to improve it. The
accuracy of the results obtained is still fairly poor and this
characteristic is common to all measurements of this nature; the
results are in good qualitative agreement with theory as to the
shape of the flow density and temperature curves although the
latter sometimes stabilizes after a few seconds operation. The
equivalent heat exchange coefficient $\bar{h}$, in the converging section,
decreases with time, which conforms to the increase in the condensed
layer thickness as shown in the formula:

$$\bar{h} = \frac{h'}{1 + \frac{\lambda}{\lambda_s} h'} \ .$$

The thickness Δ deduced by this formula of the theoretical value h' and the experimental value $\bar{h}$ is completely comparable to that determined experimentally ($\Delta \approx 0.3$ mm). Finally we will note the existence of tests on shielding the nozzle converging section by a gas film supplied by a non-metallized and therefore cooler propellant (2400°K instead of 3300°K) which confirm both the good operation of the flowmeters and correct interpretation of the phenomena; the heat flow is small when firing begins, i.e., in the most active phase of this system, as indicated in Figure 32, and the layer deposited on the converging section of the nozzle is far less abundant.
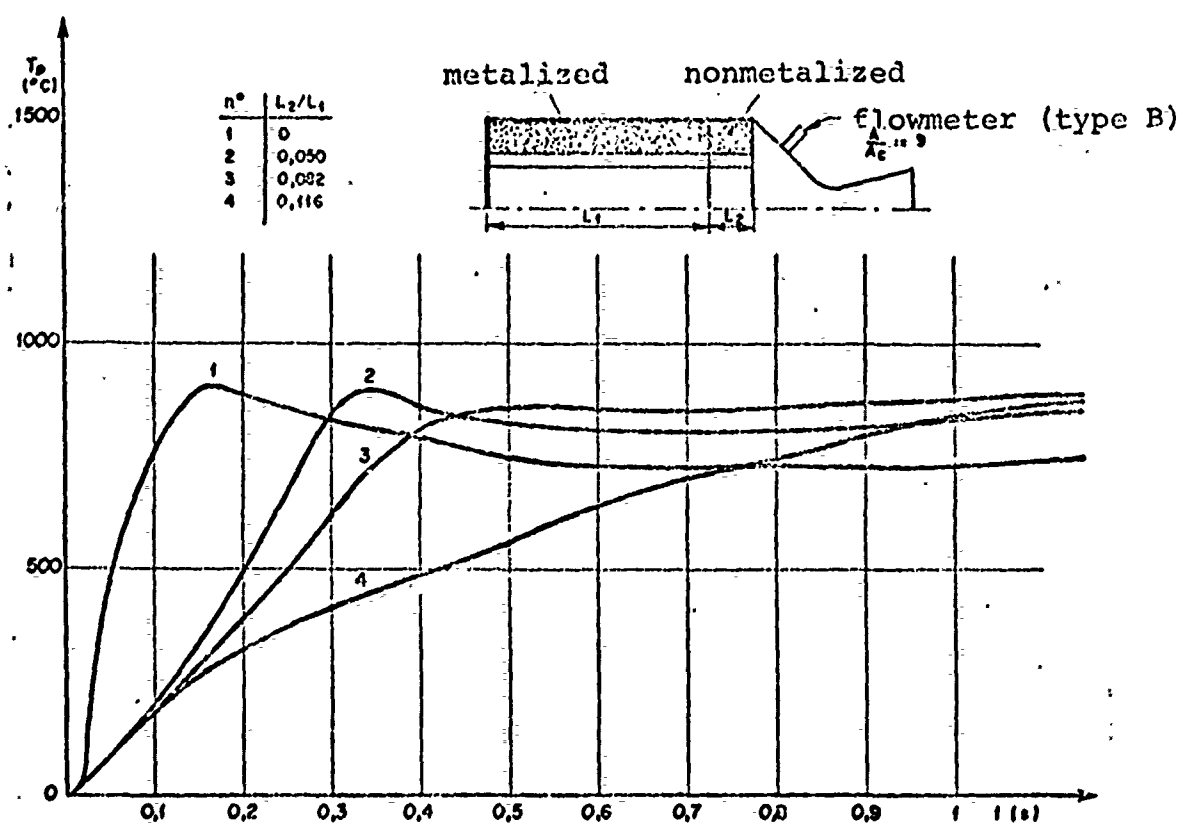

Figure 32. Temperature Rise of a Nozzle Protected by a Cold Film.

To summarize, the experimental study of wall phenomena necessitated development of a specific material, a development which proved difficult and must be pursued. Although the results are

still scattered they are still close to those predicted by theory.
If we remember that the objective of this study is to find the
specific impulse loss due to wall phenomena, which loss does not
exceed a few percent in relative terms, this simple statement is
sufficient in the first stage as it validates the calculations
employed.

5.5. ESTIMATE OF SPECIFIC IMPULSE LOSS DUE TO WALL PHENOMENA

Since, strictly speaking, the wall phenomena are linked to the
condensed phase problem, in principle we should study successively
the particle trajectories in the flow, the particle impacts taking
into account any rebounds and desegregations, and wall exchanges
coupled to development of the condensed phase. Due to the com-
plexity of the general problem we will confine ourselves to a
simplified approach. We calculate a priori the heat exchange
coefficient h' and the friction stress τ_p without being concerned
about the condensed phase. The impacts produce supplementary
mass, momentum, and energy contributions. The captured mass enables
us to define a specific impulse loss as if the captured mass remained
on the nozzle; in fact we know that it is reinjected into the flow
in the form of droplets slightly accelerated due to their size,
which authorizes the preceding interpretation. The development
of the condensed flow perturbs the flow transmitted to the wall
and the friction, but this layer is poorly known and we have shown
that perturbation is moderate as long as the layer is solid. We
will thus leave it out of count in the material following so that
we come back to calculating impulse loss due to friction τ_p and
flux $\bar{q}$. With regard to the latter, the mean value $\bar{q}$ depending on
the operating time must be considered as shown in Paragraph 5.3.a.

The equations for one-dimensional flow perturbed by heat trans-
fer and wall friction are written:

$$\begin{cases} \overline{\rho}\,\overline{u}\,A = \overset{\circ}{m}\,, \\[4pt] \overline{\rho}\,\overline{u}\,d\overline{u} + d\overline{p} = -\dfrac{\tau_p \cos\theta}{A}\,dA_p\,, \\[4pt] d\overline{h} + \overline{u}\,d\overline{u} = -\dfrac{\overline{q}}{\overset{\circ}{m}}\,dA_p\,, \\[4pt] \overline{P} = \overline{\rho}\,r\,\overline{T}\,. \end{cases}$$

The area A_p relates to the lateral surface of the nozzle while A is the area of the straight section; θ is the angle made locally between the meridian and the nozzle axis such that:

$$\cos\theta\,dA_p = 2\pi r\,dx\,.$$

It is interesting to transform these equations to show the non-adiabatic and non-isentropic character of the flow. The energy equation gives:

$$\overline{h} + \frac{\overline{u}^2}{2} = -\frac{1}{\overset{\circ}{m}}\int_0^x \overline{q}\,dA_p \simeq -\frac{1}{\overset{\circ}{m}^{(e)}}\int_0^x \overline{q}\,dA_p = (\delta h)_a\,.$$

From the Gibbs equation for frozen flow:

$$d\overline{h} = \overline{T}\,d\overline{s} + \frac{d\overline{p}}{\overline{\rho}}\,,$$

we deduce, with the aid of energy and momentum equations, the expression,

$$d\overline{s} \simeq \frac{1}{T^{(e)}}\left[\frac{\tau_p \cos\theta\,dA_p}{A\rho^{(e)}} - \frac{\overline{q}\,dA_p}{\overset{\circ}{m}^{(e)}}\right]\,.$$

We thus form:

$$(\delta s)_a = \frac{1}{\overset{\circ}{m}^{(e)}}\int_0^x \frac{u^{(e)}\cos\theta\,\tau_p - \overline{q}}{T^{(e)}}\,dA_p\,.$$

The increase in entropy is thus due both to heat transfer and to friction.

Bringing out the differences δu, δp, $\delta \rho$, δt with respect to the unperturbed problem as in Paragraph 4.6.1, we come back to the system of equations:

$$
\begin{cases}
\dfrac{\delta u}{u^{(o)}} + \dfrac{\delta p}{p^{(o)}} = \dfrac{\delta \overset{\circ}{m}}{\overset{\circ}{m}{}^{(o)}} \,, \\[2mm]
C_{pf}^{(o)} \dfrac{\delta T}{T^{(o)}} - r \dfrac{\delta p}{p^{(o)}} = (\delta s)_a \,, \\[2mm]
C_{pf}^{(o)} \delta T + u^{(o)} \delta u = (\delta h)_a \,, \\[2mm]
\dfrac{\delta p}{p^{(o)}} - \dfrac{\delta \rho}{\rho^{(o)}} - \dfrac{\delta T}{T^{(o)}} = 0 \,.
\end{cases}
$$

Resolution of this system by a matrix method leads to the following explicit solutions:

$$
\begin{cases}
\delta u = -u^{(o)} \dfrac{\dfrac{\delta \overset{\circ}{m}}{\overset{\circ}{m}{}^{(o)}} + \dfrac{(\delta s)_a}{r} - \dfrac{(\delta h)_a}{a_f^{(o)2}}}{\dfrac{u^{(o)2}}{a_f^{(o)2}} - 1} \,, \\[4mm]
\delta p = \rho^{(o)} \dfrac{u^{(o)2} \dfrac{\delta \overset{\circ}{m}}{\overset{\circ}{m}{}^{(o)}} + \dfrac{C_{pf}^{(o)} T^{(o)} + u^{(o)2}}{C_{pf}^{(o)}}(\delta s)_a - (\delta h)_a}{\dfrac{u^{(o)2}}{a_f^{(o)2}} - 1} \,, \\[4mm]
\delta \rho = \rho^{(o)} \dfrac{\dfrac{u^{(o)2}}{a_f^{(o)2}} \dfrac{\delta \overset{\circ}{m}}{\overset{\circ}{m}{}^{(o)}} + \dfrac{(\delta s)_a}{r} - \dfrac{(\delta h)_a}{a_f^{(o)2}}}{\dfrac{u^{(o)2}}{a_f^{(o)2}} - 1} \,, \\[4mm]
\delta T = \dfrac{1}{C_{pf}^{(o)}} \cdot \dfrac{u^{(o)2} \dfrac{\delta \overset{\circ}{m}}{\overset{\circ}{m}{}^{(o)}} + u^{(o)2} \dfrac{(\delta s)_a}{r} - (\delta h)_a}{\dfrac{u^{(o)2}}{a_f^{(o)2}} - 1} \,,
\end{cases}
$$

The geometric throat ($u^{(o)} = a_f^{(o)}$) is a single point for which the numerators of the second members cancel out simultaneously if the following condition is true:

$$
\frac{\delta \overset{\circ}{m}}{\overset{\circ}{m}{}^{(o)}} + \frac{(\delta s)_a^{*}}{r} - \frac{(\delta h)_a^{*}}{a_f^{(o)2*}} = 0 \,.
$$

We thus get:

$$\frac{\delta \mathring{m}}{\mathring{m}^{(o)}} = -\frac{1}{\mathring{m}^{(o)}} \left[\frac{1}{a_f^{(o)2*}} \int_0^{\infty^*} \overline{q} \, dA_p + \frac{1}{\Gamma} \int_0^{x^*} \frac{u^{(o)} \cos\theta \; \overline{c}_p - \overline{q}}{T^{(o)}} dA_p \right].$$

The relative variation in the characteristic conventional velocity is deduced immediately:

$$\frac{\delta c^*}{c^*} = -\frac{\delta \mathring{m}}{\mathring{m}^{(o)}} = \frac{(\delta s)_a^*}{\Gamma} - \frac{(\delta h)_a^*}{a_f^{(o)2*}} \; .$$

Friction tends to increase the characteristic velocity in an obvious manner. The heat flux influence is linked to the sign of the quantity:

$$\frac{M}{a_f^{(o)2*}} - \frac{1}{\Gamma T^{(o)}} \qquad , \qquad \left(T^* \leqslant T^{(o)} \leqslant T_o^{(o)} \right) \; .$$

In view of the range of temperature variation $T^{(o)}$ we can establish:

$$-\frac{\gamma^* - 1}{\gamma^* \Gamma T^*} < \frac{1}{a_f^{(o)2}} - \frac{1}{\Gamma T^{(o)}} < -\frac{(\gamma^* - 1)(\gamma_o - 1) + 2(\gamma^* - \gamma_o)}{2(\gamma^* - 1)\gamma_o \Gamma T_o^{(o)}} \; .$$

Thus the characteristic velocity decreases with heat flux and the simultaneous influence of the wall phenomena is not known a priori.

The specific impulse loss is calculated as in Paragraph 4.6.1. with respect to a suitable reference flow. Once more we obtain:

$$\frac{\delta I}{I^{(o)}} = \frac{\delta u_s}{u_s^{(o)}} + \frac{\delta p_s}{\rho_s^{(o)} u_c^{(o)2}} \; .$$

Replacing δu_s and δp_s by their expressions, we get:

$$\frac{\delta I}{I^{(o)}} = -\frac{1}{u_s^{(o)2}} \left(T_s^{(o)} (\delta s)_{as} - (\delta h)_{as} \right) ,$$

or again:

$$\left|\frac{\delta I}{I^{(o)}}\right| = \frac{1}{u_s^{(o)2} \; \dot{m}^{(o)}} \left[T_s^{(o)} \int_0^{x_s} \frac{u^{(o)} \cos\theta \; \tau_p}{T^{(o)}} dA_p + \int_0^{x_s} \left(1 - \frac{T_a^{(o)}}{T^{(o)}}\right) \bar{q} \, dA_p \right].$$

as we might expect, each of the wall phenomena has a positive con-
tribution to make to specific impulse losses.

*   *

*

6. PREDICTION OF SPECIFIC IMPULSE LOSSES

In this final section we propose to apply the results estab-
lished above to a concrete case and compare the estimate thus
obtained of total specific impulse loss to the value determined
experimentally.

Tests were performed on a design motor represented schemati-
cally in Figure 33. The reference operating conditions chosen are
the following:

- propellant:

    The propellant is a polyurethane binder composite containing
    16.4% aluminum. It is used in the shape of a cylindrical grain
    with a star hole (Olive type by SNPE), with outer diameter 121 mm
    and length 430 mm (throat diameter $\emptyset_c$ = 20 mm and chamber pres-
    sure 70 atm.).

- nozzle:

    The nozzle is wholly made of graphite and supported by a metal
    ring. Its contour is biconical with a constant radius of cur-
    vature at the throat; the half-angle of the converging section

is 45°, that of the diverging section 15°, and the throat radius of curvature is equal to the diameter of the nozzle (20 mm). The ratio of the outlet section is 9 which approximately ensures that the nozzle is suitable for chamber pressure of 70 atm.

Neither in scale nor configuration is the motor representative of flight motors for which the specific impulse loss problem arises. We are forced to operate on a small scale for obvious financial reasons; utilization of the one-piece non-integrated nozzle was due from a choice made to simplify the phenomena as far as possible in the first analysis.
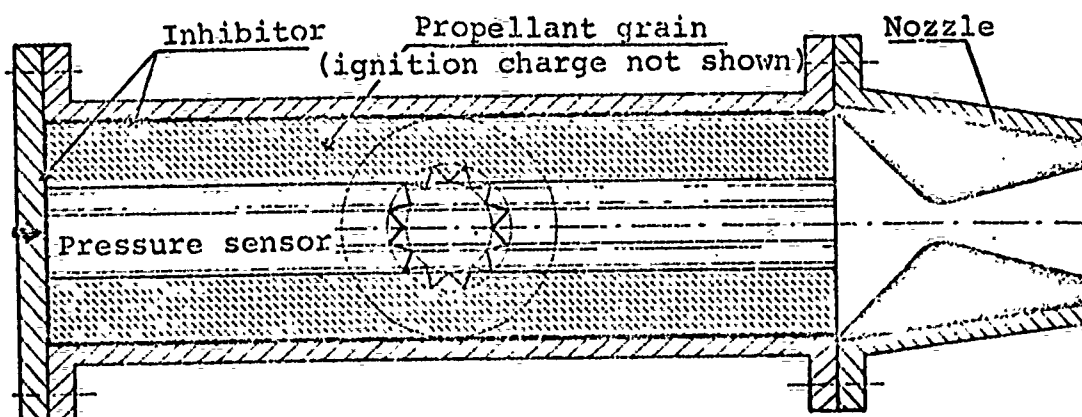

Figure 33. Motor for Studying Specific Impulse Losses

6.1. THEORETICAL ESTIMATES

In view of the importance of the particle size of the condensed phase we must start off from fairly certain data. The values taken are the result of numerous measurements made by capture. We give the values of the principal mean diameters at the nozzle inlet and after particle solidification, the latter values being far more precise than the preceding values:

	inlet	outlet
d_{10} µm	0.5	1
d_{30} µm	0.6	1.3
d_{53} µm	0.8	3.6

Each loss will be calculated in succession. We note to begin with that loss due to incomplete combustion of aluminum is 0.4% at most.

6.1.1. Loss Due to Phase Lags

We first of all looked to see whether it was possible to apply the formulas of Paragraph 4.6. here. In the near equilibrium the condition to be checked is written approximately at the geometric throat:

$$\frac{\ell \, \overline{\tau_u}}{\overline{\gamma}+1} \sqrt{\frac{\overline{\gamma} \, \overline{r} \, T_0}{r_c \, R_c}} \ll 1 \ .$$

Computer application was performed with the following values:

- $d_{53}^{*} = 1{,}9 \, \mu m$, in the throat (the variation in d_{53} between 0.8 and 3.6 µm are deduced from Figure 17),

- $\rho_c = 2{,}17 \times 10^{3} \, kg/m^{3}$, (liquid alumina according to [83]),

- $\mu = 4{,}9 \times 10^{-5} \, kg/ms$,

- $\overline{\gamma} = 1{,}131$,

- $\overline{r} = 208{,}2 \, J/kg \, °K$,

- $T_0 = 3352 \, °K$,

- $R_c = 2 r_c = 2 \times 10^{-2} \, m$.

We get:

$$\frac{\ell \, \overline{\tau_u}}{\overline{\gamma}+1} \sqrt{\frac{\overline{\gamma} \, \overline{r} \, T_0}{r_c \, R_c}} = 0{,}52$$

It appears thus that the near frozen hypothesis is not respected
for our small motor; we note that the hypothesis would begin to
be valid with constant particle size for a throat diameter greater
than 100 mm. Application of the proposed formula would thus lead
to sharply over-estimating the loss due to the condensed phase (in
fact, calculation gives a value greater than 20%).

The condition to be checked for the near frozen theory is:

$$\frac{\left[2 \int_{0}^{x} \frac{\overline{\tau u_c}}{\tau u} u^{(0)} dx \right]^{\frac{1}{2}}}{\sqrt{\overline{\tau u_c}} \, u^{(0)}} \ll 1 \ .$$

Calculation requires us to know $u^{(0)}$ as a function of x and
particle growth with the same hypotheses. $u^{(0)}$, a local velocity
of the gaseous combustion products in the nozzle, if they expanded
on their own, is not given by existing computer programs. Calcu-
lation must be performed as indicated in [84] for frozen expansion:
the JANAF thermodynamic table and composition at equilibrium in the
chamber enable us to calculate the mass entropy, the mass enthalpy,
and the mass heat at constant pressure for the mixture and each
temperature; the isentropic hypothesis enables us to connect tem-
perature to pressure, and conservation of energy gives the velo-
city as a function of temperature and reasoning on the flow deter-
mines the section ratio. In the preceding formula we neglect
particle size variations upon expansion and we calculate $\overline{\tau u}$ with
a mean diameter.

The minimum value of the left member of the inequality for the
largest mean diameter than can be chosen is 0.54. This says that
the near frozen theory is not applicable and the motor regime cor-
responds to mean relaxation between phases which makes it neces-
sary to calculate on the computer.

We note that near frozen flow furnishes the upper limit of
two-phase loss. Indeed, specific impulse is always between the

value corresponding to two-phase equilibrium (thermodynamic computer programs) and that corresponding to expansion of gaseous products only (considering the entire mass of burnt propellant). If we agree to calculate the loss with respect to two-phase equilibrium (frozen chemical composition) we find that it cannot exceed 35.7%. This limit results from numerous differences in the two extreme flows; "gaseous" flow is characterized by slight inadaptation at the nozzle outlet, a far higher isentropic exponent (1.26 < γ < 1.32 instead of 1.19 < $\overline{\gamma}$ < 1.21) and especially by the fact that the heat of solidification of the particles is not recuperated in expansion which explains why the maximum specific impulse loss exceeds the maximum flow loss.

Development of a realistic calculation method should be the logical follow-up to the detailed examination of the physical phenomena constituting the greater part of this study. Estimation just of the specific impulse loss due to phase lags, which it is possible to make at this stage, is based on the simplified model of Paragraph 4.5.1. which gave rise to development of a computer program. Due to the low representativity of t.. simplified model, we can only hope to obtain an order of magnitude. To chose the most representative constant mean diameter we based ourselves on a series of calculations performed for the near equilibrium theory with both solid and liquid particles; this reasoning led us to take $\overline{d} = 1.3$ μ. The loss so calculated is:

$$\left|\frac{\delta I}{I^{(o)}}\right| \simeq 2.4\%$$

6.1.2. Loss Due to Two-Dimensional Effects

The loss due to non-uniform distribution of the condensed phase in the combustion products does not exceed 0.4%. That connected with jet divergence can be calculated by the classic formula:

$$\left|\frac{\delta I}{I^{(o)}}\right| = \frac{1 + \cos\alpha}{2} \simeq 1.7\%$$

6.1.3. Wall Losses

The maximum loss due to impacts of alumina particles on the converging section is estimated with the aid of the formula in Paragraph 5.2. Calculation gives:

$$\left|\frac{\delta I}{I^{(0)}}\right| \leq 0,1\ \%$$

This loss is thus practically negligible. It corresponds to a mass deposited on the nozzle on the order of 5g: these are on the average masses of deposits measured after firing.

Losses due to friction and heat flow on the nozzle are obtained with the formula of Paragraph 5.5. The friction contribution is written in the reduced form:

$$\left|\frac{\delta I}{I^{(0)}}\right| = \frac{T_A}{T_0}\left(\frac{u_A}{u_R}\right)^{-2} \int_0^{\frac{x_0}{r_c}} \left(\frac{T}{T_0}\right)^{-1} \frac{u}{u_R}\ \frac{r}{r_c}\ \tau^* d\left(\frac{x}{r_c}\right) ,$$

where u_R is a reference velocity and τ^* is the reduced friction given by the expression:

$$\tau^* = \frac{2\sqrt{\frac{\gamma-1}{2\gamma}}}{\Gamma(\gamma)}\ \frac{\tau_p}{P_0} .$$

τ_p is known from Figure 23.
Calculation gives for the friction loss: $\left|\frac{\delta I}{I^{(0)}}\right| = 1,7\ \%$.

Contribution of the heat flow is expressed by:

$$\left|\frac{\delta I}{I^{(0)}}\right| = \left(\frac{u_A}{u_R}\right)^{-2} \int_0^{\frac{A_A}{r_c}} \left[1 - \frac{T_A}{T_0}\left(\frac{T}{T_0}\right)^{-1}\right] \frac{r}{r_c}\ q^* d\left(\frac{A}{r_c}\right) ,$$

where q^* is a mean reduced flow density given by:

$$q^* = \frac{2\sqrt{\frac{\gamma-1}{2\gamma}}}{\Gamma(\gamma)} \times \frac{q}{P_0 u_R} .$$

The exchange coefficient h' is known from Figure 23. We go from h' to $\bar{q}$ by the formula already given:

$$\bar{q} = h' \Theta_t \; f\left(\sqrt{\frac{a_p h'^2 t_p}{\lambda_p^2}}\right) \; .$$

For the loss due to heat flow we get:

$$\left|\frac{\delta I}{I^{(0)}}\right| = 1\%$$

We will now recapitulate all the results in a table:

Origin of Loss	Loss
Combustion	< 0.4 %
Two-Phase Flow Effects	2.4 %
Two-Dimensional Effects:	
- segregation of condensed phase	< 0.4 %
- jet divergence	1.7 %
Walls:	
- impacts	< 0.1 %
- friction	1.7 % } 2.7%
- heat flow	1 %

The total specific impulse loss which is most probable is close to 6.8 %. The accuracy of this result is limited by the inaccuracy of data on particle size of the condensed phase and at the nozzle boundary layers; it could not be more than 10%.

The most important losses are, for the application given and in decreasing order:

- wall losses;
- losses due to presence of condensed phase in flow;
- loss due to jet divergence.

The latter can be strongly diminished by adopting a contoured diverging section; in this case and in the absence of two-phase effects we find the order of magnitude of the minimum losses of a non-metallized propellant.

There are but few results in the literature to which this loss breakdown can be compared. The work of Kliegel and Nickerson was done on nozzles with diameter 67 mm but practically without a diverging section. The results of Miller and Barrington [85] under fairly comparable conditions:

$$\beta \approx 60^\circ, \alpha = 19{,}6^\circ, R_c = r_c, P_o = 660 \text{ psia}, \frac{A_s}{A_c} = 46{,}8,$$

seem to indicate a substantial over-rating of two-phase effects (more than 6%), however to the detriment of wall losses (less than 1%); the effect of the condensed phase is calculated with a constant particle diameter and values for this diameter resulting from captures and cannot thus claim to accuracy. Recent attempts made in France by various manufacturers have similar defects.

6.2. COMPARISON OF THEORETICAL ESTIMATES AND EXPERIMENTAL RESULTS

By measuring the thrust and mass of propellant consumed we determine a mean specific impulse in the laboratory, a result to be compared with the theoretical values. Here we find two main problems:

- While the theory was established in well-determined conditions (operating pressure, nozzle geometry, etc.), the experiments are not usually performed under the same ideal conditions; we have to live with the fact that the operating pressure is not strictly constant due to variation of the combustion surface with the burnt thickness and throat erosion, and with spurious phenomena such as partial combustion of the inhibitor for example;

- We are trying to find out the influence of various operating parameters on specific impulse. Since the expected deviations represent only a small percentage of specific impulse we can only expect to demonstrate them if measurement accuracy is excellent. Despite the difficulties inherent in laboratory measurements, our target accuracy was about 1% or a little more than 0.2 sec. on the specific impulse. As the results will show, this target was almost reached; this success was achieved only be meticulous choice of equipment and measuring and analysis techniques.

6.2.1. Equipment

The thrust-testing bench proper was a modification of an existing assembly (PL32 motor). It is shown schematically in Figure 34: the motor is suspended on a very rigid frame by a set of flexible blades and its thrust is transmitted to a sensor calibrated by a physical system.

With this type of assembly it is desirable to use extremely stiff sensors. The flexibility of the suspension blades must not be too great to avoid spurious undamped vibrations when the motor is ignited.
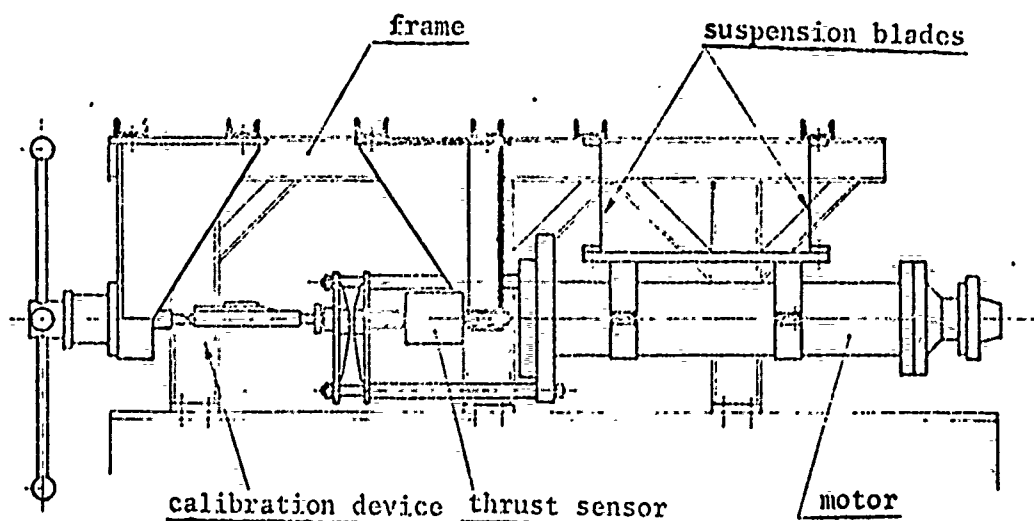

Figure 34. Diagram of Thrust-Testing Bench

The sensor used is a gauge sensor made by Baldwin-Lima-Hamilton. One must see that the motor axis and the sensor axis are perfectly aligned; also, to avoid measurement perturbation by spurious torques the sensor is connected to the frame and the component to the motor by joints. The assembly is such that the sensor is always slightly prestressed.

For calibration we chose a physical system. A screw and thrust bearing device ensured that a standard dynamometric ring

and the gauge sensor were placed under traction simultaneously. The assembly was calibrated before and after firing for each test. The hysteresis found upon calibration was generally small. The front bottom was equipped with pressure gauges which could receive a wide variety of sensors (C.E.C. gauge sensors in general).

To remove random effects, each series of tests for studying one parameter was performed in a small length of time, i.e., under the same climatic conditions. If need be, when the outside temperature fell too low, the motor temperature could be maintained at 15°C by a heating band wound over the main ring and a heat regulating system. All the grains used in the same series of tests were machined in blocks from the same casting. The operating conditions, except for the parameter studied, were maintained as constant as possible from one firing to another; in particular the nozzle was changed for each test, the ignition charge was always the same, and the motor was always cleaned between firings.

We are interested here only in the principal operating characteristics of the motor, namely pressure and thrust. At the outputs of the measuring bridges, for the gauge sensors, we had voltage signals representing the instant phenomena with excellent precision if the sensors were of good quality. The problem was to record them with sufficient care for their later use. This question is not independent of the operating method used of which we will speak further.

The viewpoint adopted was the following: the phenomenon must be exactly reproduced but there was no point in going down to time scales that were too small for fluctuations of physical origin would then appear (non-homogeneity of propellant) or of electronic origin (noise). It was sufficient to be able to confer on the regular time intervals a very precis measurement representing the integral of the signal over these intervals, i.e., the mean value plus or minus a known factor.

Analog processing of the signal was limited from the accuracy viewpoint. Thus digital processing was chosen. The measuring system is shown in block diagram form in Figure 35. The first elements are voltage-frequency converters (Hewlett-Packard 2212 A) which deliver impulses at a frequency proportional to the input level; these converters operate around zero and have three measuring ranges: 1 V, 0.1 V, and 0.01 V. Synchronized digital counters (Hewlett-Packard 5325 B) give, for each time interval, the number of impulses delivered by the converters, which numbers are proportional to the integral of the signal over the time interval. The zero reset time of the counters is less than 100 microseconds; it can thus be neglected without making an error greater than 10^{-3} sec. The practically contiguous time intervals, plus or minus the zero reset time, were chosen within the range of the counter which was of the universal multimeter type; this choice was simple since in practice one is limited by the performance of the Hewlett-Packard 5050 B rapid printer (20 lines per second at maximum rate): the interval is 0.1 sec. This value permits excellent reproduction of the almost-permanent firing phase but does not authorize reproduction of the transient phases (ignition, thrust decay); we then used a classic graphic recorder of which the accuracy was sufficient in this case.

The other measurements necessary for determining the performance parameters were:

- measurements of masses; the propellant grain was weighed after machining and after inhibition of its front surface; the masses of inhibitor unburnt after firing, the deposits in the motor or on the nozzle before and after firing were also measured;

- measurements of throat diameter before and after firing;

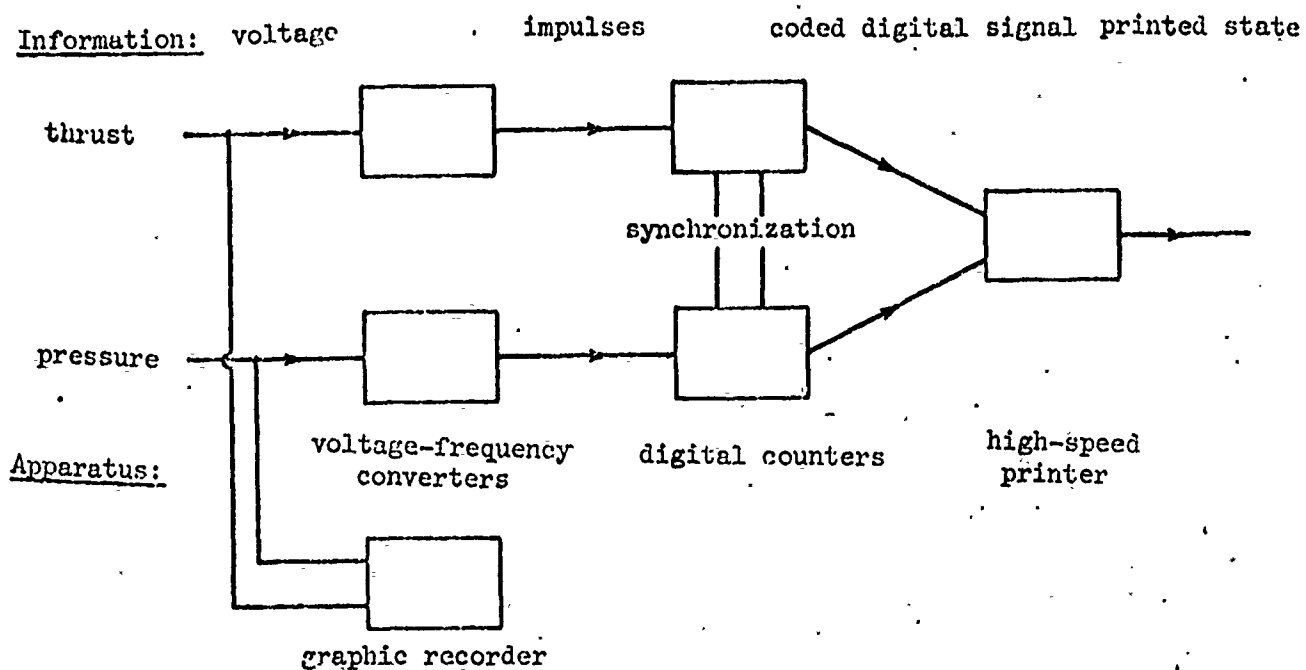- atmospheric conditions (pressure and temperature).

thrust

synchronization

pressure

Apparatus:

voltage-frequency
converters

digital counters

high-speed
printer

graphic recorder

Figure 35. Block Diagram of Measuring System.

6.2.2. Method of Analysis

Since we knew the changes in thrust and pressure during the
test, the problem was now to go back to specific impulse. Analysis
proceeded in several stages, the quality of which increases:

a) Overall analysis

The first information on specific impulse is given by average
application of the definition formula. We write:

$$I \simeq \frac{(F)_{moyen}}{(\overset{\circ}{m})_{moyen}\ g_0}$$
$$= \frac{\int_0^{t_p} F\, dt}{\Delta m\ g_0} \ .$$

The total thrust impulse is calculated from the data recorded by the printer by adding, after corrections if necessary for zero drift (assumed linear through time).

The mass Δm is the mass of propellant consumed. In actual fact part of the inhibitor has been burned; to take this into account we assumed that the mass of burnt inhibitor and half the mass of propellant were the same [86]. We then calculated successively:

- for a given grain, the masses of propellant and inhibitor (lateral inhibitor and front surface inhibitor),

- the mass of inhibitor burned during firing,

- the equivalent mass of consumed propellant.

The characteristic velocity is also given in the first approximation by the formula:

$$C^* \simeq \frac{(p_0 A_c)\,\text{mean}}{(\mathring{m})\,\text{mean}} \simeq \frac{\int_0^{t_f} p_0 dt \times \overline{A_c}}{\Delta m} \ .$$

We note that since we do not know the variation in time of the throat diameter we have to separate the terms p_0 and A_c. The total pressure impulse is determined by adding the printed data after correction, and the average throat section is calculated from the arithmetic mean of the diameters before and after firing.

The first rough results I and C^* correspond to average operating conditions and a correction is necessary to bring them to the theoretical operating conditions. The first problem arising is to define an average combustion time and average relative operating pressure. The two values are connected by:

$$\overline{p_{0\,rel}} \times \overline{F} = \int_0^{t_f} p_{0\,rel}\, dt \ .$$

There is some arbitrariness in calculating the means values. Various conventions can be adopted [85]; in France the Powders and Explosives Study Committee standardized the definition of the self-propulsion parameters; the standard determines $\bar{t}$ as the time interval between the passages of the curve at $\overline{P_0}_{rel}/2$.

$\overline{P_0}$ being calculated in this way and atmospheric pressure P_A being known, we bring I and C^* to the ideal conditions (p_{OR} and p_{AR}) by formulas whose coefficients are deduced from thermodynamic calculations. Thus we establish:

$$I_1 = (I) \text{ corrected} = \frac{I + \frac{\gamma_s C^*}{g_0} \frac{P_A - P_{AR}}{P_0}}{1 + (\alpha + \beta)(\overline{P_0} - P_{0R})} ,$$

$$C_1^* = (C^*) \text{ corrected} = \frac{C^*}{1 + \beta(\overline{P_0} - P_{0R})} .$$

We can also calculate an approximate value for the rate of combustion by a conventional burnt thickness and a mean time $\bar{t}$; a pressure correction, based on a known coefficient, enables us to bring u_b to the reference pressure.

b) Mean analysis in the almost-permanent phase

Overall analysis furnishes rapid information which, however, has a systematic error: in the transient phases a certain mass of propellant is consumed but it does not contribute very effectively to propulsion (low pressure, unsuitable nozzle). In this second analysis we propose to use the preceding calculations, but taking into account only the portion of the test for which the values are stabilized. The problem is then to calculate the mass of propellant consumed during the transient phases.

Let t_1 and t_2 be the limits of the almost-permanent firing phase; these times are to be taken as a function of the data from the printed state. For ignition, and as pressure varies rapidly

(the time for rising from 0 to 70 b is about 0.1 sec) we chose to use the combustion rate of the propellant as the basic datum (u_b is determined as a relative value by a standard curve and as an absolute value by the first analysis). At the beginning of the test the change in the combustion surface is well known as a function of the burnt thickness and we calculate the mass flow taking into account corrosive effects in the central channel, if any. The mass consumed during ignition is taken as being equal to:

$$\delta m_1 = \int_0^{t_1 \cdot \tau_s} \mathring{m} \, dt \quad ,$$

where τ_s is the dwell time in the chamber at the beginning of firing.

The thrust decay is slower (the time for decending from 70 b to 0 b is greater than 0.5 sec.). The instant mass flow is calculated with the aid of the characteristic velocity given by the first analysis and corrected as a function of pressure and the final nozzle diameter: by integration we obtain:

$$\delta m_2 = \int_{t_2}^{t_r} \mathring{m} \, dt \quad .$$

The propellant mass to be taken into consideration is thus here:

$$\Delta m' = \Delta m - (\delta m_1 + \delta m_2) \quad .$$

Analysis proceeds as in a) above; the time, however, is perfectly known now such that the correction is more significant. These second values for specific impulse and characteristic velocity will be denoted I_2 and C^*_2.

c) Local analysis

We could be tempted to push corrections further and apply them to instant values. The theoretical expression for thrust is:

$$F = \overset{\circ}{m}\,v_s + A_s(p_s - p_A).$$

The first correction would be calculating the thrust in the case where atmospheric pressure is standard:

$$F^* = F - A_s(p_{AR} - p_A)$$

The second correction is due to the unsuitability of the nozzle for instant pressure p_o. However we know that thrust is at its maximum when the nozzle is suitable, i.e., for a certain value $\tau_{sa}(p_o)$ of the ratio of the nozzle outlet section; as in practice one never departs very far from suitability one can show that the correction can be neglected.

The last correction is due to the difference between p_o and the reference value p_{oR}. The correction formulas used are respectively, for the thrust coefficient and the characteristic velocity:

$$C_F(p_o) = C_F(p_{oR})\left[1 + \alpha(p_o - p_{oR})\right],$$

$$C^*(p_o) = C^*(p_{oR})\left[1 + \beta(p_o - p_{oR})\right].$$

The coefficients α and β are given by thermodynamic calculation.

Writing:

$$\Delta p_o = p_o - p_{oR},$$

we can thus write:

$$F^* = \overset{\circ}{m}\,g_o\,I(p_o) = \overset{\circ}{m}\,g_o\,I_R\left[1 + (\alpha + \beta)\,\Delta p_o\right],$$

or:

$$I_R = \frac{\displaystyle\int_{t_1}^{t_2} \frac{F^*}{1 + (\alpha + \beta)\Delta p}\,dt}{\Delta m'\,g_o}.$$

Calculation shows that this third specific impulse value differs
very little (less than 0.2 sec) from I_2; this new determination
should rather be considered as a check.

We also have:

$$\frac{F^{*}}{(1 + \alpha \Delta p_o)\, p_o \, A_{co}} = \frac{A_c}{A_{co}} \, C_{FR}.$$

We thus determine the variations in time of the throat section;
we must check that A_{cf}/A_{co} does indeed correspond to the measure-
ments taken before and after firing, and we finally calculate
C_{FR} then C_R^*.

Figure 36 gives an example of the various curves that can be
plotted. The first analysis gives:

$$I_1 = 236{,}8 \text{ s} , \quad C_1^R = 1546 \text{ m/s}$$

The second analysis leads to:

$$I_2 = 237{,}8 \text{ s} , \quad C_2^* = 1553 \text{ m/s} .$$

We see that I_2 is greater than I_1 by 1 second: the transient
phases correspond to 4% (ignition) and 5.1% (thrust decay) of the
consumed mass but only to 8.7% of the thrust impulse. This result
is very general: for all tests the relative differences found
between I_1 and I_2 are between 0.4 and 1.2%. The rough experimental
values must thus not be used without precautions and standardization
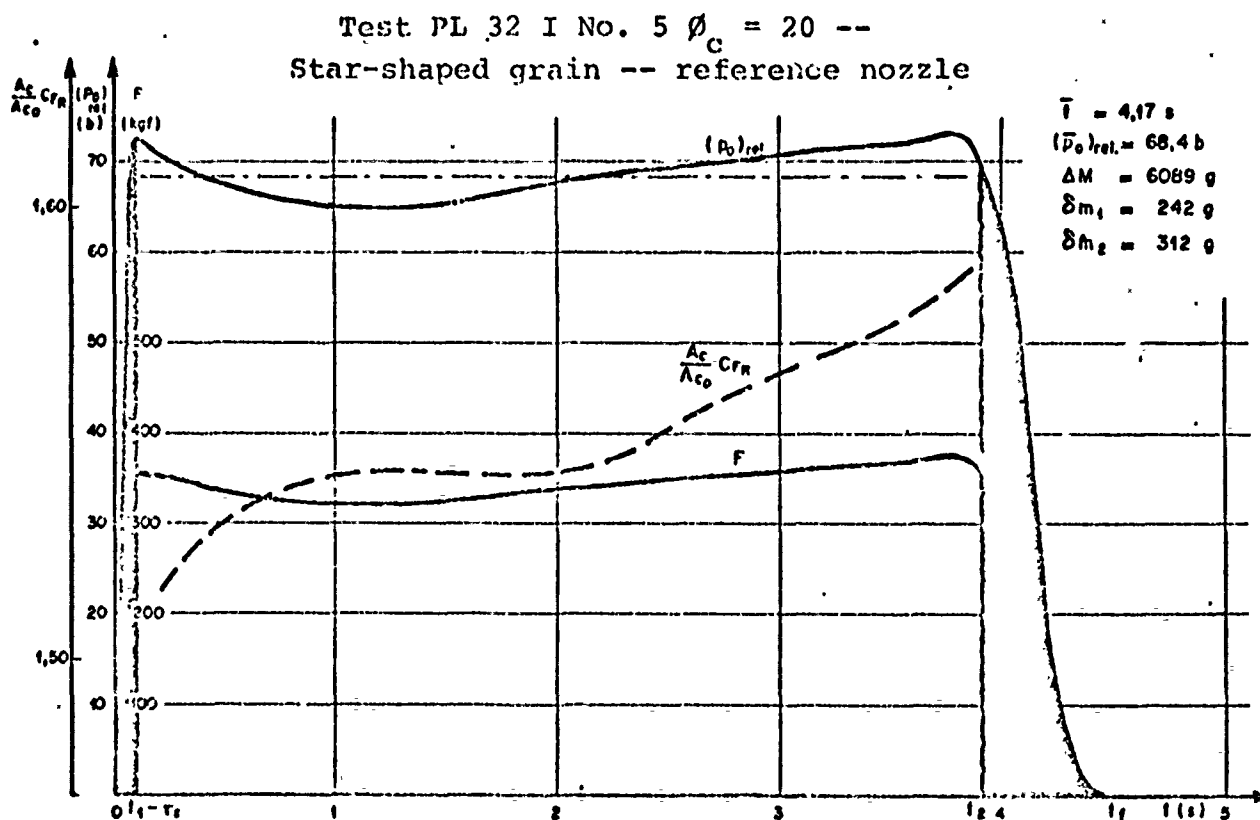of methods of analysis is thus desirable.

Figure 36. Example of Analysis

6.2.3. Experimental Results

We can first of all mention that the accuracy finally obtained
is about that for which we aimed: the maximum difference between
the specific impulses of the two tests carried out under identical
conditions is about 0.2%.

With respect to the total specific impulse loss, we agreed to
calculate it with respect to thermodynamic calculation for a chem-
ically frozen flow; this hypothesis seems the most realistic due
to the small size of the motor. We may note that the result in
the "frozen in throat" hypothesis differs from the preceding result
only by 0.4% while the result for thermodynamic equilibrium is
greater by 1.7%.

The average of the experimental results in the reference conditions is:

$$\overline{I_R} = 238{,}1 \, s \, .$$

It corresponds to an experimental loss of 7.4%. This result differs only slightly from the theoretical estimate (6.8%); it leads one to assume that the loss due to phase lags was under-estimated and would be 3% rather than 2.4%.

Several series of tests were run to determine the influence of various operating parameters on the specific impulse loss. We investigated only one propellant, only one motor size (20 mm $\leq$ $\phi_c \leq$ 22 mm), a constant operating pressure (70 atm., expansion ratio 70:1). We report the results obtained briefly with respect to the influence of the loading design, the geometry of the inlet zone, and the nozzle geometry.

a) Loading design

To ensure neutrality of motor operations, i.e., an essentially constant chamber pressure, we made star-shaped cylindrical perforations; the blocks were obtained by casting the propellant around a star-shaped core. A new method of grain preparation consists of beginning with a circular cylindrical perforation and machining a number of notches into the propellant; optimization of the geometric elements of these notches enables satisfactory neutrality to be obtained. This technique is relatively flexible but the structure of the flow in the perforation is distinctly more complex than in the cylindrical case; thus we tried to find out whether the specific impulse loss was affected by this.

The nozzles used have the following characteristics:

$$\beta = 41°30' \, - \, \alpha = 15° \, - \, \phi_c = 22 \, - \, \frac{R_c}{r_c} = 1{,}36 \, .$$

For a star grain the loss is 7.9% while for a machined grain
we find 8.4%; the difference between these two losses is 0.5% and
it is significant. Analyses of the corresponding particle size
have not been done thus far.

Another loading design aimed at reducing wall losses has
already been reported (Paragraph 5.4. and Figure 32). Figure
37 gives the variation in specific impulse loss with the proportion
of non-metallized and metallized propellant (same nozzle character-
istics as before). The reduction in loss that might be expected
by this system is very small and the increased motor complexity
cannot be offset. No systematic particle size variation in the
condensed phase was found in this case. We would also note that
the variation in characteristic velocity can be expressed by a
suitably weighted mean of the theoretical characteristic velocities
of the two propellants, and that nozzle deposits decrease with
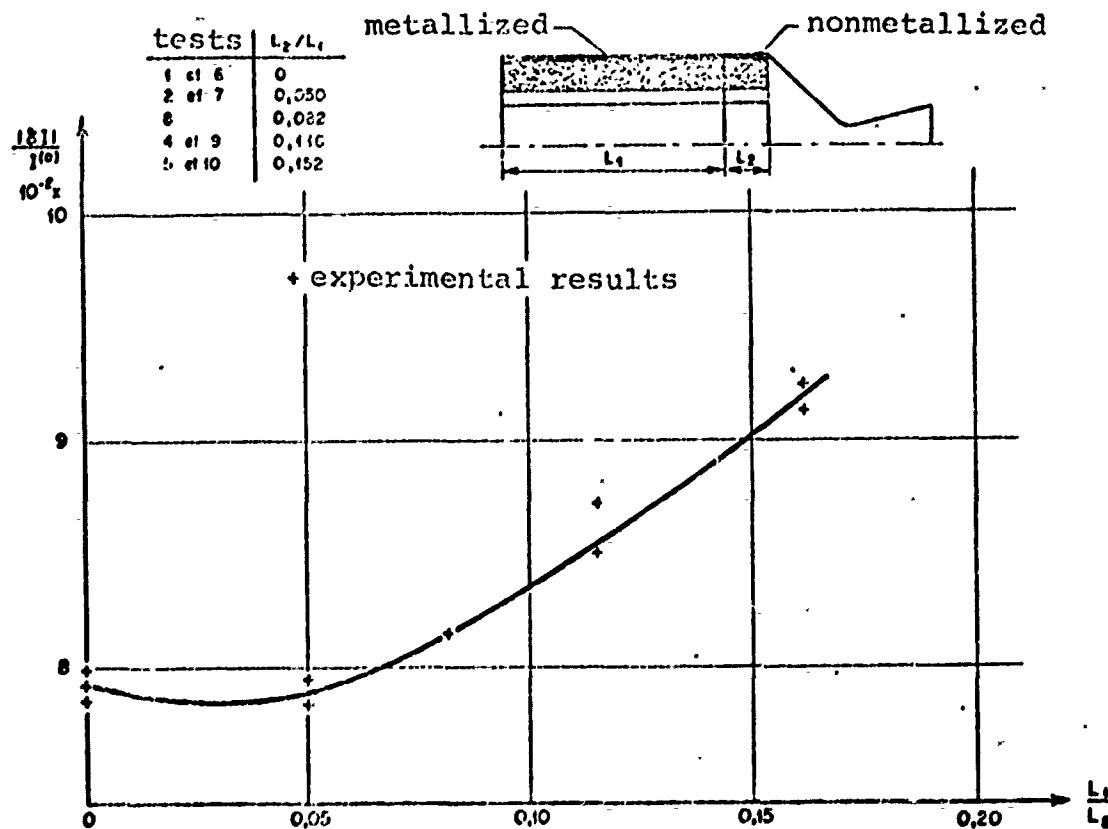increasingly heavy shielding but throat erosion is more or less
independent of this.

Figure 37. Reduction of Wall Losses by a Cold Film.

-188-

b) Geometry of inlet zone

The motor's outside dimensions can be reduced by using nozzles with a very small inlet ratio, i.e., practically without a converging section, or by arranging the converging section inside the motor itself ("integrated" or "submerged" nozzle). The existence of a "dead" zone in the first case and the flow around the integrated part of the nozzle in the second case could be the cause of changes in the condensed phase.

The nozzle used for studying the inlet ratio have the following common characteristics:

$$\beta = 45° . \quad \alpha = 15° . \quad \phi_c = 20 . \quad \frac{R_e}{r_c} = 2 .$$

Figure 38 shows that the effect of the inlet ration becomes large only below the value of $r_e/r_c = 4$. The extra loss in specific impulse could exceed 1% for inlet ratios slightly above 1.

The results on integration of the nozzle were obtained for a nozzle with the following characteristics:

$$\beta = 41°30' . \quad \alpha = 18° . \quad \phi_c = 22 . \quad \frac{R_e}{r_c} = 1,36 . \quad \frac{r_e}{r_c} = 2,35 .$$

(relative integrated length: $L_I/L_p = 0.094$).

The extra specific impulse loss due to integration, in comparison with that of a reference biconical nozzle, is 1%. We can compare this result with that of the formula proposed by Kordig and Fuller [87] which would be written with our notations:

$$\left|\frac{\delta I}{I_\phi}\right| = 0,74 \times 10^{-2} \times \frac{\varepsilon}{\eta_a} \times \left(\frac{L_I}{L_p}\right)^{0,38} \times \left(\frac{r_a}{r_c}\right)^{0,28} \times \left(\frac{r_c}{r_c}\right)^{-1,60} \times \left(\frac{P_0 L_p}{\mu C^x}\right)^{0,80}$$
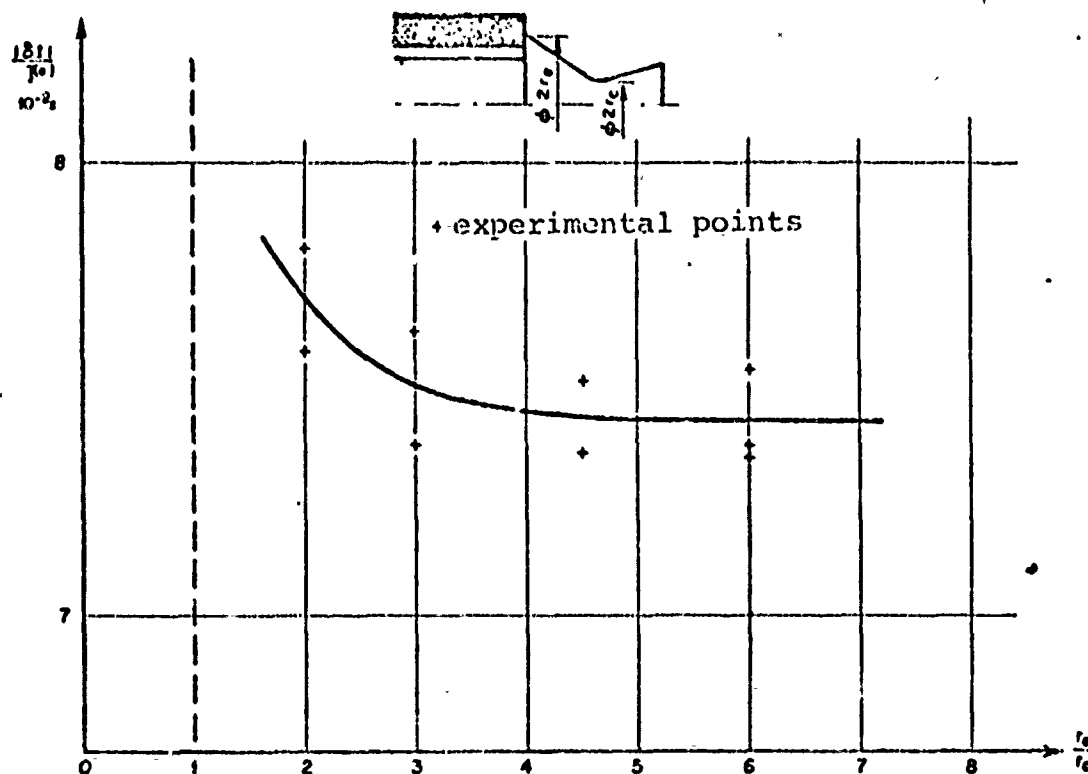
Figure 38. Influence of Inlet Section Ratio on Specific Impulse Loss.

Computer application leads to:

$$\frac{|\partial I|}{I_s^{(0)}} \approx 0{,}5\% \ .$$

To this value we must add the extra loss due to the low inlet ratio, or 0.2% (Figure 39) which gives a total of 0.7%. This is the order of magnitude obtained experimentally.

Particle size measurements confirm that the extra loss is indeed due to action on the condensed phase. When the inlet ratio varies from 6 to 2, the mean diameters increase regularly; in this case we observe that d_{10} varies rather little while the variation in d_{53} is more than 30%; this difference is due to the increase in the number of large particles as r_e/r_c decreases. The increase in

-190-

mean diameters for an integrated nozzle is more uniform, 11% for
d_{10} to 13% for d_{30}; these values enable us to find the extra
specific impulse loss if we assume that this loss is proportional
to the square of a certain mean radius. The growth mechanism of
the condensed phase appears rather different with regard to the
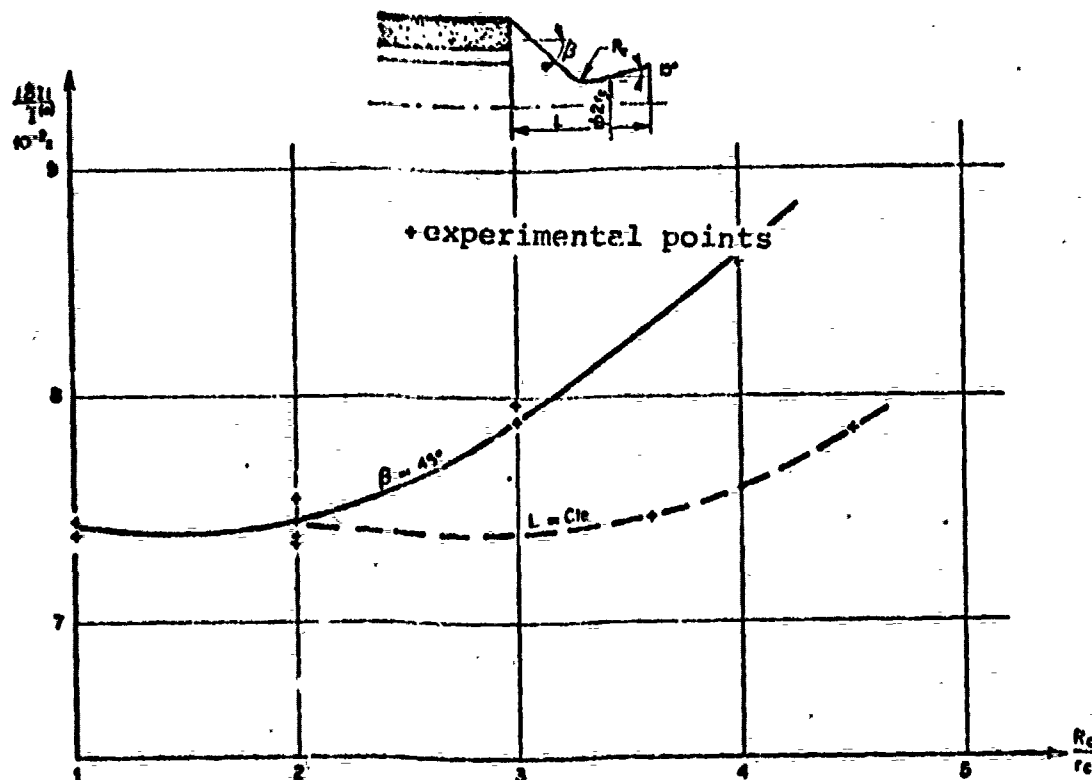respective influence of the inlet ratio and integration of the
nozzle.

Figure 39. Influence of Nozzle Geometry on Specific Impulse
Loss.

In the case of integration, heat losses are probably increased
due to the very design of the nozzle. We try to protect the nozzle
by the cold film method mentioned above. The gain obtained for
$L_1/L_2 = 0.082$ is 0.2%, i.e., the limit of significance; the influ-
ence on particle size is not clear either.

c) **Nozzle geometry**

The loading design and geometry of the inlet zone play an active part in initial particle size and possibly in loss due to particle impacts on the wall, which loss is always very small. The nozzle geometry, on the other hand, has a direct influence on the most important losses: phase lags, wall friction and heat flow, and of course jet divergence.

Tests were limited to biconical nozzles to minimize the number of geometric parameters. The first run of tests was on nozzles with a constant throat radius of curvature, and constant throat diameter and diverging section half-angle (20 mm and 15°).

Figure 39 gives two curves. The first is for constant nozzle length and simultaneous variation of the convergent half-angle and throat radius of curvature. The second relates to a constant convergent half-angle, the increase in the throat radius of curvature implying increase in nozzle length. We find that short nozzles and small radii of curvature are always preferable. The increase in loss with the radius of curvature cannot be linked to the condensed phase since no systematic variation in particle size could be demonstrated and the most progressive throats reduced the phase lags; thus the wall loss influence must be substantial. The characteristic velocity varies little with constant nozzle length; it decreases regularly when the radius of curvature of the throat increases.

With the aim of reducing phase lags at the throat we performed some tests with nozzles identical to the reference nozzle from the standpoint of converging section, diverging section, and total length but with a cylindrical throat of 4 mm connected by two sections with constant radius of curvature to the converging section and diverging section instead of a throat with constant radius of curvature ($R_c/r_c = 2$). The difference found between the two

-192-

series of tests is less than 0.2% and is thus not significant. Throat erosion is also marked in both cases; the cylindrical throat thus has no advantage with respect to performance.

6.2.4. Result of Comparing Theory to Experiment

The theoretical analysis of the problem appears to be good since it is well borne out by the experimental results both qualitatively, enabling loss increases to be explained under certain conditions, and quantitatively. With respect to the latter point accuracy is still limited by the absence of a realistic flow pattern in the nozzle and by particle size data for the condensed phase.

Good knowledge of the condensed phase at the nozzle inlet is essential; other investigations will be necessary before the particle size can be predicted at the preliminary design stage, not only as a function of operating pressure and motor scale but also according to the loading design and the nozzle inlet zone.

6.3. OPPORTUNITIES FOR REDUCING LOSSES

The problem to which we will now address ourselves relates to motor optimization, i.e., choice of operating parameters enabling losses to be minimized. All optimization is subjected to some limitations: we will assume that the principal dimensions of the motor are well defined and that the nature of the propellant, the operating pressure, and the throat diameter are given. We can vary the propellant composition and the motor's geometric characteristics.

6.3.1. Variations in Propellant

We must first note that the practical optimum for propellant metal content is always beyond the value given by thermodynamic calculation; since condensed phase losses depend both on the metal content and motor size, the gap between theoretical optimum and

practical optimum depends on the application in view. This gap can be as much as 5% for small motors.

Since the performance level is established we can diminish losses by reducing either the proportion of condensed phase in the combustion products or the particle size. To reduce the condensed phase beginning from an essentially constant metal content we can first think about forming a maximum of volatile components. This aspect of the problem is linked to the choice of metal: a body such that, in this respect, the bore would have some advantage (oxide vaporization temperature about 2400°K) although it is somewhat unfavorable from the energy standpoint (formation of products with high molar masses somewhat unstable at high temperatures and difficult to burn). The choice of metal is thus a compromise. When metals difficult to burn are used, metal mixtures could be tried [88]. Another means of reducing the condensed phase is to add to the propellant an additive likely to produce volatile products; fluoride compounds are interesting from this viewpoint (they can also accelerate propellant inflammation). An example of the effect of fluoride products has been supplied by modulation studies. The basic propellant has a polyurethane binder containing 16.4% aluminum; the functioning of this propellant with an injection of ℓF_3 (mass fraction 10%) reduces the metal content to 14.8%. The proportion of condensed phase in the chamber at 70 atm. is on the other hand reduced by 42% such that the 2.5% impulse loss due to injection should only now be 1.2% if we assume that the loss due to the condensed phase is about 3% for the reference propellant.

Due to the considerable influence of particle size it would be desirable to reduce the proportion or size of large particles. According to the presumed mode of formation of the latter the mass of aluminum particles entrained by the gaseous phase should be reduced; this could be achieved by avoiding agglomeration of liquid aluminum particles to the propellant surface by an appropriate surface treatment. Moreover, it is always desirable to avoid surface

-194-

oxidation of metal particles in the propellant, which may be achieved by deposition when the particles are made [89]; this technique would also permit lithium to be used -- useful from the energy standpoint.

6.?.2. Variations in Motor

The first elements for a response were furnished by tests and could also be given by a parametric study [57]. The objective here is to determine directly by calculation what the optimum motor design would be and the gain entailed. The influence of loading design and inlet zone is translated by modifications in condensed phase particle size in the nozzle inlet section. This influence has been found out by experiment but thus far we have no theory to predict it; we may consider, qualitatively speaking, that it would be useful to limit the velocity gradients and avoid overspeed zones, jet mixtures, and any device likely to increase turbulence in the chamber. Optimization will thus here be limited to the nozzle.

a) Relative influence of various nozzle zones

The loss due to phase lags stresses the primordial importance of the diverging section if we consider particle growth, since it is at the nozzle outlet that these particles are the largest. This is confirmed by near equilibrium calculations done with the formula of Paragraph 4.6.1. for biconical nozzles: the contribution of the converging section to loss is negligible and that of the throat is small; an appreciable part of the loss is produced during solidification of the alumina in the diverging section.

The role of various nozzle zones in wall losses is fairly complex. In the example taken and for heat loss the diverging section is responsible only for 25% while for friction loss this is 94%.

The jet divergence loss is directly linked to the diverging section contour and there are classic techniques in homogeneous fluid for choosing contours more suitable than the conical contour [90, 91]; the maximum contour half-angle must not exceed a calculable limit value, failing which the expansion waves would be focused -- unfavorable from the flow stability standpoint. We must also take care that these particles cannot encounter the terminal part of the nozzle [52].

It thus appears that the diverging section is the most important part of the nozzle and that flow must be studied from the two-dimensional viewpoint.

The difficulty of calculation forces us to proceed by under-optimization, i.e., considering only one nozzle zone or one type of loss. Nozzle contour optimization with respect to wall losses is a problem upon which little work has been done; the most that we know is that for a constant length of the subsonic part of the nozzle a concave converging section should be chosen with a moderate throat radius of curvature [92]. Existing studies may be broken down into two groups: the first studies the loss linked to the condensed phase throughout the nozzle in one-dimensional flow and the second relates to losses in the diverging section taking the condensed phase and the two-dimensional aspect of flow into account.

b) Optimization of entire nozzle for two-phase loss

The first result in this direction was obtained by Marble [93] for the simplified two-phase flow model (constant and uniform particle diameter) and by application of near equilibrium methods. We extended his calculations and began from more exact equations in the near equilibrium, considering a more realistic flow.

Analytical optimization methods are fairly numerous [91]; among them variational calculation has been successfully applied

to nozzle problems [95]. Here we chose to apply the maximum principle (Pontryagin). To avoid cumbersome calculation we included only kinetic phase lags (p = 1) which leads us to use the isentropic exponent of the mixture in equilibrium (denoted here simply by γ for simplication in writing). The reduced equations to be used , are thus:

$$\frac{dm}{dx} = -\frac{m\left(2m + \frac{\gamma-1}{\gamma}\right)}{\frac{1}{\gamma} - m} F - \left(1 + \frac{2\gamma}{\gamma-1} m + Kn^2\right) K \left[\frac{1-n}{n} + (1+m)\frac{\left(\frac{\gamma-1}{\gamma}n-1\right)\frac{1-n}{n}}{\frac{1}{\gamma} - m}\right],$$

$$\frac{dn}{dx} = -\frac{mn F}{\frac{1}{\gamma} - m} + \left(1 + \frac{2\gamma}{\gamma-1} m + Kn^2\right)\left[\frac{1-n}{n} - Kn \frac{\left(\frac{\gamma-1}{\gamma}n-1\right)\frac{1-n}{n}}{\frac{1}{\gamma} - m}\right].$$

For the optimal problem the control function will not be F but an auxiliary function able to eliminate the singularity of the equations. The function chosen is linked to pressure variations:

$$u = \overset{o}{f}(x) = \frac{d}{dx}\left(\text{Log }\frac{P_o}{P}\right).$$

We then get:

$$\begin{cases} \frac{dm}{dx} = -m\left(2m + \frac{\gamma-1}{\gamma}\right)u + K\left(1 + \frac{2\gamma}{\gamma-1} m + Kn^2\right)^{\frac{1}{2}}\left[2m + \frac{\gamma-1}{\gamma}(1-n)\right]\frac{1-n}{n}, \\ \frac{dn}{dx} = -mnu + \left(1 + \frac{2\gamma}{\gamma-1} m + Kn^2\right)^{\frac{1}{2}}(1 + Kn)\frac{1-n}{n}. \end{cases}$$

Here optimization is performed with a constant nozzle length and constant outlet pressure (adapted nozzle). We then show that specific impulse is proportional to the integral:

$$S = \int_0^{x_A} \frac{m}{\left(1 + \frac{2\gamma}{\gamma-1} m + Kn^2\right)^{\frac{1}{2}}} u\, dx.$$

Writing:

$$a_m = -m\left(2m + \frac{\gamma-1}{\gamma}\right),$$

$$a_n = -mn,$$

$$b_m = K\left(1+ \frac{2\pi}{\delta-1}m + Kn^2\right)^{\frac{1}{2}}\left[2m + \frac{\sigma-1}{\delta}(1-n)\right]\frac{1-n}{n},$$

$$b_n = \left(1+ \frac{2\pi}{\delta-1}m + Kn^2\right)^{\frac{1}{2}}(1+Kn)\frac{1-n}{n},$$

$$g = \frac{m}{\left(1+ \frac{2\pi}{\delta-1}m + Kn^2\right)^{\frac{1}{2}}},$$

the problem can be written out in the following form:

"Given the system:

$$\begin{cases} \overset{\circ}{m} = a_m u + b_m, \\[4pt] \overset{\circ}{n} = a_n u + b_n, \\[4pt] \overset{\circ}{q} = u, \\[4pt] \overset{\circ}{s} = g u, \end{cases}$$

subjected to the conditions:

$$x=0, \quad q(0)=s(0)=0, \quad m(0), n(0) \text{ donnés},$$

$$x_0 \text{ et } q_0 \text{ donnés},$$

find the control $u(x) \geq 0$ which makes $S(X_p)$ a maximum."

We form the adjunct system:

$$\begin{cases} \overset{\circ}{\lambda}_m = -\lambda_m\left(\frac{\partial a_m}{\partial m}u + \frac{\partial b_m}{\partial m}\right) - \lambda_n\left(\frac{\partial a_n}{\partial m}u + \frac{\partial b_n}{\partial m}\right) - \lambda_s u \frac{\partial g}{\partial m}, \\[6pt] \overset{\circ}{\lambda}_n = -\lambda_m\left(\frac{\partial a_m}{\partial n}u + \frac{\partial b_m}{\partial n}\right) - \lambda_n\left(\frac{\partial a_n}{\partial n}u + \frac{\partial b_n}{\partial n}\right) - \lambda_s u \frac{\partial g}{\partial n}, \\[6pt] \lambda_q = Cte \\[6pt] \lambda_s = Cte \end{cases}$$

It must satisfy the conditions:

$$\lambda_m(x_0) = 0,$$
$$\lambda_n(x_0) = 0,$$
$$\lambda_s = -1,$$
$$\lambda_q . \text{ indeterminate but not zero.}$$

The Hamiltonian is written:

$$H = \lambda_m b_m + \lambda_n b_n + u\left(\lambda_m a_m + \lambda_n a_n - g + \lambda_q\right).$$

-198-

The principle of the maximum indicates that at each point H must be minimum with respect to the control. Now since H is a linear function of u we must impose restrictions on the control; we will take:

$$0 \leq u \leq u_{MAX} \ .$$

Optimum control thus breaks down into a series of arcs which belong to the following three categories:

- arcs u_{max} if $\lambda_m a_m + \lambda_n a_n - g + \lambda_g < 0$,
- arcs 0 (constant pressure) if $\lambda_m a_m + \lambda_n a_n - g + \lambda_c > 0$,
- arcs u variable if $\lambda_m a_m + \lambda_n a_n - g + \lambda_g = 0$.

Calculation gives:

$$\frac{dH}{dx} = \dot{u} \left(\lambda_m a_m + \lambda_n a_n - g + \lambda_q \right) \ .$$

H is thus constant on each of the arcs; as the arc changes by cancelling the coefficient of $\dot{u}$ in the latter equation we may conclude that H is continuous and thus constant throughout the interval.

From this result we show that the first and the last arcs can only be u_{max} arcs and that the intermediate arc is a variable u arc. Of all the possible solutions there is the solution relating to u constant corresponding to an exponential increase in pressure, which bears out the results of Marble [93]. The nozzle shape deduced is known: it has a short convex converging section, a long throat, and a very open diverging section ("trumpet" contour).

The second type of calculation begins with the formula established for near equilibrium for specific impulse loss:

$$\frac{|\delta I|}{I^{(o)}} = \varepsilon \, \overline{\tau_{u_o}} \, \frac{\overline{T_o}^{(o)}}{\overline{u_a}^{(o)2}} \int_{x_o}^{x_a} q \, \frac{\rho_e}{\rho_{eo}} \, \frac{\mu_o}{\mu} \, \frac{\overline{u}^{(o)}}{\overline{T}^{(o)}} \left(\frac{d\overline{u}^{(o)}}{dx} \right)^2 \left[1 + \frac{3}{2} \overline{\sigma}_{r_f}^{(o)} k^2 \frac{\overline{u}^{(o)2}}{\overline{c_p}^{(o)} \overline{T}^{(o)}} \right] dx \ .$$

In this formula we assume that the growth function q depends only on the section ratio or on $\bar{u}^{(o)}$. Adimensional variables can be introduced [62] which leads to minimizing an integral of the form:

$$J = \int_0^1 g(\bar{M}^{(o)}) \left(\frac{d\bar{M}^{(o)}}{dx}\right)^e dx$$

Here optimization will be performed with constant nozzle length and given outlet section ratio ($\bar{M}_\Delta^{(o)}$ fixed).

The Euler equation for the extreme problem leads to the solution:

$$g(\bar{M}^{(o)}) \left(\frac{d\bar{M}^{(o)}}{dx}\right)^e = C .$$

A $H(\bar{M}^{(o)})$ function can be defined by:

$$H(\bar{M}^{(o)}) = \int_{\bar{M}_0^{(o)}}^{\bar{M}^{(o)}} \sqrt{g(\zeta)} \, d\zeta .$$

With the conditions of the simplified model, the H function is expressed in terms of incomplete elliptical integrals [93] and in the general case we must resort to the computer.

The optimum solution is such that:

$$X = \frac{H(\bar{M}^{(o)})}{H(\bar{M}_\Delta^{(o)})} ,$$

$$C = \left[H(\bar{M}_\Delta^{(o)})\right]^e = J_{min.} .$$

Calculation was conducted under realistic conditions with or without particle growth. The contours corresponding to these two hypotheses are relatively close (Figure 40) and the optimal nozzle characteristics are accentuated by growth and solidification of particles. This shape is not usable in practice since it would lead to unacceptable heat and jet divergence losses.

Calculation can also be performed with biconical nozzles and compared to the minimum two-phase loss. We form the ratio:

$$\frac{|\delta I|}{|\delta I|_{min}} = \frac{\int_0^1 g(\bar{M}^{(e)})\left(\frac{d\bar{M}^{(e)}}{dx}\right)^2 dx}{\left[\int_{\bar{M}_0^{(e)}}^{\bar{M}_e^{(e)}} \sqrt{g(\zeta)}\, d\zeta\right]}.$$
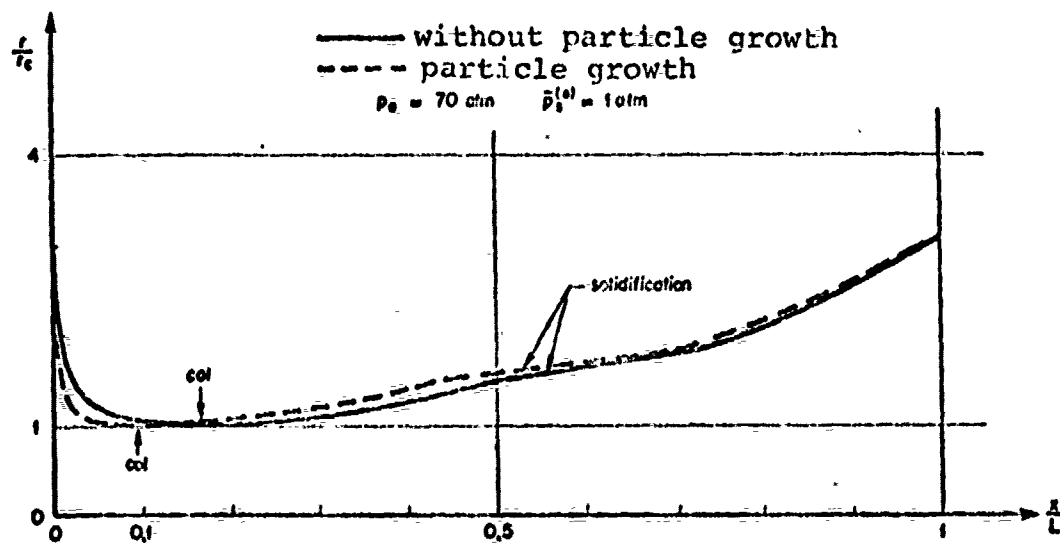

Figure 40. Optimum Nozzle Shape for Two-Phase Loss.

The results are summarized in Figure 41 and should be compared to those of Figure 39. With constant length, two-phase loss decreases as the radius of curvature increases; simultaneous increase of the heat loss can explain the upward turn of the curve representing total loss beyond $R_c/r_c = 3$. With constant converging section angle, two-phase loss increases with radius of curvature as does heat loss which causes a sharp increase in total loss.

We also find that the loss for a conical nozzle is about double that of the minimum loss; we can thus expect to recuperate, by nozzle optimization, only half of the two-phase loss at most, or 1.5%

$$\frac{|\delta I|}{|\delta I|_{min}}$$

$P_0 = 70\ atm$, $P_s^{(a)} = 1\ atm$

$\frac{r_0}{r_c} = \cdot$, $\frac{r_s}{r_c} = 3{,}104$

$\alpha = 15°$

$\beta = 45°$

$L = 0{,}8$

$\left(\frac{R_c}{r_c}\right)_{MAX}$
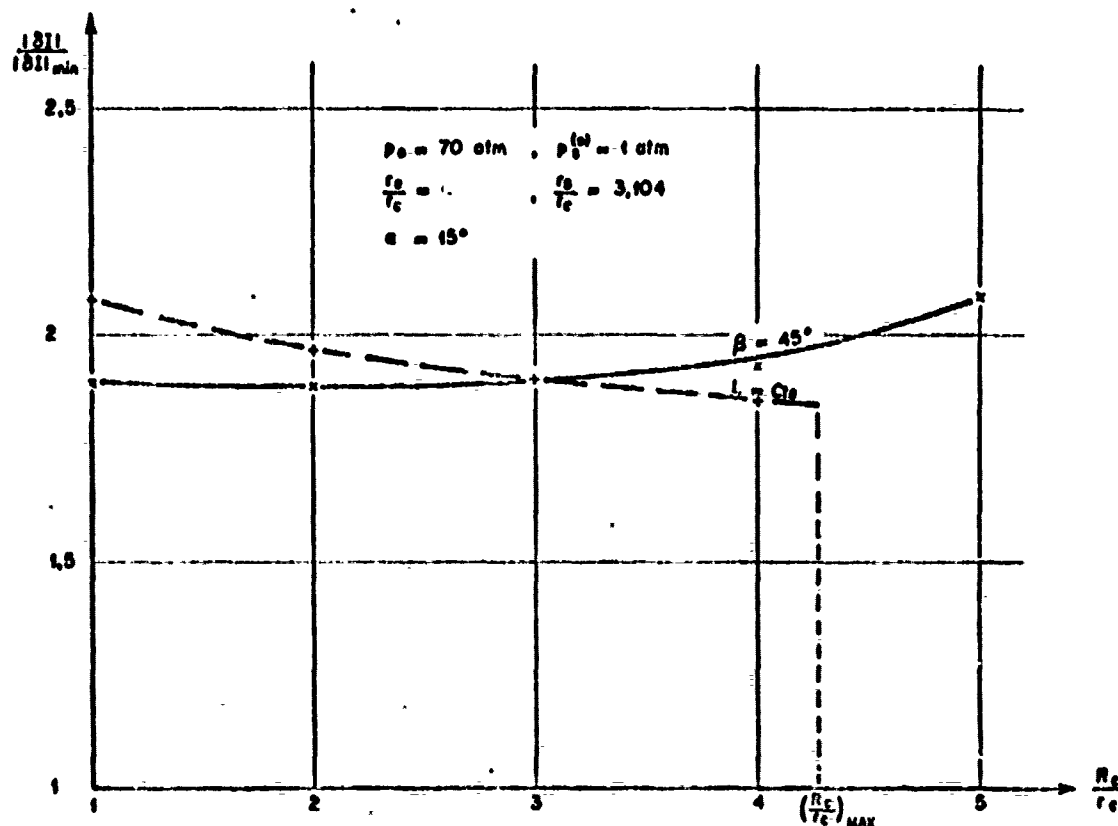
$\frac{R_c}{r_c}$

Figure 41. Influence of Nozzle Geometry on Two-Phase Loss.

for the experimental motor. This gain will be more difficult to obtain due to the compromise that must be made for wall losses and jet divergence losses.

c) Diverging section optimization

The method for calculating the flow in the diverging section is that of characteristics. It lends itself well to calculation of variations [97, 98]; we can also use nozzle contour parameters [96]. The nozzle parameters can be the length, surface, perimeter, or weight. Existing calculations assume that the particles are of constant diameter; nevertheless this simplification leads to

useful results since we show that the optimum nozzle contour is relatively insensitive to particle diameter.

Calculations show that with constant nozzle length and a moderate throat diameter (about 60 mm) optimization of the diverging section enables us to gain only 0.8% with respect to the conical nozzle with half-angle 15°. This result, together with theoretical indications in near equilibrium, show that the hoped-for gains can only be small ones.

*   *

*

7. GENERAL CONCLUSIONS

The increase in specific impulse losses of solid metallized propellants proves to be linked to the existence of a condensed phase in the combustion products. The influence of this condensed phase appears to be rather general and the main difficulty of the problem is that the particle size changes during expansion of the combustion products. We thus had first to specify the character-istics of the condensed phase before undertaking a flow analysis.

The experimental techn.que used for determining particle size is fairly classical but the efforts made to improve the method of analysis and interpretation of the results brought about a clear gain in accuracy; use of the electron microscope proved particularly useful. The particle distribution function is now better known throughout the span of diameters; captures made inside the motor showed the importance of particle growth; the influence of the motor's operating parameters is better understood qualitatively.

Theoretical analysis of condensed phase behavior in the motor was performed for each zone of interest: propellant combustion zone, motor combustion chamber, and nozzle. In order to separate the flow

problem from the condensed phase evolution problem we schematized
the behavior of the gaseous phase in each of these zones; this
schematization led us to relatively simple models and enabled us
in the first analysis to reach qualitative conclusions and estab-
lish orders of magnitude. We demonstrated the formation, during
combustion, of two classes of particles with very different diameters;
the dwell time of the combustion products acts more on distribution
of the condensed phase between the two classes than on particle
distribution within each of these classes.

The phenomena causing collisions are different in the com-
bustion chamber and in the nozzle. In the nozzle, acceleration
of the gaseous phase is the preponderant phenomenon. In the
combustion chamber the collision functions are still poorly
known; they seem to be different for small and large particles.

The main effect of the condensed phase, from the specific
impulse loss standpoint, is that concerning expansion of com-
bustion products in the nozzle. The two-phase nature of the
flow led us to set up condensed phase, gaseous phase, and mixture
equations. These basic equations rest upon very general hypotheses
but hypotheses which are adapted to flow of suspensions showing
the existence of relaxation phenomena deriving from irreversible
exchanges between phases and degrading the quality of expansion.
The equations were first of all applied to a very simplified nozzle
flow (uniform and constant particle diameters in an ideal gas) in
order to show the essential characteristics. This pattern was
progressively modified to represent the real phenomenon. In all
cases fairly complex computation was necessary. However, we
showed that the analytical formulas for specific impulse loss
could be established in extreme cases for very small or very large
motors. The second case, fairly representative of existing motors,
is the most interesting; the analytical formula enables us to pre-
dict simply the influence of the operating parameters of the motor
on the specific impulse loss.

The condensed phase also acts upon the more classic losses which still subsist when the propellant is not metallized: jet divergence loss and wall losses. The divergence loss, which is not physical in nature but results from the need to calculate on sectional flow, is more difficult to calculate for a suspension than for a homogeneous fluid due to segregation of the condensed phase in the center of the flow. We showed, with the aid of a calculation method for perfectly stratified flow, that this phenomenon, although it only slightly modifies the classic divergence loss formula, causes a slight extra loss in specific impulse.

Wall losses are affected by the formation of a condensed alumina layer on part of the nozzle. This phenomenon, about which little had been known, was studied from the viewpoint of its formation, its evolution, and its effects. The alumina layer is formed by impingement of alumina particles in suspension in the combustion products; this is a capture problem linked to flow in the inlet zone of the nozzle. This capture, corresponding to an ejected mass defect, causes no significant specific impulse loss. Development of the alumina layer is linked to its heating and its physical conditions; when its surface reaches the alumina melting point the effect of friction forces becomes substantial. The layer adheres to the nozzle throat in fine droplets by a liquid film instability mechanism. Calculation showed that despite the alumina layer the wall losses can be calculated in the classical manner: friction is only slightly sensitive to velocity and to the layer's surface temperature, and the heat exchange coefficient between combustion products and nozzle changes only slightly. Due to the transient nature of nozzle heating we established an original formula giving the mean flow density at a point of the wall over time. Surface temperature measurements and the flow calculations derived therefrom are in good agreement with theory. A formula was given to express the specific impulse loss due to wall phenomena.

The results were applied to a small motor for which we
determined the total specific impulse loss in the laboratory.
This measurement necessitated a judicious choice of experimental
means and method of analysis; the accuracy finally obtained was
close to 0.2% and permited a comparison between theory and exper-
iment. The cross check was satisfactory as discrepancies came
within the margin of accuracy due to the simplifying hypotheses
used and to the still imperfect knowledge of the condensed phase.
Tests conducted to find out the influence of the motor configura-
tion on specific impulse 'oss confirmed the close link between
the latter and the particle size of the condensed phase. We
demonstrated that it is difficult to reduce specific impulse
loss by optimizing motor geometry, but it is a more attractive
proposition to vary the propellant.

The improvement in predictions necessarily has two inter-
mediate stages: better knowledge of the condensed phase and
more precise description of the expansion of combustion products.
The main obstacle slowing down progress in particle size derives
from their growth, which growth is expressed theoretically by
the necessity of taking collisions into account and experimentally
by the need for new measuring methods. These measuring methods
must give local knowledge of particle distribution without per-
turbing the flow and enable the collision functions to be defined
and the particle size at the nozzle inlet to be predicted as a
function of the operating parameters. The nozzle calculation must
be two-dimensional and the condensed phase must be described
realistically; the first stage will be to define the behavior of
the combustion products in the throat region of the nozzle since
this zone has proved very important from the standpoint of the
gaseous phase as well as the condensed phase (rapid particle growth,
condensed phase segregation). At this stage we must expect compu-
ting difficulties which should partially be resolved by the successive
approximation method. Calculations must be able to take into
account the inertial forces resulting from motor acceleration (we
know experimentally that the combination of centrifugal inertial

forces due to rotation of the motor about its lengthwise axis and longitudinal inertial forces is the cause of the supplementary specific impulse loss; this particular aspect of the general problem could not be dealt with here).

The three preoccupations which guided us through this study were: to take stock of present-day knowledge; to contribute by theory and experiment to better understanding of these phenomena; and to lay out the paths for future work. An answer was given to each of these three points and it appears that new progress has been contributed to present-day investigation in both the fundamental and experimental domains.

Académie de Paris   PRINTING PERMIT
Université de Paris VI
4, Place Jussieu - 75230.Paris - CEDEX 05

Student Department

Education Office, Third Cycle

Telephone: 336-25-25 - 325-12-21

            Doctorate: Government

            Thesis: Physics

            Name: Mr. Kuentzmann

            First Names: Paul

            Born on November 21, 1940 in Paris, Seine.

                              .

            First Thesis. "Contribution to the Study of Specific

            Impulse Loss in Solid Propellant Rockets."

            Second Thesis: (Topic suggested by University):

            "The Pogo Effect in Liquid Propellant Rockets."

Chairman: Mr. Fortier

Examiners: Mr. Siestrunck
             Mr. Barrère

                                      Examined and Approved
                                      Paris, July 5, 1973
                                      The President
          [Seal:] Académie de Paris   of the University of
                  Université Paris VI Paris VI

                                      [signature]

REFERENCES

[1] B. CRAMPEL – Chimie des constituants des propergols
Note technique ONERA n° 113, 1967.

[2] M. BARRERE – Problèmes énergétiques de la propulsion
Cours ENSA, 1965.

[3] S.E. COLUCCI – Experimental determination of solid rocket nozzle heat transfer coefficient
Ballistic Missile and Space Technology, vol. II, p. 303. Academic Press, 1960.

[4] J.D. HOFFMAN – An analysis of the effect of gas particles mixtures on the performance of rocket nozzles.
Jet Propulsion Center. Purdue University. Report TM 63-1, 1963.

[5] F.E. MARBLE – Dynamics of a gas containing small solid particles
Combustion and Propulsion fifth AGARD colloquium. Pergamon Press, p. 175, 1963.

[6] S.L. SOO – Dynamics of multiphase flow systems
Project SQUID. Technical Report ILL 18,P, 1964.

[7] F.A. WILLIAMS – M. BARRERE – N.C. HUANG – Fundamental aspects of solid propellant rockets.
AGARD ograph 116. Technivison Services, 1969.

[8] P. KUENTZMANN – Etude expérimentale de la phase condensée d'un propergol solide métallisé.
La Recherche Aérospatiale, n° 153, mars-avril 1973.

[9] B. BROWN – K.P. MAC ARTY – Particle size of condensed oxides from combustion of metallized solid propellants.
Eight Symposium on Combustion. The Williams and Wilkins Company, 1962.

[10] H. CHEUNG – N.S. COHEN – On the performance of solid propellant containing metal additives.
AIAA Solid Propellant Rocket Conference. Preprint n° 64 116, Palo Alto, Jan., 1964.

[11] L.A. POVINELLI – P.A. ROSENSTEIN – Alumina size distributions from high pressure composite solid propellant combustion
AIAA Journal, vol. 2, n° 10, p. 1754, oct. 1964.

E.W. PRICE – J.E. CRUMP – H.C. CHRISTENSEN – R. SEGHAL – Comments.
AIAA Journal, vol. 3, n° 9, p 1790, sept. 1965.

[12] R.A. DOBBINS – L.D. STRAND – A comparison of two méthods of measuring particle size of Al_2O_3 produced by a small rocket motor
AIAA Journal, vol. 8, n° 9, p. 1544, sept. 1970

[13] J. BRULARD – Contribution à l'étude de la combustion des particules d'aluminium
La Recherche Aérospatiale, n° 118, Mai-Juin 1967.

[14] J. CRABOL - Caractéristiques thermiques d'un jet de fusée contenant des particules
d'alumine
Publication ONERA n° 133, 1970.

[15] R.N. JAMES - W.R. BABCOCK - H.S. SEIFERT -
A laser doppler technique for the measurement of particle velocity
AIAA Journal, vol.6, n° 1, p. 160, Jan. 1968.

[16] M.E. FOURNEY - J.H. MATKIN - A.P. WAGGONER - Aerosol size and velocity determi-
nation via holography.
The review of scientific instruments, vol.40, n° 2, p. 205, fev. 1969.

[17] E. BRUN - R. CARON - M. VASSEUR - Introduction à l'étude de la mécanique des
suspensions.
Rapport technique GRA n° 15, 1945.

[18] W. LEWIS - R.J. BRUN - Impingement of water droplets on a rectangular half body
in a two dimensionnal incompressible flow field.
NACA TN 3658.

[19] P. KUENTZMANN - Formation de la phase condensée dans un propulseur à propergol
solide métallisé.
Note technique ONERA n° 210, 1973.

[20] P. KUENTZMANN - Agglomération des particules d'alumine dans l'écoulement de
tuyère d'un propergol métallisé.
La Recherche Aérospatiale, n° 131, juillet - août 1969.

[21] M. BARRERE - Résultats expérimentaux récents sur la combustion de l'aluminium
et d'autres métaux.
ONERA, T.P. n° 735, 1969.

[22] M. BARRERE - R. PRUD'HOMME - Aérothermochimie des écoulements homogènes.
Mémoires de Sciences Physiques, Gauthier Villars, 1971.

[23] G. GYARMATHY - Zur Wachstumgeschwindigkeit kleiner Flüssigkeitstropfen in einer
übersättigen Atmosphär.
Z.A.M.P., vol. 14, p. 280, 1963.

[24] R.M. JENKINS - R.T. HOGLUND - A unified theory of particle growth in rocket
chambers and nozzles.
AIAA Paper, 69 541.

[25] F.E. MARBLE - Some gas dynamic problems in the flow of condensing vapors.
Astronautica Acta, vol. 14, p. 585, 1969.

[26] R. CARUSO - Behavior of ultra small colloïd particles.
AFOSR 67 0933, 1967. Thiokol Chemical Corporation.

[27] H.L. FEIN - A theorical model for predicting aluminium oxide particles size dis-
tributions in rocket exhausts.
AIAA 2nd Aerospace Sciences Meeting, 1965.

[28] C.T. CROWE - P.G. WILLOUGHBY - A study of particle growth in a rocket nozzle.
AIAA Journal, vol. 5, n° 7, p. 1300, 1967.

[29] S.D. GRISHIN - A.P. TISHIN - R.Y. KHAIRUTDINOV - Ecoulement biphasique en désé-
quilibre dans une tuyère de Laval avec la coagulation des particules du condensat
polydispersé.
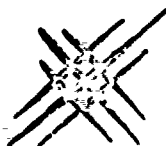Akademiïa Nauk. SSSR. Izvestiïa Mekhanika Zhidkosti i Gaza, n° 2, p. 112, 1969.

[30] G.L. BABUKHA - L.E. STERNIN - A.A. SCHRAIBER - Calcul des pertes diphasées dans une tuyère dues à la phase condensée.
Akademiia Nauk. SSSR. Izvestia Mekhanika Zhidkosti i Gaza, n° 1, p.175, 1971.

[31] F.E. MARBLE - Droplet agglomeration in rocket nozzles caused by slip and collision
Astronautica Acta, vol. 13, n° 2, p. 159, 1967.

[32] J.F. REGAN - H.D. THOMPSON - R.F. HOGLUND - Two dimensional analysis of transonic gas particles flow in axisymmetric nozzles.
AIAA Paper, n° 69 572.

[33] P. KUENTZMANN - Aérothermochimie des suspensions.
Mémoires de Sciences Physiques n° 72. Gauthier Villars, 1973.

[34] A. FORTIER - Mécanique des suspensions.
Masson 1967.

[35] R. PANTON - Flow properties for the continuum view point of a non equilibrium gas particle mixture.
Journal of fluids mechanics, vol. 31, part. 2, p. 273, 1968.

[36] D.A. DREW - L.A. SEGEL - An averaging approach to the theory of two phase flows.
International symposium on two phase flow. Paper 6-30. Haïfa, 1971.

[37] B.P. SELBERG. J.A. NICHOLLS - Drag coefficient of small spherical particles.
AIAA Journal, vol. 6, n° 3, p. 401, March 1968.

[38] D.J. CARLSON - R.F. HOGLUND - Particle drag and heat transfer in rocket nozzles.
AIAA Journal, vol. 2, n° 11, p. 1980, Nov. 1964.

[39] C.T. CROWE - Inaccuracy of nozzle performance predictions resulting from the use of an invalid drag law.
Journal of Spacecraft and Rockets, vol. 7, n° 12, p. 1491, dec. 1970.

[40] R.W. BARTLETT - L.J. DELANEY - Effect of liquid surface tension on maximum particle size in two phase flow.
Pyrodynamics, vol. 4, p. 397, 1966.

[41] L. NAPOLITANO - Thermodynamique des systèmes composites en équilibre ou hors d'équilibre.
Mémoire de Sciences Physiques. Gauthier Villars, 1971.

[42] F.A. WILLIAMS - Combustion theory.
Addison Wesley. Publishing Company, 1965.

[43] V. QUAN - J.R. KLIEGEL - Axisymmetric two phase reacting gas non equilibrium nozzle flow.
NASA CR 92058, Aug. 1967.

[44] J.R. KLIEGEL - One dimensional flow of a gas particle system.
IAS Paper n° 60-5, 1960.

[45] P. DUBAN - J.NICOLAS - Influence de la présence de particules solides sur l'écoulement dans une tuyère.
La Recherche Aéronautique n° 92, Janv.-Fév. 1963.

[46] H.A. HASSAN - Exact solutions of gas particle nozzle flows.
AIAA Journal, vol. 2, n° 2, p. 395, feb. 1964.

[47] T.C. DELLINGER - H.A. HASSAN - Analysis of gas particle flows in rocket nozzles.
Journal of Spacecraft and Rockets, vol. 3, n° 4, p. 601, Apr. 1966.

[48] W.D. RANNIE – Perturbation analysis of one dimensional heterogeneous flow in rocket nozzles.
Progress in astronautics and rocketry, vol. 6. Detonation and two phase flow. Academic Press. 1962

[49] V.D. VENEDIKTOV – Two phase flow in turbines and reaction nozzles.
NASA TTF 613. Jun.1970.

[50] E.F. LYPE – One dimensional analysis of non isentropic two phase flow.
ARS Preprint 1605-61. 1961.

[51] R.D. CLAUZ – Combined subsonic supersonic gas particle flow.
ARS Preprint 1717-61. 1961

[52] W.S. BAILEY – E.N. NILSON – R.A. SERRA – T.F. ZUPNIK – Gas particle flow in a axisymmetric nozzle.
ARS Journal, vol. 31, p. 793, Jun 1961.

[53] J.A. HULTBERG – S.L. SOO – Flow of a gas solid suspension through a nozzle.
AIAA Paper 65-6, 1965.

[54] R.F. HOGLUND – Recent advances in gas particle nozzle flows.
ARS Journal, p. 662, May 1962.

[55] G. RUDINGER – Dynamics of gas particle mixtures with finite particle volume.
AIAA Paper n° 65-9.
Relaxation in gas particle flow.
Project SQUID T.R. CAL 96 PU. Jul. 1968.
Gas particle flow in convergent nozzles at high loading ratios.
Project SQUID T.R. CAL 98 PU. Jul. 1969.

[56] J.R. KLIEGEL – G.R. NICKERSON – Flow of gas particle mixtures in axially symmetric nozzles.
Progress in astronautics and rocketry, vol. 6, p. 173. Detonation and two phase flow. Academic Press 1962.

[57] J.D. HOFFMAN – S.A. LORENC – A parametric study of gas particle flows in conical nozzles.
AIAA Journal, vol. 3, n° 1, p. 103. Jan. 1965.
Correlation of performance of conical and contoured nozzles for gas particle flow.
AIAA Journal, vol. 4, n° 1, p. 169, Jan. 1966.

[58] H. SAUERWEIN – F.E. FENDELL – Method of characteristics in two phase flow.
The Physics of fluids, vol. 8, n° 8, p. 1564, 1965.

[59] D. MIGDAL – V.D. AGOSTA – Supersonic gas particle flow with chemical reactions.
The Physics of fluids, vol. 10, n° 4, p. 620, 1967.

[60] G.R. JOHNSON – Supersonic gas solid particle flow in a axisymmetric nozzle by the method of characteristics.
Von Karman Institute,T.N. 78, Aug. 1971.

[61] L.P. VERESHAHAIKA – N.S.GALIUN – A.N.KRAIKO – L.E.STERNIN – Résultats du calcul d'un écoulement gazeux avec des particules dans des tuyères axisymétriques par la méthode des caractéristiques et comparaison avec les résultats de l'approximation unidimensionnelle.
Akademiia Nauk. SSSR. Izvestia Mekhanika Zhidkosti i Gaza, n° 3, p. 123, (1968).

[62] P. KUENTZMANN – Perte d'impulsion spécifique des propergols métallisés.
Entropie, à paraître.

[63] P. KUENTZMANN – Influence de l'hétérogénéité de la distribution de la phase condensée sur la performance des propergols solides.
La Recherche Aérospatiale n° 1970-3, p. 145.

[64] J.R. KLIEGEL – Gas particle nozzle flows.
9th International Combustion Symposium, Ithaca, Aug. 1962.

[65] R.C. PARKINSON – Convective heat transfer in rocket engines. Part 2. Heat transfer to the nozzles.
Rocket Propulsion Establishment. T.R. n° 67/16.

[66] J.R. HOWELL – M. KERN STRITE – H. RENKEL – Heat transfer analysis of rocket nozzles using very high temperature propellants.
AIAA Preprint n° 64-62, 1964.

[67] D.R. BARTZ – Turbulent boundary layer heat transfer from rapidly accelerating flow of rocket combustion gases and of heated air.
Advances in Heat Transfer, vol. 2, p. 1. Academic Press, 1965.

[68] R. MICHEL – Cours sur les couches limites professé à l'ENSA, 1963.
Développement de la couche limite en tuyère hypersonique.
ONERA T.P. n° 91, 1964.

[69] D.R. BARTZ – An approximate solution of compressible turbulent boundary layer development and convective heat transfer in convergent divergent nozzles.
ASME Paper n° 54-A-153.

[70] R.J. ZEAMER – Survey paper on erosion produced by two phase flow in solid propellant rocket motors.
AGARD Conference Processings, n° 52, 1970.

[71] E.W. UNGER – Heat transfer to a solid propellant rocket motor.
ARS Solid propellant rocket conference, 1962. Paper 2333-62.

[72] H.S. CARSLAW – J.C. JEAGER – Conduction of heat in solids.
Oxford at the Clarendon Press, 1965.

[73] A.S. LYCHEVSKII – Sur la stabilité des pellicules liquides dans les moteurs thermiques.
Traduction SEDOCAR n° 650329.

[74] I. DEE CHANG – P.E. RUSSELL – Stability of a liquid layer adjacent to a high speed gas stream.
The Physics of fluids, vol. 8, n° 6, p. 1018, Jun 1965.

[75] A. SHERMAN – J. SCHETZ – Breakup of liquid sheets and jets in a supersonic gas stream.
AIAA Journal, vol. 9, n° 4, Apr. 1971.

[76] A.H. NAYFEH – W.S. SARIC – Stability of a liquid film.
AIAA Journal, vol. 9, n° 4, Apr. 1971.

[77] M. SCAGNETTI – J. CRABOL – Sondes thermométriques à film de platine à réponse rapide.
La Recherche Aérospatiale n° 97, Nov. Déc. 1963, p. 23.

[78] M. SCAGNETTI – J. CRABOL – Mesure des flux de chaleur pendant la phase d'allumage d'un propergol solide.
La Recherche Aérospatiale n° 123, Mars – Avril 1968, p.45.

[79] D. BALAGEAS - Conduction non linéaire unidimensionnelle. Méthode par différences finies du type explicite.
Notes Techniques ONERA non publiées.

[80] A.V. LUIKOV - Methods of solving the non linear equations of unsteady state heat conduction.
Heat Transfer. Soviet Research, vol. 3, p. 1, May - June 1971.

[81] M.A. BIOT - New methods in heat flow analysis with application to flight structures.
Journal of the aeronautical Sciences, vol. 24, n° 2, p. 857, Dec. 1957.

[82] M.A. BIOT - H.C. AGRAWAL - Variational analysis of ablation for variable properties.
ASME Paper 63-WA 207, 1964.

[83] A.D. KIRSHENBAUM - J.A. CAHILL - The density of liquid aluminium oxide.
J. Inorg. Nucl. Chem. vol. 14, n° 3-4, p. 283, 1960.

[84] M. BARRERE - Problèmes énergétiques de la propulsion.
Cours ENSA, spécialisation M.A.S., 1965.

[85] W.H. MILLER - D.K. BARRINGTON - A review of contemporary solid rocket motor performance prediction techniques.
Journal of Spacecraft and Rockets, vol. 7, n° 3, p. 225, March 1970.

[86] L.J. GORDON - Ballistic effect of pyrolyzed liner in solid propellant motor firings.
ARS Journal, vol. 30, n° 5, p. 502, May 1960.

[87] J.W. KORDIG - G.H. FULLER - Correlation of nozzle submergence losses in solid rocket motors.
AIAA Journal, vol. 5, n° 1, p. 175, Jan. 1967.

[88] A.W. BLACKMAN - D.K. KUEHL - Use of binary light metal mixtures and alloys as additives for solid propellants.
ARS Journal, vol. 31, n° 9, p. 1265, Sept. 1961.

[89] A.M. MELLOR - I. GLASSMAN - Augmented ignition efficiency for aluminium.
Combustion Science and Technology, vol. 1, p. 437, 1970.

[90] E.M. LANDSBBAUM - Contour nozzles.
ARS Paper 734-58, 1958.

[91] E. LE GRIVES - Tuyères propulsives à grand rapport de détente.
Combustion and Propulsion fifth AGARD Colloquium.
Pergamon Press, p. 217, 1963.

[92] T.K. BOSO - T.R. SANKARANARAYANAN - Heat transfer optimization of convergent section of a hypersonic flow nozzle.
Journal of Spacecraft and Rockets, vol. 8, n° 10, p. 1090, Oct. 1971.

[93] F.E. MARBLE - Nozzle contours for minimum particle lag loss.
AIAA Journal, vol. 1, n° 12, p. 2793, Dec. 1963.

[94] G. LEITMANN - Optimization techniques with applications to aerospace systems.
Academic Press, New-York, 1962.

[95] R.R. HESS - Optimum nozzle contours for a dissociating gas with a catalyst.
Ph. D. Dissertation. Kansas State University, 1966.

[96] G.V. DRITOV – A.P. TISHIN – Choix d'un profil de tuyère pour un écoulement de gas et de particules condensées.
Akademila Nauk. SSSR. Izvestia Mekhanika Zhidkosti i Gaza, n° 1, p. 170, (1971).

[97] J.D. HOFFMAN – H.D. THOMPSON – A general method for determining optimum thrust nozzle contours for gas particle flows.
AIAA Paper n° 66-538, 1966.

[98] A.A. ELSBERND – J.D. HOFFMAN – Maximum thrust nozzles for gas particle flows.
AIAA Paper n° 72-1189, 1972.